The Role of Quorum Sensing
in Bacterial Colony Dynamics

Cicik Alfiniyah

Doctor of Philosophy

University of York

Mathematics

September 2017

Abstract

The quorum sensing (QS) signalling system allows colonies of bacteria to coordinate gene expression to optimise behaviour at low and high cell densities, giving rise to individual and group responses, respectively. The main aim of this thesis is to understand better the important roles of QS in bacterial colony dynamics. Thus a mathematical description was developed to thoroughly explore key mechanisms and parameter sensitivity. The nature of the QS system depends very much on the species. *Pseudomonas aeruginosa* was chosen as a model species for this study. *P. aeruginosa* is a Gram-negative bacterium that is responsible for a wide range of chronic infections in humans. Its QS signalling system is known to involve the *las, rhl* and *pqs* systems; this thesis focuses on the first two. The *las* system includes the LasR regulator and LasI synthase, which direct the synthesis of autoinducer 3O-C12-HSL. Similarly, the *rhl* system consists of the RhlR regulator and RhlI synthase, directing the synthesis of autoinducer C4-HSL.

The mathematical model of the *las* system displays hysteresis phenomena and excitable dynamics. In essence, the system can have two stable steady states reflecting low and high signal molecule production, separated by one unstable steady state. This feature of the *las* system can give rise to excitable pulse generation with important downstream impact on the *rhl* system. The *las* system is coupled to the *rhl* system in two ways. First, LasR and 3O-C12-HSL activate the expression of their counterpart in the *rhl* system. Second, 3O-C12-HSL blocks activation of RhlR by C4-HSL. Furthermore, the *las-rhl* interaction provides a 'quorum memory' that allows cells to trigger rhamnolipid production when they are at the edge of colony. It was demonstrated how the dynamical QS system in individual cells and with coupling between cells can affect the dynamics of the bacterial colony.

Contents

List of Tables

List of Figures

Acknowledgements

Declaration

Some material presented in this thesis has been published in the following paper: Alfiniyah C, Bees MA, Wood AJ (2017) Pulse Generation in the Quorum Machinery of Pseudomonas aeruginosa. Bulletin of Mathematical Biology 79(6): 13601389. http://doi.org/10.1007/s11538-017-0288-z.

Except where stated by reference or acknowledgement, I declare that this thesis is a presentation of my original work, written by me, and has not previously been submitted for an award at this, or any other, University.

Chapter 1

General introduction

1.1 Introduction

Bacteria are tiny microorganisms, typically a few micrometres in length. They are classified as prokaryotes which along with archaea and eukaryotes form the three main branches of the tree of life (Brown and Doolittle, 1997). Each organism consists of a single cell with a simple internal structure and may be classified using a number of different criteria. One of the most important is by the bacterial cell-wall composition; by using the Gram stain technique (Gram, 1884) bacteria are classified into two groups: Gram-positive and Gram-negative bacteria. The cell wall of bacteria is defined as the rigid structure present below the capsules, sheaths and flagella and external to the cell membrane of the cell that gives shape to the cell. The rigid layer in the cell wall of bacteria is called peptidoglycan or murein. Gram-positive cell walls contain a thick peptidoglycan layer with techoic acids (bacterial copolymers of glycerol phosphate). Meanwhile, Gram-negative cell walls contain a thin peptidoglycan layer without techoic acids that is surrounded by a thick plasma membrane, encasing a separate compartment, the periplasm (Lowy, 2009).

In the environment, bacteria are not usually found individually, but typically grow in communal groups, colonies or biofilms. In a similar manner to multicellular organisms, bacteria have the ability to build and manage complex social interactions and to exhibit diverse behavioural responses. Furthermore, bacteria utilise the process by which genetic codes are used to direct gene product synthesis, called gene expression. Bacteria employ a communication mechanism that is called quorum sensing (QS) to facilitate these activities. QS bacteria produce and release chemical signal molecules that are called autoinducers. Both Gram-positive and Gram-negative bacteria use QS circuits to regulate gene expression for both behavioural interactions and physiological activities (Miller and Bassler, 2001). In general, Gram-negative and Gram-positive bacteria use acylated homoserine lactones as autoinducers and processed oligo-peptides to communicate, respectively. For example

these processes include expression of virulence genes in *Pseudomonas aeruginosa* (Pearson et al, 1995; Davies et al, 1998; De Kievit et al, 1999), formation of biofilms and growth in *Escherichia coli* (Pratt and Kolter, 1998; Anand and Griffiths, 2003), extracellular polymeric substance biosynthesis and pathogenicity in *Erwinia* (Von Bodman and Farrand, 1995), antibiotic production in *Photorhabdus luminescences* (Ma et al, 2014), bioluminescence and symbiosis in *Vibrio fischeri* (Winson et al, 1995; Miller and Bassler, 2001; Mok et al, 2003).

In addition, QS plays a role in the growth and motility of bacterial colonies, which affects how bacteria spread on surfaces. In this thesis, we study the growth of bacteria on surfaces and present an analytical approach to model the phenomenon incorporating both biological and physical aspects. As micro-organisms impact human life, it is essential that we study how they grow and transform into different types of bacterial cell, communicate with other cells regulated by QS and spread on surfaces.

Bacteria are usually considered to be associated with dirt, diseases, and death, although certain bacteria are good for humans and we cannot live without some beneficial bacteria. Here, we focus on bacteria that cause large-scale disease for plants and humans, which are called pathogens. This has led to recent research on how bacterial communication allows bacteria to coordinate gene expression, to control production of virulence factors and other gene products that appear to have an important role in changing the spatial structure of the bacterial colony on the surface. Initially, we employ data on colony growth and QS signal molecule production of a plant-pathogen *Erwinia carotovora* as to parameterize a basic general model. Then we take the human-pathogen i.e bacterium *Pseudomonas aeruginosa* to study QS signalling systems in detail. In terms of the general QS structure of a Gram-negative bacteria, it consists of a homologous pair, a synthase autoinducer and a regulator that binds the autoinducer to activate certain genes. Different types of Gram-negative bacteria have different homologous pairs. Well-known notation for the synthase autoinducer and regulator uses "I" and "R" symbols respectively in the last homologous pair names. *P. aeruginosa* has a complex QS signalling system, and is a Gram-negative bacteria with two pairs of homologous systems (both LasI/LasR and RhlI/RhlR). Thus it might accommodate signalling dynamics for other gram-negative bacteria with only one pair of homologous systems, for example LuxI/LuxR in *Vibrio fischeri* (Eberhard et al, 1981), TraI/TraR in *Agrobacterium tumefaciens* (Zhang et al, 1993), AhyI/AhyR in *Aeromonas hydrophila* (Swift et al, 1997), CepI/CepR in *Burkholderia cepacia* (Lewenza et al, 1999), and so forth.

We use our modelling and analysis to identify key parameters that are essential for bacterial communication and can influence gene expression. By using mathematical modelling it is possible to study complex systems involving cell-cell communication, and to identify

those processes which are essential for the system. Thus the focus of this thesis is to develop mathematical models of bacterial interaction that are affected by both internal and external factors, such as gene regulation inside each cell and physical processes in each cell's environment, that subsequently affect the spatial structure of bacterial colony expansion.

1.2   Growth of bacteria and nutrient consumption

Bacteria increase their cell numbers by replication through binary fission, whereby one single cell splits into two single cells. At first, cells increase in size, then after the chromosome replicates, a partition is formed and the cell divides.

Ingraham et al (1983) demonstrated that growth of bacteria typically involves four phases: termed the lag, log or exponential, stationary and death phases. In the lag phase, cell replication does not occur even though the cells may be increasing in mass or volume, synthesizing enzymes, proteins, mRNA and increasing in metabolic activity. The bacterial cells are adapting to the new environment before binary division. In the log or exponential phase, cells divide through binary fission. The growth rate in this phase is dependent on the type of medium, growth conditions, and the species of bacteria. Insufficient nutrient is one of many factors that trigger bacterial growth to progress from the exponential to the non-replicating stationary phase. Finally, the number of bacterial cells decreases (see Fig. 1.1).

An increasing population density affects the rate of nutrient decline. Many references explore different models of bacterial growth (for example, (Grover, 1997; Koch et al, 1998; Panikov, 1995; Smith and Waltman, 1995; Tilman, 1982)). There are three principle variations on population growth models: the exponential growth or unlimited growth, the logistic model or space limited growth, and the monod model or resource limited growth. We briefly introduce these in turn.

Let $N(t)$ be the concentration of bacteria at time t. Exponential population growth is described by the simple differential equation (Malthus, 1798)

$$\frac{dN}{dt} = rN, \tag{1.1}$$

where parameter $r > 0$ is the per-capita growth rate of bacterial cells. If the initial condition is N_0, the solution is

$$N(t) = N_0 e^{rt}, \tag{1.2}$$

and the output from the exponential model is an exponential curve (see Fig. 1.2a)

Exponential growth of bacterial cells would happen only if sufficient nutrient is always available (with no other limiting factors) and is very rare in the real world. In the natural environment, bacteria live in communities competing for the available nutrients. Active
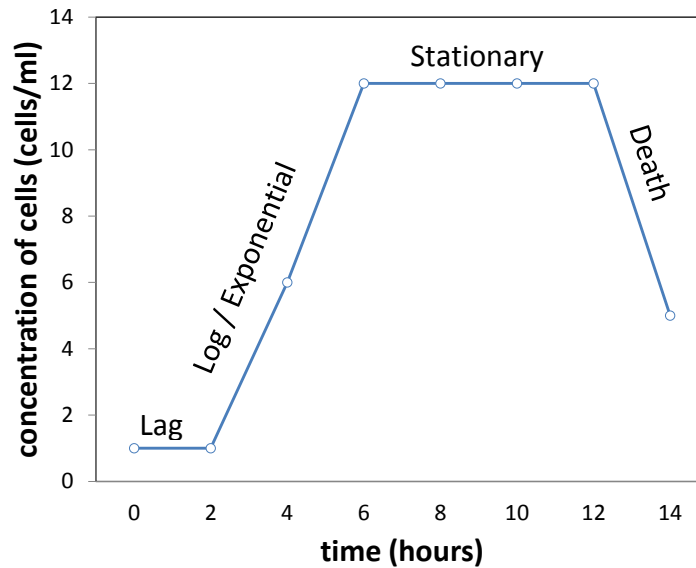
Figure 1.1: A typical bacterial growth curve. It represents the four-phase pattern of bacterial cell growth. "See text for detail explanation in each phase" (reproduced from Ingraham et al (1983))

motility of bacterial cells requires a high level of nutrient, as does growth. When the number of individual cells becomes large, nutrient will get depleted and the bacterial growth rate reduces. This is reasonable that we use up our resources when the population is too large. Verhulst (1838) demonstrated the following differential equation as a logistic growth model such that

$$\frac{dN}{dt} = rN \left(1 - \frac{N}{K} \right). \tag{1.3}$$

K is the carrying capacity of the bacterial population. When N is very small the carrying capacity does not affect the growth and the population increases exponentially. However, when N is large, the expression on the right-hand side is close to zero (if $N = K$) or negative (if $N > K$) resulting in slow growth or population decline, respectively. Therefore, logistic growth is a more realistic model of population growth than exponential growth. The output from the logistic model is a sigmoidal curve as illustrated in Fig. 1.2b.

The last type of bacterial growth model is the Monod model. Monod (1947) argued that a sigmoidal curve that the growth rate is inversely proportional to substrate concentration. For bacterial growth, Monod proposed that the growth rate gradient is large at low concentrations of substrate and small at high concentrations of substrate, reaching saturation level at large concentration (Fig. 1.2c). Thus the Monod growth model is restricted by substrate
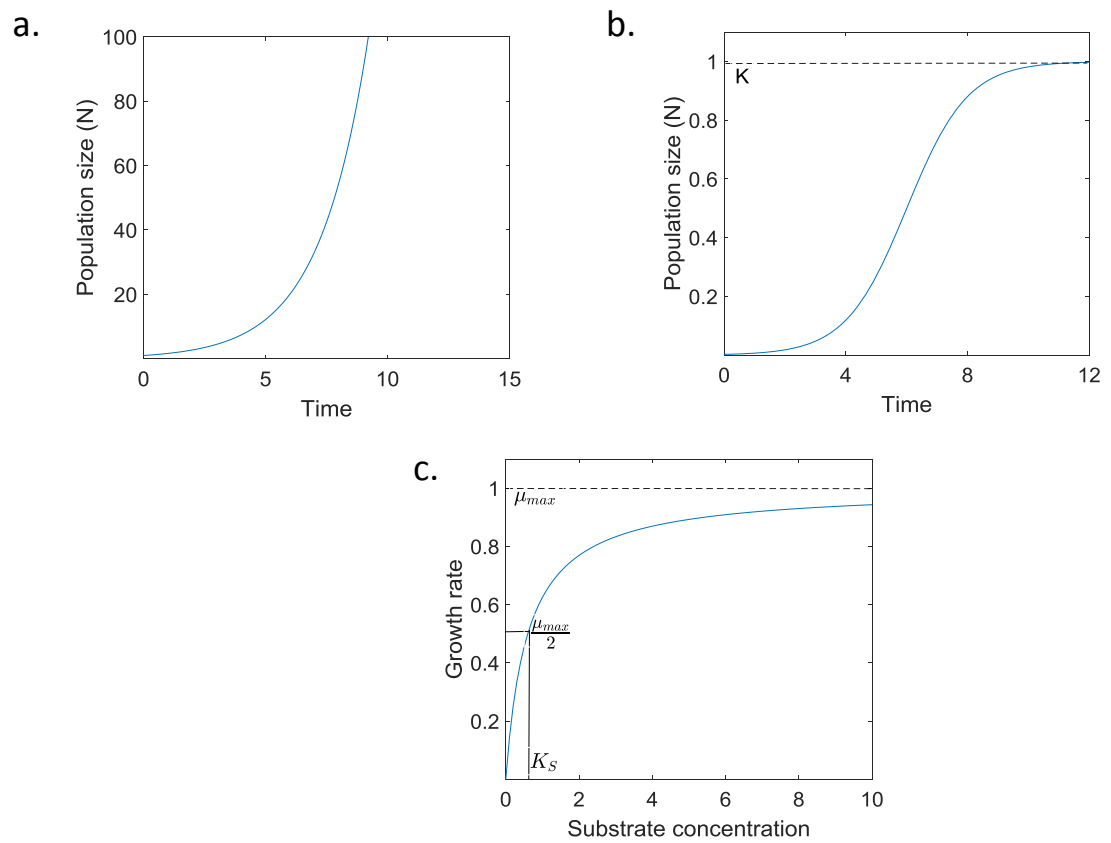
Figure 1.2: Different types of population growth: (a) exponential growth, (b) logistic growth, and (c) monod growth. The solid-line depicts the growth rate of the population, and the dashed-line depicts the maximum population size.

concentration, such that

$$\mu = \mu_{max}\frac{S}{K_S + S},\tag{1.4}$$

where μ_{max} is the maximum growth rate, and K_S is the Monod-constant, the substrate concentration at which half of the maximum growth rate is achieved.

The Monod model is the most commonly used of these growth models for bacterial populations with simple substrates (Contois, 1959). We explore generalizations of the above models in later chapters.

1.3 Gene regulation

Bacteria usually inhabit an ever-changing environment in which nutrient availability may vary significantly. Bacteria respond to the various environments by altering gene expression; nutrient availability affects the expression of different enzymes (Ralston, 2008a).

Gene regulation is a mechanism for controlling which genes are expressed. In other words, it is a process of switching genes "on" and "off" (Berg et al, 2002). Regulation of gene expression also helps an organism to respond to its environment at proper times and conditions.

Every cell has mechanisms to control gene expression. In this thesis, we only discuss the regulation of gene expression for *prokaryotic* cells (bacteria). The process of gene expression consists of two main stages, transcription and translation (Fig. 1.3). At first, messenger RNA (mRNA) is produced by the enzyme RNA polymerase, resulting in mRNA molecules (transcription). After that, mRNA directs protein synthesis (translation) (Berg et al, 2002). Unlike transcription and translation in *Eukaryotes*, these two processes are linked in time and space. Both machineries can occupy the same mRNA. They facilitate direct contact between transcribing RNAPs and translating ribosomes. The translation process occurs immediately after the ribosome binding sites are transcribed (McGary and Nudler, 2014).

In *prokaryotic* gene regulation, related genes are often located in a cluster on the chromosome, where they are transcribed from one promoter (RNA polymerase binding site) as a single unit. A cluster of genes that is controlled by a single promoter is called an operon (Berg et al, 2002). In general, operons contain genes that function in the same process. Not only made up of the coding sequences of genes, the operon also contains regulatory DNA sequences that control its transcription (Fig. 1.3). Typically, these sequences are binding sites for regulatory proteins, which control how much of the operon is transcribed. Regulatory proteins in bacterial gene expression are categorized as either positive or negative regulators, which are called activators and repressors, respectively (Berg et al, 2002). When a positive regulatory protein is bound to its DNA binding site, transcription of the operon
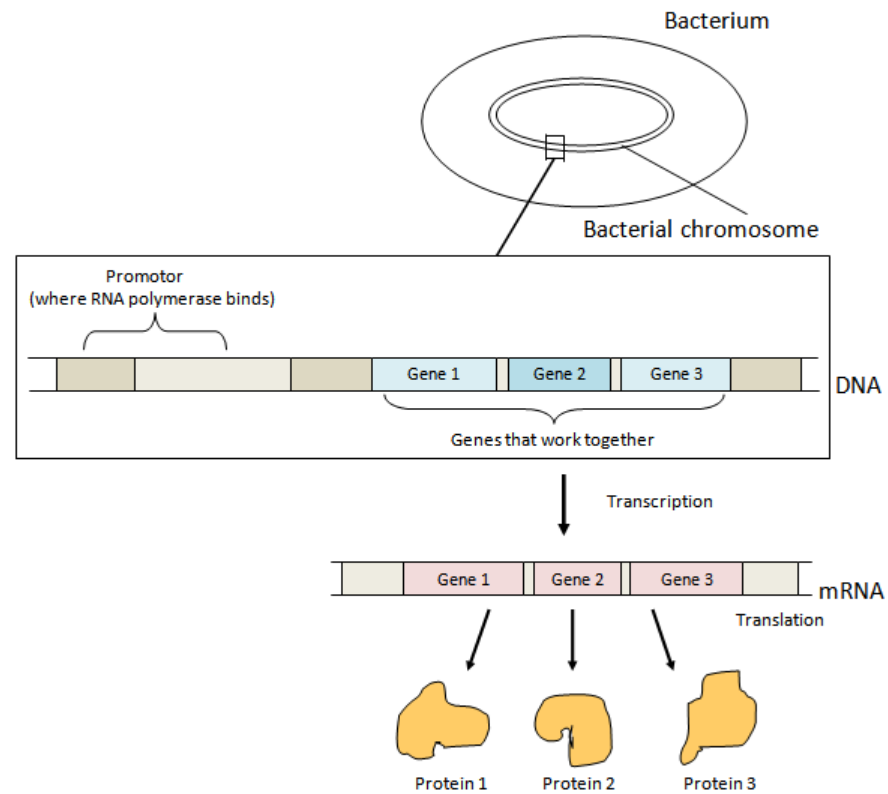
Figure 1.3: In a cluster on the chromosome, genes are found and transcribed from one promotor where RNA polymerase binds. For the prokaryotic case, DNA gene sequences are organized as an operon. They are transcribed to produce mRNA, then it is immediately translated to a protein without additional processing. (Reproduced from (Khanacademy, 2017), retrieved 20-04-17)

goes up (Fig. 1.4a). Conversely, when a negative regulatory protein is bound to a piece of DNA, it reduces the transcription of the operon (Fig. 1.4b). The arrangement of this sequence of binding sites for the regulatory proteins acts to turn expression of the operon either "up" or "down".
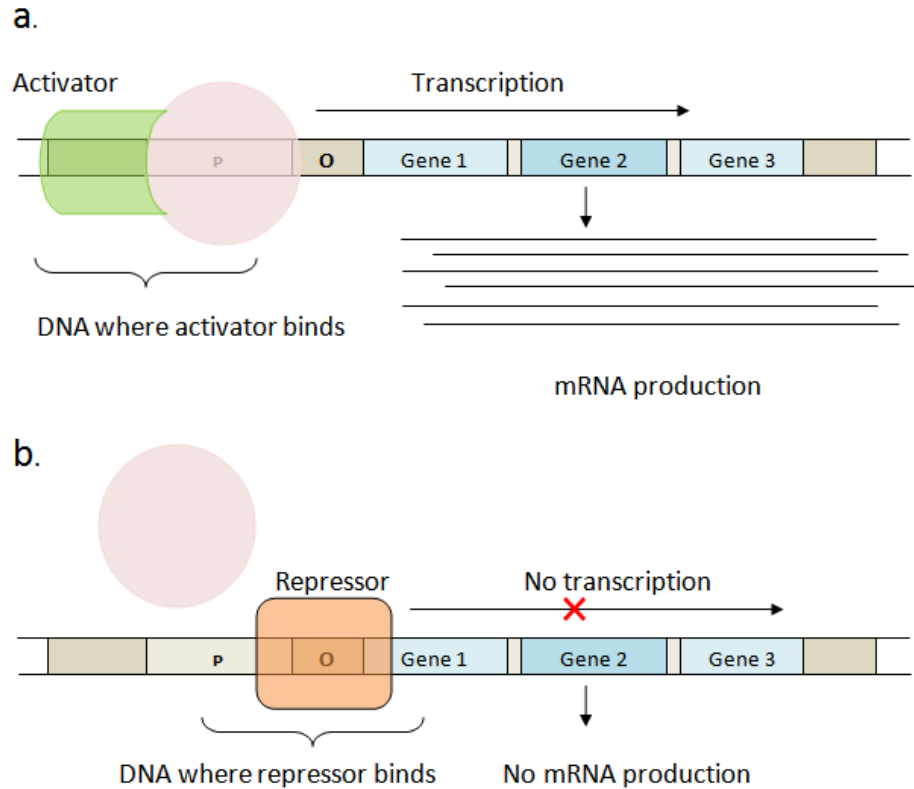
Figure 1.4: Regulatory proteins by (a) activator; the activator binds the DNA binding site. This binding helps RNA polymerase binds promotor. Consequently, it increases transcription. (b) Repressor; the repressor binds the operator, another side of DNA. This binding blocks RNA polymerase from binding on DNA. Consequently, there is no transcription process. (Reproduced from (Khanacademy, 2017)), retrieved 20-04-17

1.4 Quorum sensing-what is it?

Quorum sensing describes cell communication mechanisms that allow bacterial cells to control gene expression in relation to the cell density (Miller and Bassler, 2001). Communication occurs through the interchange and detection of small signal molecules. Although bacteria produce different chemical signals (see Fig. 1.5), in every case the ability to communicate with other types of bacteria allows a degree of collective coordination in gene expression (Bassler, 2002).

Quorum sensing (QS) was discovered over 40 years ago associated with the expression

a. Acyl-Homoserine Lactone Autoinducers

V. fischeri/LuxI
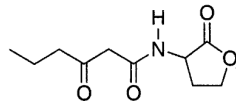
P. aeruginosa/LasI
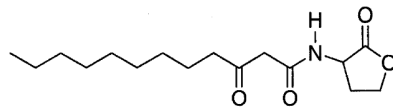
P. aeruginosa/RhlI
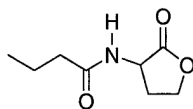
P. Stewartii/EsaI
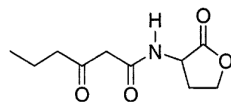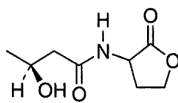
V. harveyi/LuxLM

b. Oligopeptide Autoinducers

B. subtilis/ComX

ADPITRQWGD

B. Subtilis/CSF

ERGMT

S. aureus/subgroup 1

YSTCDFIM
S—C=O

S. aureus/subgroup 2

GVNACSSLF
S—C=O

S. aureus/subgroup 3

YINCDFLL
S—C=O
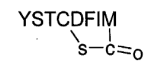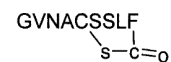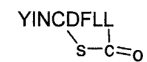
S. aureus/subgroup 4

YSTCYFIM
S—C=O
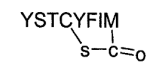
C. AI-2

V. harveyi/LuxS
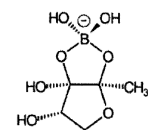
Figure 1.5: Representative bacterial autoinducers and Enzymes that produce them. (a) Gram-negative AHL autoinducers. (b) Gram-positive oligopeptide autoinducers. The asterisk denotes an unknown modification. (c) *V. harveyi* AI-2. (Adapted from Bassler (2002))
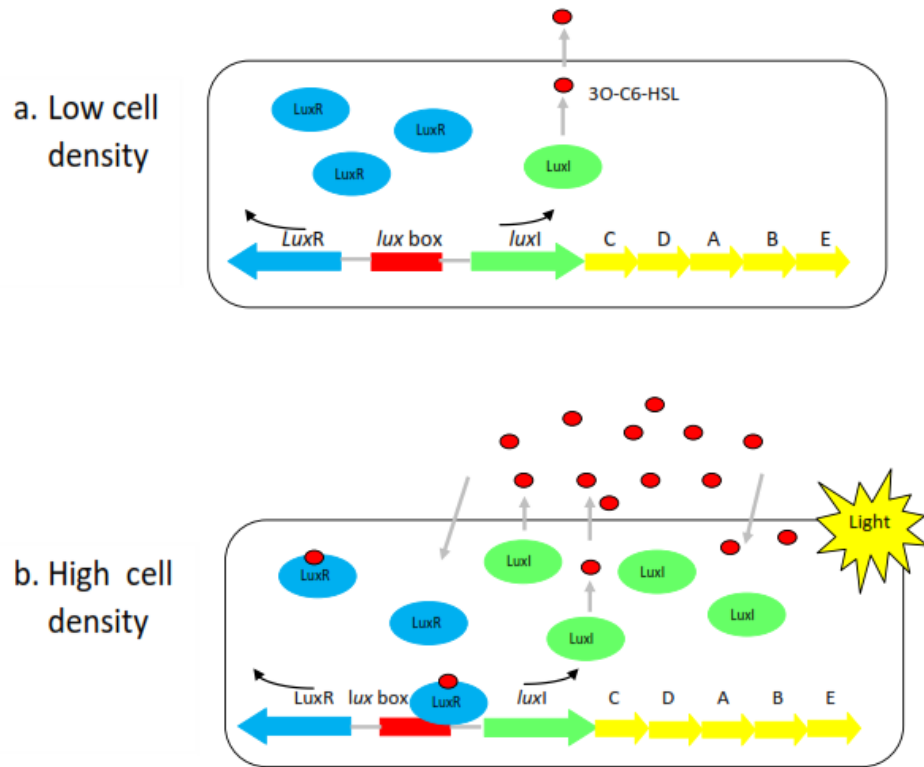
Figure 1.6: Mechanism of quorum sensing and bioluminescence activation in *V. fischeri*. When there are few bacteria, the *luxICDABE* genes are transcribed constitutively at a low concentration of signal molecule (red circles). Signal molecules are produced, diffuse out of the cell and dilute in the environment. When there are many bacteria, there are a large number of inducer molecules that will induce a large expression of the lux genes. Signal molecules accumulate in the local environment and within the cell. They bind to LuxR to form complexes then increase transcription of *luxICDABE* and result in light production (they release free energy in the form of blue-green light, thus light is not seen unless the bacteria are in high concentration). (a) Transcription is not activated at low cell density. (b) Transcription is activated at high cell density. (reproduced from Li and Tian (2012))

of bioluminescence in the Gram-negative marine bacterial species, *Vibrio fisheri* and *Vibrio harveyi* (see Fig. 1.6) (Nealson et al, 1970; Nealson and Hastings, 1979). They produce a small, diffusible molecule that is called an autoinducer (Nealson et al, 1970; Eberhard, 1972) and identified as an acylated homoserine lactone (AHL) (Eberhard et al, 1981). In general, Gram-negative bacteria use N-acyl homoserine lactones (HSLs) as signals while Gram-positive bacteria use oligopeptides (Miller and Bassler, 2001). The quorum sensing structure of *Vibrio fischeri* has been well explored. The enzymes responsible for light production are encoded by eight genes (*luxA-E, luxG, luxI* and *luxR*). LuxI is a synthase protein that encodes an enzyme called an autoinducer synthase. Then, LuxR is a transcription regulator protein that binds to the autoinducer and activates the *luxA-E* and *luxI* operon (Miller and Bassler, 2001).

At a low population density of bacteria, the concentration of signal molecules is low because only a low level of *luxI* genes are expressed (Liu et al, 2004). However, as the population of cells increases, the concentration of signal molecules increases in the surrounding environment. Consequently, the diffusion gradient is reversed and the signals start to diffuse back into the cell. As Redfield (2002) argues, it is more accurate to say that bacteria are using the signal molecule concentration to measure diffusion limitation in the local environment.

As described in the previous paragraph, the regulation of bioluminescence in the marine bacterium *V. fisheri* is the earliest known example of QS. At low cell density, it is non-bioluminescent, and cultures of *V. fisheri* appear dark. Once the concentration of AHLs reaches a particular threshold level, which corresponds to critical density, this bacterium is bioluminescent (Fig. 1.6).

1.5 What is rhamnolipid?

In 1949, Jarvis and Johnson (1949) demonstrated that *Pseudomonas aeruginosa* characteristically produces the biosurfactant rhamnolipid, a glycolipidic surface-active molecule. However, in last decade Hussler et al (1998); Tuleva et al (2002); Gunther Iv et al (2005) showed that *Pseudomonas putida, Pseudomonas chlororaphis* and *Burkholderia pseudomallei* also produce other varieties of rhamnolipids. Different types of bacteria produce specific types of rhamnolipids. *P. aeruginosa* produces four types of rhamnolipids, namely $RhC_{10}C_{10}$, RhC_{10}, $Rh_2C_{10}C_{10}$, and Rh_2C_{10} (Rahman et al, 2002). Rhamnolipids are typically formed of a dimer of 3-dydroxyfatty acids linked through a beta glycoside bound to a mono- or di-thamnose (see Fig. 1.7)(Chaves et al, 2005).

The production of rhamnolipids is regulated by two quorum sensing systems, *las* and *rhl* system (Van Delden and Iglewski, 1998). *P. aeruginosa* produces two essential autoin-
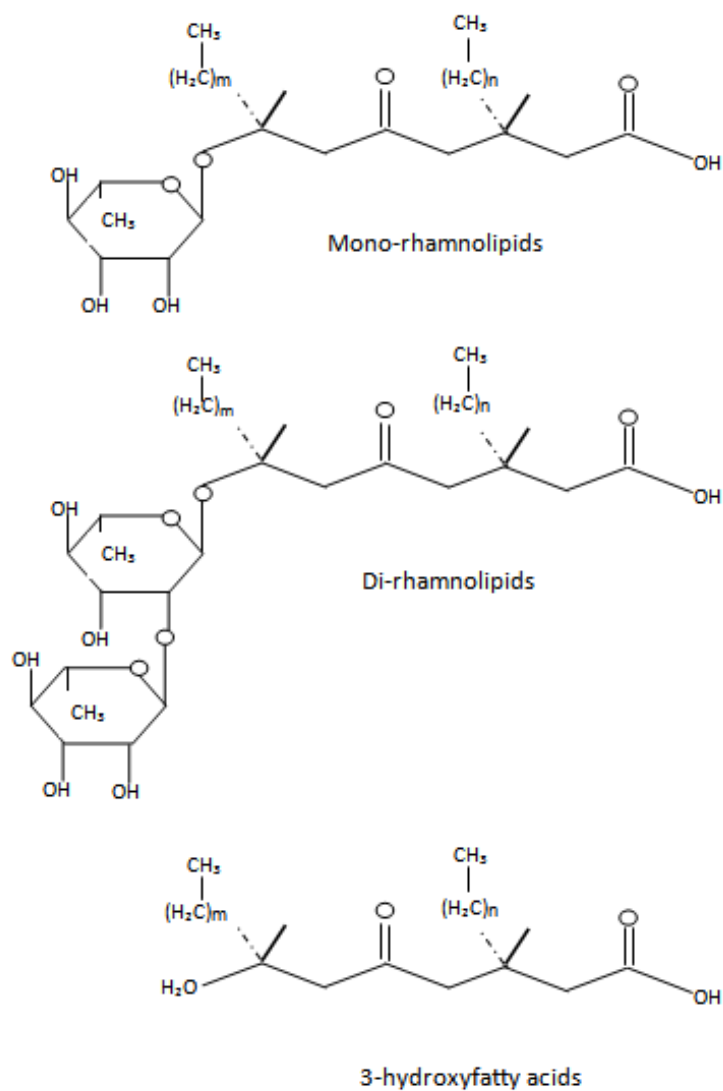
Figure 1.7: Chemical structure of rhamnolipids, $m, n = 4$ to 8. Replotted (Chaves et al, 2005).
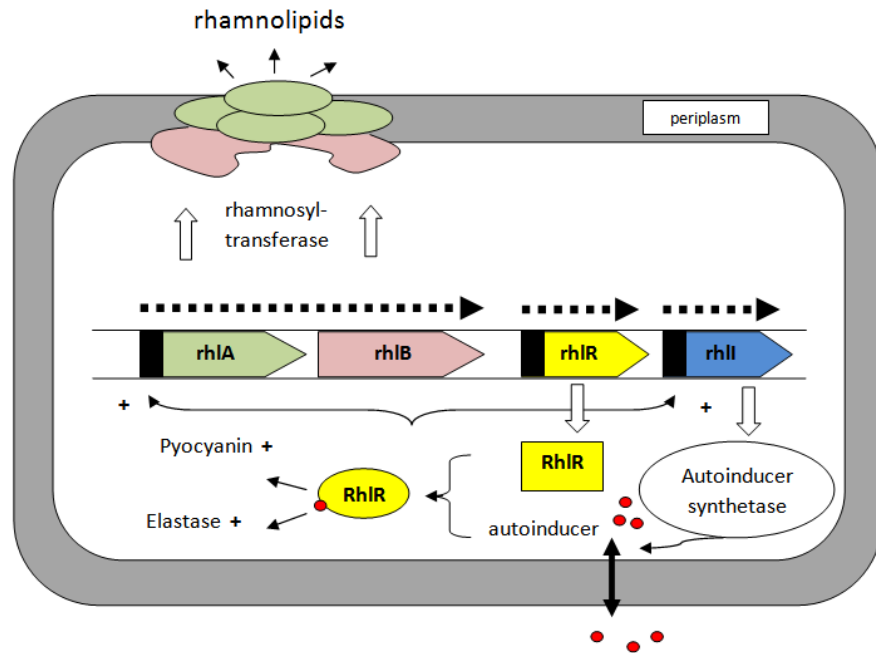
Figure 1.8: Model for the regulation of rhamnolipid production in *P. aeruginosa*. Replotted (Ochsner and Reiser, 1995).

ducers, *N*-3-oxododecanoyl-HSL (3O-C12-HSL) and *N*-butanoyl-HSL (C4-HSL), which are synthesized by LasI and RhlI, respectively (Pesci et al, 1997). 3O-C12-HSL and C4-HSL bind LasR and RhlR respectively, to activate gene expression (Seed et al, 1995; De Kievit et al, 1999; Miller and Bassler, 2001). The complex of LasR/3O-C12-HSL promotes several genes, including genes that encode the transcriptional regulator RhlR (Latifi et al, 1996; Pesci et al, 1997), which links to the *rhl* system. Once RhlR bind C4-HSL, it promotes the expression of *rhlAB* genes (Ochsner and Reiser, 1995) and *rhlC* genes (Rahim et al, 2001). The transcription of *rhlAB* encodes rhamnosyltransferase 1 (see Fig. 1.8) (Ochsner and Reiser, 1995), and *rhlAB* encodes rhamnosyltransferase 2 (Rahim et al, 2001). Moreover, RhlR activates *rhlAB* gene expression if coupled with C4-HSL, but represses if coupled with 3O-C12-HSL (Medina et al, 2003). Thus transcriptional regulation of *rhlAB* not only depends on RhlR and C4-HSL, but also diffusible molecules of 3O-C12-HSL.

Rhamnolipids have been extensively studied due to their important functions, chemical structures, physico-chemical properties, etc. Syldatk et al (1985); Stanghellini and Miller (1997) demonstrated that rhamnolipids play essential roles in bacterial cell motility, cell interaction, cell differentiation and formation of water channels. In a series of papers, Maier and Soberon-Chavez (2000); Chaves et al (2005) explored physico-chemical properties of rhamolipids in terms of surface activity and potential application. These important functions have inspired the use of rhamnolipids in bioremediation of contaminated soils and polluted

waters. In medical treatment, rhamnolipids are very important as antimicrobials, on wound healing and in organ transplants (Stipcevic et al, 2006).

1.5.1   Effects of rhamnolipid-biosurfactant on surfaces

The Rhamnolipid-biosurfactant produced by *Pseudomonas* affects cell surface structures. The rhamnolipid causes reduction of total cellular LPS (lipopolysaccharides), which can be associated with an increase in cell hydrophobicity. Sotirova et al (2009) demonstrated that increasing rhamnolipids-biosurfactant concentration up to a certain level increased extracellular protein concentration but did not affect the growth. Biosurfactant concentration increases the amount of extracellular protein, perhaps due to increased cell permeability. LPS are the major component of the outer membrane of Gram-negative bacteria and are responsible for stabilizing the overall membrane structure involved in the cell impermeability characteristics (Denyer and Maillard, 2002). The experiment data by Sotirova et al (2009) showed that the cell surface becomes more hydrophobic with the high concentration of rhamnolipid-biosurfactant associated with a reduction of the total cellular LPS (see Fig. 1.9).
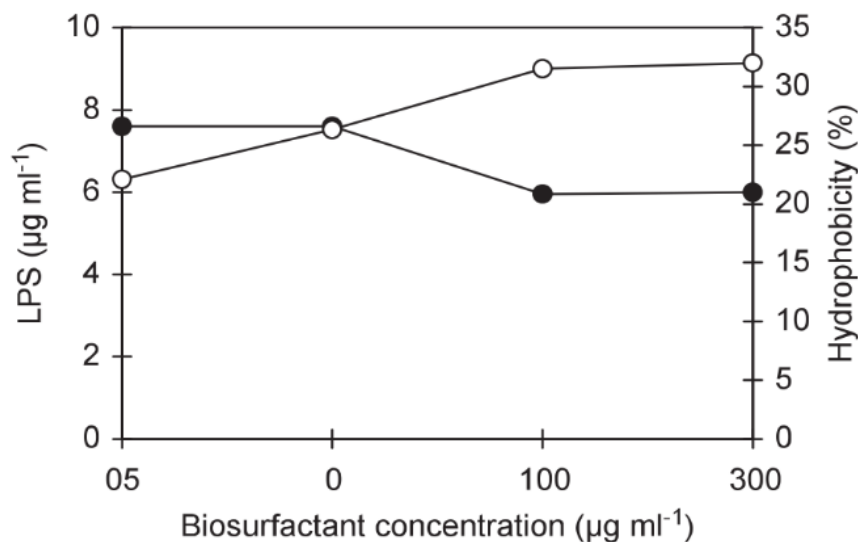
Figure 1.9: Effect of rhamnolipid-biosurfactant on cell hydrophobicity (○) and LPS content (●) in outer membrane of *P. aeruginosa*. Adapted (Sotirova et al, 2009).

In addition, the structure of rhamnolipid-biosurfactant consists of hydrophobic and hydrophilic areas that can alter the properties of the liquid-solid interface through aggregation at the vapor-liquid and solid interfaces, which reduces surface tension. Renfro (2013) ob-

Table 1.1: Contact angles measured with (θ^{Pol}= polypropylene, θ^{Pmma}= poly(methyl, methacrylate), θ^{Nylon}= polyamide). Adapted (Renfro, 2013).

Concentration rhamnolipid	θ^{Pol} (^{0})	θ^{Pmma} (^{0})	θ^{Nylon} (^{0})
6.25	105.1	65.0	69.1
12.5	103.9	64.4	68.0
25	102.3	63.4	66.4
50	96.9.1	58.9	60.0
75	94.3	58.3	57.9
100	95.4	61.6	60.8

served that rhamnolipid-biosurfactant can reduce water surface tension. When rhamnolipids disperse in water, the hydrophilic monomer head groups of rhamnolipid molecules accumulate at the interface. From his observation, Renfro (2013) demonstrated that water surface tension decreased linearly with regard to rhamnolipid biosurfactant concentration until it reached a critical threshold value. Water surface tension will stabilize above this critical value (see Fig. 1.10).
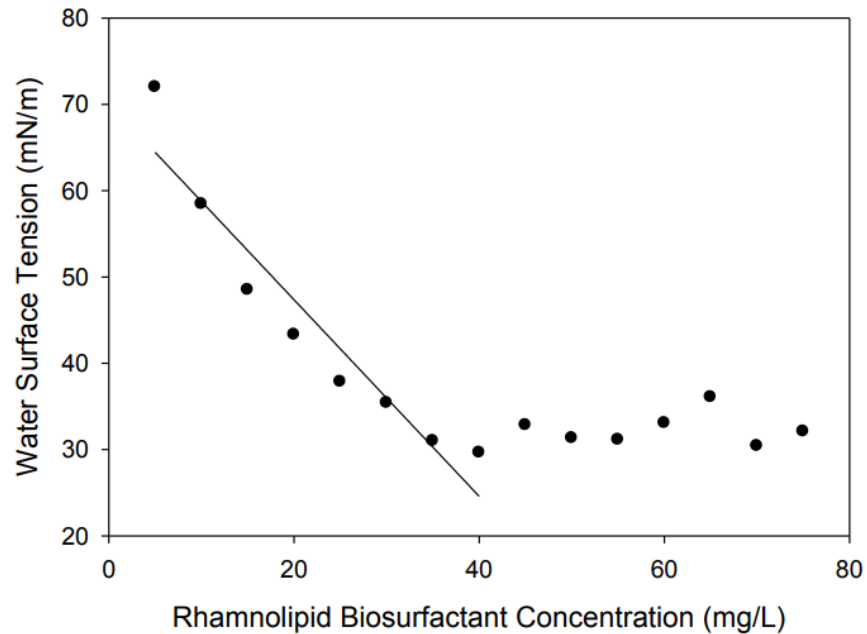
Figure 1.10: Water surface tension drop as a function of rhamnolipids biosurfactant concentration. Adapted (Renfro, 2013).

Furthermore, rhamnolipid-biosurfactant can be applied as wetting agent. It is used to break down the barriers, allowing liquid to easily spread. Wetting profiles showed that the

contact angle of fluid droplets on the solid surface and concentration of rhamnolipid have a converse relationship (tabulated in table 1.1). There is a big contact angle when it has for low concentration of rhamnolipid, and when the concentration of rhamnolipid is increased, the contact angle decreases (Costa et al, 2009). Contact angles reveal the level of wettability (Musselman and Chander, 2002).

1.6 Bacterial colony

Typically, a single bacterial colony consists of two or more individual cells. Cell coordination is a requirement for the bacterial colony for further growth. Since the observation of complex bacterial colony patterns (Fujikawa and Matsushita, 1988; Matsuyama et al, 1989), there has been renewed theoretical and biological interest in the mechanisms and processes for bacterial colony growth.

Various types of bacterial colonies reveal different spatial patterns, depending on the growth medium, the hardness of the agar and the nutrient levels. Bees et al (2000) constructed a mathematical model of growth in thin fluid films on surfaces of different hardness and nutrient availability (see Fig.1.11). Ward and King (2012) used thin film to investigate biofilm growth and QS. They examined shear stress-free and no-slip as boundary conditions between the biofilm and the solid surface. In addition, there has been a considerable number of papers modelling bacterial colony patterns with particular interest in their dynamical behaviour. Their spreading creates interesting spatial structure and branching instability (see Fig.1.12). For example: Matsushita and Fujikawa (1990) include diffusion limited in nutrient concentration, Ben-Jacob et al (1994) consider random walkers that move in response to gradients in nutrient concentration, and Golding et al (1998) incorporate a reaction-diffusion model with non-linear diffusion.

Two common cell movement mechanisms involve chemotaxis and diffusion. Chemotaxis describes directed cells movement in response to a spatial chemical gradient. Meanwhile, diffusion describes random motion of cells. In this research, we only consider diffusional cell movement.

A significant amount of research on bacterial colony behaviour has been carried out that considers coupled physical and biological aspects. Jacob (2008) demonstrated collective pattern formation by swarming bacteria and explained how bacteria develop complex colonial patterns by employing communication capabilities including quorum sensing. Mimura et al (2000) explored bacterial pattern models that focused on the dynamics of colony development with two types bacterial cells, active and inactive, based on nutrient concentration. Also there are numerous studies that focus on QS signal molecule production. For example, Ward et al (2001) explored bacterial growth and QS signal molecule production in *V. fischeri*
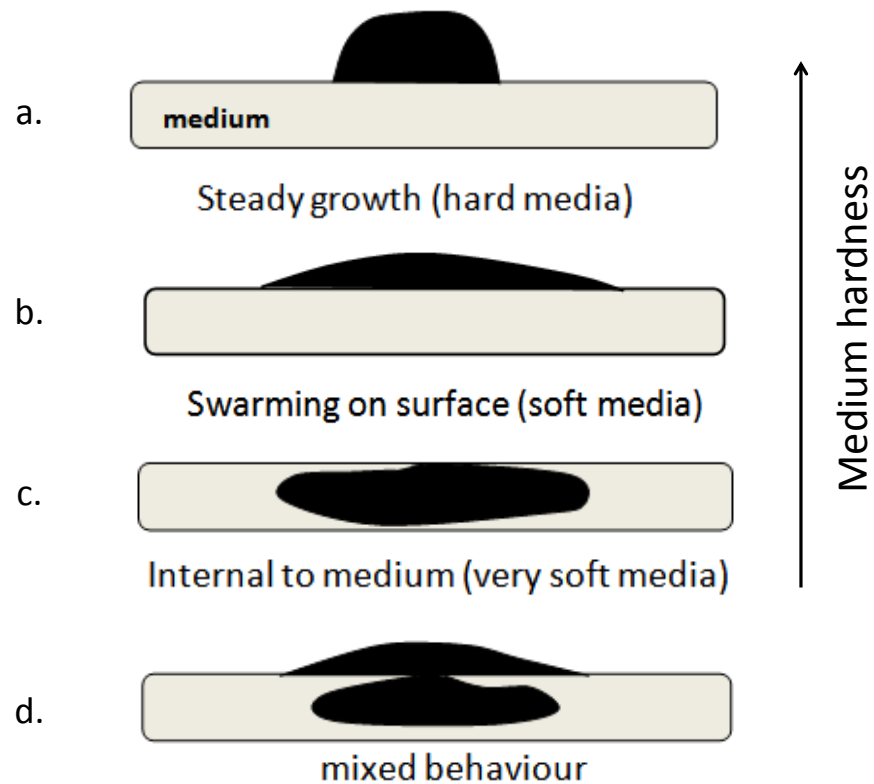
Figure 1.11: Illustration of colony expansion: (a) steady growth of bacteria on hard media, (b) bacteria are able to extract fluid from the soft media, (c) bacteria are able to swim in the soft media, (d) bacteria in media that has intermediate hardness between b and c. (Adapted from Bees et al (2000))

rather than biochemical mechanism by using a population dynamics approach, Daniels et al (2004) investigated the effect of QS on swarming migration of bacteria by describing how QS may disperse biofilm existence, and Frederick et al (2011) construct a mathematical model of quorum sensing but their focus is QS effects on biofilm formation rather than colony growth. However, to the best knowledge of the authors, none of the studies about QS signal molecules link directly to the interesting spatial structure of bacterial spreading.
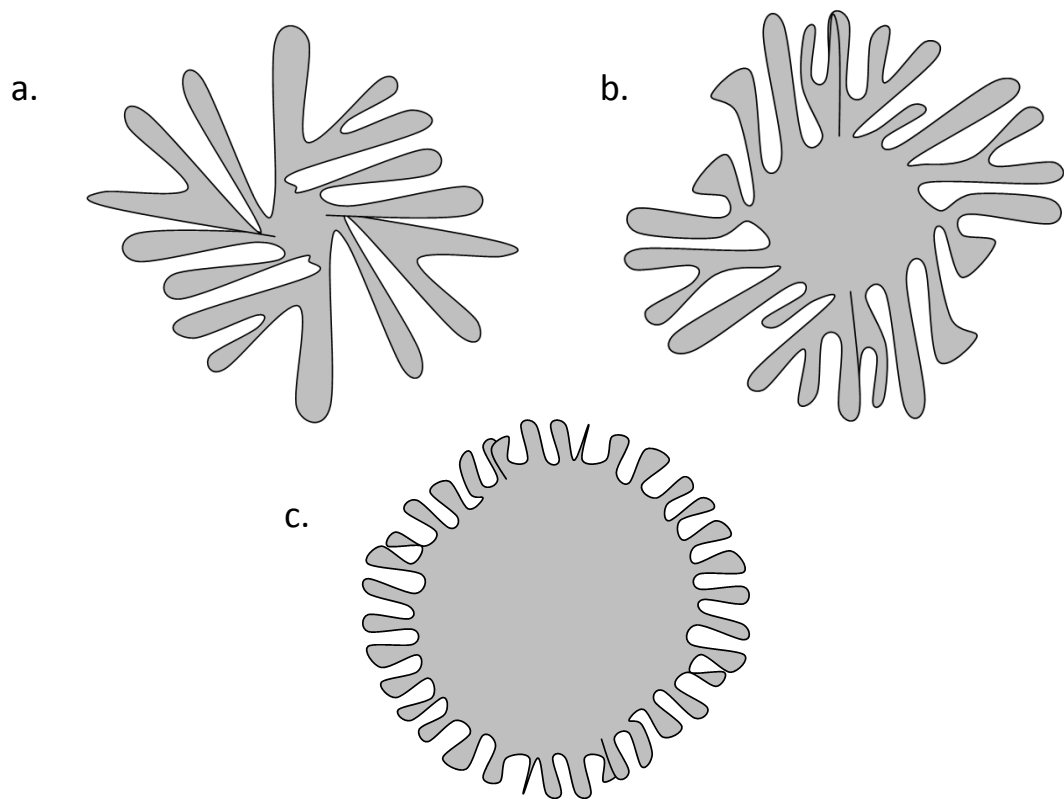
Figure 1.12: Finger patterns on colony spreading observed in biological experiments. These patterns are affected by nutrient source and hardness of surfaces. In the experiment, they use peptone as nutrient sources. (a) 4 g/l peptone and 2.5% agar concentration (b) 2.5 g/l peptone and 2.5% agar concentration (c) 15 g/l peptone and 2.25% agar concentration. (Reproduced from Golding et al (1998))

1.7 Objective research questions

Bacterial quorum sensing (QS) has received significant interest by mathematicians and biologists. Experimental work has supported biological hypotheses that the QS signalling system regulates gene expression, including for production of extracellular virulence factors and motility behaviour. By using QS signalling, bacteria engage in cell-to-cell communication using diffusible molecules. Thus this signal molecule is very important for social behaviour

and pathogenesis. Typically, a QS system consists of several components: autoinducer synthase, transcriptional activator and autoinducer. In order to get better understanding of the dynamics of the QS systems, mathematicians construct mathematical models of QS system and parameterize the system from experimental evidence.

In the last few years, the QS signalling system of *P. aeruginosa* has received much attention. *P. aeruginosa* is a Gram-negative opportunistic pathogen for humans and animals, it produces a variety of virulence factors that can result in severe infections and other serious illnesses. On the other hand, *P. aeruginosa* also produces virulence factors that coordinate biofilm formation, which might give benefit on biotechnological applications such as wastewater treatment by removing toxic chemicals via the formation of biofilm (Kokare et al, 2009), bioremediation by removing pollutants that threaten public health (Schachter, 2003), soil remediation by improving the agriculture soil quality (increasing the bioavailability of nutrient) via bio-surfactants that is produced (Ramesh Kumar and Kumar, 2017). Thus *P. aeruginosa* is considered as an interesting species for research that is important in human life. Furthermore, the QS signalling system of *P. aeruginosa* is accessible due to a large amount of biological literature. In addition, it has a complex QS system that consists of at least the *las*, *rhl* and *pqs* subsystems. It is challenging for mathematicians to model this system in order to manage biological knowledge, interpret complex system interaction, and predict the dynamical system's behaviour.

The aim of this thesis is to investigate the role of the QS system in bacterial colony expansion. The first objective of this part of the thesis was to construct a simple bacterial interaction model that includes basic concepts, such as bacterial growth, transition of bacterial types, QS production, and diffusion of signal molecules. This individual based QS model is expected to establish a framework to explore the impact of QS signal molecules on bacterial growth. The second objective of the QS modelling was to understand in more detail how the QS system works as a central controller that regulates almost all gene expression. This model takes a particular species, *P. aeruginosa*, with some reasons that we have explained in the previous paragraph.

1.8   Thesis outline

The research work to address the above aims is presented in different chapters as follows.

Chapter 2 describes the introductory model, which consist of up-regulated cells, down-regulated cells, and quorum-sensing as main components of the model. It describes the biological interactions involved in three process: bacterial growth, transition of bacterial types, and signal molecule production. This model will be used to investigate the constant diffusion effect of QS signal molecule production. In this introductory model, we do not con-

sider motile behaviour and quorum sensing in a specific organism. However, we investigate *Erwinia carotovora* data as an example.

Chapter 3 reviews the literature on mathematical modelling of the QS signalling system. This chapter also investigates all papers that cite Dockery and Keener (2001) (key reference) and classifies them into four different categories, including papers that correspond to features relevant to biological and physical implications, secondary relevance, and unrelated to our research. This chapter demonstrates how biological theories can be developed into different sets of equations to model QS in *P. aeruginosa*. Thus this chapter also reviews the systems of equations in published models.

Chapter 4 develops a mathematical description of the hierarchical quorum sensing system in *P. aeruginosa*, especially for the *las* subsystem. This model will be used to investigate the excitable pulse generation of HSL concentration due to the *las* subsystem. This chapter shows how this model will give important downstream consequences to the *rhl* subsystem, which affects rhamnolipid production. This chapter presents the published work "Pulse Generation in the Quorum Machinery of *Pseudomonas aeruginosa*".

Chapter 5 provides further analysis of the *las* system, including investigation on dynamical behaviour of the *las* system by changing model assumptions, also investigation on binding types of RsaL in the intergenic region that consist of competitive, uncompetitive, and non-competitive inhibition types. This chapter also explains detailed phase diagrams associated with each region in parameter space of bifurcation diagram that were derived from the bifurcation analysis on chapter 4. Furthermore, This chapter demonstrates the downstream impact of the *las* to *rhl* system.

Chapter 6 demonstrates two different models, one simple and one complex to study the expansion of bacterial colony. The simple model develops an introductory model in chapter 2 by considering motile behaviour, which will be used to investigate how the diffusion coefficient on motile cells and nutrient availability affect colony spreading. After introducing that simple model, this chapter develops the model by imposing the dynamical system of QS signal molecule production that has been explored in chapters 3 to 5. This complex model will be used to investigate the implications of excitable pulse generation of HSL concentration for colony cells, which lead to travelling waves and the production of rhamnolipid at the edge of colony.

Chapter 7 summarizes and discusses all of the results. Furthermore, it suggests how the findings from this research can be extended.

Chapter 2

A review of mathematical modelling of quorum sensing

2.1 Introduction

Pseudomonas aeruginosa is a Gram-negative opportunistic pathogen, well known for causing a variety of diseases such as wound infections, and lung infections in cystic fibrosis patients. *P. aeruginosa* has been used as an interesting research object because of the frequency with which it is involved in human disease, and can infect any part of the body, including the liver, brain, bones and sinuses. It is also known for its innate resistance to many antibiotics. It has efflux pump systems, which are responsible for transporting compounds, including toxic substances and antibiotics, from within cells into the external environment (Webber and Piddock, 2003). In addition, the bacteria's ability to form biofilms also makes the cells more resistant to antibiotics (Todar, 2015). Furthermore, several published works demonstrate quorum sensing (QS) as a communication mechanism between cells, which is used to coordinate the expression of virulence factors relevant to infectious diseases (De Kievit and Iglewski, 2000; Kong et al, 2006; Castillo-Juarez et al, 2015).

In this chapter, we review the mathematical models that have been constructed of the QS signalling system, especially the QS model by Dockery and Keener (2001). The modelling of QS signalling systems in *P. aeruginosa* has received significant attention from a large number of researchers. Moreover, in recent years, there have been a number of research articles focusing on the structure of QS systems. These model the signalling system by incorporating some factors or assumptions that have not been considered in the previous models in order to capture other interesting dynamical behaviours of the system. Van Delden and Iglewski (1998) published a biological research paper "Cell-to-cell signalling and *P. aeruginosa* infections" as the first paper that discusses the hierarchy of the QS signalling system on *P. aeruginosa*. In addition, James et al (2000) constructed the first mathematical model of the

QS signalling system in *Vibrio fischeri* and this has guided much of the subsequent work on QS systems in some Gram-negative bacterial species. Thus these two papers are most important for researchers who work on modelling the QS signalling system in *P. aeruginosa*.

2.2 Quorum sensing in *P. aeruginosa*

The QS signalling system of *Pseudomonas aeruginosa* has been studied intensively because it controls many important virulence genes. Van Delden and Iglewski (1998) demonstrated that around one third of the QS regulated genes in *P. aeruginosa* encode virulence factors. *P. aeruginosa* produces many extracellular products, including virulence factors that have been shown to be controlled by the signalling system.

In this organism, the QS signalling system is highly complex and regulated by two hierarchical LuxI/LuxR homologue circuits consisting of LasI/LasR and RhlI/RhlR (Miller and Bassler, 2001) and a separate PQS system. The QS system of *P. aeruginosa* is responsive to two chemically different signal molecules, based on Homoserine-Lactones (HSLs) and 4-quinilines (4Qs).

In this research, we only focus on Homoserine-Lactones (HSLs) since this is the main chemical signalling in *Pseudomonas aeruginosa* that regulates many activities of bacteria, including symbiosis, virulence factors, motility, production of antibiotics, and formation of biofilm. To simplify the model, we do not consider the production of the 4-quinilines (4Qs) chemical; sometimes referred to as the PQS system (Pesci et al, 1999; Dubern and Diggle, 2008).

The first QS system regulates expression of the elastase LasB, and is therefore named the *las* system. Enzyme elastase LasA and LasB are responsible for elastolytic activity, which destroys elastin-containing human lung tissue and causes pulmonary haemorrhages associated with *P. aeruginosa* infection (Galloway, 1991). The second QS system is able to control the production of rhamnolipid, and is therefore named the *rhl* system. Rhamnolipid is a biosurfactant product that also functions as a wetting agent and affects the motility of bacteria in colonies of *P. aeruginosa*. Rhamnolipids are particularly important in swarming motility in that they are postulated to lower the surface tension of the surface through their surfactant properties, allowing the bacterial colony to swarm (Glick et al, 2010). As a human pathogen, rhamnolipid has a glycolipid (detergent-like) structure; that serves to degrade lung surfactant and thus inhibits the function of the human respiratory system (Van Delden and Iglewski, 1998; Dockery and Keener, 2001).

Formation of HSL autoinducer 3O-C12 HSL and C4-HSL are catalyzed by LasI and RhlI, respectively. LasI is an autoinducer synthase and LuxI homologue that synthesizes 3O-C12-HSL, whereas LasR is a LuxR homologue and the transcriptional activator for 3O-
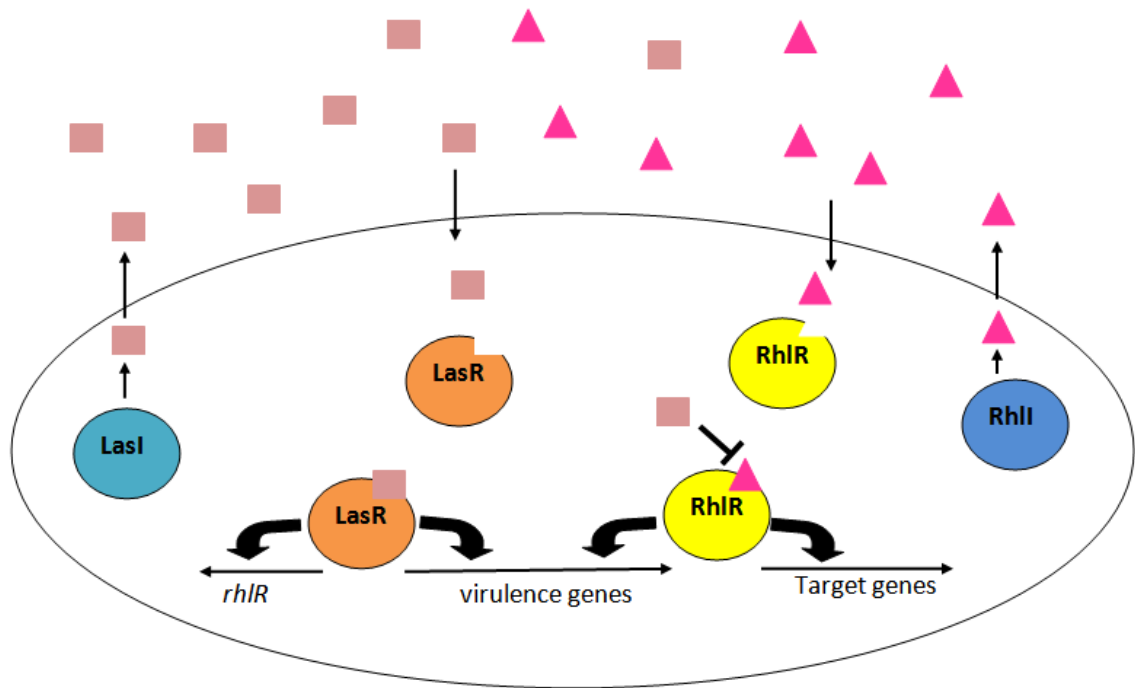
Figure 2.1: *las-rhl* signalling system in *Pseudomonas aeruginosa* consisting of LasI/LasR-RhlI/RhlR. Replotted and adapted (Miller and Bassler, 2001)

C12-HSL (Pesci et al, 1997). The LasR/3O-C12-HSL complex controls production of many virulence factors (Pearson et al, 1997; Davies et al, 1998; Pesci et al, 1999). In addition, the LasR/3O-C12-HSL complex binds to the *lasI* gene that allows an increase in autoinducer synthesize LasI, which in turn increases the concentration of 3O-C12-HSL binding to LasR (Seed et al, 1995). On the other side, the LasR/3O-C12-HSL complex also binds to the *rsaL* gene thus allowing an increase in transcriptional regulator RsaL, which represses expression of *lasI*. Consequently, it blocks transcription of the autoinducer synthesis LasI, which in turn decreases the concentration of 3O-C12-HSL binding to LasR (De Kievit et al, 1999).

In addition, RhlI is an autoinducer synthase that synthesizes C4-HSL, and RhlR is the transcriptional activator for C4-HSL (Van Delden and Iglewski, 1998). The main difference between the *las* and *rhl* systems is that the *las* system has the inhibitor (*rsaL*) in the inside of the system itself, regulating the production of the synthase and hence the autoinducer production.

It should be noted, however, that the *las* and *rhl* signalling system have their own specific autoinducers, and thus have no activating transcriptional activator protein in another system (see Fig. 2.1). For example, while 3O-C12-HSL activates *lasR*, it blocks the binding of
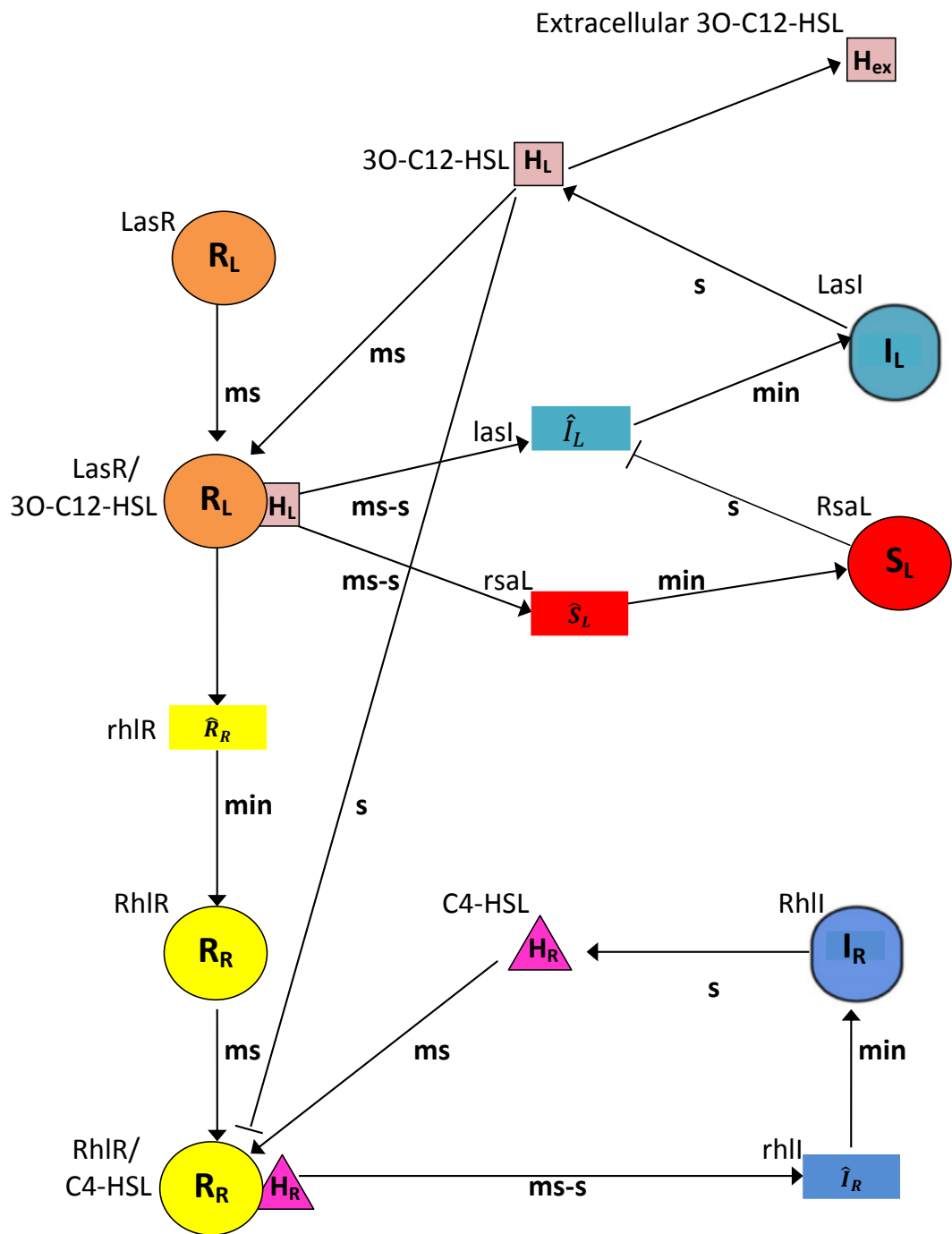
Figure 2.2: The quorum sensing signalling system in *Pseudomonas aeruginosa* is composed of *las* and *rhl* systems. Arrows and barred arrows indicate activating (positive) and inhibiting (negative) regulatory interactions, respectively. Shapes on the diagram depict autoregulation terminology. Letters associated with each arrow reflect the associated time scale (ms = millisecond, s = second, and min = minute). Replotted and adapted (Van Delden and Iglewski, 1998)

C4-HSL to its transcriptional activator *rhlR* (Pesci et al, 1997). Likewise, while C4-HSL activates *rhlR*, it is unable to activate *lasR* (Latifi et al, 1995; Pearson et al, 1997). The *las* system can therefore be considered to be above the *rhl* system through the activation of *rhl* by LasR/3O-C12-HSL (Pesci et al, 1997) (see Fig. 2.2). In other words, the *las* system controls the *rhl* system in a hierarchical signalling cascade (Latifi et al, 1996; Pesci et al, 1997).

2.3   A review of modelling techniques

Formal mathematical models of QS on *Pseudomonas aeruginosa* have been extensively studied by numerous scientists. One of the aims of this review is to create an awareness of the development of the mathematical modelling of QS in *P. aeruginosa* within the mathematical biology community. To provide a broad overview, we analyze the first paper that was written by Dockery and Keener (2001). After this, we investigate papers that cite Dockery and Keener (2001). There are 91 of 114 papers that cite Dockery and Keener (2001) until in the mid-2015, the time when we constructed our model. We analysed those papers before formulating our model, but have added 21 new papers during the last two years. Moreover, we also review some other papers out of those 114 papers, in order to get a better understanding of how the QS system in *P. aeruginosa* works and therefore make the mathematical model more realistic in terms of its biophysical aspects.

We classify papers that cite Dockery and Keener (2001) into four different categories, based on the subject of their research. Table 2.1 shows a timeline of research exploring the first formal mathematical model of QS in *P. aeruginosa*. Timeline items in green and brown correspond to aspect relevant to our research, namely papers covering biological and physical implications, respectively. Timeline items in purple are less related to our research focus, but there is a possibility that those papers might provide additional information for our research. Meanwhile, timeline items in red are unrelated to our research focus. We therefore focus on green timeline items to develop a mathematical model for quorum sensing in *P. aeruginosa*, using these to confirm that our model provides results that have not been published before. In addition, brown timeline items also have an important role in this research, since they present possible physical aspects of colony behaviour arising from the QS dynamic system. Together, these studies introduce a multiscale model for studying bacterial growth that incorporates the main role of QS schemes and their environment interaction.

Before starting the review, it should be mentioned that pure biological papers on the QS signalling system in *P. aeruginosa* have also progressed in the last decade. Some works, including the papers by Alon (2006); Rampioni et al (2007a,b) and Gloag et al (2015), will also be examined here to improve the model.

Table 2.1: Expansion work from first formal model of QS signalling system in *P. aeruginosa* (Papers that cite Dockery and Keener (2001)'s model), from 2001-2015. Green and brown are primary relevance sources to our research and cover biological and physical implications, respectively; purple for secondary relevance, and red for not-relevance sources to our research.

2001

1. Nilsson et al (2001) model how the concentration of AHLs inside bacterial cells and in a biofilm changes over time as a function of the population growth rate, and diffusion of AHLs.

2. First of Ward's series of papers on QS. Ward et al (2001) created a mathematical model that describes bacterial population growth and quorum sensing in a system.

2002

1. Koerber et al (2002) created a mathematical model of QS in *P. aeruginosa* in the early stage of the infection process.

2. Chopp et al (2002) introduced a mathematical model of QS in biofilm grow.

3. McMillen et al (2002) revealed the presence of synchronizing genetic relaxation oscillators by internal signalling.

4. Zhao et al (2002) developed models for the influence of inoculum size on the growth kinetics.

2003

1. Fagerlind et al (2003) demonstrated the role of regulators in the expression of QS in *P. aeruginosa*.

2. Second of Ward's series of papers on QS, Ward et al (2003).

3. Second of Chopp's series on QS in biofilm, Chopp et al (2002).

4. King et al (2003) modelled host tissue degradation by extracellular signal molecule.

5. Wolf and Arkin (2003) demonstrated motifs, modules, and games in bacteria.

2003

6. Stewart (2003) discussed the profound influence of the physics of the diffusion process in biofilm.

.

1. Viretta and Fussenegger (2004) introduced the QS regulatory network of *P. aeruginosa.*

2. Anguige et al (2004) showed how the complex hierarchy of the QS signalling system regulates the formation of biofilm differentiation.

2004

3. Third of Ward's series of paper on QS, Ward et al (2003).

4. Repressilators coupled by QS, Garcia-Ojalvo et al (2004).

.

1. Fagerlind et al (2005) developed a QS model using 3O-C12-HSL.

2. Goryachev et al (2005) constructed a stochastic model of "on-off" gene expression QS.

3. Simple spatial mathematical model on an early stage of biofilm, Anguige et al (2005).

4. Deterministic and stochastic model for QS by a single bacterium, Koerber et al (2005).

2005

5. Chen et al (2005) provided a general model and an analytic tool to examine the cooperative behaviour of a multicell system.

6. Gustafsson et al (2005) characterized the dynamics of the QS in *Staphylococcus aerus.*

7. P-system model of QS, Terrazas et al (2005).

8. Wang and Chen (2005) established a theoretical foundation and a quantitative basis for understanding the essential cooperative dynamics.

.

2006

1. Muller et al (2006) reveal the cell-cell communication by QS, including the regulatory network and its bistable behaviour.

2. Goryachev et al (2006) analysed the QS network.

3. Anguige et al (2006) developed a multi-phase model of a maturing *P. aeruginosa* biofilm.

4. A mechanistic P-system model of the *P. aeruginosa* QS model, Bianco et al (2006).

5. Keener (2006) presented a mathematical model for the growth of the flagellar motor of *Salmonella typhimurium*.

6. Gallegos et al (2006) analyzed the phenomenon of bacterial spreading.

7. Gheorghe (2006) demonstrate a new computational approach in the P-system.

8. Zhao et al (2006) show existence of QS in *Clostridium botulinum 56A*.

2007

1. Karlsson et al (2007) modelled the regulation of the competence-evoking QS.

2. In a series of studies, Frieden and Gatenby (2007); Gatenby and Frieden (2007) promoted application of IT to the study of living systems.

2008

1. Haseltine and Arnold (2008) investigated rewiring bacterial QS.

2. Khan et al (2008) presented mechanistic model of bacterial growth in heterogeneous media.

3. Zhang et al (2008) constructed a model competition between bacteria and the immune system.

4. Duddu et al (2008) developed computational techniques for understanding biofilm growth.

2009

1. Goryachev (2009) presented a system biology perspective on the structure of the QS regulatory network.

2. Navid et al (2009) showed three different approaches for modelling on microbial communities: rate equation, individual-based modelling, and population dynamics.

3. Janakiraman et al (2009) described QS and biofilm formation in microfluidic channels.

4. Tinsley et al (2009) demonstrated the spatiotemporal dynamics of QS on collective behaviour in groups.

5. Duddu et al (2009) constructed a two-dimensional biofilm growth model incorporating fluid flow and shear stress.

6. Alberghini et al (2009) demonstrated the consequences of relative cellular positioning on quorum sensing and bacterial cell-to-cell communication by applying equations governing the physical diffusion of the autoinducer molecules.

7. In a series of papers, Barbuti et al (2009,b) presented stochastic calculus looping sequences suitable to model cellular pathways.

8. Cogan and Chellam (2009) show incorporated pore blocking, cake filtration, and EPS production in a model for constant pressure bacterial fouling.

9. Zhang and Suo (2009) analyzed an epidemic model with a QS mechanism.

2010

1. Barbarossa et al (2010) created a delay model for quorum sensing of *Pseudomonas putida*.

2. Fekete et al (2010) explained the dynamic regulation of N-acyl-homoserine lactone production by combining microbial, chemical and mathematical approaches.

3. Jabbari et al (2010) modelled the agr operon in *Staphylococcus aureus*.

4. Brown (2010) modelled gene expression in the Gac/Rsm QS network.

5. Kepseu et al (2010) demonstrated the dynamics of the transition to phatogenicity in *Erwinia chrysanthemi*.

6. Klapper and Dockery (2010) described the microbial community in order to model some important aspects, including QS.

7. Jabbari et al (2010) used numerical and asymptotic techniques to examine the effects of inhibitor therapy on three putative phosphorylation cascades.

8. Carstea et al (2010) analysed a transcriptional modular network cascade.

9. Muller et al (2010) promoted *P. aeruginosa* PAO1 as a model of rhamnolipid production in a bioreactor system.

10. Russo and Slotine (2010) analysed the synchronization phenomenon in a QS network.

11. Tinsley et al (2010) demonstrated experimental studies of interacting excitable and oscillatory catalytic particles.

2010

.

1. Frederick et al (2011) modelled QS and EPS production in a growing biofilm.

2. Goryachev (2011) described the QS genes network and bacterial cell-cell communication.

3. Du et al (2011) constructed a multiscale model of *P. aeruginosa* swarming by combining a liquid thin film equation and convection-reaction-diffusion equations.

4. Automata modelling for QS, Abadal and Akyildiz (2011).

2011

.

2011

5. Barbuti et al (2011) presented a spatial structure in an extension of the calculus of looping sequences.

6. Cogan et al (2011) identified areas where the theory lags behind the experimental understanding : biofilm and infectious diseases.

.

1. Hense et al (2012) showed that the autoinducer regulator network generates spatially heterogeneus behaviour, especially under nutrient-controlled conditions.

2. Kepseu et al (2012) modelled the onset of virulence in pathogenic bacteria.

2012

3. Potapov et al (2012) demonstrated QS generated multistability and chaos in a synthetic genetic oscillator.

4. Du et al (2012) showed that high density waves of the bacterium *P. aeruginosa* in propagating swarms result in efficient colonization of surfaces.

5. Beckmann et al (2012) investigate QS in a digital organism.

.

1. Fujimoto and Sawai (2013) modelled group-level decisions (i.e. switch state as a group) in a cell population.

2. Muller and Uecker (2013) studied a dynamical model of QS in a diffusive medium.

3. Weber and Buceta (2013) presented the dynamics of QS switch.

2013

4. Hunter et al (2013) formulated and parameterized a novel mathematical model of *V. harveyi* and *V. cholerea*.

5. Metabolic model for QS in *P. aeruginosa*, Schaadt et al (2013).

6. Garca-Contreras et al (2013) reviewed the evidence that bacteria can evolve resistance to quorum-quenching compounds.

.

2013

7. Cogan (2013) explain concepts in the disinfection of bacterial populations.

8. Zhang et al (2013) introduced a general theory for integrated analysis of growth, gene, and protein expression in biofilm.

9. Brown (2013) connected molecular and population process in a mathematical model of QS, showing that many published models fail to satisfy physical constraints.

1. Langebrake et al (2014) investigated travelling waves in response to a diffusing QS in spatially extended bacterial colonies.

2. Trovato et al (2014) presented a quantitative analysis of Quorum vs diffusion sensing.

3. Uecke et al (2014) considered a model for N cells which communicate with each other via signalling with a background flow.

4. Horn and Lackner (2014) modelled a biofilm system, incorporating it by solving the Navier-Stokes equation for the liquid phase above the biofilm.

5. Abadal et al (2014) promoted signal amplification for molecular communication in nanonetworks.

2014

6. Agrawal et al (2014) demonstrated how a genetic ring oscillator network with QS feedback can operate as a robust logic gate.

7. Balco et al (2014) demonstrated the process of bacterial diffusion into the biopolymeric hydrogel core.

8. Hunter and Keener (2014) described the affinity of Qrr and its expression relative to the master transcriptional regulator.

9. A neoteric approach for designing a virulence regulation model, Jalihal et al (2014).

10. Scutera et al (2014) used a novel approach for the design and discovery of QS inhibitors.

2014

11. Liu et al (2014) demonstrated the sensitivity of parameters in the model of pH regulation of lactic acid production by *Lactobacillus bulgaricus*.

.

1. Emerenini et al (2015) constructed a mathematical medel of quorum sensing induced cell dispersal to control biofilm growth.

2. Zhonghua et al (2015) presented a stability and bifurcation analysis for a QS model of bacteria immunity.

3. Perez-Velazquez et al (2015) investigated QS regulation and its heterogeneity in Pseudomonas on leaves.

4. Wei et al (2015) analysed the social network dynamics and biofilm metrics.

5. Zhang et al (2015) formulated a delay model characterizing the competition between bacteria and the immune system.

2015

6. By controlling the dynamics of a bacterial cell-to-cell communication network, Lo et al (2015) presented a paradigm change in reducing bacterial phatogenesis.

7. Paton et al (2015) created a model of growth regulation in Mesophyll celd.

8. Jarrett et al (2015) created a model for human nasal carriage.

9. Li et al (2015) developed a mathematical model to describe the molecular diffusion.

10. Szabo (2015) demonstrated Oregonator generalization as a minimal model of quorum sensing in a Belousov-Zhabotinsky reaction with catalyst confinement in large populations of particles.

.

1. Mund et al (2016) analysed the dynamics of bacterial quorum sensing and its evolutionary stability under signal and enzyme production.

2016

.

2016

2. Barbarossa and Kuttler (2016) presented a simple system of delay differential equations for quorum sensing of *Pseudomonas putida* with one positive feedback plus one negative feedback mechanism.

3. Perez-Velazquez et al (2016) presented the progress of mathematical modelling of QS, both Gram-positive and Gram-negative bacteria (review paper).

4. Zhao et al (2016) developed a 3D hydrodynamic model to investigate the mechanism of antimicrobial persistence in heterogeneous multi-species biofilms.

5. Nikolaev and Sontag (2016) presented monotone dynamical systems theory on the synchronization of QS switches.

6. Quan et al (2016) examined how desynchronized QS leads to bimodality and patterned behaviour.

7. Bressloff (2016) analysed ultrasensitivity in a model of *Vibrio harveyi* quorum sensing.

8. Wei et al (2016) proposed a computational framework in the evaluation of the impacts of quorum sensing inhibition on strain competition.

9. Marenda et al (2016) demonstrated QS model system trade-offs between bacterial cell density and system extension from an open boundary.

.

2017

1. Bressloff (2017) provided a review of stochastic switching biology, genotype to phenotype.

.

We also investigate some theoretical biology papers that were published before Dockery and Keener (2001) constructed their model, including papers by Latifi et al (1995, 1996), Pearson et al (1997) and Pesci et al (1997) in order to track the biological theories that support the form of the model.

Latifi et al (1995) demonstrate that multiple homologues of LuxI and LuxR in *P. aeruginosa* control the expression of virulence. They show that the expression of elastase (an enzyme that breaks down protein) depends on the interaction between the transcriptional activator and autoinducer N-(3-oxododecanoyl)-HSL, which is directed by LasI. In the following year, Latifi et al (1996) showed that the QS signalling system in *P. aeruginosa* regulates many virulence factors in concert with cell density. They demonstrated that the LuxR homologues LasR and RhlR are activated by N-(3-oxododecanoyl)-HSL and N-butanoyl-HSL respectively. The *lasR* and *rhlR* are connected to the *luxI* homologues *lasI* and *rhlI*, which are responsible for synthesis of N-(3-oxododecanoyl)-HSL and N-butanoyl-HSL, denoted by 3O-C12-HSL and C4-HSL, respectively. In experimental work, Latifi et al (1996) also provide evidence that *rhlR* expression is regulated by LasR/3O-C12-HSL, and that RhlR/C4-HSL regulates *rhlI*.

In 1997, Pearson, Pesci, and Iglewski presented the roles of the *las* and *rhl* QS signalling system of *P. aeruginosa* in the control of elastase and rhamnolipid production (Pearson et al, 1997). Both *las* and *rhl* QS systems regulate the expression of virulence genes. They explained that the *las* system is composed of a transcriptional activator LasR, and synthase LasI, which direct the synthesis of the autoinducer N-(3-oxododecanoyl)-HSL. Then, LasR and the autoinducer are required for induction of *lasB* (encoding elastase) and other virulence genes. Meanwhile, the *rhl* system is composed of the transcriptional activators, RhlR and RhlI, which direct the synthesis of the autoinducer N-butanoyl-HSL. Rhamnolipid production requires *rhlAB* (encoding rhamnosyltransferase), which is controlled by the *rhl* system. They subsequently demonstrated the regulation of the *las* and *rhl* QS signalling system of *P. aeruginosa*, (Pesci et al, 1997). Through experimental data, they show that the *las* QS system controls the *rhl* system in two ways. First, LasR and N-(3-oxododecanoyl)-HSL activated *rhlR* transcription. Second, N-(3-oxododecanoyl)-HSL blocked N-butanoyl-HSL from binding to RhlR, inhibiting the expression of *rhlA*.

2.3.1 Models of the QS system

The mathematical modelling of QS started with James et al (2000). This paper explores the QS signalling system of the Gram-negative bacteria *Vibrio fischeri* and concentrated on the molecular mechanism. It focused on the regulatory system within a single cell considering intracellular and extracellular autoinducers. Their equation system results in two stable

states, which correspond to luminescent and non-luminescent phenotypes. The nonlinear ODE system has three steady states, two are stable and one is unstable which lead to a "on-off switch" behaviour of the regulation system. By using chemical kinetics on the model, James et al (2000) examined the production and loss of regulatory proteins and signal molecules.

In a simultaneous publication, Dockery and Keener (2001) introduced the first model of the QS signalling system in *Pseudomonas aeruginosa* and also concentrated on the molecular mechanism. As explained in the previous section, these bacteria have more complex signalling systems composed of two regulatory systems called the *las* and *rhl* systems. In Dockery and Keener (2001)'s paper, they focussed on the *las* system and presented it through an eight-dimensional ODE system (for the concentration of LasR, 3-oxo-C12-HSL, LasR/3-oxo-C12-HSL, LasI, RsaL, *lasR* mRNA, *lasI* mRNA, and *rsaL* mRNA) considering the expression of genes in a Michaelis-Menten type reaction. By applying different timescales for every reaction in the model, they simplified this ODE system to three equations (for the concentration of LasR, 3-oxo-C12-HSL, LasR/3-oxo-C12-HSL). The timescale for the LasR and LasI enzymes are longer than for *lasR* mRNA and *lasI* mRNA, respectively. Dockery and Keener (2001) demonstrate that the system has three steady solutions, with two stable states and one unstable state. The stable states depend on the parameters of the local density of bacterial cells, permitting the switch from a low level to a high level of autoinducer, and vice versa (bistability). Then, they added a spatial variable to get a more realistic model in a homogeneous environment.

Shortly after the first published paper on QS signalling, i.e. the model of *P. aeruginosa* by Dockery and Keener (2001), Ward et al (2001) constructed a mathematical model of the QS system parameterised against *P. aeruginosa*. Ward et al (2001)'s model concentrated on cell growth and signal molecule production rather than the biochemical mechanism of the QS regulatory network. By using a population dynamics approach, they focussed on the dynamics of the down-regulated and up-regulated populations. They also investigated switching behaviour with increasing autoinducer production, describing this by means of a three-dimensional ODE system (for concentration up-regulated cells, down-regulated-cells, and autoinducer), and analysed it numerically. They compared the system to experimental data, so this work was specifically designed to estimate the parameter values of the model. Their results suggested that the production of autoinducer in the up-regulated cells is much faster than in the down-regulated cells. Nilsson et al (2001)'s work, still related to the production of autoinducer, introduced a mathematical model that described the changes in the autoinducer concentration and investigated the impact on biofilm growth. They determined the concentration of autoinducer within the cell and in the biofilm medium

through two coupled ODEs, then they tracked the changes, and analysed the stability of the equilibrium system graphically. They showed that high concentrations of autoinducer within the bacterial cell are positively affected by a slow diffusion rate out of the cell and biofilm in the early stages of the growth rate. A mathematical model for growing *P. aeruginosa* biofilm coupled with a QS *las* systems was demonstrated by Chopp et al (2002) and extended in Chopp et al (2003). In addition, it was also extended by Ward et al (2003), who added the release and diffusion of QS molecules into their previous model, Ward et al (2001). They considered growth on the surface during biofilm formation that is affected by QS activity.

Based on Ward et al (2001)'s model, Koerber et al (2002) constructed a deterministic model of PDEs for the *las* system of *P. aeruginosa*. By adopting Ward et al (2001)'s work, they accounted for up-regulated and down-regulated populations and also utilised their parameter values, focussing on the role played by QS in wound infections. They investigated the evolution of autoinducer concentration and the fraction of up-regulated and down-regulated cells under various wound colonization situations.

In the following year, Fagerlind et al (2003) developed Dockery and Keener (2001)'s model, especially the way the *las* and *rhl* systems interact. Similar to Dockery and Keener (2001), they constructed a mathematical model for a single bacterium cell. They described the system as eight ODEs (for the concentration of LasR, RhlR, RsaL, 3O-C12-HSL, C4-HSL, LasR/3O-C12-HSL, and RhlR/C4-HSL). Fagerlind et al (2003) investigated the behaviour of the QS signalling system by examining the response of the LasR/3O-C12-HSL complex to the concentration of extracellular AHL as a bifurcation parameter. Their system has two steady states, controlled by the concentration of the autoinducer 3O-C12-HSL, which is regulated in turn by RsaL and Vfr. Then, they analysed the role of Vfr as a modulator and RsaL as an inhibitor.

Anguige et al (2004) developed a model of the QS system to investigate strategies to disrupt autoiducer interaction, and destroy its signal molecules. They constructed their model based on Ward et al (2001)'s model by assuming a spatially homogeneous population of cells. The model consisted of five ODEs. They investigated the model behaviour based on a standard antibiotic treatment and found that certain doses of the anti-QS agent decreased autoinducer concentration. After that, Anguige et al (2005) extended this work by including a well-mixed, spatially structured planktonic *P. aeruginosa*. These works were followed by a third paper by Anguige, Anguige et al (2006) that uses a multiphase approach to model biofilm formation of *P. aeruginosa*, which includes Extracellular Polysaccharides (EPS) production. By using numerical solutions, they explored the role of QS in EPS production. The results agree with experimental observation, which is that the concentration of LasR/autoinducer dimer affects EPS production.

Viretta and Fussenegger (2004) introduced a deterministic model of the QS regulatory network of *P. aeruginosa*, including the *las*, *rhl* and *pqs* systems. They focused on virulence factor production by *P. aeruginosa*. Their model described the dynamics of the QS signalling system as a set of qualitative states and transitions between these states. Their simulated dynamic QS network is in agreement with experimental results, and their model suggests that quorum sensing responds to pharmacological interference.

Fagerlind et al (2005) extended Fagerlind et al (2003) by including a QS molecule antagonist for 3O-C12-HSL, which is called a QS blocker. They introduced different affinity values with R-protein, and different rates of 3O-C12-HSL induced degradation of R-protein. Unlike QS, QS blockers bind, but do not activate LasR. They described their system using fourteen ODEs included QS blockers that form a new complex with LasR and RhlR, i.e a LasR/3O-C12-HSL antagonist and a RhlR/3O-C12-HSL antagonist. They adopted Fagerlind et al (2003)'s result to investigate the effect of adding QS blockers by considering high stable steady states and growing the colony until the cell population was enough to induce QS. Their model suggested that QS blockers have the ability to take this stable state down by inducing LasR degradation.

Goryachev et al (2005) constructed a stochastic model for an "on-off" gene expression switch in an *Agrobacterium* population. They formulated the model by considering mass-action rate laws to describe the chemical kinetics of the *Agrobacterium* QS network. Then, they reduced the dimensionality of the full QS network model to only two equations, for TraRd and an intracellular autoinducer. They solved these numerically and demonstrated that the quorum sensing switch needs a much higher threshold cell density in a liquid medium than in biofilm. Koerber et al (2005) developed both deterministic and stochastic models to describe the endosome escape process of *Staphylococcus aureus* in the case of a single bacterium. Since we know that QS controls virulence factors, *S. aureus* enters the cell and becomes up-regulated inside the endosome, leading to the destruction of the membrane.

Similar to the previous work, Goryachev et al (2006) considered a chemical kinetic approach based on the mass-action rate law to describe intracellular QS dynamics. They show that dimerization of the transcriptional factor, and the presence of the auxiliary positive feedback loop are the key factors in the "switch-like" behaviour of the regulatory network, which they relate to the QS model of *V. fischeri* by James et al (2000) and *P. aeruginosa* by Dockery and Keener (2001).

In the same year, 2006, Muller et al (2006) describe cell-cell communication by QS and constructed a model that consists of an equation describing autoinducer production involving a Hill-type function and another one describing cell growth. This model has bistability with the possibility of hysteresis. They analysed how autoinducer production depends on the

complex. Moreover, they examined how homoserine and homoserine-degrading enzymes interact by adding abiotic degradation and an AHL-degrading enzyme into the system. They also proposed a spatial single-cell model of QS. This model combined the ODE model with a PDE model in order to provide spatial structure. They assumed that there is no spatial structure within the cell. The dynamics are affected by the influx/efflux of AHL through the cell membrane. Activities related to the signalling substance outside the cell are described by a PDE, while they coupled ODEs and PDEs to describe the mixed boundary conditions at the cell surface.

Karlsson et al (2007) developed a non-linear model for the regulation of the competence-evoking QS in *Streptococcus pneumoniae*. Its QS system controls serotype switching, virulence factors, and antibiotic resistance. Then, Haseltine and Arnold (2008) investigated the *lux* circuit of *V. fischeri* and how QS operons in this bacteria affect bistability in the regulation of bacterial pathogens, i.e *Agrobacterium tumefaciens* as a plant pathogen and *P. aeruginosa* as a human pathogen. They therefore examined three different systems, including the factor that determines the threshold for bistable gene expression. They formulated the model so that the steady states were shown to be a function of the population density. They demonstrated how induction density affects how virulence can switch between "on" and "off".

Goryachev (2009) presented a review of the system biology perspectives on the structure of QS regulatory networks. He started with an explanation of what a quorum sensing network is, QS signal molecules, and their synthase systems. He also presented the core network of LuxR/LuxI in Gram-negative bacteria, which determine the switching between "on" and "off". Lastly, he examined the integration of QS into a global gene network.

The study of Fekete et al (2010) is another model of the QS mechanism. Through experimental work, they measured the autoinducer concentration at different phases of bacterial growth, and formulated one equation for the AHL net production by involving a Hill-type function and another equation for cell growth. Their model results in hysteresis. Similar to Muller et al (2006)'s model, they added abiotic degradation and an autoinducer-degrading enzyme that is regulated through an "on" and "off" switch. Based on Fekete et al (2010)'s model, Barbarossa et al (2010) investigated the autoinducer dynamics for a delayed model of QS *Pseudomonas putida*, including bifurcation and oscillation regimes that are presented by both positive and negative feedbacks. The model consists of bacterial (logistic) growth, autoinducer concentration, LuxR receptor protein, LuxR/autoinducer complex, and lactonase concentrations. Lactonase is metalloenzyme; it targets and inactivates autoinducer. By using experimental data, they estimated parameter values for growth and autoinducer concentration. They introduced a time delay for the activation of the lactonase and suggest

that bacteria activate and produce lactonase only after a certain time.

Jabbari et al (2010), meanwhile, model the QS mechanism of an opportunistic bacteria, *Staphylococcus aureus*. Unlike previously published models, which connect between autoinducer concentration threshold and quorum size or population density, they focused on the autoinducer concentration threshold needed to activate virulence. They show that the *agr* operon is the primary operon in the QS signalling system of *S. aureus*, and that it consists of two transcription units, with the receptor protein AgrC detecting the presence of signal molecules and then activating the response regulator protein AgrA. They then follow Dockery and Keener (2001) model methods, which formulate the ODE system describing the intracellular components of the full *agr* operon. The system consists of three layers, i.e the inside of the cell, the cell membrane and the outside of the cell. Initially, by using parameters from the literature, they present numerical simulations in order to get the overall dynamics. After that, they performed time-dependent asymptotic analysis in order to investigate reactions that dominate the behaviour of the system at several time points to understand how an up-regulated state is reached (i.e. how the bacterium becomes virulent), if sufficient signal molecules still remain in the environment of cells. As is typical of research on QS system modelling, they also observed bistability in the system.

By involving two QS systems of *P. aeruginosa*, Klapper and Dockery (2010) explored some aspects of biofilm models, which are QS, growth, and antimicrobial tolerance mechanisms. This model is followed by Frederick et al (2011)'s mathematical model for QS system and EPS production in biofilm growth. They analysed how QS-regulated EPS production affects biofilm. Their model consists of reaction-diffusion equations, and they solved it by numerical simulation. They suggest that biofilms that induce EPS production do not get the high cell populations of low-EPS-producing biofilms, but are able to rapidly increase their volume to high-EPS-producing. The biofilm switching behaviour from colonization to protection modes is regulated by QS that induces EPS production.

Goryachev (2011) described the QS network theoretically in more detail, introducing the integration of the QS network with the bacterial decision making, and explaining why bacteria need to communicate with others.

In 2013, by using both stochastic and deterministic approaches, Weber and Buceta (2013) showed that the transition of the QS switch is slower in respect to the critical autoinducer concentration. They analysed the response and dynamics at the single-cell level and compared them to the global response at the population level. In the same year, similar to Weber and Buceta (2013)'s work, Hunter et al (2013) used a deterministic approach to analyse the QS signalling system in *V. harveyi* and *V. cholerae*, which regulate the production of virulence factors and bioluminescence, respectively.

Muller and Uecker (2013) developed Muller et al (2006)'s work, they investigated N-bacterial cells that communicate via diffusive signalling substances. The dynamics in the inside and outside of the cell are described by ODE and linear diffusion equations, respectively. They started with the case of a single cell and showed that the dynamics of the system can be approximated by solutions of an ODE. Then, they introduced another technique for the solution of $N \geq 2$ cells (see Muller and Uecker (2013) for more detail). They investigated QS by examining 27 cells arranged in a cubic patterned colony, and determined the effect of distance between cells on activation of QS signals.

Schaadt et al (2013) constructed a regulatory model for QS in *P. aeruginosa*. Using a multi-level logical approach, they model the *las*, *rhl* and *pqs* systems to investigate how the formation of autoinducers and virulence factors is affected by inhibitors and receptor antagonists.

Langebrake et al (2014) modeled how the LuxR/LuxI circuit regulates QS behaviour. They investigated travelling waves in response to a wave of QS activation through a spatially extended bacterial colony, which is plausible. They also explore how the speed of a wave of QS activation is affected by both the autoinducer diffusion constant and the per capita AHL decay rate. Their work is related to Ward et al (2003)'s work. The difference between these works, however, is that Ward et al (2003) constructed a spatially extended QS system that incorporates biofilm production and demonstrated a wave propagation of up-regulation through the colony. They do not, however, show the existence of a travelling wave mathematically in their model, unlike Langebrake et al (2014)'s model. Langebrake et al (2014) demonstrated that the travelling wave speed of QS activation increases with the diffusion rate of QS signal molecules. Then, it decreases with the decay rate of QS signal molecules. Thus a travelling wave is no longer sustainable when the decay rate of QS is quite high.

Perez-Velazquez et al (2015) investigated factors that would affect QS across colonies, including water availability and diffusional losses of QS signalling molecules. Their experiment focused on *Pseudomonas syringae*, a Gram-negative bacterium that live on leaf surfaces. By using experimental data, they explored the heterogeneity of the QS activation of this bacterium. Their work suggested that QS activation is an indicator of diffusional limitation: i.e., when the diffusion of the autoinducer signal decreases, whether due to water availability or loss by diffusion, QS is increased.

Emerenini et al (2015) demonstrated QS induced biofilm detachment. Since QS is a communication mechanism that is used to coordinate gene expression and colony behaviour, it can also lead to cell dispersal. This process is an efficient mechanism for bacteria to control biofilm colony size. They also showed that bacterial dispersal affects the structure

and architecture of the biofilm colony.

Every time that we discuss a QS signalling model, it is inseparable from the bistability of the system due to positive and negative feedbacks loop. Zhonghua et al (2015) presented stability and bifurcations for a QS model of bacterial immunity. It is well known that QS coordinates gene expression among a local population. They model competition between bacteria and a host immune system, where signal molecules help survival against immune cells. They focused on investigating bifurcation phenomenon in the system, including a saddle-node, Hopf, homoclinic and Bogdanov-Takens bifurcations.

Mund et al (2016), meanwhile, analysed the dynamics of bacterial QS and its evolutionary stability under cooperation between signal and enzyme production by using an age-dependent colony model. Their model describes mutation rates, and switches between growth of planktonic and biofilm state. Their work showed that switching between growth in colonies and biofilms promotes the evolutionary stability of QS-regulated cooperation.

In another model of a QS signalling system, Barbarossa and Kuttler (2016) constructed a mathematical model of bacterial communication in continuous cultures. They presented a delay differential equation system of *Pseudomonas putida* QS, which consists of one positive and one negative (delayed) feedback mechanism. They investigated the qualitative behaviour of the system, including its stationary states and bistability. They also showed how sensitive the model is because of parameter values. For certain parameter values, the system presents stability switches with respect to the delay. Meanwhile, Hopf bifurcations could occur with respect to the negative feedback parameter value if the delay is set to zero. They fitted parameter values to experimental data in order to get a better understanding of biological observations that indicate a delay system.

From the review of papers that cite Dockery and Keener (2001)'s work, we should acknowledge that the modelling of QS regulation networks has developed significantly.

2.4 Main components of *P. aeruginosa* QS

2.4.1 *las* system

The *las* signalling system is composed of two main regulatory feedback loops, the LasI and RsaL loops. There are three main components of the LasI loop: LasI, autoinducer N-(3-oxododecanoyl)-HSL, and LasR. LasR operates as a transcriptional activator in the presence of N-(3-oxododecanoyl)-HSL. LasR would bind N-(3-oxododecanoyl)-HSL when critical cell density is reached, and this leads to a complex chemical form of LasR/3O-C12-HSL. Following this process, the complex chemical form of LasR/3O-C12-HSL would bind and activate the *lasI* genes creating a positive feedback for the LasI loop (Fagerlind et al,

2005). The transcription and translation process on *lasI* genes induces the production of autoinducer synthase protein LasI, which increases the amount of *N*-(3-oxododecanoyl)-HSL available to bind to LasR.

The RsaL loop is composed of RsaL, LasR/3O-C12-HSL complex, *lasI* genes and *rsaL* genes. As explained above, the LasR bound autoinducer becomes the LasR/3O-C12-HSL complex. This activates some virulence genes, including *lasI* and *rsaL* immediately. The RsaL transcriptional regulator, encoded by the *rsaL* gene, represses LasI expression by binding to the promoter of *lasI*, and thus RsaL negatively autoregulates by functioning in opposition to LasR and reduces *N*-(3-oxododecanoyl)-HSL signal molecule production by binding to the promotor *lasI*.

2.4.2 *rhl* system

The *rhl* system is another homologue of the Lux system. Most of the research about the QS signalling system of *P. aeruginosa* only focuses on the *las* system, consisting of the negative and positive feedback loops. The *rhl* system, however, has a similar pattern of positive feedback loop to the *las* system. Thus we can predict that the dynamics of the *rhl* system are mathematically analogous to the *las* system. The *rhl* system is composed of RhlR, RhlI, and autoinducer *N*-(butyryl)- HSL (Pesci et al, 1997).

The *rhlR* genes encode a transcriptional activator protein RhlR (Pearson et al, 1995; Latifi et al, 1995). RhlR would bind C4-HSL when critical cell density is reached, and this leads to a complex chemical form of RhlR/C4-HSL. Following this process, the complex chemical form of RhlR/C4-HSL would bind and activate the *rhlI* genes which induce the production of autoinducer synthase protein RhlI, thus increasing the amount of C4-HSL available to bind to RhlR.

Consequently, a number of *rhl* research articles concentrate on its role in bacterial behaviour rather than the underlying dynamic system. For example: the role of the *rhl* system in controling elastase and rhamnolipid biosynthesis genes (Pearson et al, 1997), in control of twitching motility (Glessner et al, 1999), in *rhlI* regulation (De Kievit et al, 2002), in proteome analysis of extracellular proteins (Nouwens et al, 2003), in secretion (Kong et al, 2009), infection and inflammation in rats (Nelson et al, 2009), and in cooperation and cheating in *P. aeruginosa* (Wilder et al, 2011).

Even though most research does not focus on the *rhl* system itself, Fagerlind et al (2003) developed the first QS modelling of *P. aeruginosa* that explicitly includes the *rhl* system. They investigate how the *las* and *rhl* systems, along with RsaL, interact to control quorum sensing in *P. aeruginosa*. Since they examined steady states for the whole system, their focus was not only on the *las* but also the *rhl* system. Their results indicated that the

whole system has two stable steady states: the system will suddenly switch from a low steady state to a high steady state when it reaches a specific threshold concentration of extracellular *N*-acyl-homoserine lactones. In terms of the dynamic system, if we focus on the *las* system only, we also find this same system behaviour as in Fagerlind et al (2003)s' work. It is, therefore, reasonable that most of researchers only focus on the *las* system for modelling purposes. In our case, we also focus on the dynamic *las* system only, although we will briefly explore the downstream impact on the *rhl* system in the next chapter. As a hierarchical QS signalling system, we consider *rhl* as a system that receives the impact of the behaviour of the *las* system.

2.5   Mathematical descriptions of *P. aeruginosa* QS

Mathematical models of QS in *Pseudomonas aeruginosa* have received a lot of attention. They provide the formalism to summarize current understanding, as well as the means to explore mechanisms and evaluate emergent solution behaviour. Here, we develop a model description, employing recent genomic information and bioinformatic techniques, and explore mechanisms for the generation of pulses and memory effects for downstream rhamnolipid production (in the next chapter).

Before we develop the published models of the QS system in *P. aeruginosa*, we begin with an investigation of the development of the equations for QS system modelling since Dockery and Keener (2001) published their work.

The LuxR/LuxI homologue is used by a variety Gram-negative bacteria to regulate QS signalling systems that correspond to the expression of certain genes (referred to as *lux* genes) in response to population density (Sitnikov et al, 1995). The modelling of QS system has been developed to investigate how the expression of these *lux* genes produces and responds to the QS signal molecule known as autoinducer or acylated homoserine lactones (AHL). The *luxR* gene encodes a regulator LuxR through transcription and translation, which binds AHL to form a complex of regulator/AHL (Sitnikov et al, 1995). Meanwhile, the *luxI* gene encodes a synthase for the autoinducer. Typically most of QS system modelling focuses on three to four coupled differential equations in order to capture the main components in the system. In order easily to recognize the differences between various model systems that have been published, we apply the same symbols to the variables used in all the analysed models (see table 2.2).

Table 2.2: Variables employed in the analysis of QS model.

Symbol	Type	Examples; adapted from Diggle et al (2008)
A	Autoinducer(AHL)	3O-C6-HSL in *V. fischeri*; 3O-C12-HSL, C4-HSL and C6-HSL in *P. aeruginosa*; C4-HSL and C6-HSL in *Aeromonas hydrophila*; 3O-C6-HSL in *E. carotovora*
R	Regulator	LuxR in *V. fischeri*; LasR, RhlR and QscR in *P. aeruginosa*; AhyR in *A. hydrophila*; ExpR and CarR in *E. carotovora*
C	Complex of regulator/AHL	LuxR/3O-C6-HSL in *V. fischeri*; LasR/3O-C12-HSL and RhlR/C4-HSL in *P. aeruginosa*; AhyR/C4-HSL in *A. hydrophila*; CarR/3O-C6-HSL in *E. carotovora*
I	Synthase	LuxI in *V. fischeri*; LasI and RhlI in *P. aeruginosa*; AhyI in *A. hydrophila*; CarI in *E. carotovora*

2.5.1 James et al (2000)'s model

The mathematical equation to describe the QS signalling process started with James et al (2000) who formulated the QS system on *Vibrio fischeri* into three coupled differential equations.

$$\frac{dA}{dt} = k_2 C - k_1 AR - nA + p\frac{fC}{1 + fC},\tag{2.1}$$

$$\frac{dR}{dt} = k_2 C - k_1 AR - bR + q\frac{fC}{1 + fC},\tag{2.2}$$

and

$$\frac{dC}{dt} = k_1 AR - k_2 C.\tag{2.3}$$

The equation for the rate of change of A and R have a similar form. Both A and R are used in the production of C at rate k_1. They also naturally degrade at rate n and b for A and R, respectively. Both A and R are produced by degradation of C at rate k_2, and by gene activity at rate p and q, respectively. Gene activity involves binding C to the "black box" that has a positive effect on the expression of A and R (Shadel and Baldwin, 1991; Sitnikov et al, 1995). They use $\frac{fC}{1+fC}$ to describe gene activity. Meanwhile, the differential equation for C explains how C is formed from the law of kinetic mass action at rate k_1 through association of R and A, and the natural degradation at rate k_2.

2.5.2 Dockery and Keener (2001)'s model

After James et al (2000) established the QS mathematical model, Dockery and Keener (2001) constructed a QS mathematical model for a different bacterial species, *P. aeruginosa*. The number of pair LuxI/LuxR homologues systems makes a difference between the QS signalling system of *P. aeruginosa* and that of *Vibrio fischeri*, i.e. two and one pair, respectively. Dockery and Keener (2001) only focused on the *las* system, which involves one pair of LuxI/LuxR homologues systems (LasI and LasR). At first, they derived an eight-dimensional ODE from the *las* system. Then, they reduced the system to become a three-dimensional ODE system which is similar to the one in James et al (2000)'s work. These three equations are:

$$\frac{dA}{dt} = k_2 C - k_1 AR - nA + p\frac{C}{K_L + C} + A_0, \tag{2.4}$$

$$\frac{dR}{dt} = k_2 C - k_1 AR - bR + q\frac{C}{K_R + C} + R_0, \tag{2.5}$$

and

$$\frac{dC}{dt} = k_1 AR - k_2 C. \tag{2.6}$$

Dockery and Keener (2001) demonstrated that both A and R are used in the production of C and naturally degrade. They also presented both A and R are produced by degradation of C and gene activity. Similar to James et al (2000)'s model, Dockery and Keener (2001) also consider Michaelis-Menten in the gene reaction, and specifically in *luxI* and *luxR* genes that denote encoding for LasI and LasR in the QS system of *P. aeruginosa*. The difference between James et al (2000) and Dockery and Keener (2001)'s models in terms of the Michaelis-Menten formula lies only in the value of the affinity constant between Complex of regulator/AHL and LuxI (K_L), or Complex of regulator/AHL and LuxR (K_R). In this case, the value of K_L and K_R (Dockery and Keener, 2001) is equal to $\frac{1}{f}$, where f denotes the affinity constant between Complex of regulator/AHL and LuxI or LuxR in James et al (2000)'s model. Thus, basically, they use the same formula of Michaelis-Menten. The difference in the values of the affinity constant might be due to the different types of QS signal molecules in their model, *V. fischeri* and *P. aeruginosa* for James et al (2000) and Dockery and Keener (2001), respectively. Furthermore, Dockery and Keener (2001) add basal production with small value, A_0 and R_0, to both the differential equations for A and R, whereas basal production does not exist in James et al (2000)'s model. Meanwhile, there is no difference in the differential equation of C between the two models, in that they both use the law of kinetic mass action to describe the formation of C.

2.5.3 Fagerlind et al (2003)'s model

Fagerlind et al (2003) developed a mathematical model of the hierarchical quorum sensing in *P. aeruginosa*. They investigate how the *las* and *rhl* system, along with RsaL and Vfr, interact to control quorum sensing in *P. aeruginosa*. Their model is similar to Dockery and Keener (2001)'s model, with the difference lying in the form of the differential equation for RsaL. Fagerlind et al (2003) consider the inhibition process by RsaL in the *las* system, thus the governing equations become:

$$\frac{dA}{dt} = k_2 C - k_1 A R - nA + p\frac{C}{K_L\left(1 + \frac{S}{K_{SL}}\right) + C} + A_0, \tag{2.7}$$

$$\frac{dR}{dt} = k_2 C - k_1 A R - bR + q\frac{C}{K_R + C} + R_0, \tag{2.8}$$

and

$$\frac{dC}{dt} = k_1 A R - k_2 C. \tag{2.9}$$

They demonstrated that the production of autoinducer 3O-C12-HSL is positively affected by the LasR/3O-C12-HSL complex. On the other hand, it is also negatively influenced by RsaL. In Fagerlind et al (2003)'s model, RsaL acts as a competitive inhibitor, and therefore they improved the Michaelis-Menten formula in Dockery and Keener (2001)'s model. They apply a competitive inhibition formula to the autoinducer 3O-C12-HSL equation. RsaL binds promotor *lasI* in order to inhibit activation of *lasI* genes by the LasR/3O-C12-HSL complex, which reduces the production of autoinducer 3O-C12-HSL. S represents the concentration of RsaL and K_{SL} determines the affinity between RsaL and *lasI*.

2.5.4 Fagerlind et al (2005)'s model

After Fagerlind et al (2003) developed Dockery and Keener (2001)'s model, Fagerlind et al (2005) extended Fagerlind et al (2003)'s model by introducing a QS molecule antagonist into the system, referred to as QS blockers (QSB), which are assumed to diffuse through the cell membrane and bind to both LasR and RhlR. They developed a system of ordinary differential equations by adding a differential equation for N-(3-oxododecanoyl)-HSL antagonist (A_A), that includes LasR/3O-C12-HSL antagonist complex (C'),

$$\frac{dA}{dt} = k_2 C - k_1 A R - nA + p\frac{C}{K_L\left(1 + \frac{S}{K_{SL}}\right) + C} + A_0, \tag{2.10}$$

$$\frac{dR}{dt} = k_2 C - k_1 A R - bR - k_3 A_A R + dC' + q\frac{C}{K_R + C} + R_0, \tag{2.11}$$

$$\frac{dC}{dt} = k_1 A R - k_2 C, \tag{2.12}$$

and

$$\frac{dA_A}{dt} = k_4 C' - k_3 A_A R - n_A A_A, \tag{2.13}$$

$$\frac{dC'}{dt} = k_3 A_A R - dC' - k_5 C'. \tag{2.14}$$

Their model suggests that QSBs affect the degradation of LasR. We will not consider this factor in our model, however, since we only focus on the dynamic main structure of the *las* system.

2.5.5 Goryachev (2009)'s model

Goryachev (2009) presented a QS model by giving a systems biology perspective on the system of regulatory networks that control QS. According to the network, he described the rate of R and autoinducer HSL change as follows:

$$\frac{dR}{dt} = k_7 r - bR - k_1 AR + k_2 C, \tag{2.15}$$

$$\frac{dA}{dt} = k_5 I - k_1 AR + k_2 C + k_6 (A_e - A_i). \tag{2.16}$$

The equation for the rate of R change is composed of four terms that represent mRNA translation, protein degradation, formation of complex C, and its dissociation, respectively. Meanwhile, the last term on the rate of autoinducer HSL change represent passive diffusion between intra and extracellular QS signal molecules. He then developed stochastic model on the system to explore the transition of QS switching, although this is beyond the scope of our research.

Biochemical theories of regulatory networks of the QS system in *P. aeruginosa* have continuously evolved since the publication of the first model in 2001. Biochemical evidence established that LasR exists as a dimer in solution, with each monomer liganded by a single HSL (*N*-(3-oxododecanoyl)-HSL) molecule (Rampioni et al, 2007a). This evidence supports higher multimers upon DNA binding (Schuster and Greenberg, 2006). The biochemical evidence is therefore consistent with a Hill number much higher than one. On the other hand, De Kievit et al (2002) presented that the RsaL transcriptional repressor is a helix-turn-helix protein that binds the promotor of *lasI*. De Kievit et al (1999)'s finding also supported that of Rampioni et al (2007a) that the RsaL transcriptional repressor exists as a monomer in the cell, which leads to a Hill number of one. Rampioni et al (2007b) demonstrated that RsaL binds simultaneously with LasR to *rsaL-lasI* bidirectional promotor, thereby preventing the LasR-dependent activation of both genes; *N*-(3-oxododecanoyl)-HSL production continues to increase throughout growth. To the best of our knowledge, however, this biochemical

evidence has not been included in the published model on the QS signalling system of *P. aeruginosa.*

2.6 Parameter values

Generally, most studies of quorum sensing signalling systems have been based on empirical approaches, and only a few studies have taken advantage of theoretical guidance to identify the key parameters that are essential for cell-cell communication based on gene expression. Bacterial communication that may involve multiple regulatory circuits makes it difficult to predict and determine which parameters will be key to the system. By relying solely on experimental approaches, therefore, cell-cell communication models are intractable due to the complexity of this system. Thus mathematical modelling approaches try to identify key parameters and further the understanding of the system.

Although there are many mathematical models that demonstrate quorum sensing signalling system, however, only a few of these published works try to employ experimental data in the model. Most mathematical modelling studies employ arbitrary parameter values for modelling purposes only in order to capture the interesting behaviour of dynamic systems. In addition, not all of the parameter values are easy to find from experimental work. This means that researchers who work in mathematical modelling have to estimate some parameter values, or take parameter values from another species with particular reasons or assumptions.

The first model of QS system in *V. fischeri* by James et al (2000), for example, employed arbitrary parameter values for modelling purposes. James et al (2000) investigated the change in the concentration of AHL, R-regulator, and R-regulator/AHL complex when exposed to different concentrations of extracellular AHL. The model predicted that the QS system in *V. fischeri* has two stable steady states. Not only James et al (2000), but Dockery and Keener (2001) also determine parameter values based on modelling purposes. Dockery and Keener (2001) focused on the production and diffusion between intracellular and extracellular of AHL. They demonstrated that the QS system exhibited hysteresis in its switching behaviour between two stable steady states. We can see a comparison of parameter values by James et al (2000) and Dockery and Keener (2001) model in the table 2.3.

Meanwhile, Ward et al (2001) focused on the effect on the population growth of rapid increases of AHL concentration. Ward et al (2001) employ experimental data for their parameter values, but these data are more focussed on the relation between concentration of QS signal molecules and population growth rather than biochemical interaction within the QS system. A similar modelling approach by Nilsson et al (2001) also explored the temporal

Table 2.3: Comparison of the parameter values for QS system modelling used by James et al (2000), Dockery and Keener (2001) and Fagerlind et al (2005).

Par	Description	James et al (2000)	Dockery and Keener (2001)	Fagerlind et al (2005)
k_1	Rate constant of binding reaction between AHL and regulator	20 $l^3 m^{-1} t^{-1}$	1	0.16 $\mu M^{-1} s^{-1}$
k_2	Rate constant of dissociation reaction between AHL and regulator	10 t^{-1}	1	0.25 s^{-1}
n	Diffusion constant of AHL through the cell membrane	10 t^{-1}	0.02	0.12 s^{-1}
b	Degradation constant of regulator	3 t^{-1}	0.7	0.15 s^{-1}
p	The maximum rate at which AHL is produced	30 $ml^{-3} t^{-1}$	2	1 $\mu M s^{-1}$
q	The maximum rate at which R-regulator is produced	5 $ml^{-3} t^{-1}$	2	0.7 $\mu M s^{-1}$

Note: Dockery and Keener (2001) did not put units on their parameters and determined the values only for modelling purposes. Thus, they actually cannot be compared to the other parameter values in other references. However, in the context of the model they can be used as preliminary values for QS modelling to investigate behaviour.

changes of AHL concentration as cell density increased. Thus Nilsson et al (2001) also only focused on the rates of three parameters (population growth, AHL diffusion, and AHL autoinduction). Unlike Ward et al (2001) however, Nilsson et al (2001) employ arbitrary values of parameters for modelling purposes only.

In addition, Anguige et al (2004) developed a model of the Las system in *P. aeruginosa*. This model was a based on the QS model by Dockery and Keener (2001). In contrast to Dockery and Keener (2001), however, in which population density was set by a fixed parameter value, Anguige et al (2004) assumed logistic growth of the *P. aeruginosa* population, similar to the approach adopted by Ward et al (2001) and Nilsson et al (2001). Basically, Anguige et al (2004) try to adapt the assumptions and approaches of the published work by Dockery and Keener (2001), Ward et al (2001) and Nilsson et al (2001). The QS model by Anguige et al (2004) demonstrated the existence of hysteretic switching between two stable steady states in the QS system of *P. aeruginosa*, one with low and another one with high concentrations of AHL. Although they adopt existing parameters from the published work, most of the parameter values are the same as those in Dockery and Keener (2001), moreover, the assumed ratio of up- and down-regulated AHL production rates is close to

the experimentally-verified parameter values in Ward et al (2001).

Table 2.4: Comparison of the parameter values used for QS system modelling by Alon (2006), and Wei et al (2016).

Par	Description	Alon (2006)	Wei et al (2016)
k_1	Rate constant of binding reaction between AHL and regulator	$nM^{-1}min^{-1}$ (ratio $\frac{k_2}{k_1} = 1000 - 2000nM$)	$0.1 \ s^{-1}$
k_2	Rate constant of dissociation reaction between AHL and regulator	min^{-1} (ratio $\frac{k_2}{k_1} = 1000 - 2000nM$)	$0.1 \ s^{-1}$
n	Diffusion constant of AHL through the cell membrane	0-10000 min^{-1}	$0.0001 \ s^{-1}$
b	Degradation constant of regulator	$0.01 \ min^{-1}$	$0.0001 \ s^{-1}$
p	The maximum rate at which AHL is produced	1 nM min^{-1} (estimate)	$0.002 \ s^{-1}$
q	The maximum rate at which R-regulator is produced	1 nM min^{-1} (estimate)	$0.002 \ s^{-1}$

Fagerlind et al (2005) also developed a model of the QS system in *P. aeruginosa*. They tested several hundreds of different parameter values and these consistently give the same results. Most of the parameter values used in their model system have not been experimentally generated. Principally, Fagerlind et al (2005)'s model extended Fagerlind et al (2003)'s model by introducing different affinity values between LasR and AHL. Thus most parameter values are adopted from Fagerlind et al (2003) in order to match the work on the steady state concentration of AHL that was done in 2003.

The parameters in Fagerlind et al (2005) have been subsequently adopted in other later papers on *P. aeruginosa* modelling. These parameters (see table 2.3 column 3) were compared to biological estimates (see table 2.4) and were found to be significantly different, for example Alon (2006); Melke et al (2010) and the recent article by Wei et al (2016). The parameters used in Fagerlind et al (2005) suggest that the typical lifetime of a transcription factor is of the order of seconds. Biological estimates, however, typically describe transcription factors as stable proteins with a lifetime of the same order as the cellular turnover time, i.e. hours for *P. aeruginosa*. We therefore decided that most of our parameter values should be adopted from the systems biology book by Alon (2006). These parameter values are not significantly different to those used in the paper published by Wei et al (2016), which were in turn adopted from experimental results by Melke et al (2010) (see table 2.4).

2.7 Results and discussion

The theoretical and experimental understanding of bacterial communication has made remarkable progress on QS modelling. By reviewing and discussing the development of models of QS signalling systems of *P. aeruginosa*, we identify some important factors that have not been involved in the previous models. Moreover, by using new findings from biochemical theory, we can develop and refine the previous models.

First, Dockery and Keener (2001) model focused on activity regulatory networks and the production of signalling molecules. The transcription process at the *lasI* promoter site is activated by the LasR/3O-C12-HSL complex (R_{LH}). The production process is assumed to follow a Hill form with a Hill number p. Recent biochemical evidence strongly suggests a Hill number > 1 in contrast to the arguments of Dockery and Keener (2001). Furthermore,the activated form of lasR is at least dimeric (Schuster and Greenberg, 2006) and it is possible that it forms a tetramer on the DNA.

Second, in the QS signalling system of *P. aeruginosa* it is very clear that the transcriptional repressor RsaL inhibits the activation of LasI, which causes a decrease in the downstream production of N-(3-oxododecanoyl)-HSL. This process has been involved in the QS models constructed by Dockery and Keener (2001) and Fagerlind et al (2005). In 2007, Rampioni et al (2007b) demonstrated that the RsaL transcriptional repressor bind to the *lasI-rsaL* intergenic region. The transcription of both genes is promoted and regulated via binding of the two proteins to the same intergenic region between the *lasI* and *rsaL* operons, hence the functional form for the transcription is identical, with the exception of the numerical values of the transcription and loss rates. Note that this implies a negative feedback relation between the RsaL protein and its own production, which has not been historically represented in graphical depictions of the *las* system, although it is strongly implied by the analysis of Rampioni et al (2007a). From these biological findings, we can add a "repressor-line" from RsaL transcriptional repressor to *rsal* genes.

Third, biochemically there is insufficient evidence to determine whether the binding in the intergenic region results in competitive, uncompetitive or non-competitive binding of other systems, or indeed whether there is a symmetry in the expression rates in each direction with all configurations of binding at the intergenic region. Thus we will analyse those possibilities in our model.

Fourth, in terms of the parameter values that have been discussed above, it is mentioned in James et al (2000)'s and Dockery and Keener (2001)'s work that they apply arbitrary parameter values for modelling purposes. Meanwhile, the parameter values in Fagerlind et al (2005) are significantly different to the biological estimates and have not been experimentally investigated.

These four findings will therefore be incorporated into the model we construct in the next chapter.

Chapter 3

A simple model of non-motile bacterial interactions

3.1 Introduction

The aim of this chapter is to establish a rational description that can be used to explain simple biological interactions between up-regulated and down-regulated bacteria. Furthermore, we wish to explore a colony-level quorum switch as the colony expands.

Here, we investigate colony growth with a mathematical model that is affected by nutrient concentration and signal molecule production. The process of quorum sensing is regulated by the production and monitoring of a chemical signal molecule that increases in concentration as a function of cell density (Miller and Bassler, 2001; Ward et al, 2001). Cells produce, detect, and release low-molecular-mass signal molecules called autoinducers, or recently quormon (Daniels et al, 2004; Long et al, 2009). However, Goryachev et al (2005) suggest that most of the signal molecules are lost to the environment by diffusion.

After the full non-linear equations are solved using numerical techniques, we define new variables to make analytical progress. The new variables are ratios between the amount of biomass of each kind of bacteria, up-regulated and down-regulated, over the total biomass.

Finally, we investigate the effect of constant diffusion of quorum sensing signal molecules on the bacterial colony growth. In this model, we do not consider quorum sensing for a specific species. However, we employ data on the colony growth and QS signal molecule production of a Gram-negative plant pathogen, *Erwinia carotovora*, as an example.

3.2 Up-regulated and down-regulated bacteria

In this chapter, general biological interactions are investigated. In particular, we explore bacterial growth, transition process of bacteria to another type of bacteria, and signal molecules

production (see Fig. 3.1).
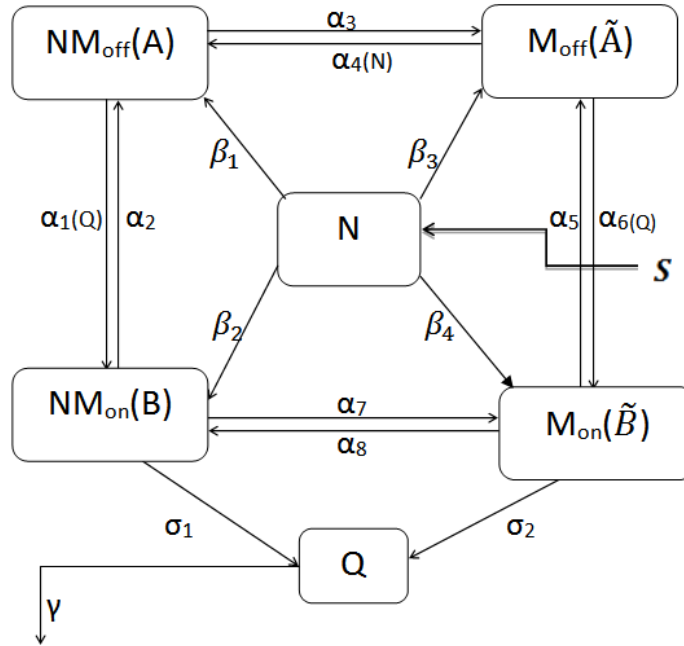
Figure 3.1: A flow diagram to describe the biological interactions between different types of bacteria (NM_{off}, NM_{on}, M_{off}, and M_{on}) that involve three processes: growth, transition, and signal molecule production. The growth of bacteria is affected by nutrient concentration, N, which gets S as nutrient source. β_i, $i = 1, ..., 4$ associated with each *arrow* reflect the associated growth rate for different types of bacteria. NM = non-motile bacteria, M = motile bacteria, then "off" and "on" subscript represent down-regulated and up-regulated bacteria. α_i, $i = 1, ..., 8$ associated with each *arrow* reflect the associated transition rate between different types of bacteria. The quorum sensing signal molecules, Q, are produced by the up-regulated bacteria at constant rate σ_i, $i = 1, 2$. These molecules are degraded and diffused from the system at rate γ.

In the biological terminology of production of gene products by organisms, up-regulation and down-regulation are the processes by which a cell increases and decreases the quantity of protein, respectively (Shankaran et al, 2007). Bacterial cells are able to receive and process signal molecules from the outside through their cell walls, which they do by receptor located in the cell membrane. Once a signal molecule binds to a receptor, it effectively activates a regulatory protein that then binds to specific DNA and results in a quorum dependent protein (Miller and Bassler, 2001). Thus bacterial cells that respond to chemical signal molecules depend on the existence of a receptor tuned to the message. Receptors are created and expressed by a cell's DNA. When receptors are increased or deceased significantly they are termed up-regulated or down-regulated, respectively.

In this chapter, we employ the up-regulation and down-regulation terminology, but we try to simplify the language for our basic model. Bacterial cells produce signal molecules and release the signal molecules to the environment. The concentration of signal molecules in the environment affects how many receptors are tuned to the signal molecules. Based on the production rate of signal molecules, we differentiate bacterial cells between two types: up-regulated and down-regulated bacteria, which produce signal molecules with high and low-rates, respectively.

In the next chapter, we also take into account interactions between non-motile and motile bacterial cells. Motile cells are able to move actively to access nutrient by using their flagella, unlike non-motile cells.

3.2.1 Model construction of interacting non-motile bacteria

The following non-spatial model gives specialized attention to nutrient acquisition and QS signal molecule production on non-motile bacterial colonies and involves four dependent variables: N for the concentration of nutrients, A for biomass of down-regulated bacteria with quorum sensing circuits switched off (off-QS), B for biomass of up-regulated bacteria with quorum sensing circuits switched on (on-QS), and Q for the concentration of signal molecules. Nutrient acquisition influences the growth and activities of the bacterial colony. The model is summarized in the schematic in Fig. 3.2.
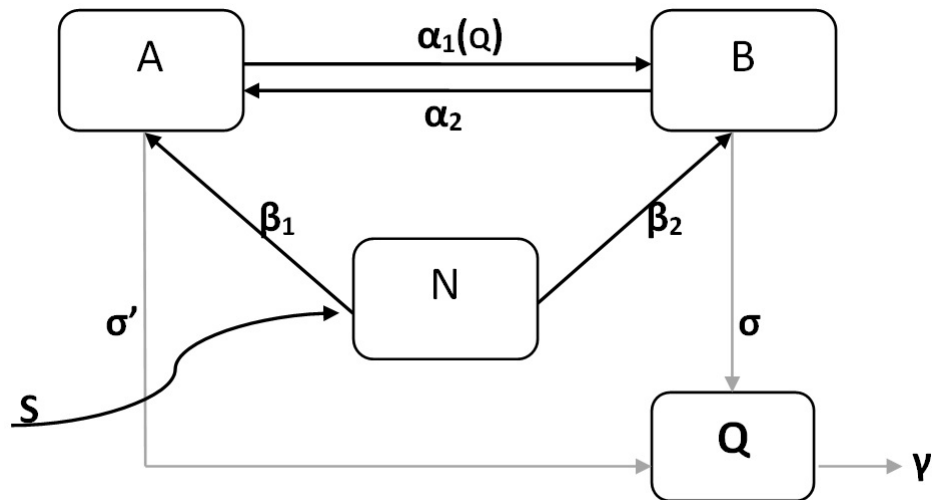
Figure 3.2: A flow diagram to describe the biological interaction on non-motile bacteria that involve three processes: growth, transition, and signal molecule production

The biomass of non-motile bacteria with off-QS (A) is formed via the law of mass action at growth rate β_1. It is increased and decreased through the transition process of non-motile bacteria with on-QS (B) to off-QS (A) and vice versa, at rate α_2 and α_1, respectively. Thus

(a)

(b)

(c)
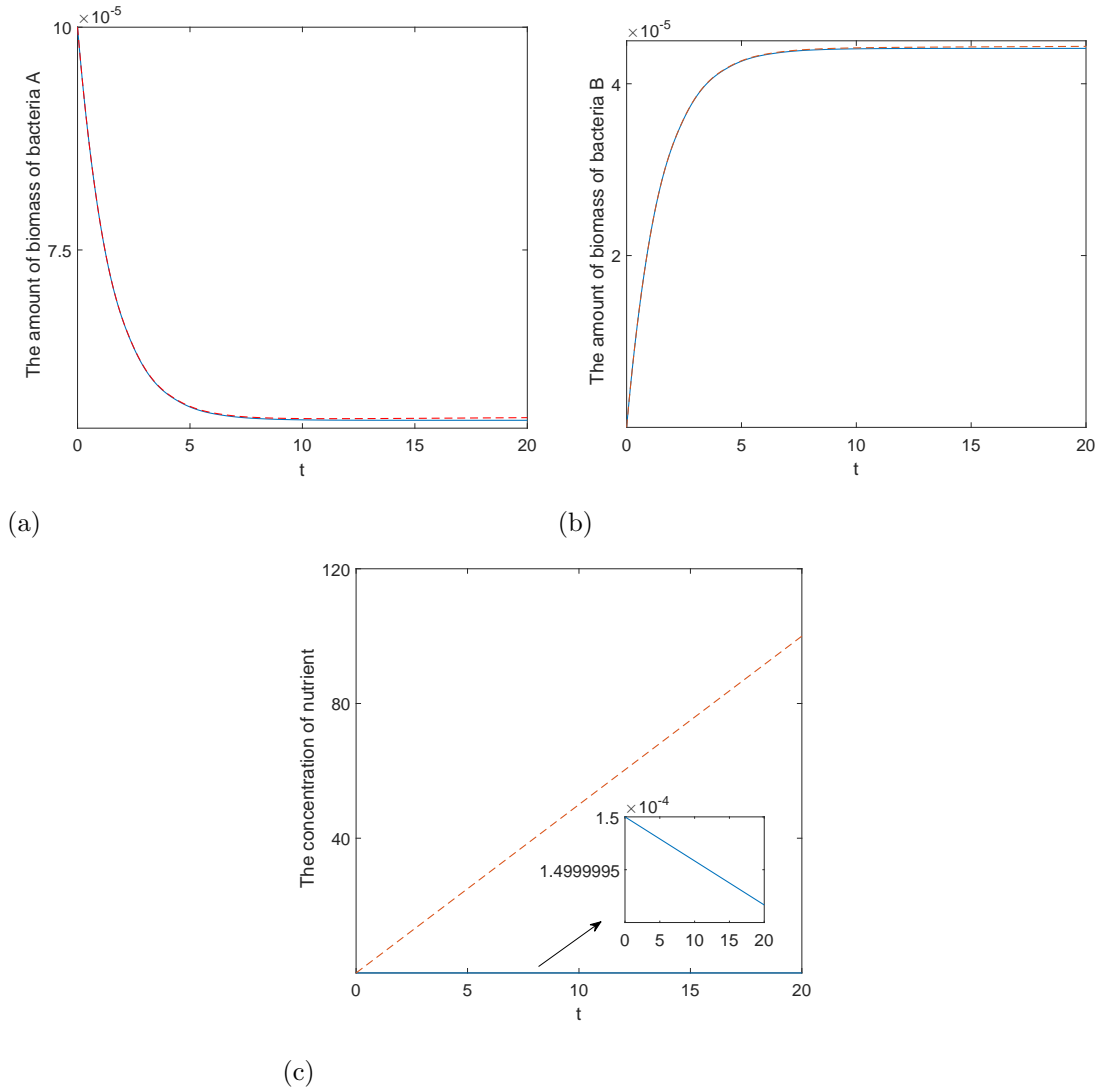
Figure 3.3: Numerical solutions of equations (3.1) to (3.3) of (a) bacteria A, (b) bacteria B, and (c) nutrient. Blue-dashed and red-solid lines depict the solution for the system when $S \neq 0$ (with a nutrient source) and $S = 0$ (without a nutrient source), respectively. Here, $\alpha_1 = 0.3$ s^{-1} and all other parameters are given in Table. 3.1

the biomass of bacteria (A) can be modelled as

$$\frac{dA}{dt} = \frac{\beta_1 NA}{K+N} + \alpha_2 B - \alpha_1 A. \tag{3.1}$$

In a similar manner, we formulate an equation for the biomass of non-motile bacteria with on-QS (B) at bacterial growth rate β_2 are modelled such that

$$\frac{dB}{dt} = \frac{\beta_2 NB}{K+N} + \alpha_1 A - \alpha_2 B. \tag{3.2}$$

For simplicity down-regulated and up-regulated are assumed to have the same growth rate, $\beta_1 = \beta_2$. In general α_1 and α_2 depend on Q, the concentration of QS signal molecules. However, initially we will assume that they are constants.

It is clear that nutrient in the suspension is consumed by both off-QS and on-QS bacteria. The rate of change of nutrient, N, can be written as

$$\frac{dN}{dt} = S - \frac{\beta_1 NA}{K+N} - \frac{\beta_2 NB}{K+N} \tag{3.3}$$

where S is a nutrient source term.

As the solutions of the system that are illustrated in Fig. 3.3, we consider the effect of nutrient source on the system. We shall compare the solution for the two cases if $S \neq 0$ and $S = 0$. If $S = 0$, the amount of biomass of bacteria A and B increases gradually. Furthermore, if $S \neq 0$ the increase is slightly greater (see Fig. 3.3a and Fig. 3.3b). Nutrient is one of the essential factors that affects bacterial growth (Van Der Tol and Scholten, 1997; Su et al, 2012) as indicated in Fig. 3.3a and Fig. 3.3b (see refs Bowden and Li (1997); Mata et al (2012)). If the system has no source of nutrients ($S = 0$), the concentration of nutrients will deplete to zero. Conversely, it will not reach zero when there is a source of nutrients ($S \neq 0$), (see Fig. 3.3c).

3.2.2 Ratios and dynamics of bacterial biomass

To make analytical progress, we define new variables

$$x = \frac{A}{A+B} \qquad \text{and} \qquad y = \frac{B}{A+B}. \tag{3.4}$$

Here, x is the ratio between the amount of biomass of off-QS bacteria and the total biomass, and y is the ratio between the amount of biomass of on-QS bacteria and the total biomass. Hence, $x + y = 1$, and substituting into equations (3.1) and (3.2) yields

$$\begin{aligned}
\frac{dx}{dt} &= \frac{d}{dt}\left(\frac{A}{A+B}\right) \\
&= \frac{1}{(A+B)^2}\left[\frac{dA}{dt}B - \frac{dB}{dt}A\right] \\
&= \frac{1}{(A+B)^2}\left[B(\frac{\beta_1 NA}{K+N} + \alpha_2 B - \alpha_1 A) - A(\frac{\beta_2 NB}{K+N} + \alpha_1 A - \alpha_2 B)\right] \\
&= \left(\frac{\beta_1 N}{K+N}\right)xy + \alpha_2 y^2 - \alpha_1 xy - \left(\frac{\beta_2 N}{K+N}\right)xy - \alpha_1 x^2 + \alpha_2 xy,
\end{aligned}$$

(3.5)

and

$$\begin{aligned}
\frac{dy}{dt} &= \frac{d}{dt}\left(\frac{B}{A+B}\right) \\
&= \frac{1}{(A+B)^2}\left[\frac{dB}{dt}A - \frac{dA}{dt}B\right] \\
&= \frac{1}{(A+B)^2}\left[A(\frac{\beta_2 NB}{K+N} + \alpha_1 A - \alpha_2 B) - B(\frac{\beta_1 NA}{K+N} + \alpha_2 B - \alpha_1 A)\right] \\
&= \left(\frac{\beta_2 N}{K+N}\right)xy + \alpha_1 x^2 - \alpha_2 xy - \left(\frac{\beta_1 N}{K+N}\right)xy - \alpha_2 y^2 + \alpha_1 xy.
\end{aligned}$$

(3.6)

From the above differential equation system (Eq. 3.5 and 3.6), we get the solution in Fig. 3.4. The amount of x decreases to a certain value, and the amount of y increases up to a particular level.
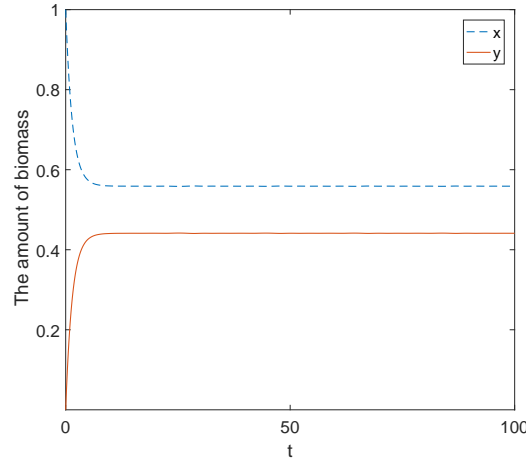
Figure 3.4: The solution of equation system that describes the fraction of biomass, x and y. Here, $\beta_1 = \beta_2 = 0.023$, α_1 and α_2 are considered constant, such that $\alpha_1 = 0.023$, and $\alpha_2 = 0.046$.

Let τ be the total amount of biomass of bacteria, such that

$$\tau = A + B.$$

(3.7)

For the sake of simplicity, here we shall assume the shape of the culture is a cylindrical slab (see Fig. 3.5). Thus the total amount of biomass of bacteria (τ) is proportional to the volume

of culture $\left(\pi r^2 h\right)$. We also assume the increase of bacterial cells leads to the proportional growth of colony radius and nutrient is accessible to the colony. All new growth of bacterial cells is immediately transferred to the colony edge, while the death of bacterial cells results in decrease in the cell density locally. Consequently, we can justify that the entire area of the culture is occupied by nutrient source (S). In relation to these assumptions, the nutrient source (S) is not only proportional to the radius of culture (r), but also to the square root of total amount of biomass $(\tau^{1/2})$. Therefore, if the radius of bacterial colony is assumed to increase linearly with time, the increase rate of total biomass is

$$\frac{d\tau}{dt} = C\tau^{1/2}, \tag{3.8}$$

where C is a constant.

$V = \pi r^2 h$, and $V \propto A + B$

$S \propto r$.

Thus

$r^2 \propto A + B$
$r \propto (A + B)^{1/2} \rightarrow S \propto \tau^{1/2}$
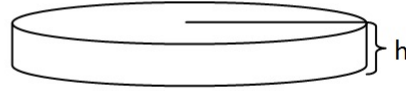
Figure 3.5: Illustration of a simplified model of a cylindrical bacterial culture that is allowed to spread radially. A, B and S represent the biomass of non-motile bacteria with off-QS, the biomass of non-motile bacteria with on-QS, and source of nutrient, respectively. V, r and h symbolize volume, radius and height of culture, respectively. "See text for detail explanation".

We assume that there is a supply of nutrients $S\left(\tau\right)$, a function that depends on the total number of bacteria. Hence, we write

$$\begin{aligned}
\frac{dN}{dt} &= S(\tau) - \frac{\beta N}{K + N}\tau \\
&= f(S(\tau), N, \tau),
\end{aligned} \tag{3.9}$$

and see Fig. 3.6 as the simulation result.

3.2.3 Modelling quorum sensing

In our mathematical model (Fig. 3.2), we assume both bacteria A and B produce QS signal molecule with constant rates σ' and σ with $\sigma' \ll \sigma$. The signal molecules produced may be lost from the system due to diffusion. Thus the concentration of QS signal molecules
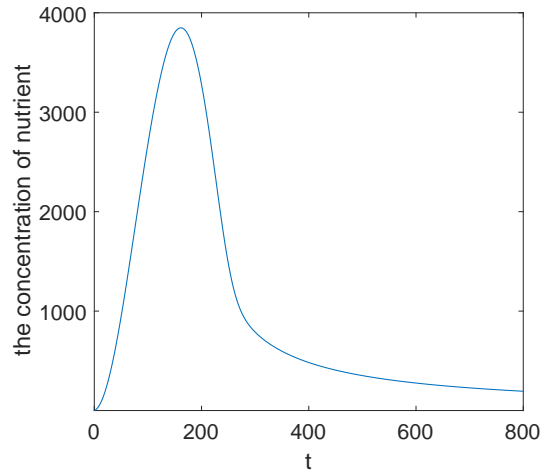
Figure 3.6: The concentration of nutrient plotted as a function of time. Here $\beta = 0.023$.

changes as

$$\frac{dQ}{dt} = \sigma' A + \sigma B - \gamma Q, \qquad (3.10)$$

where γ represents the rate of loss of signal molecules via both degradation and diffusion from the system.

As with x and y, a more tractable variable is the amount of signal molecules per bacterium, q, defined as

$$q = \frac{Q}{A + B}. \qquad (3.11)$$

The amount of signal molecules influences the transition rate α_1 between off-QS and on-QS bacteria. Thus α_1 represents a function of the amount of signal molecules, which can be written in the base mathematical model $\alpha_1(Q)$. Associated with the amount of biomass and the concentration of signal molecules per bacterium, α_1 is described as transition rate, such that $\alpha_1(q)$. Following Langebrake et al (2014), the transition rate from off-QS to on-QS bacteria can be approximately modelled with a Hill function of the form $\alpha_1(q) = C_0 + (C_1 - C_0) \frac{q^n}{\kappa^n + q^n}$, providing control over the location of the transition (Frank, 2013). Thus there are three phases in the transition process. This is consistent with evidence from molecular biology for both *Vibrio fischeri* and the related QS system, suggesting that the signal molecule binds as a ligand to the DNA, which promotes the operon that produces more QS molecules (James et al, 2000).

The four parameters of the Hill equation are C_0, C_1, κ and n. The Hill function coefficient n determines the shape; the value of the Hill coefficient $n > 1$ describes positively cooperative binding. For this case, we also consider the tangent hyperbolic function as a suitable replacement for the Hill function in order to obtain analytic solutions for the bifurcation points. It can describe the transition process properly, and is defined by $\alpha_1 = C_0 + (C_1 - C_0) \tanh(\kappa (q - q_0))$, where κ is a constant that determines the slope tran-
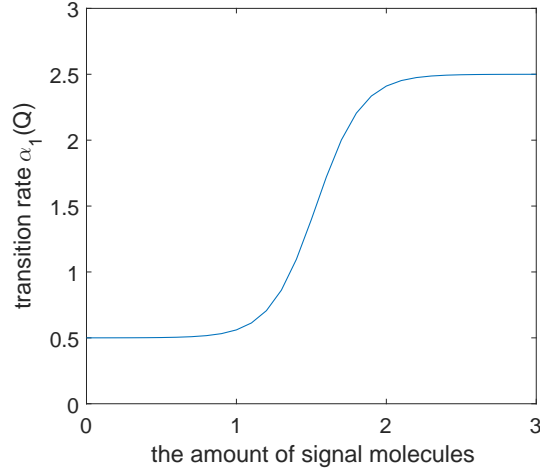
Figure 3.7: Transition process rate affected by the amount of signal molecules. Here, $C_0 = 1.52$, $C_1 = 2.52$, $\kappa = 3.265$ and $q_0 = 1.53$.

sition rate from off-QS to on-QS bacteria, replacing the Hill function coefficient (n). This function also allows control over the location of transition (see Fig. 3.7). Thus the amount of signal molecules to switch between the phases varies with the particular parameter of the transition rate, α_1. Meanwhile, we assume that the transition rate from on-QS to off-QS, α_2, is a constant.

Moreover, the signal molecule production rate per bacterium is

$$
\begin{aligned}
\frac{dq}{dt} &= \frac{d}{dt}\left(\frac{Q}{A+B}\right) \\
&= \frac{(A+B)\frac{dQ}{dt} - \left(\frac{dA}{dt} + \frac{dB}{dt}\right)Q}{(A+B)^2} \\
&= \frac{dQ/dt}{(A+B)} - \frac{S(\tau)Q}{(A+B)^2} \\
&= \sigma'x + \sigma y - \gamma q - \frac{S(\tau)q}{A+B} \\
&= \sigma'(1-y) + \sigma y - q\left(\gamma + \frac{S(\tau)}{\tau}\right) \\
&= \sigma'(1-y) + \sigma y - q\left(\gamma + \frac{\delta\tau^{1/2}}{\tau}\right).
\end{aligned}
\tag{3.12}
$$

If we assume that $\gamma' := \gamma + \delta\tau^{-\frac{1}{2}}$ changes at a slower rate than the other processes, then we can think of γ' as a control parameter. Hence,

$$
\frac{dq}{dt} = \sigma'(1-y) + \sigma y - q\gamma'.
\tag{3.13}
$$

Here γ' represents an effective rate of loss of the QS molecules, which decreases slowly over a long time scale as the colony grows. By applying the assumption that the bacterial colonies to have the same growth rate for both types $(\beta_1 = \beta_2)$, we can construct the relation between

signal molecules and biomass of bacteria, which can be described by the pair of equations,

$$\frac{dy}{dt} = \alpha_1(1-y) - \alpha_2 y,$$

(3.14)

$$\frac{dq}{dt} = \sigma'(1-y) + \sigma y - q\gamma'.$$

It is reasonable to assume that the production of QS molecule is much faster than cell growth, thus $\frac{dq}{dt}$ tends to 0 relative quickly. If the value of γ' is considered as a constant, we obtain that the amount of signal molecule q in proportion to y, such that,

$$q = \frac{\sigma'(1-y) + \sigma y}{\gamma'}.$$

(3.15)

As $\sigma' \ll \sigma$, we may substitute $q \approx \frac{\sigma y}{\gamma'}$ into $\frac{dy}{dt}$, so that it becomes

$$\frac{dy}{dt} = \left(C_0 + (C_1 - C_0)\tanh\left(\kappa\left(\frac{\sigma y}{\gamma'} - q_0\right)\right)\right)(1-y) - \alpha_2 y,$$

(3.16)

where κ represents the slope of the transition rate.

3.2.4 Analysis of fixed points

Fixed points (steady states) are points at which time derivatives vanish (Edelstein, 2005). For the current system, steady states correspond to a constant fraction of up-regulated bacteria within the system, even though the amount of up-regulated bacteria may continue to increase or decrease.

The steady states are given by the solution of $\frac{dy}{dt} = 0$. To assist graphical analysis we write the equation for the steady state of 3.16 as

$$C_0 + (C_1 - C_0)\tanh\left(\kappa\left(\frac{\sigma y}{\gamma'} - q_0\right)\right) = \frac{\alpha_2 y}{1-y}.$$

(3.17)

The right-hand term is a curve with asymptote at $y = 1$, and the left-hand term represents a hyperbolic function.

The curves have three intersection points that can be seen in Fig. 3.8. As explained before, transition processes between off-QS and on-QS bacteria are typically modelled with Hill functions. If we had used a Hill function instead we would need $n \geq 3$ in order to get bifurcation phenomenon related with an "on-off" switch. Instead, we use the tangent hyperbolic function to allow for a relatively simple analytic solution.

3.2.5 Bifurcation analysis

Varying the values of parameters in the model modifies the qualitative structure of the flow and controls the fold bifurcation appearance (Medved, 1992). A saddle-node bifurcation occurs when the gradients of the two sides of 3.17 match, such that

$$\kappa\frac{\sigma}{\gamma'}\left(1 - \tanh^2\left(\kappa\left(y\frac{\sigma}{\gamma'} - q_0\right)\right)\right) = \frac{1}{C_1 - C_0}\frac{\alpha_2}{(1-y)^2}.$$

(3.18)
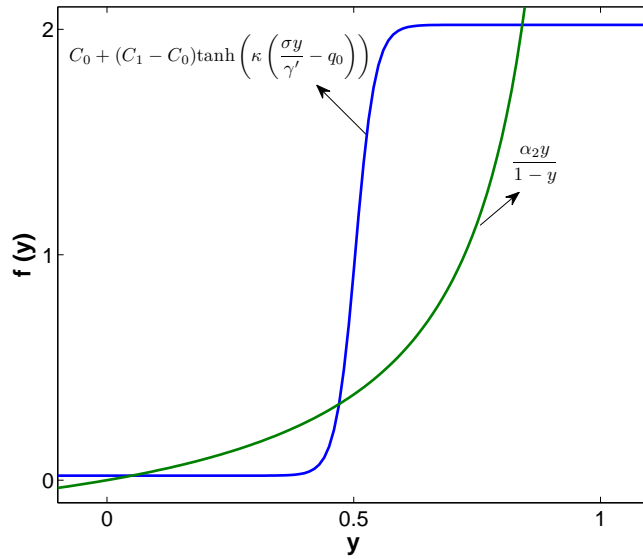
(a)
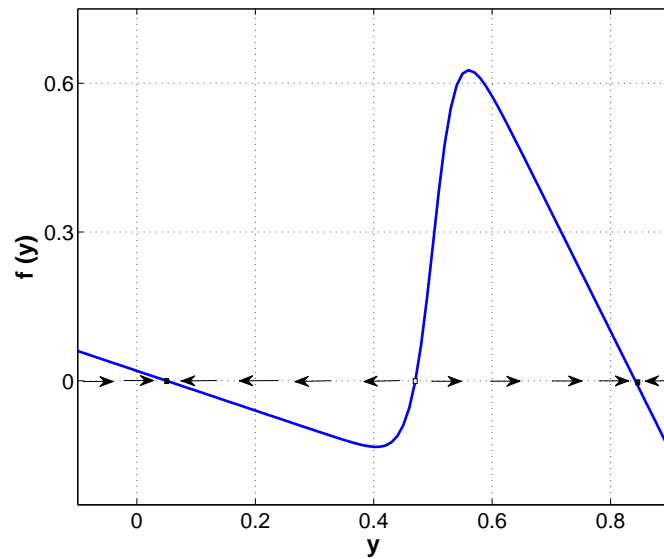
(b)

Figure 3.8: Three solutions are found in figure (a) as the intersections of curve $\alpha_2 y/(1-y)$ and curve $C_0 + (C_1 - C_0)\tanh(\kappa(\sigma y/\gamma' - q_0))$. The slope of the curve at the intersection determines the stability of fixed points. (b) The stability of fixed points of $f(y)$. Here, $C_0 = 1.02$, $C_1 = 2.02$, $\sigma = 7.72 \times 10^{-6}$, $\alpha_2 = 0.38$, $\gamma' = 4.86 \times 10^{-5}$, and $\kappa = 40$.
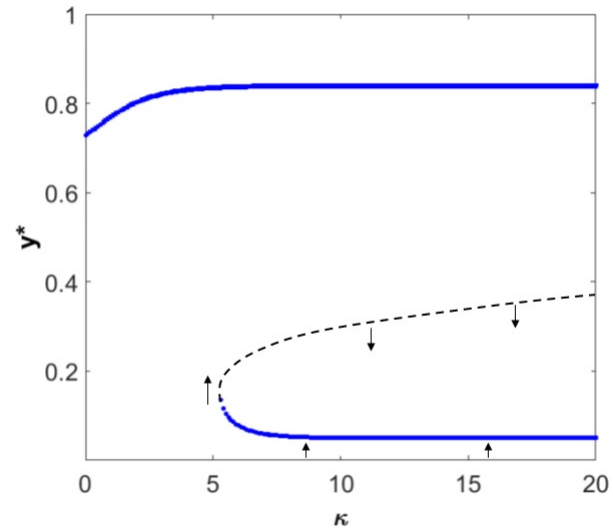
(a)
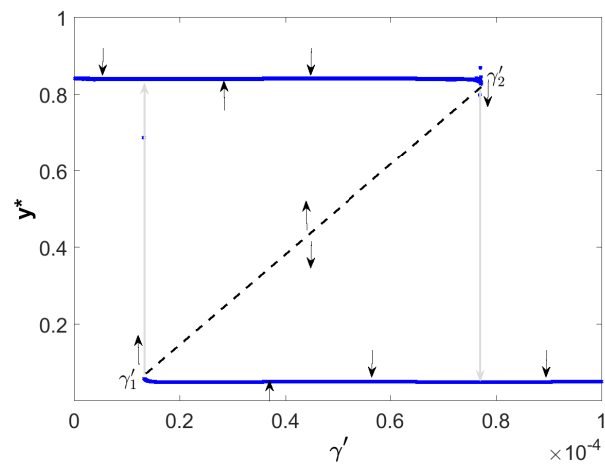
(b)

Figure 3.9: Bifurcation diagrams. The arrows indicate the direction of change from the unstable states to stable states. The stable states are represented by solid lines on the upper and lower branches, while unstable states are represented by a dashed line in the middle section. (a) κ as bifurcation parameter and $\gamma' = 4.86 \times 10^{-5}$. (b) γ' as bifurcation parameter and $\kappa = 40$. Other parameter values are $C_0 = 1.02$, $C_1 = 2.02$, $\sigma = 7.72 \times 10^{-6}$, and $\alpha_2 = 0.38$.

Substituting (3.17) into (3.18) yields

$$\frac{\kappa\sigma}{\alpha_2\gamma'}\left((C_1-C_0)(1-y)^2-\frac{\alpha_2^2y^2}{C_1-C_0}+\frac{2\alpha_2C_0y(1-y)}{C_1-C_0}-\frac{C_0^2(1-y)^2}{C_1-C_0}\right)=1. \qquad (3.19)$$

It is clear that $\frac{\kappa\sigma}{\alpha_2\gamma'}\neq 0$, thus

$$\alpha_2=\frac{(2C_0y-C_0)\pm\sqrt{(C_0-2C_0y)^2+(y-y^2)\left(8C_1C_0-4C_1^2\right)}}{-2y}. \qquad (3.20)$$

Furthermore, we can write 3.17 in the form

$$\kappa=\frac{\gamma'}{\sigma y-\gamma'q_0}\text{arctanh}\left(\frac{\alpha_2y-C_0+C_0y}{(C_1-C_0)(1-y)}\right). \qquad (3.21)$$

Substituting (3.20) into (3.21) gives

$$\kappa=\frac{\gamma'}{\sigma y-\gamma'q_0}\times$$
$$\text{arctanh}\left(\frac{-C_0\pm\sqrt{(C_0-2C_0y)^2+y\left(8C_1C_0-4C_1^2\right)-y\left(8C_1C_0-4C_1^2\right)^2}}{2(C_1-C_0)(1-y)}\right). \qquad (3.22)$$

By using the same way the calculation of bifurcation, we can get bifurcation diagram with γ' as bifurcation parameter. Substituting $\alpha_2(y)$ into 3.17 yields

$$\gamma'=\frac{\sigma\kappa y}{\left(\kappa q_0+\text{arctanh}\left(\frac{-C_0\pm\sqrt{(C_0-2C_0y)^2+y\left(8C_1C_0-4C_1^2\right)-y\left(8C_1C_0-4C_1^2\right)^2}}{2(C_1-C_0)(1-y)}\right)\right)}. \qquad (3.23)$$

The multiple steady states due to variation of parameter values affect bifurcation occurrence (Strogatz, 2000). This can be easily seen by analyzing the steady state in the system for some values of parameter. Two stable steady states coexist and are separated by an unstable region (Murray, 1989).

The parameter κ affects the stability of the system as it determines the shifted slope of the transition rate from off-QS to on-QS bacteria. If κ has small positive values, there is only one point of intersection. However, above a certain positive value of κ, there are three intersection points: associated with two stable and one unstable steady state. The bifurcation diagram (Fig. 3.9a) shows that with κ as bifurcation parameter the system has only one bifurcation point a fold bifurcation. For certain high positive values of κ, the gradient of the transition curve will only change slightly as we employ a hyperbolic function ($tanh$) that determines the slope of transition. There is almost no change in the steady states for large values of κ. As a consequence, there is no collision of the high and intermediate steady states. They will never meet for the large κ.

Fig. 3.9b explains that if γ' is very large, then the stable points of the fractional up-regulated bacteria are very low, corresponding to the "off" state. As γ' is decreased, we move through the bistable region until γ' reaches γ'_1 and y^* shifts discontinuously to the higher

state. Such shifting induces a higher production of QS signal molecules that corresponds to the "on" state. Conversely, when γ' increases to γ_2', y^* shifts discontinuously to the lower state, which results in a lower production of QS signal molecules that corresponds to the "off" state.

3.2.6 Estimation of parameters

The model parameters represent rates of the bacterial interactions involving cell growth, signal molecule production and diffusion, and cell transition. Values for several parameters, including β_1, β_2, σ and γ', were taken from experimental data, related to previous work (Byers et al, 2002). Other parameter values, α_1 and α_2 can be inferred from the model to investigate bifurcation phenomena.

(a) (b)
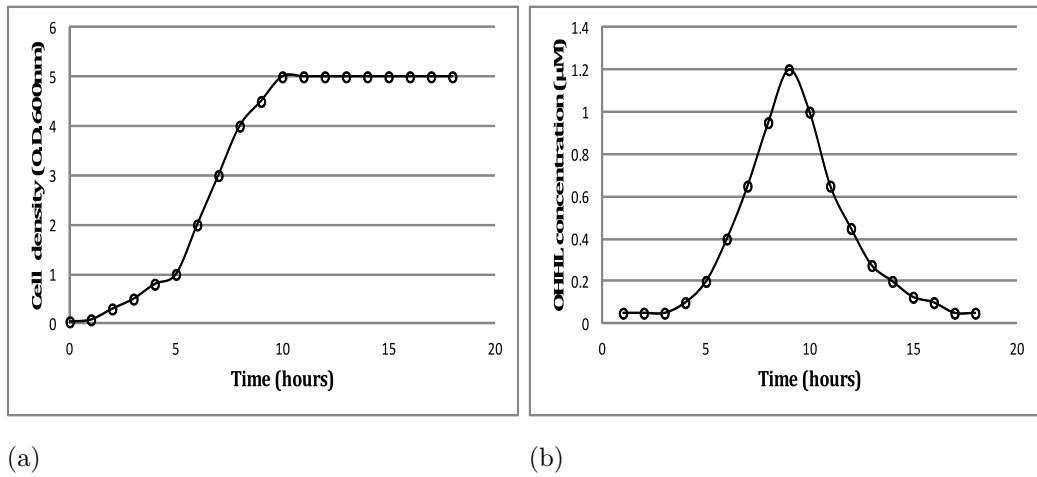
Figure 3.10: (a) bacterial growth and (b) signal molecule (OHHL) concentration, as obtained from experiment on *E. carotovora*. Replotted from data in Byers et al (2002), pp 1165.

The value of bacterial growth rate (based on assumption that β_1 and β_2 have similar values) is obtained from the rate of change cell density in exponential phase. The value of γ is calculated based on the decay phase of signal molecules concentration, where we assume that there is no signal molecule production during the decay phase. From the mathematical model in the previous section, we have assumed that the rate-of-change of bacteria cells is determined by growth rate (β_1) and amount of bacteria (B), such that $B = B_0 e^{\beta_1 t}$ where B_0 represents initial amount of bacteria. Thus, the differential equation for signal molecules Q becomes

$$\frac{dQ}{dt} = \sigma B_0 e^{\beta_1 t} - \gamma Q, \tag{3.24}$$

and we have an equation for Q that can be used to obtain the value of the signal molecule production rate (σ), which is

$$Q = \frac{\sigma}{\beta_1 + \gamma} B_0 e^{\beta_1 t} + C e^{-\gamma t}. \tag{3.25}$$

Table 3.1: Parameter estimates for simple model of non-motile bacterial interactions.

Name	Value	Unit	Description	Ref
β_1	2.78×10^{-4}	s^{-1}	growth rate of bacteria off-QS	Byers et al (2002)
β_2	2.78×10^{-4}	s^{-1}	growth rate of bacteria on-QS	Byers et al (2002)
σ	7.72×10^{-6}	μm s^{-1}	signal molecules production rate	Byers et al (2002)
γ	4.86×10^{-5}	μm s^{-1}	signal molecules loss rate	Byers et al (2002)
α_2	0.38	s^{-1}	transition rate on-QS to off-QS	estimated

Table 3.1 lists some parameter values from above calculation taken from Byers et al (2002), either obtained from the graph (β_1, β_2, and γ) or the equation (σ), whereas the parameter value of α_2 (transition rate "off " to "on") remains difficult to determine a specific number. The reason for this corresponds to the fact that determining the exact value is quite complicated. Many papers have focused on explaining temporal transition between "off " to "on " state, and conversely [e.g. Ward et al (2001) states that a corresponding bacterial colony will "switch on" their trait depending on their density once a specific concentration of Q is reached. Goryachev et al (2006) and Langebrake et al (2014) investigate interim transitions between "off and on " state]. In this case, the parameter value for the transition rate is an arbitrary constant chosen to obtain bistability behaviour. This is a familiar behaviour that represents the dynamical system of the QS signal molecule. The bacteria have a low steady state (off) from which it is possible to jump past an unstable state to a stable high steady state (on) (Dockery and Keener, 2001; Ward et al, 2001; Song et al, 2007).

The results in Fig. 3.10, provide the value of bacterial growth rate, $\beta_1 = 2.78 \times 10^{-4}$ /s (β_2 as well). They also give the value of loss rate of signal molecules is $\gamma = 4.86 \times 10^{-5}$ $\mu m/s$. Then, from the equation of Q, we obtain $\sigma = 7.72 \times 10^{-6} \mu m/s$.

3.3   Results and discussion

We have presented a simple model of bacterial interaction that gives particular attention to nutrient acquisition and QS signal molecule production as an important aspect of the transition rate of bacterial types. We develop the model through specifying the dynamics of off-QS and on-QS non-motile bacteria.

In the simulations, several different parameter values are tested and the outputs consistently showed the same behaviour. The parameter values used were adopted from Byers et al (2002); we employ data on *E. carotovora* to proceed our model. From the simulation

we show the relation between cell transition rate and the amount of QS signal molecule. The increase of QS signal molecule concentration raises the transition rate (from off-QS to on-QS of bacteria). In order to explore the dynamical behaviour of the proposed model, a bifurcation analysis has been carried out by considering the slope transition rate from off-QS to on-QS bacteria (κ) and loss effective rate of signal molecules (γ') as bifurcation parameters. The system has a fixed point solution which exhibits a fold bifurcation. The numerical result shows that an effective rate of diffusion of the QS signal molecule decreases on a slow time scale as the colony grows. In a related study, Ward et al (2001) found switching behaviour for *Vibrio fischeri* in which there was a cell transition as the colony increased in size. Ward et al (2001) presented a mathematical model which describes bacterial population growth and quorum sensing. The population of bacteria consist of down-regulated and up-regulated sub-populations, with signal molecules being produced at a much faster rate by the up-regulated cells.

The hysteresis phenomenon is predicted by the model, yet it has not been verified experimentally. In addition, we set the bacterial colonies to have the same growth rate for both types. In contrast, bacterial colonies have different growth rate that depends on temperature and light (Ingraham et al, 1983), availability of nutrient (Todar, 2015; Goryachev et al, 2006). In that regard, it would be more interesting to use assumptions that can resemble real conditions by considering factors that influence the growth rate of bacteria through experiment.

Bees et al (2002) state that there will be translocation and expansion through surfaces of medium by swarming bacterial colonies to get access to a wider source of nutrient, which is a main factor in establishing the success of a specified colony. In a later chapter, this type of model will be developed by considering not only non-motile bacteria, but motile bacteria. The underlying reason of this is that QS signal molecules in swarmer colonies may allow optimal spreading of bacterial cells when a population density increases. In addition, sufficient nutrient acquisition promotes formation of the flagellar that enables bacteria to be more active and expand to the larger area. This expectation is in accordance with Kim et al (2012), who show the supply of higher nutrient concentration produces more active cells.

Furthermore considering the theoretical research regarding QS systems, the results need to be developed into regulation system of QS model in order to look deeply of bistability phenomena on QS signal molecule behaviour per se. James et al (2000) demonstrated QS model of *V. fischeri*, which has two stable metabolic states corresponding to the expression of the luminescent and non-luminescent phenotypes. The system has three steady states that has a "switch-like" behaviour. In simultaneous work, Dockery and Keener (2001) showed the

biochemical switch between two stable steady states on QS model of *P. aeruginosa*, one with low level and another one with high level of signal molecules, is the key to how QS works in relation to the population density. Like James et al (2000) and Dockery and Keener (2001), Fagerlind et al (2003) developed a model of a QS system of *P. aeruginosa* and presented that the system has two steady states which are regulated by signal molecules. Therefore, these published works motivate us to look in more detail at the biochemical behaviour of QS systems in the following chapter.

Chapter 4

Pulse generation in the quorum machinery of *P. aeruginosa*

4.1   Abstract

Pseudomonas aeruginosa is a Gram-negative bacterium that is responsible for a wide range of infections in humans. Colonies employ quorum sensing (QS) to coordinate gene expression, including for virulence factors, swarming motility and complex social traits. The QS signalling system of *P. aeruginosa* is known to involve multiple control components, notably the *las*, *rhl* and *pqs* systems. In this paper, we examine the *las* system and, in particular, the repressive interaction of *rsaL*, an embedded small regulative protein, employing recent biochemical information to aid model construction. Using analytic methods we show how this feature can give rise to excitable pulse generation in this subsystem with important downstream consequences for rhamnolipid production. We adopt a symmetric competitive inhibition to capture the binding in the lasI-rsaL intergenic region and show our results are not dependent on the exact choice of this functional form. Furthermore, we examine the coupling of *lasR* to the *rhl* system, the impact of the predicted capacity for pulse generation and the biophysical consequences of this behaviour. We hypothesise that the interaction between the *las* and *rhl* systems may provide a quorum memory to enable cells to trigger rhamnolipid production only when they are at the edge of an established aggregation.

keywords : *Pseudomonas aeruginosa*, Quorum sensing, Excitable behaviour, Bifurcation analysis.

4.2   Introduction

Pseudomonas aeruginosa is a common Gram-negative bacterium responsible for a wide range of infections, including those of the urinary and gastrointestinal tract, the skin, and, most prominently, the respiratory system in immunocompromised hosts and sufferers of Cystic Fibrosis (CF). *P. aeruginosa* is a well-studied opportunistic pathogen in many contexts; it is well-known for its ability to form biofilms (O'Loughlin et al, 2013; Singh et al, 2015), its swarming behaviour (Daniels et al, 2004; Shrout et al, 2006), its rapid acquisition of resistance to antibiotics (Shih and Huang, 2002) and its quorum sensing (QS) behaviour (Fuqua et al, 2001). QS in *P. aeruginosa* is of particular interest because the mechanism is more complex than the originally-discovered, prototypical Lux homolog positive-feedback loop (e.g., James et al, 2000; Shadel and Baldwin, 1991) and the number of genes regulated by QS is large (Sitnikov et al, 1995), especially those associated with virulence (O'Loughlin et al, 2013). Mathematical models of QS in *Pseudomonas aeruginosa* have received a lot of attention. They provide the formalism to summarize current understanding as well as the means to explore mechanisms and evaluate emergent solution behaviour. Here, we develop a model description, employing recent genomic information and bioinformatic techniques, and explore mechanisms for the generation of pulses and memory effects for downstream rhamnolipid production.

In *P. aeruginosa* quorum sensing is governed by a hierarchical LuxI/luxR system, which consists of two homolog pairs: LasI/LasR and RhlI/RhlR (Miller and Bassler, 2001). Under this process, formation of the HSL autoinducers *N*-(3-oxododecanoyl)-HSL and *N*-(butyryl)-HSL are synthesised by LasI and RhlI, respectively (see Fig. 4.1). It should be noted, however, that signalling systems of *las* and *rhl* are specific in their activation of autoinducers, i.e. *N*-(3-oxododecanoyl)-HSL is unable to activate RhlR and, similarly, LasR cannot be activated by *N*-(butyryl)- HSL (Latifi et al, 1995; Pearson et al, 1997). Although biochemically independent, the *las* system is able to exert control of the *rhl* system through the transcriptional promotion of the RhlR gene by LasR/*N*-(3-oxododecanoyl)-HSL (Pesci et al, 1997; Latifi et al, 1996). As well as gene regulation effects, the *rhl* system has an important function of modulating rhamnolipid production via *rhlAB*. Rhamnolipids are particularly important in swarming motility where they are postulated to lower surface tension and allow expansion of the colony through their surfactant and wetting properties, driving the bacteria to swarm on surfaces (Glick et al, 2010; Kohler et al, 2000). In addition, a quinolone system (Dubern and Diggle, 2008) may also modulate these interconnecting feedback loops (for simplicity, we do not model this aspect of QS here).

The first models of QS in *P. aeruginosa* were of the Lux (James et al, 2000) and the Las systems (Dockery and Keener, 2001). Both descriptions, and subsequent models, highlight
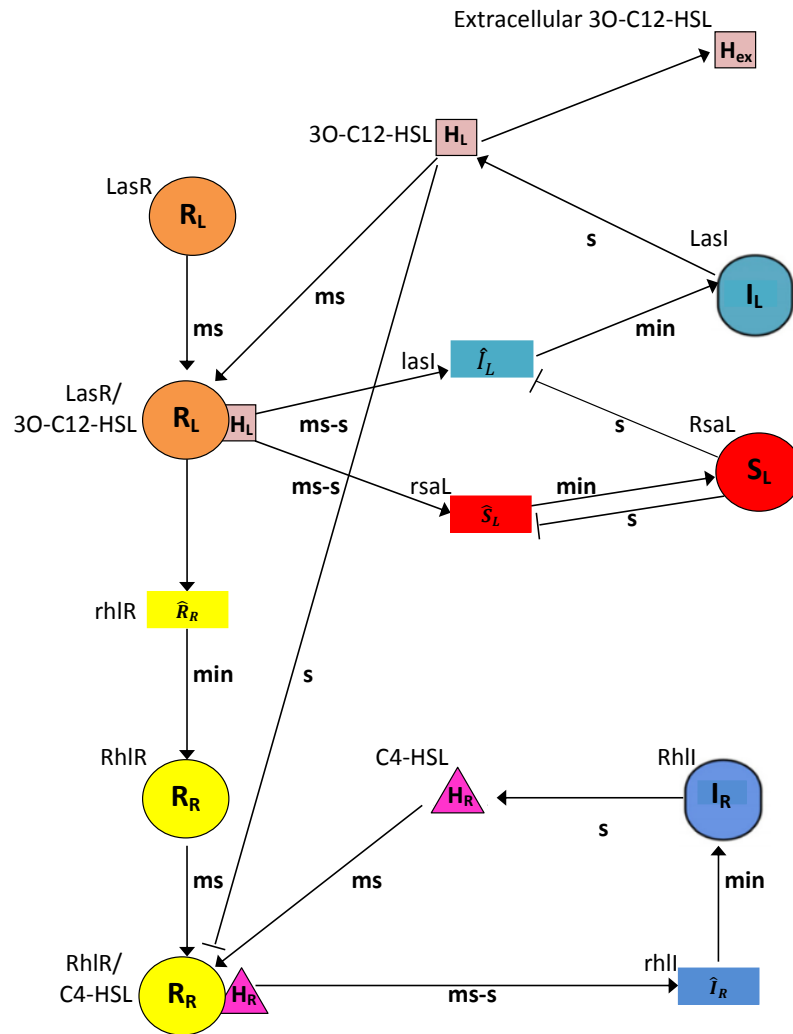
Figure 4.1: The quorum sensing signalling system in *Pseudomonas aeruginosa* is composed of *las* and *rhl* systems. Arrows and barred arrows indicate activating (positive) and inhibiting (negative) regulatory interactions, respectively. Shapes on the diagram depict autoregulation terminology. Letters associated with each arrow reflect the associated time scale (ms = millisecond, s = second, and min = minute). Symbols associated with each shape are detailed in Table 4.1.

the existence of a fold bifurcation structure for the concentration of the response regulator in response to bulk cell concentration. The seminal paper by Dockery and Keener (2001) provides the foundation for the emergence of QS based on formal mass action arguments. However, there have been significant increases in biochemical knowledge of this system in the last 15 years. Fagerlind et al (2003) constructed a large mass action model of the coupled Las and Rhl systems, including the effects of both RsaL and Vfr. This work also emphasises the existence of the classic two-fold bifurcation diagram for the activation level of the system (typically for the levels of liganded LasR) with respect to the external concentration of HSL. Subsequent work Fagerlind et al (2005) then explored how anti-virulence drugs (followed by Skindersoe et al (2008)) are able to quorum quench this system. The qualitative model of Viretta and Fussenegger (2004) does not include the effect of the *rsaL* negative loop and lacks the capacity to deal with the non-linear effects predicted here. The production of rhamnolipid was modelled and tested empirically by Chen et al (2004). The exhaustive rule-based approach of Schaadt et al (2013) includes the effect of *rsaL* but does not include the kinetic possibilities that emerge from non-linear interactions. There are many other studies on this system but, increasingly, these are based on the perspective of computational rather than mathematical modelling (e.g., Dockery and Keener, 2001; Fagerlind et al, 2005; Schaadt et al, 2013), typically with a non-mechanistic emphasis.

In this article we focus in detail on the Las system and its internal regulation and modulation for individual cell. The *las* system is composed of LasI, autoinducer N-(3-oxododecanoyl)-HSL, LasR and RsaL (Pesci et al, 1997). Importantly, biochemical evidence has now firmly established that LasR exists as a dimer in solution, with each monomer liganded by a single HSL (N-(3-oxododecanoyl)-HSL) molecule with additional evidence supporting higher multimers upon DNA binding (Schuster and Greenberg, 2006). This is in contrast to assumptions of Dockery and Keener (2001) who assume a simpler mechanism for binding. Mathematically, the biochemical evidence is consistent with a Hill number of at least two and possibly much higher. In contrast, the RsaL transcriptional repressor is a helix-turn-helix protein that binds the promoter of *lasI* (De Kievit et al, 2002) and exists as a monomer in the cell (Rampioni et al, 2007a), leading to a Hill number of one. The transcription of both genes is promoted and regulated via binding of the two proteins to the same intergenic region between the lasI and rsaL operons, so except for rates the functional form for the transcription is likely to be identical (but we discuss variations of this in the next chapter). This improvement in biochemical knowledge offers clear guidance for expected mathematical forms in the equations.

We begin with an investigation of the behaviour of gene regulation by constructing a mathematical model of a single cell. In order to focus on a biologically plausible region of

parameter space we conduct an extensive search of published data, noting deviations from modelling choices in the literature. The dynamical system exhibits a range of interesting solution behaviour. We find that bistable solutions and oscillations are possible and explore the bifurcation structure. Of significant interest is the potential for excitability in the system, in the presence of both single and multiple steady states, such that a modest perturbation from a low level steady state triggers a large-amplitude excursion around phase space that eventually returns the system to low steady state. The extracellular concentration of HSL can have a significant impact on the dynamics. As signal molecules can accumulate and diffuse in the external environment we demonstrate how pulse generation of the *las* system can be propagated in space.

This paper is organised as follows. In section 2, we describe in greater detail the biological system as well as the mathematical approach. In Section 3, we conduct a numerical exploration of our model, highlighting the key parameters in determining LasI and RsaL equilibria. We then employ extracellular concentration as a driving factor in the dynamical behaviour of the system. We conclude by discussing our findings, identify challenges and suggest future work in Section 4.

4.3 Methods

We construct the governing equations using mass action kinetics, except where noted, guided by the literature (e.g., Fagerlind et al, 2003). First, consider the LasR regulator (R_L), its binding activator, the autoinducer 3O-C12-HSL (H_L), and the complex LasR/3O-C12-HSL (R_{LH}). If LasR associates at rate k_L^+, dissociates at rate k_L^-, is produced at a rate β_0 and degrades or dilutes at rate γ_L, then we may write

$$\frac{dR_L}{dt} = -k_L^+ R_L H_L + k_L^- R_{LH} + \beta_0 - \gamma_L R_L, \tag{4.1}$$

In a similar manner, we formulate an equation for the complex, with degradation or dilution rate γ_{RL}, such that

$$\frac{dR_{LH}}{dt} = k_L^+ R_L H_L - k_L^- R_{LH} - \gamma_{RL} R_{LH}. \tag{4.2}$$

where $\beta_0, \gamma_L, \gamma_{RL}$ are positive constants.

New biochemical data have indicated approximately steady cellular levels (Ishihama et al, 2014) of many transcription factors and, therefore, we hypothesise it is the change in activation rather than production *per se* that dictates the dominant dynamics; unlike previous studies that consider the regulated production of LasR. Therefore, we shall assume the association and dissociation processes occur over a sufficiently fast time scale that the production and loss terms can be safely neglected: we disregard terms multiplied by β_0, γ_L and γ_{RL}.

Table 4.1: Description of dimensional variables of *las* system.

Variable	Description	Unit
R_L	LasR	nM
H_L	3O-C12-HSL	nM
R_{LH}	LasR/3O-C12-HSL complex	nM
I_L	LasI	nM
$\hat{I}_L$	lasI mRNA	nM
S_L	RsaL	nM
$\hat{S}_L$	rsaL mRNA	nM
R_R	RhlR	nM
H_R	C4-HSL	nM
R_{RH}	RhlR/C4-HSL complex	nM
$\hat{R}_R$	rhlR mRNA	nM
I_R	RhlI	nM
$\hat{I}_R$	rhlI mRNA	nM

The autoinducer 3O-C12-HSL (H_L) is created in the system via the activity of the LasI synthase (I_L), which we take to be at rate β_{HL}, and is naturally lost from the system at rate γ_{HL}. The most significant loss of the autoinducer from the cell is via diffusion through the cell membrane, a process we account for separately. Taking a simplified description of diffusion we can express the diffusive term as being proportional to the concentration difference across the membrane of H_L, where we take the extracellular concentration to be H_{ex}. Therefore, D_{HL} represents an additional loss rate, which is multiplied by the concentration difference, $H_L - H_{ex}$, yielding

$$\frac{dH_L}{dt} = \beta_{HL}I_L - \gamma_{HL}H_L - D_{HL}(H_L - H_{ex}). \tag{4.3}$$

The enzyme LasI (I_L) is produced by the lasI gene through a transcription and translation process of lasI-mRNA ($\hat{I}_L$) at rate α_L and degrades at rate γ_{IL}, such that

$$\frac{dI_L}{dt} = \alpha_L\hat{I}_L - \gamma_{IL}I_L. \tag{4.4}$$

In a similar fashion, the inhibitor RsaL (S_L) is produced by rsaL genes through transcription and translation of rsaL-mRNA ($\hat{S}_L$) at rate α_S and degrades at rate γ_S, providing

$$\frac{dS_L}{dt} = \alpha_S\hat{S}_L - \gamma_S S_L. \tag{4.5}$$

Transcription at the lasI promoter site ($\hat{I}_L$) is activated by the LasR/3O-C12-HSL complex (R_{LH}). The production process is assumed to follow a Hill form with a Hill number

p. Recent biochemical evidence strongly suggests a Hill number > 1 in contrast to the arguments of Dockery and Keener (2001); the activated form of lasR is at least dimeric (Schuster and Greenberg, 2006) and it is possible that it forms a tetramer on the DNA. For mathematical simplicity we adopt the smaller potential value, $p = 2$, in the analysis that follows. In addition, the RsaL transcriptional repressor has been shown to bind to the lasI-rsaL intergenic region but, unlike LasR, RsaL is a helix-turn-helix protein that exists as a monomer in the cell (Rampioni et al, 2007a), and thus we will adopt Hill number $q = 1$ for the inhibition factor for production of RsaL ($\hat{S}_L$), mathematically equivalent to a Michaelis-Menten equation. The transcription of both genes is promoted and regulated via binding of the two proteins to the same intergenic region between the lasI and rsaL operons, so the functional form for the transcription is identical, with the exception of the numerical values of the transcription and loss rates. Note that this implies a negative feedback relation between the RsaL protein and its own production, which has not been historically represented on graphical depictions of the *las* system, but strongly implied by analysis of Rampioni et al (2007a). Biochemically there is insufficient evidence to determine whether the binding in the intergenic region results in competitive, uncompetitive or non-competitive binding system, or indeed whether there is a symmetry in the expression rates in each direction with all configurations of binding at the intergenic region. In the analysis below we adopt a symmetric competitive binding form (we choose $K_L = K_S$ in the analysis below), but show in detail in the next chapter (section 5.5) that qualitatively the results are not dependent on this functional choice. With basal expression of β_{L0} and a loss rate of γ_{mL} this leads to the following expression for lasI:

$$\frac{d\hat{I}_L}{dt} = \beta_L \frac{R_{LH}^p}{K_L^p(1 + S_L^q/K_{SL}^q)^p + R_{LH}^p} - \gamma_{mL}\hat{I}_L + \beta_{L0}. \tag{4.6}$$

Similarly, with basal expression of β_{S0} and a loss rate of γ_S for rsaL we obtain

$$\frac{d\hat{S}_L}{dt} = \beta_S \frac{R_{LH}^p}{K_S^p(1 + S_L^q/K_{SL}^q)^p + R_{LH}^p} - \gamma_{mS}\hat{S}_L + \beta_{S0}. \tag{4.7}$$

The numerical values of the temporal processes are such that we are able to make a number of assumptions regarding the timescales to simplify the system. We assume that the dominant, slowest processes are protein production from mRNA via translation and folding. Therefore, other processes, namely the liganding of regulators, DNA binding, synthetase operation, and the transcription of DNA are much faster and we can assume that four of our differential equations are at a quasi-steady state, such that

$$\hat{I}_L = \frac{\beta_L R_{LH}^p}{\gamma_{mL}\left(K_L^p\left(1 + \frac{S_L^q}{K_{SL}^q}\right)^p + R_{LH}^p\right)} + \frac{\beta_{L0}}{\gamma_{mL}}, \tag{4.8}$$

and

$$\hat{S}_L = \frac{\beta_S R_{LH}^q}{\gamma_{mS}\left(K_S^p\left(1 + \frac{S_L^q}{K_{SL}^q}\right)^p + R_{LH}^p\right)} + \frac{\beta_{L0}}{\gamma_{mS}}. \tag{4.9}$$

From equation (4.1) and (4.2), we have a *Moiety conservation* equation

$$\frac{dR_{LH}}{dt} + \frac{dR_L}{dt} = 0 \Rightarrow R_{LH} + R_L = R_{L0}, \text{ where } R_{L0} \text{ is a constant.} \qquad (4.10)$$

Initially, we make the simplifying assumption that HSL diffusion is rapid and, therefore, that the equation for HSL, H_L can also be written in a quasi-steady state, providing

$$H_L = \frac{\beta_{HL} I_L}{D_{HL}} + H_{ex}. \qquad (4.11)$$

Later, we relax this constraint. With the simplifications above, the system of equations for the *las* system, constructed for the LasI and RsaL loops, become just two differential equations. By assuming there is negligible basal production of lasI and rsal genes ($\beta_{L0} = 0$ and $\beta_{S0} = 0$) the governing equations become

$$\frac{dI_L}{dt} = \frac{\alpha_L \beta_L}{\gamma_{mL}} \frac{R_{L0}^2 H_L^2}{K_L^2 \left(1 + \frac{S_L}{K_{SL}}\right)^2 \left(H_L + \frac{k_L^-}{k_L^+}\right)^2 + R_{L0}^2 H_L^2} - \gamma_{IL} I_L, \qquad (4.12)$$

and

$$\frac{dS_L}{dt} = \frac{\alpha_S \beta_S}{\gamma_{mS}} \frac{R_{L0}^2 H_L^2}{K_S^2 \left(1 + \frac{S_L}{K_{SL}}\right)^2 \left(H_L + \frac{k_L^-}{k_L^+}\right)^2 + R_{L0}^2 H_L^2} - \gamma_S S_L, \qquad (4.13)$$

with H_L as in equation (4.11).

We nondimensionalize this model by writing

$$\eta = \frac{\beta_{HL} k_L^+}{D_{HL} k_L^-} I_L, \; \xi = \frac{S_L}{K_{SL}}, \text{ and } \tau = \frac{\alpha_L \beta_L \beta_{HL} k_L^+}{\gamma_{mL} D_{HL} k_L^-} t, \qquad (4.14)$$

so that (4.12) and (4.13) become

$$\frac{d\eta}{d\tau} = \frac{(\eta + a_1)^2}{a_2 (1 + \xi)^2 (\eta + a_1 + 1)^2 + (\eta + a_1)^2} - a_3 \eta, \qquad (4.15)$$

$$\frac{d\xi}{d\tau} = \frac{a_4 (\eta + a_1)^2}{a_2 (1 + \xi)^2 (\eta + a_1 + 1)^2 + (\eta + a_1)^2} - a_5 \xi, \qquad (4.16)$$

where

$$a_1 = \frac{H_{ex} k_L^+}{k_L^-}, \qquad a_2 = \left(\frac{K_L}{R_{L0}}\right)^2, \qquad (4.17)$$

$$a_3 = \frac{\gamma_{IL} \gamma_{mL} D_{HL} k_L^-}{\alpha_L \beta_L \beta_{HL} k_L^+}, \qquad a_4 = \frac{\alpha_S \beta_S}{\gamma_{IL} \gamma_{mS} K_{SL}} a_3,$$

$$a_5 = \frac{\gamma_S}{\gamma_{IL}} a_3.$$

Here, a_1, a_2, a_3, a_4, and a_5 are positive constants. The biological interpretation of this model is that ξ inhibits the expression of both η and ξ, which describes negative feedback from competitive inhibition by RsaL to the expression of both *lasI* and *rsaL* genes. The binding of RsaL to the bidirectional *lasI-rsaL* counters positive feedback, thereby balancing levels of HSL. In addition, both η and ξ degrade exponentially. The model thus constructed is a type of incoherent feed forward motif (Alon, 2006) as can be seen from Fig. 4.1.

Table 4.2: Parameters employed in the model of *las* system.

Par	Description	Standard value	Unit	Value/Range	Comments (Based on)/Ref
k_L^+	rate of binding reaction between LasR and 3O-C12-HSL		$\text{nM}^{-1}\text{min}^{-1}$		ratio $\frac{k_L^-}{k_L^+} \sim 1000 - 2000$ nM
k_L^-	dissociation reaction rate of LasR/3O-C12-HSL		min^{-1}		ratio $\frac{k_L^-}{k_L^+} \sim 1000 - 2000$ nM, (Welch et al, 2000)
α_L	rate at which LasI produced by lasI mRNA	0.5	min^{-1}	0.5	2 min to translate protein, (Alon, 2006)
α_S	rate at which RsaL produced by rsaL mRNA	0.5	min^{-1}	0.5	2 min to translate protein, (Alon, 2006)
β_{HL}	rate at which 3O-C12-HSL produced by LasI	8×10^2	min^{-1}	8×10^2	(Raychaudhuri et al, 2005)
β_L	max. production rate of LasI when lasI mRNA is activated by LasR/3O-C12-HSL	1	nM min^{-1}	1	estimate
β_S	max. production rate of RsaL when rsaL mRNA is activated by LasR/3O-C12-HSL	1	nM min^{-1}	1	estimate
β_{L0}	basal production rate of lasI mRNA	0.1	nM min^{-1}	0.1	basal transcription rate of a protein, (Alon, 2006)

Table 4.2. continued

Par	Description	Standard value	Unit	Value/Range	Comments (Based on)/Ref
β_{S0}	basal production rate of rsaL mRNA	0.1	nM min^{-1}	0.1	basal transcription rate of a protein, (Alon, 2006)
K_L	affinity constant between LasR/3O-C12-HSL and lasI mRNA	116	nM	1-1000	(Alon, 2006)
K_S	affinity constant between LasR/3O-C12-HSL and rsaL mRNA	116	nM	1-1000	(Alon, 2006)
K_{SL}	dissociation constant of inhibitor RsaL to lasI mRNA	185	nM	1-1000	(Alon, 2006)
γ_L	degradation rate of LasR	0.01	min^{-1}	0.01	(Alon, 2006)
γ_{IL}	degradation rate of LasI	0.01	min^{-1}	0.01	(Alon, 2006)
γ_S	degradation rate of RsaL	0.0025	min^{-1}	0.01	(Alon, 2006)
γ_{HL}	degradation rate of 3O-C12-HSL	0.01	min^{-1}	0.01	(Alon, 2006)
γ_{RL}	degradation rate of LasR/3O-C12-HSL	0.01	min^{-1}	0.01	(Alon, 2006)
γ_{mL}	degradation rate of lasI mRNA	0.2	min^{-1}	0.2	5 min halflife of RNA, (Alon, 2006)
γ_{mS}	degradation rate of rsaL mRNA	0.2	min^{-1}	0.2	5 min halflife of RNA, (Alon, 2006)
D_{HL}	diffusion constant of 3O-C12-HSL	60	min^{-1}	$0-10^4$	(Pai and You, 2009)
H_{ex}	concentration of extracellular 3O-C12-HSL	10	nM	10-100	estimate
R_{L0}	total concentration of LasR and LasR/3O-C12-HSL	200	nM	200	QseB in *E. coli*, (Ishihama et al, 2014)

Table 4.3: Non-dimensional Parameters involved in the model of *las* system.

Name	Description	Standard value	Range
a_1	the effect of extracellular signal molecules	0.01	$5 \times 10^{-3} - 10^{-1}$
a_2	a squared ratio of concentration of Las components	0.3	$25 \times 10^{-6} - 25$
a_3	the degradation of LasI relative to signal molecule production	0.3	$0 - 100$
a_4	the control of binding of RsaL to LasI	0.4	$0 - 25 \times 10^3$
a_5	the degradation of RsaL relative to signal molecule production	0.075	$0 - 25$

4.4 Results

The non-dimensional set of differential equations (4.15) and (4.16) have been investigated analytically with the assistance of Mathematica (10; Wolfram) and solved numerically using Matlab (R2016a; MathWorks). We note that the fixed points of this system lie upon the straight line $a_3 a_4 \eta = a_5 \zeta$ but substitution of this expression into either nullcline leads to a quintic equation for the fixed points that does not provide sufficient further simplification to yield general expressions for stability bounds.

4.4.1 Parameter ranges in the system

Table 4.2 lists parameters that have either been adopted from the literature based on experimental evidence or estimated, as stated. Moreover, some parameters are chosen for the following reasons. The basal production rate of genes-mRNA can be considered as similar to the basal transcription rate of a protein. This is because the transcriptional regulator protein activates genes-mRNA in a very fast process before encoding the protein. We take typical values of total concentration of LasR and LasR/3O-C12-HSL to be 200 nM, as for the concentration of QseB in *E. coli* (Ishihama et al, 2014). As described in the previous section, we simplify the governing equations by assuming quasi-steady states for the fast reactions. This results in just 5 non-dimensional parameters (see Table 4.3).

The dimensionless variable a_1 is proportional to H_{ex}, the extracellular HSL concentration, an important factor in controlling both the intracellular HSL production and cell-cell communication. We shall see that a_1 influences the location of the key bifurcation.

Parameter a_2 depends on K_L and represents the relative binding strength of the LasR

dimer, and a_4 assigns binding control of RsaL to LasI through parameter K_{SL}, consequently it gives the relative production of RsaL to LasI. Both parameters a_2 and a_4 have a wide potential range, $25 \times 10^{-6} - 25$ and $0 - 25 \times 10^3$, respectively. This is because the affinity constant between transcriptional regulator protein to genes-mRNA is largely unmeasured and depends on the chain structure of the signal molecule (short or long chain; $1 - 1000$ nM) (Alon, 2006).

Parameter a_3 is inversely proportional to β_{HL}, the HSL production rate. It is related to a_5, which describes the degradation of RsaL relative to HSL production. It is important to note that we set $a_5 < a_3$ due to the transcription factor being more stable than the synthase. We shall see that the parameters a_3 and a_1 allow for fold and Hopf bifurcations in the system, leading to bistability and oscillations, respectively, as well as excitable dynamics, and provide suitable control parameters that can be varied in experiments.

4.4.2 Excitable dynamics in the LasI and RsaL phase plane

The simplified system (4.15) and (4.16) involves just two variables, which we investigate with phase plane analysis. By varying a_3, four phase portraits of interest can be identified, as depicted in Fig. 4.2a. We plot the two nullclines $\dot{\eta} = 0$ and $\dot{\xi} = 0$, where η and ξ represent the dimensionless of LasI and RsaL concentration, respectively. Fixed points for the system lie at their intersection.

A qualitative description of the model behaviour is now possible, with reference to classical excitable systems such as the Fitzhugh-Nagumo model (Murray, 1993). Cases I and IV (see Fig. 4.2a), which correspond to small and large values of the bifurcation parameter $a_3 = 0.1$ and 0.6, respectively, possess a single stable fixed point with the nullclines positioned so that there is no possibility of excitable behaviour (see below). For case II (Fig. 4.2a) there are two further intersections, which yield the central zone of the well-known S-shaped bifurcation diagram with three fixed points in a stable-unstable-stable configuration. This phenomenon has been reported in many experiments on autoregulation of genes (e.g., Alves and Dilo, 2005; Angeli et al, 2004; Poignard, 2014); more detail is presented in Fig. 4.3. The feedback loop that consists of both positive and negative autoregulation creates two possible LasI production states, "on" and "off" (at the large and small stable steady states, respectively), affecting signal molecule concentration. This is a familiar pattern that represents quorum sensing; the cells have a low steady state (off) from which it is possible to jump past an intermediate unstable state – either via stochastic fluctuations or changes in the external parameters, in particular the background level of HSL represented here by the parameter a_1 – to a stable high steady state (on). Crucially, the return to the low steady state typically is not reversible and the system must trace a hysteretic loop to return to the

(a)

(b)

(c)

(d)
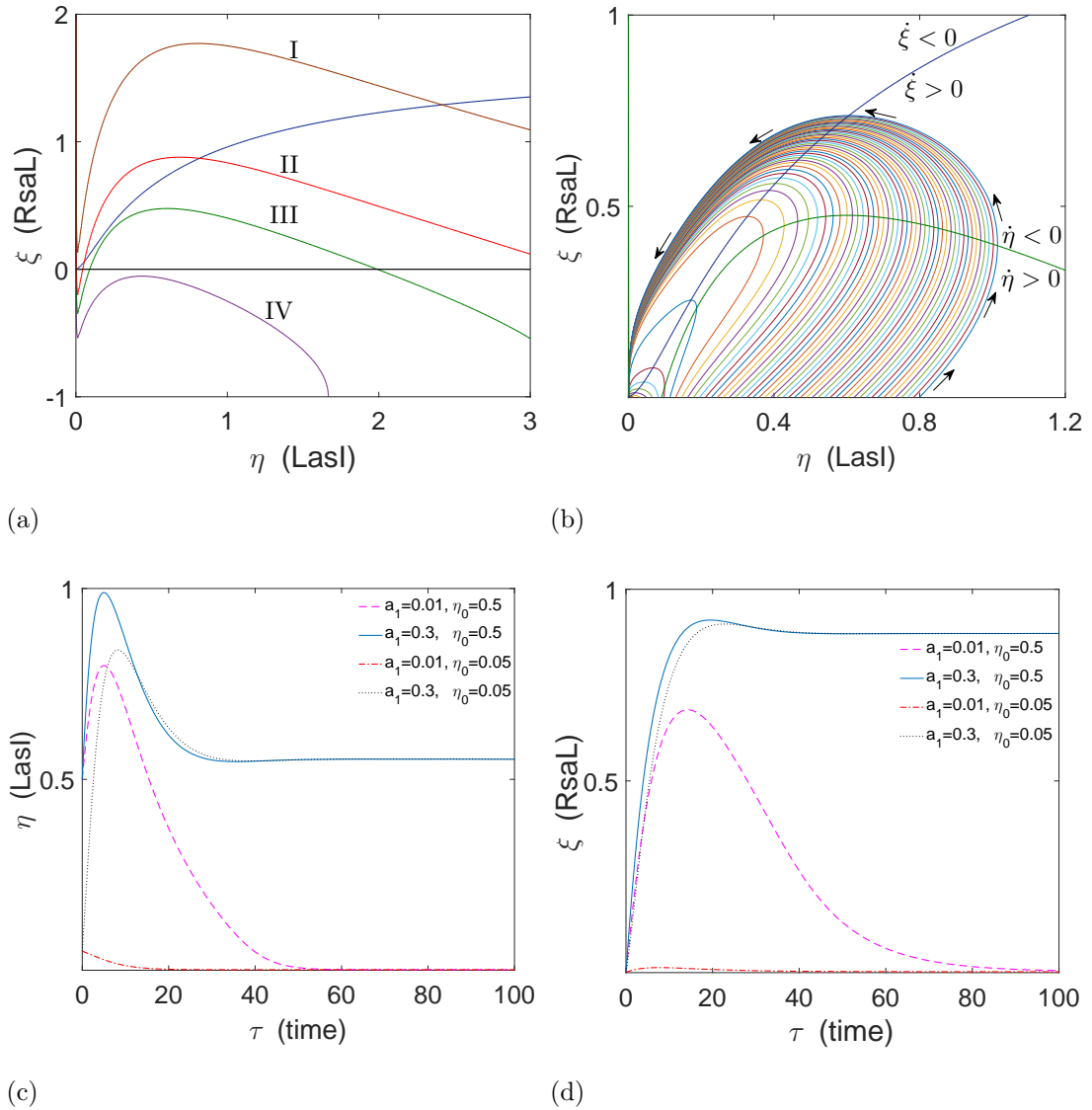
Figure 4.2: Qualitative dynamical behaviour of the *Pseudomonas aeruginosa* quorum sensing system. (a) Four phase portraits of interest resulting from intersection between LasI and RsaL (η and ξ, respectively) nullclines. As the parameter a_3 varies there can be one intersection point with no excitable dynamics (I and IV; for $a_3 = 0.1$ and 0.6, respectively), three intersection points (II; for $a_3 = 0.2$), or one intersection point with excitable dynamics (III; for $a_3 = 0.3$). (b) Excitable dynamics in the LasI and RsaL phase plane. Sufficiently large perturbations result in an excursion around the phase plane. (c,d) Time variation of η and ξ corresponding to the excitable trajectory of LasI and RsaL, respectively. All other parameters are as in Table 4.3.

low steady state via changes in the external parameters.

In Case III there is a single fixed point and the nullcline $\dot{\eta} = 0$ has a positive local maximum (which distinguishes it from cases II and IV); see Fig. 4.2a). This case allows for excitability in the LasI and RsaL phase plane caused by the $\dot{\eta}$ nullcline having cubic-like shape with a positive local maximum ($a_3 < 0.55$). By considering the behaviour of a perturbation to the steady state solution (see Fig. 4.2b), if the production of the (N-(3-oxododecanoyl)-HSL) molecule is sufficiently small, then global stability of the single fixed point ensures that the trajectory returns to the steady state. The variable ξ will engage, rapidly deplete and return the system to the small fixed point with a short loop. However, interesting behaviour occurs when there is a greater perturbation of (N-(3-oxododecanoyl)-HSL). For then the variable η pushes the system to the right in the phase plane, so that there is an excitable pulse of (N-(3-oxododecanoyl)-HSL). Consequently, there is no short route back to the stable fixed point and the trajectory undergoes a large excursion before returning. A small region of parameter space in Case II can also result in excitability ($0.27 \leq a_3 \leq 0.28$). Here there are three intersections between η and ξ nullclines, which are low stable fixed point, an intermediate saddle and a high unstable fixed points. In this region of parameter space, the saddle-unstable fixed point region is not accessible to trajectories that initiate in a zone close to the stable fixed point (see detailed analysis in the next chapter section 5.1).

The initial condition $\eta(0) = \eta_0$ and concentration of extracellular HSL have a large effect on the amplitude and duration of the excited pulse, as can be seen in Fig. 4.2. The results in Fig. 4.2b are plotted as a function of time in Fig. 4.2c and 4.2d, where the purple dashed-line and red dashed-line represent either excitable or non-excitable trajectories for large and small perturbations, respectively (for $a_1 = 0.01$ or, equivalently, $H_{ex} = 10nM$). By increasing external HSL concentration in the system via the variable a_1 (equivalent to increasing H_{ex} from $10nM$ to $= 300nM$), we find solutions tending to the single high steady state irrespective of the initial perturbation (shown in Fig. 4.2c and 4.2d by blue solid and black dotted lines; discussed later).

4.4.3 Bifurcation structure

The QS circuitry of *P. aeruginosa* is complex, with the *las* system itself consisting of both positive and negative feedback loops. The *lasI* gene is activated by LasR/3O-C12-HSL leading to increased (N-(3-oxododecanoyl)-HSL) production, positive feedback. However, LasR/3O-C12-HSL also activates the *rsaL* gene and induces expression of RsaL. RsaL inhibits expression of *lasI* and *rsaL* genes, and this process constitutes negative feedback. In general, this negative feedback loop is employed to maintain a homeostatic balance in the
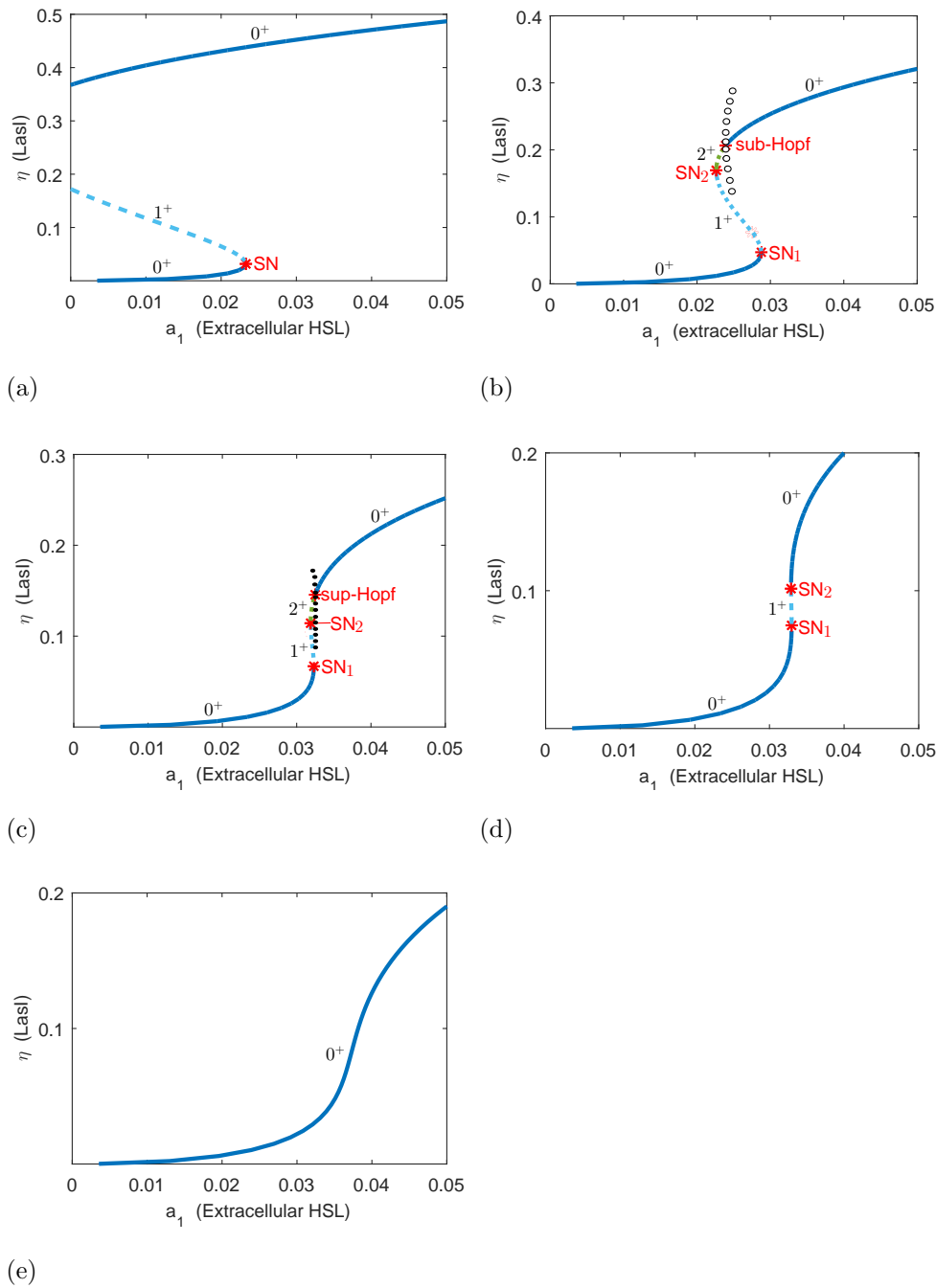
Figure 4.3: Bifurcation diagrams for autoregulation of the *las* system with respect to extracellular signal molecule concentration a_1 at five values of a_3: sub-figures a, b, c, d, and e are for $a_3 = 0.26, 0.3, 0.32, 0.323$, and 0.34, respectively. Solid lines depict stable steady states (no eigenvalues with positive real part); blue and green-dashed lines depict unstable steady states with one or two eigenvalues with positive real part, respectively; open (solid) circles denote maximum and minimum values of $\eta(\text{LasI})$ on unstable (stable) limit-cycles. The red stars indicate values of parameter a_1 and coordinate $\eta(\text{LasI})$ at bifurcations. Codimension-1 singular points marked as SN indicate a saddle-node point (or limit point); *sub*-Hopf indicates a subcritical Hopf bifurcation point; *sup*-Hopf indicates a supercritical Hopf bifurcation point. All other parameters are as in Table 4.3.
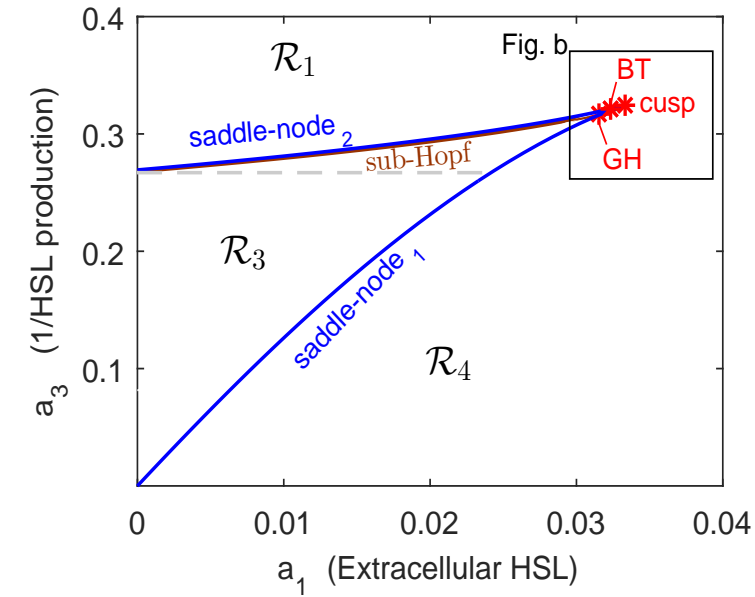
(a)
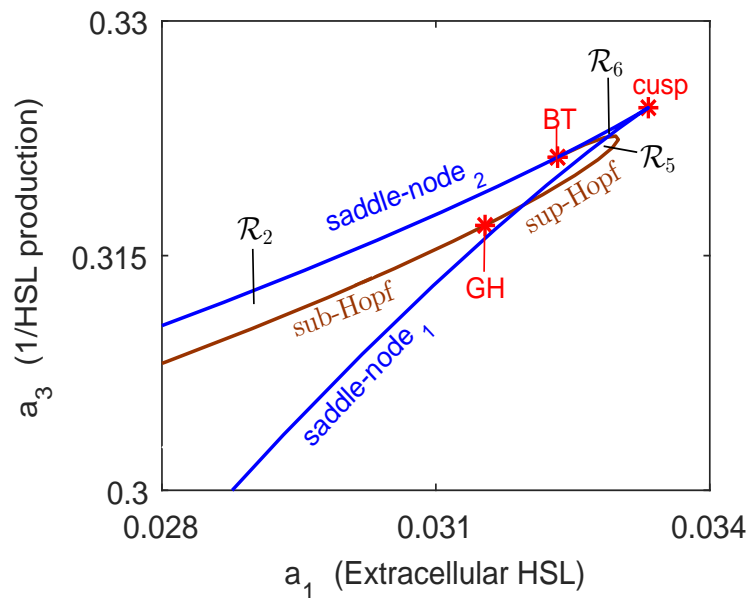
(b)

Figure 4.4: Two-dimensional bifurcation diagram for (a_1, a_3). The bifurcation lines divide the parameter domain into six regions $\mathcal{R}_1$, ..., $\mathcal{R}_6$. Each of these regions is explained in the main text. The blue lines depict the saddle-node lines, defined by the locus of saddle-node bifurcation points (or limit points), with subscripts 1 or 2 as in Figure (4.3). The Hopf lines are constructed by subcritical-Hopf and supercritical-Hopf bifurcation points, which are presented by brown lines. The bistable region, $\mathcal{R}_3$, consists of *reversible* (above of gray-dash lines) and *irreversible* (below of gray-dash lines). The red stars mark particular values of parameters a_1 and a_3 indicating a cusp, Bogdanov-Takens point (BT) or generalized-Hopf point (GH).

system. However, the interaction of both positive and negative feedback can yield bistability (and associated *hysteresis*; (Pfeuty and Kaneko, 2009)). There are many other studies on the dynamical behaviour of gene regulatory networks involving positive and negative feedback loops. Song et al (2007) demonstrated that interlocked positive and negative feedback loops play essential roles in bistability and oscillations. More complex bifurcations of co-dimension one or two have also been explored (Hat et al, 2016). Varying $a_1 > 0$, the effect of extracellular signal molecule, alters the qualitative dynamical behaviour of LasI and RsaL. Thus initially we investigated the dynamics of our system with a one-parameter bifurcation analysis of LasI versus a_1. We used continuation methods to track the evolution of solutions for η versus a_1.

Fig. 4.3a - 4.3e, depicts five qualitatively different dynamical behaviours, each at a different fixed value of a_3, the degradation of LasI relative to signal molecule production. As shown in Fig. 4.3a - 4.3d, there are at least four different bifurcation diagrams. Bifurcations of steady states do not appear in Fig. 4.3e. Fig. 4.3a, for $a_3 = 0.26$, depicts the potential for *irreversible* bistability. The left-hand saddle-node bifurcation can cross the η-axis for sufficiently small a_3, preventing a drop from the upper to the lower branch. In addition, in Fig. 4.3b - 4.3d, *reversible* bistability of LasI is evident in the range of a_1 bounded by the two limit points, SN_1 and SN_2, which denote saddle-node bifurcations. In the low steady state branch, the concentration of LasI is low until a_1 level exceeds the critical value SN_1 ($a_1 = 0.029, 0.032$, and 0.0329, for Fig. 4.3b, 4.3c, and 4.3d, respectively), at which point the concentration of LasI increases abruptly to a high value. In similar manner, starting with a_1 high, the concentration of LasI does not drop significantly until a_1 reduces below a critical value, either SN_2 ($a_1 = 0.023, 0.0318$, and 0.0328, for Fig. 4.3b, 4.3c, and 4.3d, respectively) or an earlier bifurcation such as a sub-critical Hopf bifurcation. With $a_3 = 0.3$ (Fig. 4.3b), subcritical Hopf (sub-Hopf) bifurcation points exists for the high fixed point in the bistability region, at $a_1 = 0.024$. The upper steady-state solution is unstable between SN_2 and sub-Hopf point, and stable beyond the sub-Hopf point where $a_1 > 0.24$. For $a_3 = 0.32$ (Fig. 4.3c), the two saddle-nodes (SN_1 and SN_2) move close together. Consequently, the bistability region is narrow. Here, the Hopf bifurcation becomes supercritical (sup-Hopf; at $a_1 = 0.032$). For $a_3 = 0.323$ (Fig. 4.3d), the sup-Hopf point disappears and the saddle-node bifurcations collide in Fig. 4.3e for $a_3 \geq 0.325$; the bistable regime ceases to exist.

Fig. 4.4 provides a two-dimensional bifurcation diagram in the (a_1, a_3)-plane. In general, for a value of a_1 smaller than at the cusp point, decreasing a_3 from a large value we move through a region with one relatively small stable fixed point for η to one small stable fixed point with excitable dynamics. Decreasing a_3 further provides a bistable regime before eventually reaching a region with one large stable fixed point for sufficiently small a_3. The

bistability region collapses through the collision of the two saddle-node lines at the cusp $(a_1 = 0.033, a_3 = 0.324)$, a possibility that might be inferred from Fig. 4.2a. For $a_1 > 0.033$, the bistable regime ceases to exist.

Three codimension-2 singular points, a cusp point, a Bogdanov-Takens bifurcation point (BT), and a generalized-Hopf bifurcation point (GH), are identified in Fig. 4.4. The Bogdanov-Takens bifurcation, at $(a_1, a_3) = (0.032, 0.321)$, is caused by coalescence of a saddle-node point (SN$_2$) and a Hopf bifurcation point (sup-Hopf). A sup-Hopf line extends to the lower right of the saddle-node lines close to the cusp in the bifurcation diagram. The generalized-Hopf bifurcation is at $(a_1, a_3) = (0.317, 0.002)$, a transition point from sup-Hopf to sub-Hopf. It is clear that the bifurcation structure is complex, especially close to the cusp point, although the solution space is dominated by the fold bifurcation and excitability.

The response diagram (Fig. 4.4) illustrates that the bifurcation lines divide the (a_1, a_3) parameter plane into six regions, as depicted by region $\mathcal{R}_1$, ..., $\mathcal{R}_6$. Detailed phase diagrams associated with each regions are given in next chapter (section 5.1). In summary, $\mathcal{R}_1$ has either a monostable fixed point (one stable steady state) with low concentrations of LasI and RsaL for $a_3 \geq 0.55$ (Fig. 5.1a), or excitable solutions, as discussed in the previous section (Fig. 5.1b). In the narrow region $\mathcal{R}_2$ (see Fig. 4.4b for detail figure), bounded by SN$_2$ and sub-Hopf, three steady states arise, but only the lower steady state is stable (Fig. 5.1c and Fig. 5.1d). Excitable solutions are also possible. Region $\mathcal{R}_3$ is divided into four domains with different behaviour. Three steady states arise in which the upper and lower steady states are stable, but the middle state is unstable. In the first domain, the upper state in $\mathcal{R}_3$ is surrounded by an unstable limit cycle (Fig. 5.1e). A homoclinic bifurcation arises to give the second domain (Fig. 5.1f). Upon decreasing a_3 further in this region, a high stable spiral exists with a large domain of attraction (Fig. 5.1g and Fig. 5.1h). Region $\mathcal{R}_4$ is monostable with high concentrations of LasI and RsaL (Fig. 5.1i). In the area approaching the cusp point $\mathcal{R}_5$ and $\mathcal{R}_6$, two small distinct regions arise (see Fig. 4.4b). Region $\mathcal{R}_5$ provides stable oscillations and $\mathcal{R}_6$ bistability. In summary, the bifurcation lines divide the (a_1, a_3)-plane into regions of distinct solution behaviour: monostability ($\mathcal{R}_1$ and $\mathcal{R}_4$), bistability or excitation ($\mathcal{R}_2$, $\mathcal{R}_3$, and $\mathcal{R}_6$), and oscillatory $\mathcal{R}_5$.

4.4.4 Travelling wave of a pulse in a linear chain of cells

We demonstrated the potential for the *las* system to act as a pulse generator for a single cell in the previous section. To illustrate how this effect may translate into cell-cell communication within a colony we consider a simplified linear chain of cells. The goal is to provide proof of principle that it is possible to set up a pulse train when the individual cells are coupled to the dynamics of their neighbours. For simplicity, we assume that diffusion
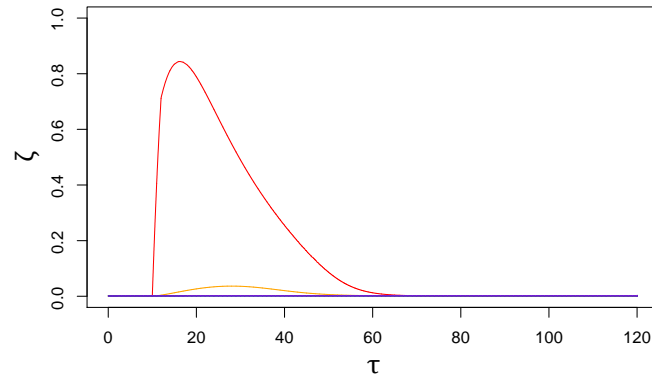
(a)
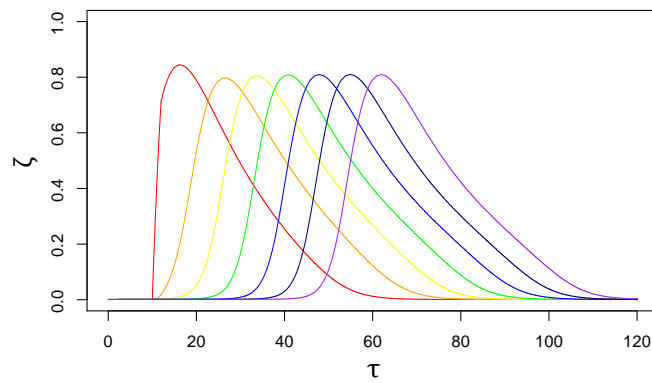
(b)
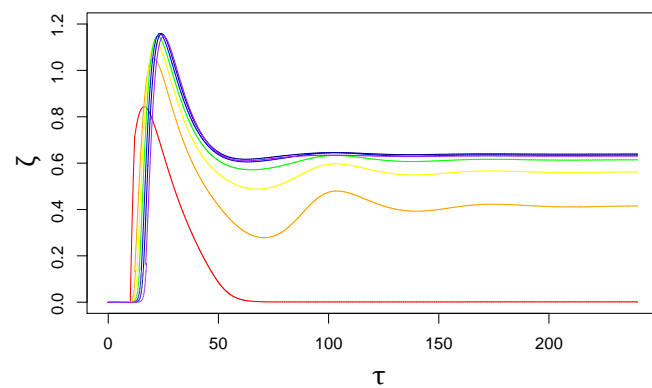
(c)

Figure 4.5: Pulse generation in the *las* system for single cells triggers a pulse train when the individual cells are coupled together. $x-$ and $y-$axes represent time variation of external HSL concentration (ζ) corresponding to the pulse train, which consist of a linear chain of seven cells. Three types of solution are found when the coupling fraction d is varied: (a) $d = 0.03$, (b) $d = 0.1$, (c) $d = 0.3$.

across each cell membrane is such that the intracellular concentration of HSL is at a kinetic equilibrium (i.e. $\frac{dH_L}{dt} = 0$, as before) and, additionally, assume that there is a neighbourhood surrounding each cell where the extracellular concentration can be modelled simply by

$$\frac{dH_{ex}}{dt} = D_{HL}(H_L - H_{ex}) - \Delta H_{ex}, \tag{4.18}$$

where Δ is the isotropic loss of H_{ex} from this loosely defined neighbourhood. Writing in a dimensionless form using equations (4.11) and (4.14) we obtain

$$\frac{d\zeta}{d\tau} = \eta - D\zeta, \tag{4.19}$$

where

$$\zeta = H_{ex}\frac{\alpha_L\beta_L\beta_{HL}}{\gamma_{mL}D_{HL}^2 K_D^2} \ , \ D = \Delta\frac{\gamma_{mL}D_{HL}K_D}{\alpha_L\beta_L\beta_{HL}} \ , \ K_D = \frac{k_L^-}{k_L^+}. \tag{4.20}$$

Additionally, we construct a chain of otherwise identical systems, (η_i, ζ_i), for $i = 1, 2, \ldots$, coupled via the external concentrations of HSL in the local neighbourhood of each cell.

$$\frac{d\zeta_i}{d\tau} = \eta_i - D\left((1 - 2d)\zeta_i + d\sum_{j=\pm 1}(\zeta_i - \zeta_{i+j}) \right)$$

$$= \eta_i - D\left(1 - \zeta_{i-1} - \zeta_{i+1}\right), \tag{4.21}$$

where ζ is the rescaled H_{ex} variable and d is now the fraction of the isotropic single loss that is retained in the single cell-cell interchange.

In this simplified system we can investigate whether it is possible for a single cell $i = 1$ to propagate a signal. To do this we trigger an arbitrary gain in the HSL, sufficient to trigger an excitable response from system $i = 1$, and examine the downstream impact. To do this we increase the levels of HSL by two orders of magnitude from the low steady state (QS off) for the equivalent lifetime of a single cell (corresponding to one dimensionless time unit) after the cells reach steady-state. Three types of solution are presented in Fig. 4.5, illustrating a range of behaviour from no propagation of the signal for small coupling, propagation of a pulse for intermediate coupling, to propagation from a mutually supported high steady state (QS on) for large coupling.

4.5 Discussion

We have described a model of the QS system in *P. aeruginosa* by considering non-linear positive and negative feedback loops associated with the production of the synthase LasI and the regulator RsaL (Fagerlind et al, 2005; Pearson et al, 1997; Rampioni et al, 2007b). These non-linear effects create the possibility of novel dynamical behaviours in the model. We have created a dimensionless set of equations to describe these behaviours and explored

how the five dimensionless parameters affect the results whilst maintaining biological plausibility. Where possible we have taken parameters from the biological literature and this has led to significant deviation in our parameter choices from existing mathematical biology manuscripts, notably the work of Fagerlind et al (2005); Fagerlind (2008), which needs commenting upon. When the parameters in these articles, which subsequently have been adopted in other later texts, were compared to biological estimates (presented for example in Alon (2006)) they were found to be significantly different. For example the parameters used in (Fagerlind et al, 2005) suggest that the typical lifetime of a transcription factor is of the order of seconds, when biological estimates typically describe transcription factors as stable proteins with lifetimes of the same order as the cellular turnover time, i.e. hours for *Pseudomonas aeruginosa*. Furthermore, it suggests mRNA molecules are *more* stable than the proteins they are translated to, which is clearly at odds with biological knowledge about the bursty nature of protein production (Xie et al, 2008).

We are confident that our dimensionless parameters thus lie within a biologically plausible region, though we acknowledge that the effects we report here are sensitive to the values of these parameters. An additional complication is the possibility of other functional forms for the rate of transcription of mRNA from the *lasI* and *rsaL* genes as a function of the active forms of both LasR and RsaL. The form we present is one from a family of different choices that result in the same qualitative behaviour: our analysis, presented in detail in the next chapter (section 5.5), suggests that competitive binding between RsaL and LasR is a requirement for excitability but symmetrical effects, resulting in the negative action of RsaL on its own production, are not required (as is shown on many diagrams of the *las* system (Dockery and Keener, 2001)). In the absence of specific biochemical data of this relationship at the intergenic region our analysis represents a significant step forward in incorporating biochemical knowledge in mathematical models of quorum sensing. There are biological instances where the binding in the intergenic region decouples and the *rsaL* and *lasI* genes are promoted and repressed independently, notably in the genetic isolates obtained from cystic fibrosis patients (Rampioni et al, 2007b). In this case the mathematical modelling of the system becomes trivial as the two systems are decoupled, and there is no possibility of excitation.

A survey of a realistic region of parameter space revealed a range of interesting numerical solution behaviour, such as limit cycles. The full equations, without approximations to reduce the number of equations, were also solved numerically and revealed similar solution behaviour (not shown). Continuation methods were employed for the reduced system in the a_1-a_3 plane to track bifurcations of the system of co-dimension one and two. The parameters a_1 and a_3 represent the information outside and inside the cell, respectively. We found fold

and Hopf bifurcations, both of co-dimension one. Furthermore, there are Bogdanov-Takens and generalized Hopf bifurcations, each of co-dimension two. For example, at a Bogdanov-Takens bifurcation, Hopf and fold curves in the plane intersect. However, most of the complex bifurcation structure is confined to a relatively small region of parameter space; the dominant behaviour is that of the fold bifurcation outside which are regions of excitable solutions.

We have demonstrated the potential for the *las* system to act as a pulse generator. As there is no explicit feedback from *rhl* to *las*, we may consider the *las* system as a black-box controller for the *rhl* system. We have demonstrated that this can lead to the generation of a pulse train when the individual cells are coupled by diffusion of the HSL signal molecule. These observations allow for a novel stigmergy (Gloag et al, 2015) in the coupled *las/rhl* system; that of a *quorum memory*. The *las* system is coupled to the *rhl* system in two distinct ways; the active LasR transcription factor promotes the transcription of its counterpart in the *rhl* system, RhlR, and due to competitive binding on the RhlR molecule of the two homoserine lactones the presence of 3-oxo-C12-HSL acts to prevent the activation of RhlR by C4-HSL. This creates an interesting unreported effect in the combined system: what one might call a 'handbraked acceleration'. Assuming the *rhl* system follows the same Lux-like dynamics of the *las* system the additional production of RhlR increases the likelihood of the system switching to its higher steady state, but this is tempered, or handbraked, by the presence of significant amounts of 3-oxo-C12-HSL preventing the activation of the rhlR system and its downstream consequences, notably rhamnolipid production. However, the effect of the pulses (the 'revs' of the 'acceleration') is still to increase the amount of RhlR, sustained due to its relative stability compared to the diffusing homoserine lactones, so that when the handbrake of 3-oxo-C12-HSL is removed the system has an increased likelihood of activating the *rhl* system. In effect the cells have been primed by the pulses and thus have a memory of experiencing higher densities of cells (or low diffusion regions (Redfield, 2002)). Cells will lose memory only when they no longer experience a local environment rich in the 3-oxo-C12-HSL from the *las* system. Therefore, the competition between the two signal molecules, one produced by the *las* system and the other produced by the *rhl* system, may enable cells to trigger rhamnolipid production only when they are at the edge of an established aggregation. This suggests a previously unreported reason for the coupled nature of the *las* and *rhl* systems and a mechanism for how they act in tandem to create a sophisticated control system for sociality and virulence in this important pathogenic organism.

4.6   Note

This chapter is a paper that has been published, Alfiniyah et al (2017). The appendixes of this paper will be discussed in the next chapter (Chapter 5).

Chapter 5

Further analysis and downstream impact of the *las* system

5.1 Introduction

The quorum sensing (QS) system of *P. aeruginosa* consists of two circuits, the *las* and *rhl* system. The theoretical studies of both systems has been discussed in the chapter 2. We have also explored and analysed the *las* system model in the chapter 4. This chapter consists of three big sections providing further investigation of QS system in *P. aeruginosa* as a continuation of the previous chapters. Those sections are further analysis of the *las* system, binding inhibition in the *las* system and downstream impact on the *rhl* system.

The first *P. aeruginosa* QS subsystem, *las* system, is composed of synthase LasI, inhibitor RsaL, autoinducer 3O-C12-HSL, and regulator LasR that binds autoinducer to form complex of LasR/3O-C12-HSL (Pesci et al, 1997). In section 5.2 - 5.4, we provide further analysis of the *las* system. The activator and repressor in the *las* system interact through positive and negative feedback loops. In order to understand the functional implications of such feedback loops, positive and negative feedback loops are investigated using bifurcation analysis in the previous chapter (chapter 4). Bifurcation analysis revealed bistability and oscillations. The stability of steady states and oscillations could be changed by parameter values. In this chapter, we demonstrated detailed investigation of phase diagrams corresponding to the labelled regions in the two-dimensional diagram that has been presented in the chapter 4. Furthermore, we also investigate the *las* system through employing another assumption, such as H_{ex} is zero.

The RsaL transcriptional regulator is encoded by *rsaL* genes. By binding the promotor of *lasI*, it represses LasI expression (De Kievit et al, 1999). In section 5.5, we show the possibilities for binding types in the inhibition of the *las* system. Then, we investigate mathematical forms in the equation that associate with all those variations.

The second *P. aeruginosa* QS subsystem, *rhl* system, is composed of synthase RhlI, autoinducer C4-HSL, and regulator RhlR that binds autoinducer to form complex of RhlR/C4-HSL (Pesci et al, 1997). The *rhl* system regulates production of rhamnolipid (Chen et al, 2004). The diagram of the QS system of *P. aeruginosa* (Fig. 4.1) shows that the LasR/3O-C12-HSL complex activates the expression of *rhlR*, which places the *las* system in a cell signalling hierarchy above the *rhl* system. Thus in section 5.6, we also briefly explore the downstream impact of *las* to the *rhl* system. Then, we can see the dynamics of the bacterial colony growth due to rhamnolipid production as a product of *rhl* system in the next chapter.

5.2   Phase diagrams of the *las* system model

We have analysed the fixed points and bifurcations of the system. There is a complex structure of bifurcation in the system, including co-dimension one and two bifurcations. The detailed explanation of bifurcation analysis has been demonstrated in the section on bifurcation in the previous chapter. In this section, we provide further investigation of the structure of two-dimensional bifurcation diagram for (a_1, a_3) parameter plane. As we know that phase plane analysis is one of the most popular techniques for investigating the behaviour of nonlinear system, since there is usually no analytical solution.

The (a_1, a_3) parameter plane is divided by bifurcation lines into six regions (see Fig. 4.4). The six corresponding phase diagrams of the dynamic solution behaviour for LasI and RsaL are illustrated below. In order to get clear understanding of qualitative behaviour for region $\mathcal{R}_1$ to $\mathcal{R}_4$, we fix parameter values for a_1, a_2, a_4, a_5 (see Table 4.3) and vary a_3 from a high to a low value. For figure 5.1a to 5.1i, $a_3 = 0.6, 0.3, 0.281, 0.28, 0.278, 0.275, 0.27, 0.2$, and 0.1, respectively.

In the region $\mathcal{R}_1$, the system has a single low stable steady state, i.e. with 0 eigenvalues with positive real part. In this region, solutions have two qualitatively different behaviours (see Fig. 5.1a and 5.1b). The difference between those two behaviours is that the large perturbation in Fig. 5.1b has a large excursion around the phase plane before it reaches the stable fixed point. In the region $\mathcal{R}_2$ after a saddle-node bifurcation, system has 0, 1, and 2 eigenvalues with positive real part in the low, middle and high steady states, respectively. Thus it consists of one stable low fixed point, one saddle and one unstable fixed point. There is a change from unstable fixed point to unstable spiral (see Fig. 5.1c and 5.1d).

In the region $\mathcal{R}_3$ after a sub-critical Hopf bifurcation, the system has 0, 1, and 0 eigenvalues with positive real part in the low, middle and high states, respectively. In this region, the system has four different qualitative behaviours. Upon decreasing a_3, the journey of qualitative dynamical behaviour can be seen clearly in Fig 5.1e, 5.1f, 5.1g, and 5.1h. First, the unstable limit cycle coexists with one saddle and two stable steady states (see Fig. 5.1e).
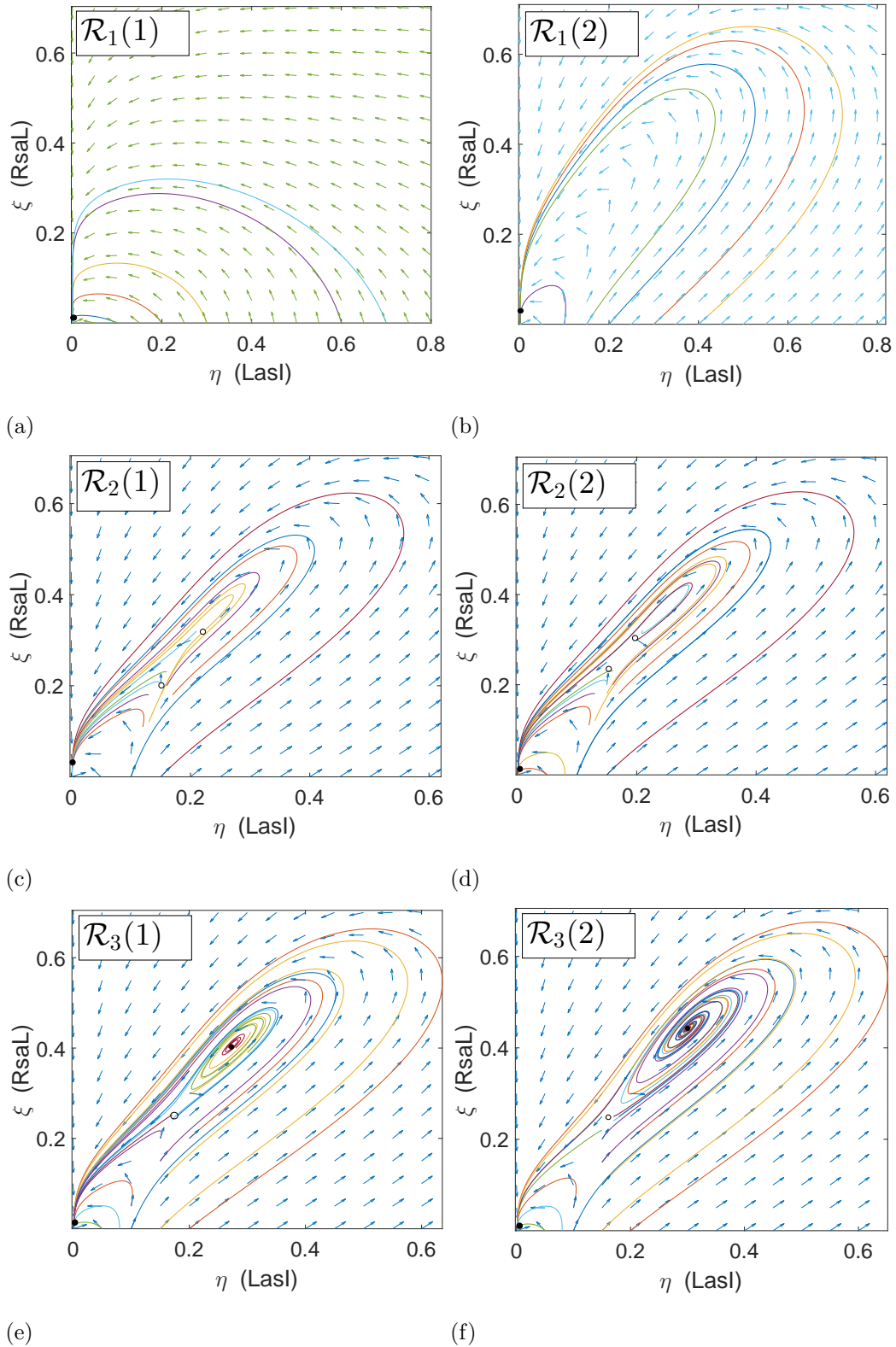
Figure 5.1: Phase diagram corresponding to the labelled regions in Figure 4.4 (figure a and b in region $\mathcal{R}_1$; figure c and d in region $\mathcal{R}_2$; figure e, f, g, and h in region $\mathcal{R}_3$; figure i in region $\mathcal{R}_4$; figure j in region $\mathcal{R}_5$). Stable (unstable) steady states are denoted by solid (open) circles.

(g)

(h)

(i)

(j)
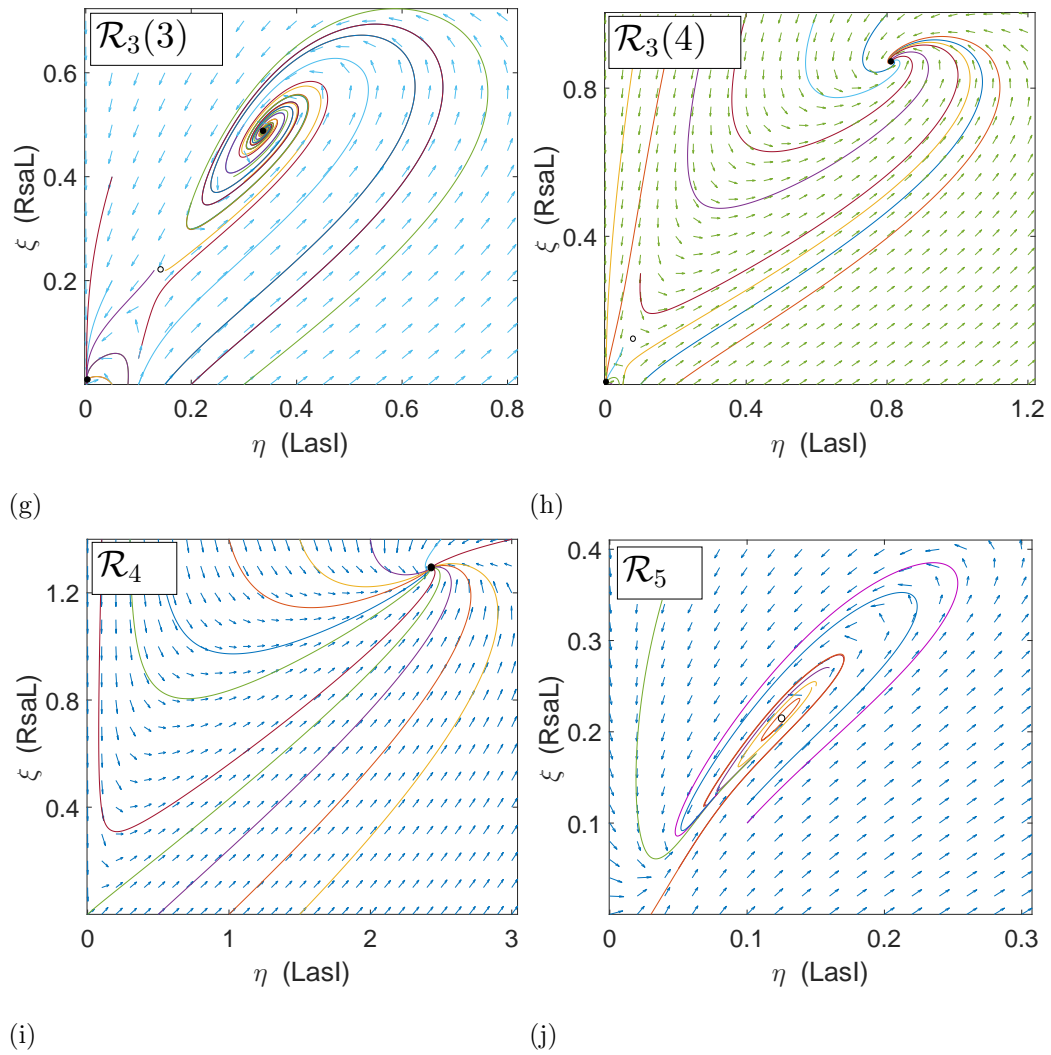
Figure 5.1: Phase diagrams... (continued)

Then, a homoclinic bifurcation occurs (a collision between the unstable limit cycle and the saddle; see Fig. 5.1e) resulting in a high state stable spiral with large basin of attraction (see Fig. 5.1f). Lastly, the saddle node moves closer to the low stable fixed point (see Fig. 5.1h) eventually colliding via a saddle-node bifurcation to yield region $\mathcal{R}_4$. This system has one high state fixed point with 0 eigenvalues with positive real part (see Fig. 5.1i).

Furthermore we find two other regions, $\mathcal{R}_5$ and $\mathcal{R}_6$. In region $\mathcal{R}_5$, a stable limit cycle and one unstable steady state exists (see Fig. 5.1j, $a_1 = 0.03298, a_2 = 0.3, a_3 = 0.3226, a_4 = 0.4$ and $a_5 = 0.075$). In region $\mathcal{R}_6$ the system has one unstable and two stable fixed points, but the region is very small as it is close to the cusp where the two saddle-node bifurcations collide.

5.3   Dynamics of the full system

(a)   (b)
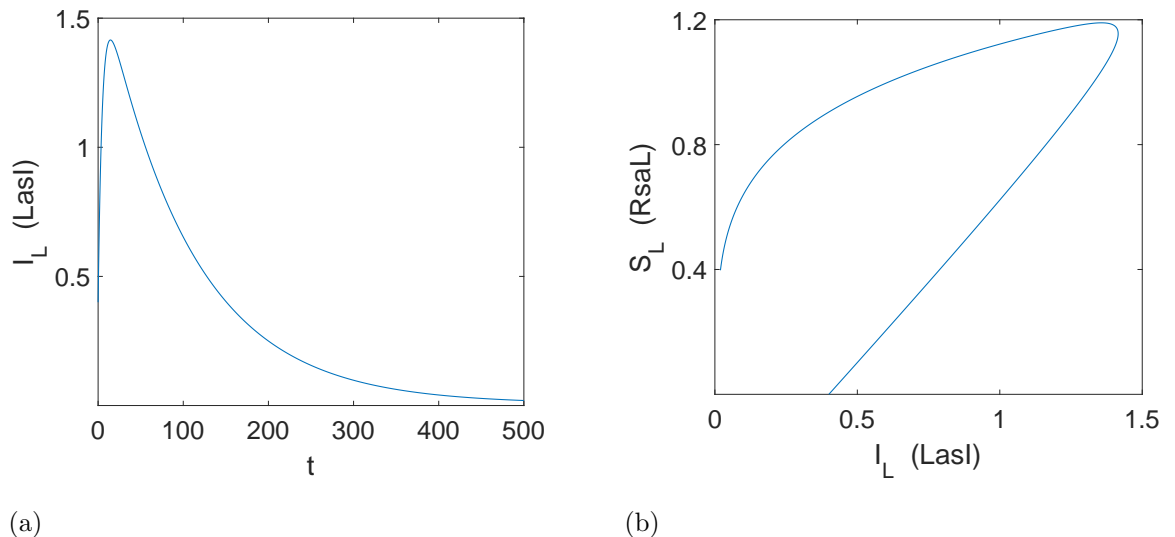
Figure 5.2: (a) Time-dependent solutions from the full system of equations before systematic reduction, corresponding to the excitable trajectory of LasI. (b) Excitable dynamics in the LasI-RsaL phase plane. As a full system, all parameters are available in table 4.2

The reduced model of the QS system for *P. aeruginosa* explored in the previous chapter reveals the potential for excitable pulse generation in the *las* subsystem. Numerical solution of the full system of seven differential equations reveals very similar solution behaviour, including excitable pulse generation. Excitation occurs when there is a sufficiently large perturbation of (N-(3-oxododecanoyl)-HSL) leading to pulse production of LasI, pushing the system to the right in the LasI-RsaL projected phase plane. Typically, this is followed by a large excursion around phase space before returning to the stable fixed point (see Fig. 5.2a and 5.2b). Other solutions are also possible analogous to those in the reduced system. These results provide confidence that the behaviour of the full system has been adequately

captured by the reduced model.

5.4 Dynamics of the system if H_{ex} equals 0

In this section we present the dynamics and stability analysis of the system if the concentration of extracellular signal equals zero, which is for mathematical simplicity.

We have tried many possibilities of the assumptions in the system before we demonstrated our published system in chapter 4, for example we assume the concentration of extracellular signal is very small, $H_{ex} \simeq 0$. In preliminary construction of the published model, we also explored the system with no binding of RsaL to the intergenic region between the *lasI* and *rsaL* operons for analytic simplicity. In this case, the functional form for the transcription is not identical to that presented in the previous chapter, having a Hill coefficient of one. From the numerical results obtained with these assumptions, we demonstrated that it also reveals the potential for excitable pulse generation in the *las* subsystem.

By assuming there is no basal production ($\beta_{L0} = 0$ and $\beta_{S0} = 0$), and also that the concentration of extracellular signal molecule is very small $H_{ex} = 0$, we can simplify the system of equations for the *las* system. Moreover, we do not employ that protein RsaL binds to the same intergenic region between *lasI* and *rsaL*, the governing system becomes

$$\frac{dI_L}{dt} = \frac{\alpha_L \beta_L R_{L0}^2 \beta_{HL}^2}{\gamma_{mL}} \left(\frac{I_L^2}{K_L^2 \left(1 + \frac{S_L}{K_{SL}}\right)^2 \left(D_{HL}\frac{k_L^-}{k_L^+} + \beta_{HL}I_L\right)^2 + R_{L0}^2 \beta_{HL}^2 I_L^2} \right) \tag{5.1}$$
$$- \gamma_{IL}I_L,$$

and

$$\frac{dS_L}{dt} = \frac{\alpha_S \beta_S R_{L0} \beta_{HL}}{\gamma_{mS}} \left(\frac{I_L}{R_{L0}\beta_{HL}I_L + K_S \left(D_{HL}\frac{k_L^-}{k_L^+} + \beta_{HL}I_L\right)} \right) - \gamma_S S_L, \tag{5.2}$$

where equations 5.1 and 5.2 refer back to the chapter 4. If we nondimensionalize this model by writing

$$\eta = \frac{\beta_{HL}}{\frac{k_L^-}{k_L^+} D_{HL}} I_L, \qquad \xi = \frac{1}{K_{SL}} S_L, \qquad \text{and} \qquad \tau = \frac{\alpha_L \beta_L \beta_{HL} k_L^{+2}}{\gamma_{mL} D_{HL} k_L^{-2}} t. \tag{5.3}$$

(5.1) and (5.2) become

$$\frac{d\eta}{d\tau} = \frac{\eta^2}{a(1 + \xi)^2 (1 + \eta)^2 + \eta^2} - b\eta, \tag{5.4}$$
$$\frac{d\xi}{d\tau} = \frac{c\eta}{h\eta + 1} - g\xi, \tag{5.5}$$

where

$$a = \frac{K_L^2}{R_{L0}^2}, \qquad\qquad b = \frac{\gamma_{mL}\gamma_{IL}D_{HL}k_L^-}{\alpha_L\beta_L\beta_{HL}k_L^+}, \qquad (5.6)$$

$$c = \frac{\gamma_{mL}D_{HL}\alpha_S\beta_S R_{L0}k_L^-}{\alpha_L\beta_L\beta_{HL}K_{SL}\gamma_{mS}K_S k_L^+}, \qquad\qquad h = \frac{R_{L0}}{K_S} + 1,$$

$$g = \frac{\gamma_{mL}\gamma_S D_{HL}k_L^-}{\alpha_L\beta_L\beta_{HL}k_L^+}.$$

Here a, b, c, g and h are positive constants. The biological interpretation of this model is ξ inhibits η through the term $\frac{d\eta}{d\tau}$, and both η and ξ are degraded linearly proportional to their concentration. These are $-b\eta$ and $-g\xi$ terms. The term $\frac{\eta^2}{a(1+\xi)^2(1+\eta)^2+\eta^2}$ shows negative feedback by ξ on the production of η, since an increase in ξ decreases the production of η, and hence indirectly reduces itself. This system represents feedback inhibition.

The nullclines for concentrations η, ξ are solutions of $\frac{d\eta}{d\tau} = 0$ and $\frac{d\xi}{d\tau} = 0$, namely

$$\dot{\xi} \;=\; 0 \Longrightarrow \xi = \frac{\frac{c}{g}\eta}{h\eta + 1}, \qquad (5.7)$$

$$\dot{\eta} \;=\; 0 \Longrightarrow \eta = 0 \quad \text{or} \quad \eta = b\left(\eta^2 + a\left(1+\xi\right)^2\left(1+\eta\right)^2\right). \qquad (5.8)$$

From equation (5.8), we have

$$\frac{\eta}{b} - \eta^2 = a\left(1+\xi\right)^2\left(1+\eta\right)^2 \quad \Rightarrow \quad \xi = \sqrt{\frac{\frac{\eta}{a}\left(\frac{1}{b}-\eta\right)}{\left(1+\eta\right)^2}} - 1. \qquad (5.9)$$

5.4.1   Stability analysis of the system if H_{ex} equals 0

We have Jacobian matrix to investigate stability of fixed points derived from equation (5.1) and (5.2),

$$J(x,y) = \begin{bmatrix} \frac{\partial}{\partial \eta}\frac{d\eta}{d\tau} & \frac{\partial}{\partial \xi}\frac{d\eta}{d\tau} \\[2mm] \frac{\partial}{\partial \eta}\frac{d\xi}{d\tau} & \frac{\partial}{\partial \xi}\frac{d\xi}{d\tau} \end{bmatrix}, \qquad (5.10)$$

where

(i) $\frac{\partial}{\partial \eta}\frac{d\eta}{d\tau} = \frac{2\eta}{a(1+y)^2(1+\eta)^2+\eta^2} - \frac{\eta^2\left(2a(1+\xi)^2(1+\eta)+2\eta\right)}{\left(a(1+\xi)^2(1+\eta)^2+\eta^2\right)^2} - b,$

(ii) $\frac{\partial}{\partial \eta}\frac{d\xi}{d\tau} = \frac{c}{h\eta+1} - \frac{hc\eta}{(h\eta+1)^2},$

(iii) $\frac{\partial}{\partial \xi}\frac{d\eta}{d\tau} = -\frac{2\eta^2 a(1+\xi)(1+\eta)^2}{\left(a(1+\xi)^2(1+\eta)^2+\eta^2\right)^2},$ and

(iv) $\frac{\partial}{\partial \xi}\frac{d\xi}{d\tau} = -g.$

Lets look at the fixed point at $(0,0)$,

$$j(0,0) = \begin{bmatrix} -b & 0 \\ e & -g \end{bmatrix}, \qquad (5.11)$$

It can be clearly seen that $\lambda_1, \lambda_2 < 0$ in which $b, g \in \mathbb{R}^+$. Thus fixed point $(0,0)$ is always stable.

(a)

(b)

(c)
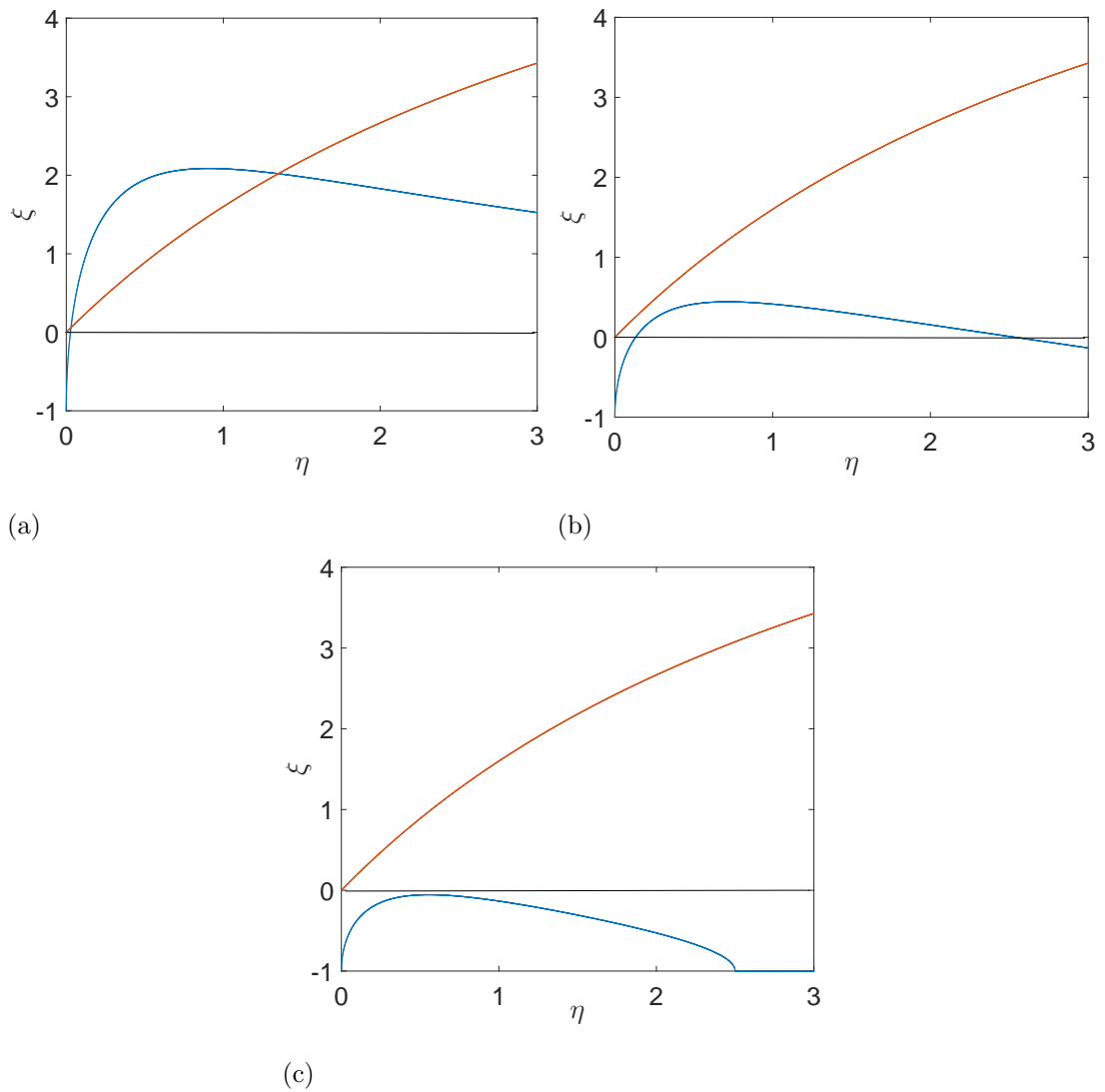
Figure 5.3: Phase plane for model system (5.4) and (5.5). As the parameter vary there can be (a) three real roots solutions for $b = 0.08$, (b) one real root solution excitable for $b = 0.2$ and (c) one real root solution unexcitable for $b = 0.6$. Here $a = 0.3$, $h = 2.1$, $c = 0.4$ and $g = 0.05$.

For another fixed points, $\frac{d\eta}{d\tau} = 0$ and $\frac{d\xi}{d\tau} = 0$, we have $\xi = \frac{\sqrt{\eta/b-\eta^2}}{\sqrt{a}(1+\eta)} - 1$ and $\xi = \frac{c/g}{h\eta+1}\eta$ respectively. By using *Descartes'* rule of signs, the equation of the system $(h^2 + 2hk + k^2 + \frac{1}{a}h^2)\eta^4 + (2h^2 + 2k^2 + 4hk + 2h + 2k - \frac{1}{ab}h^2 + \frac{2h}{a})\eta^3 + \left(4h + 4k + 2 - \frac{2h}{ab}\right)\eta^2 + \left(2h + 2k + 2 - \frac{1}{ab} + \frac{1}{a}\right)\eta + 1 = 0$ where $k = \frac{c}{g}$, has two possibilities about the number of sign changes. Assume $h, k, a, b > 0$, the coefficient of η^4 is always positive value, but the coefficient η^3, η^2 and η is possible to have negative value. Consequently, the equation has two or four sign changes.

- *The equation has two sign changes* : It has two or zero positive real roots. If it has two positive real roots, then it has no non real roots. Conversely, It has two non real roots when it has no real root.

- *The equation has four sign changes* : It has four, two or zero positive real roots.

The dimensionless model's parameters, $a, b, c, h,$ and g are composed of parameters in dimensionalization system. It reveals that the value of parameters a and b are much smaller than h. Those parameters determine the coefficient value of η, η^2 and η^3. The coefficient value of η^2 is negative and coefficient value of η^3, η are positive. Thus it is likely that the equation of system has two sign changes. In this system, there are three possibilities. Fig. 5.3a shows the system has two positive root, but Fig. 5.3b and 5.3c show the system has no positive roots.

There is important condition such that it is possible to have an interesting nullclines structure. The excitability is caused by the $\dot{\eta}$ nullcline having cubic shape, so it must have two turning points, $\xi = \frac{\sqrt{\eta/b-\eta^2}}{\sqrt{a}(1+\eta)} - 1$ from (5.4) and $\frac{d\xi}{d\eta}$ that is

$$\frac{d\xi}{d\eta} = \frac{\frac{1}{b} - \eta\left(\frac{1}{b} + 2\right)}{2\sqrt{a}(1+\eta)^2\sqrt{\frac{\eta}{b} - \eta^2}}, \tag{5.12}$$

ξ does not appear in derivative so the condition for two turning points come from $\frac{d\xi}{d\eta} = 0$, such that

$$\frac{1}{b} - \eta\left(\frac{1}{b} + 2\right) = 0,$$

$$\eta = \frac{b}{1 + 2b}. \tag{5.13}$$

By substituting (5.13) into (5.9), it yields

$$\xi|_{\eta \text{ max}} = \frac{\sqrt{\frac{1}{b(1+2b)} - \left(\frac{1}{1+2b}\right)^2}}{\sqrt{a}\left(1 + \frac{1}{1+2b}\right)} - 1,$$

$$= \frac{\sqrt{\frac{1+b}{b}}}{\sqrt{a}(2b+2)} - 1,$$

$$= \frac{1}{\sqrt{4ab(1+b)}} - 1. \tag{5.14}$$

The excitability occures when $\xi|_{\eta \ max} > 0$. Thus

$$\frac{1}{\sqrt{4ab(1+b)}} - 1 > 0 \tag{5.15}$$

$$\begin{aligned} &\Leftrightarrow \quad b\,(b+1) < \frac{1}{4a} \\ &\Leftrightarrow \quad \left(b+\frac{1}{2}\right)^2 < \frac{1}{4}\left(\frac{1}{a}+1\right) \\ &\Leftrightarrow \quad \frac{-\sqrt{1+1/a}-1}{2} < b < \frac{\sqrt{1+1/a}-1}{2} \end{aligned} \tag{5.16}$$

Lets take the case for one fixed point, which potentially has excited stability. There is one fixed point when the condition $\eta - b\left(\eta^2 + a\,(1+\xi)^2\,(1+\eta)^2\right) = 0$ has no real roots, which is $\xi = \frac{\frac{c}{g}\eta}{h\eta+1}$. In addition, the term $h\eta$ in the equation for ξ determines the stability of the system. By plotting and analysing the solutions for different values $(h\eta \gg 1, h\eta \ll 1$ and $h\eta \sim 1)$, we determine the stability for every case and find relation between the production of AHL signal molecules and the inhibitor's dissociation constant for the process of binding RsaL to the *lasI* gene.

- Case I (Fig. 5.3a)

  If $h\eta \gg 1$ at intersection then $\xi \simeq \frac{k}{h}$, where $k := c/g$. Thus there is bifurcation when $\frac{1}{\sqrt{4ab(1+b)}} - 1 = \frac{k}{h}$

  The stability of the three fixed points can be seen in Fig. 5.3a. There are two stable and one unstable steady states. The highest steady state represents the production of a lot of LasI protein.

- Case II (Fig. 5.3b)

  The excitable stability occurs when the system has condition $\frac{d\eta}{d\tau} = 0$ in which the maximum of the inner null clines is positive. If $h\eta \ll 1$ at intersection then $\xi \simeq k\eta$, where $k := c/g$. Therefore, we have

  $$\frac{\sqrt{\eta/b - \eta^2}}{\sqrt{a}\,(1+\eta)} - 1 = k\eta, \tag{5.17}$$

  and

  $$\frac{\frac{1}{b} - \eta\left(\frac{1}{b}+2\right)}{2\sqrt{a}\,(1+\eta)^2\,\sqrt{\frac{\eta}{b}-\eta^2}} = k. \tag{5.18}$$

  From (5.17), we have

  $$\sqrt{\eta/b - \eta^2} = (k\eta+1)\,\sqrt{a}\,(1+\eta), \tag{5.19}$$

  and substituting into (5.18), yields

  $$b = \frac{1-\eta}{2\left(ak\,(1+\eta)^3\,(k\eta+1)+\eta\right)}. \tag{5.20}$$

By substituting b into (5.19), such that

$$2a\eta \left(1 + \eta\right)^3 k \left(k\eta + 1\right) + 2\eta^2 - \eta^2(1 - \eta) - a(k\eta + 1)^2(\eta + 1)^2(1 - \eta) = 0. \quad (5.21)$$

Equation (5.21) obtains

$$k_1 = \frac{-2a\eta^2 - 2a\eta + \sqrt{\varphi}}{a \left(3\eta^2 + 4\eta + 1\right)\eta}, \quad (5.22)$$

and

$$k_2 = -\frac{2a\eta^2 + 2a\eta + \sqrt{\varphi}}{a \left(3\eta^2 + 4\eta + 1\right)\eta}, \quad (5.23)$$

where $\varphi = a^2\eta^4 + 4a^2\eta^3 - 3a\eta^4 + 6a^2\eta^2 - 4a\eta^3 + 4a^2\eta - a\eta^2 + a^2$.

By applying the values of k_1 and k_2 into b, we will get equation for b_1 and b_2.

There is an interesting nullcline structure (see Fig. 5.3b). In terms of qualitative behaviour, small and large perturbations would lead to different RsaL concentrations.

- Case III (Fig. 5.3c)

  If $h\eta \sim 1$ at intersection, then $\xi \simeq \frac{k\eta}{2}$, where $k := c/g$. Therefore, we have

  $$\frac{\sqrt{\eta/b - \eta^2}}{\sqrt{a}\left(1 + \eta\right)} - 1 = \frac{k\eta}{2}, \quad (5.24)$$

  and

  $$\frac{1/b - \eta \left(1/b + 2\right)}{2\sqrt{a}\left(1 + \eta\right)^2 \sqrt{x/b - x^2}} = \frac{k}{2}. \quad (5.25)$$

  From (5.24), we have

  $$\sqrt{\eta/b - \eta^2} = \left(\frac{k\eta}{2} + 1\right)\sqrt{a}\left(1 + \eta\right), \quad (5.26)$$

  and substituting into (5.25), yields

  $$b = \frac{1 - \eta}{ak \left(1 + \eta\right)^3 \left(\frac{k\eta}{2} + 1\right) + 2\eta}. \quad (5.27)$$

  By substituting b into (5.26), such that

  $$a\eta \left(1 + \eta\right)^3 k \left(\frac{k\eta}{2} + 1\right) + 2\eta^2 - \eta^2(1 - \eta) - a(\frac{k\eta}{2} + 1)^2(\eta + 1)^2(1 - \eta) = 0. \quad (5.28)$$

  Equation (5.28) obtains

  $$k_1 = \frac{2\left(-2a\eta^2 - 2ax + \sqrt{\omega}\right)}{a \left(3\eta^2 + 4\eta + 1\right)\eta}, \quad (5.29)$$

  and

  $$k_2 = -\frac{2\left(2a\eta^2 + 2a\eta + \sqrt{\omega}\right)}{a \left(3\eta^2 + 4\eta + 1\right)\eta}, \quad (5.30)$$

  where $\omega = a^2\eta^4 + 4a^2\eta^3 - 3a\eta^4 + 6a^2x^2 - 4a\eta^3 + 4a^2x - a\eta^2 + a^2$.

  By applying the values of k_1 and k_2 into b, we will get equation for b_1 and b_2.

  This last case confirms that when the production of 3O-C12-HSL signal molecules tends to infinity, it will not have an effect on binding of RsaL to *lasI* and it is not excitable system. It diminishes to zero.
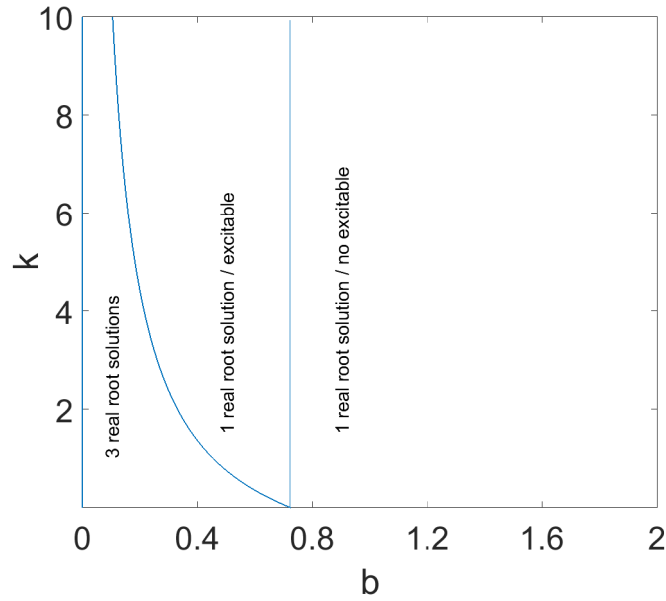
Figure 5.4: Three different regions that display effect of HSL signal molecule production to the inhibitor's dissociation constant of RsaL into *lasI* gene production.

Using the stability of the system from those three cases above, we can make a phase portrait that exhibits the solution in different regions of parameter space (see Fig. 5.4). The diagram shall display the relation between parameters b and k, in which b is proportional to the $\frac{1}{\beta_{HL}}$ and k is derived from parameter c over g, thus k is proportion to the $\frac{1}{K_{SL}}$. β_{HL} represents production rate of HSL and K_{SL} represents inhibitor's dissociation constant of RsaL into *lasI* gene.

We derive if inhibitor's dissociation constant high ($K_{SL} \to \infty$) then the value of parameter c is very small. Consequently, k also is very small (see eqn. 5.6). In addition, this condition makes I_L (production of LasI protein) is high, in which β_{HL} (production rate of signal molecules 3O-C12-HSL) has large value. Because β_{HL} is big, the value of parameter b is small (see eqn. 5.6). Thus the system has three fixed points that represent the value of inhibition rate of RsaL to *lasI* is large. Conversely, by using the same sequence of processes, if inhibitor's dissociation constant (K_{SL}) is low then b is very big ($b \to \infty$) and has no effect on the system. In other words, when the production of signal molecules 3O-C12-HSL tends to infinity (very big), it will not give effect on binding of RsaL to *lasI* and there is no excitable behaviour in the system.

Biological interpretations from the right to the left of Fig. 5.4, quorum sensing essentially on the "off" state. *lasI* increase the concentration of HSL and cross the multiple line of stability and jump up to the possibility of high production of *lasI* and switch QS to the "on" state.
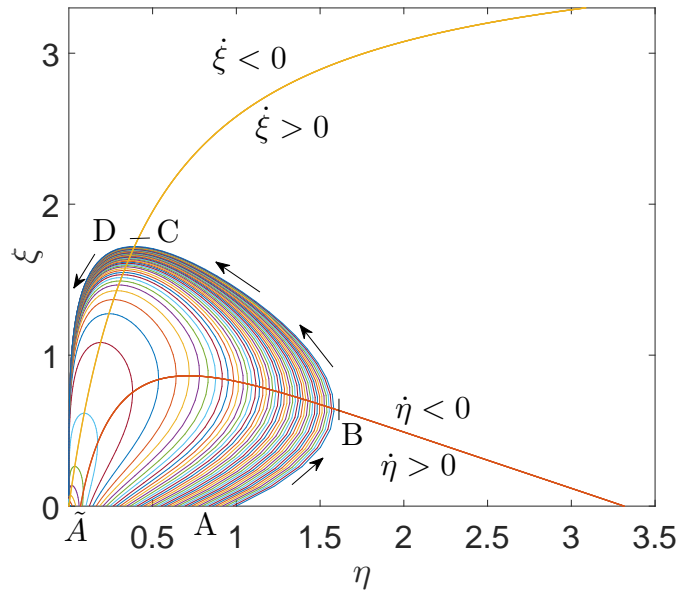
Figure 5.5: The phase portrait of model system for one fixed point. With a perturbation from the steady state $\eta = \xi = 0$ to a point $\tilde{A}$, the trajectory simply returns to the origin with η and ξ remaining small. A perturbation to A initiates a large excursion along $ABCD$ and then back to the $(0,0)$. Here, η and ξ represent the dimensionless forms of LasI and RsaL concentrations, respectively. Here $a = 0.3$, $b = 0.2$, $h = 2.1$, $c = 0.4$ and $g = 0.05$.

5.4.2   Excitability of system, if H_{ex} equals 0.

As shown in Fig. 5.3, there are three phase portraits of interest that can derive from the system. For the first case (Fig. 5.3a), it obtains common dynamical system behaviour in genes system. There will be a point of loop that is classic S-shape bifurcation diagram. Meanwhile for the third case (Fig.5.3c), it does not give interesting dynamical system behaviour in genes system. The small amount of production of LasI protein does not affect on the binding of RsaL to *lasI* due to the large value of inhibitor's dissociation constant. Therefore, we are interested in the second case (Fig. 5.3b). For this case, the dynamical system behaviour can be seen clearly through Fig. 5.5.

Consider the effect of a perturbation, Fig. 5.5 describes about an effective inhibition by RsaL to the LasI production in *las* system. If the production of 3O-C12-HSL is small enough (small perturbation is pointed by $\tilde{A}$; see Fig. 5.5), then the stability of the fixed point assures us that overtime will always return to the origin. The ξ variable will engage, deplete fast and return the system to the origin with a short loop. The interesting behaviour occurs when there is large production of 3O-C12-HSL (significant perturbation is pointed by A; see Fig. 5.5). η variable pushes the system, so that there is pulse production of 3O-C12-HSL. For the large perturbation, there is no short route back to the stable fixed point. The trajectory can no longer go directly back into the origin. This perturbation undergoes a large phase

trajectory excursion before returning to the origin. The concentration of RsaL increases with 3O-C12-HSL concentration held roughly constant. After that, the concentration of 3O-C12-HSL is able to decrease but RsaL still stays high. Finally, after an overshoot, RsaL concentration is able to decrease and together with 3O-C12-HSL concentration re-approach the fixed point from other side of the phase plane.

The results of excitable behaviour in Fig. 5.5 are plotted as a function of time in Fig. 5.6a and 5.6b where the blue and red-line represent either excitable and non-excitable trajectories for large and small perturbations, respectively.

(a)   (b)
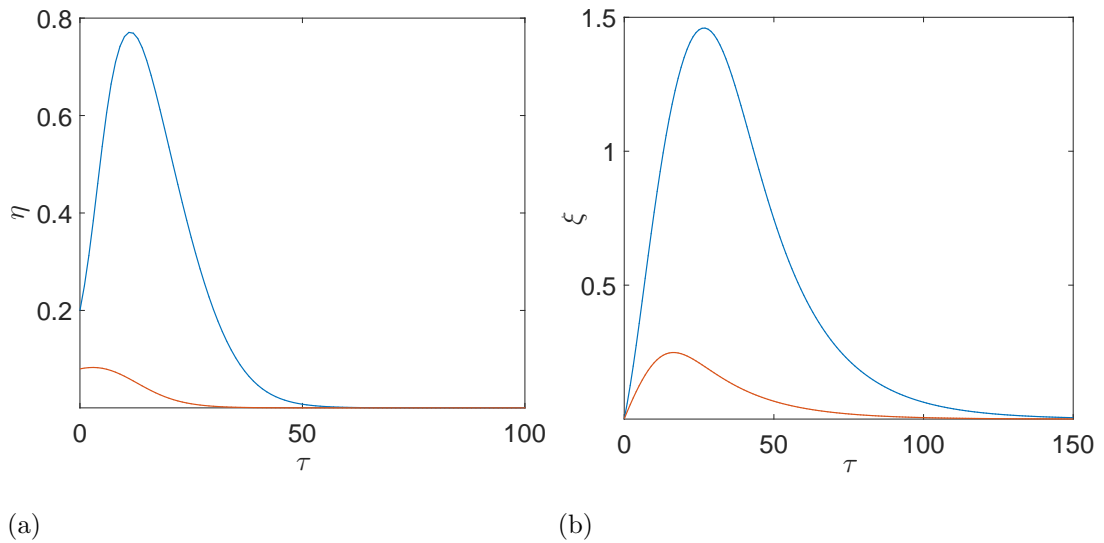
Figure 5.6: Stability of the excitable system, with large and small perturbations that are depicted by blue and red-line, respectively. (a) stability for LasI production and (b) stability for RsaL production. They represent time variation of η and ξ corresponding to the excitable trajectory. Here $a = 0.3$, $b = 0.2$, $h = 2.1$, $c = 0.4$ and $g = 0.05$, with initial condition $[\eta_0 , \xi_0] = [0.2 , 0.0001]$ and $[\eta_0 , \xi_0] = [0.08 , 0.0001]$ for large and small perturbations, respectively.

5.5   Binding inhibition in the *las* system

The *lasI* gene is activated by LasR/3O-C12-HSL complex, which constitutes part of the positive feedback loop and hence positively affects 3O-C12-HSL production. Not only positive feedback loop has important role in the QS signalling system of *P. aeruginosa*, but the QS response is also influenced by negative regulators of 3O-C12-HSL production.

It has been shown clearly in the diagram of QS signalling (see Fig. 4.2) the activation of both *lasI* and *rsaL* genes, which induce the production of synthase LasI and inhibitor RsaL, is regulated by complex of LasR/3O-C12-HSL. Moreover, the transcription *lasI* genes
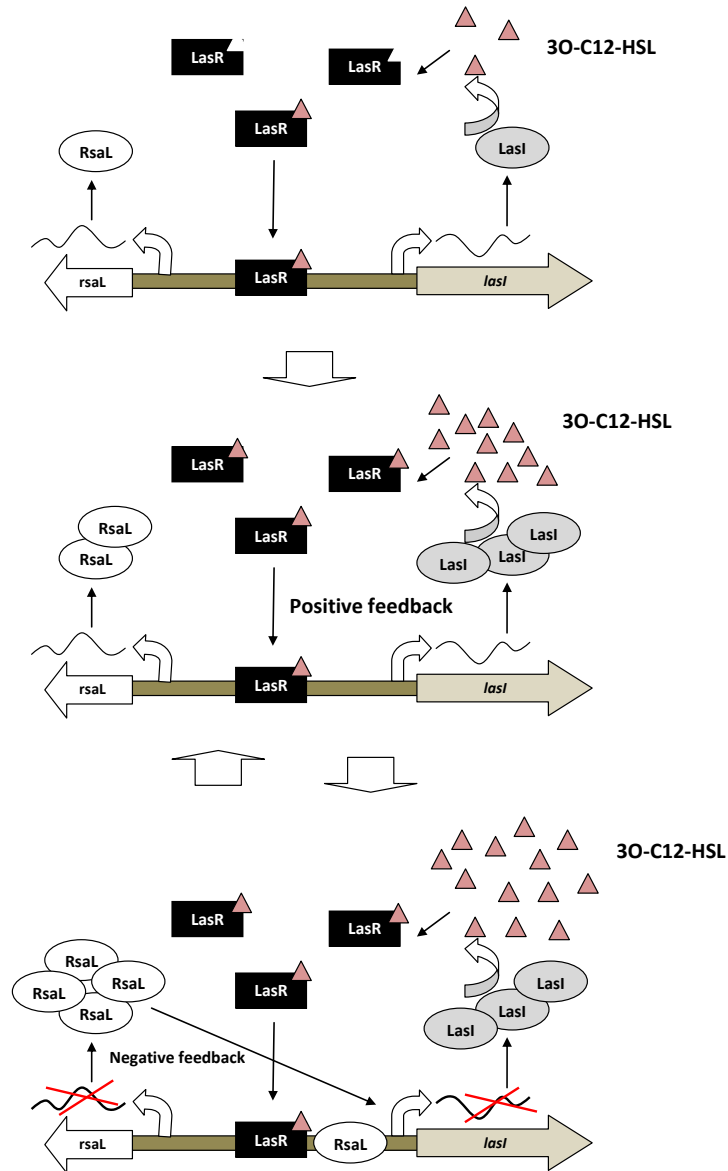
Figure 5.7: Schematic model of homeostasis mechanism in *P. aeruginosa*. Once autoinducer 3O-C12-HSL reach a quorum concentration, LasR binds the signal molecule and forms complex LasR/3O-C12-HSL. Then complex of LasR/3O-C12-HSL binds both *lasI* and *rsaL* in the intergenic region. The transcription of *lasI* induces the production of synthase LasI and hence positively affects the production of autoinducer 3O-C12-HSL. Meanwhile, The transcription of *rsaL* induces the production of inhibitor RsaL that represses the activation of *lasI* and hence negatively affects the production of autoinducer 3O-C12-HSL. After RsaL reach certain concentration, it does not repress the activation of *lasI* only, but also *rsaL*. Thus the system always in the homeostasis condition. Replotted and adopted (Rampioni et al, 2007b)

is regulated via binding of the two proteins (LasR/3O-C12-HSL complex and RsaL) to the same intergenic region between the *lasI* and *rsaL* operons. Rampioni et al (2007b) demonstrated a negative feedback by RsaL protein to that intergenic region and presented that process on graphical depictions of the *las* system (see Fig.5.7).

Rampioni et al (2007b) presented that transcription of *rsaL* is also dependent on the 3O-C12-HSL production. This *rsaL* transcription generates a negative feedback loop that counter acts the positive feedback loop. Therefore, this process implicitly always maintains the system in homeostasis condition. Furthermore, RsaL directly inhibits its own expression. Consequently, the level of this negative regulator is restricted for certain concentration. In homeostasis condition, the production of 3O-C12-HSL is also maintained by population of *P. aeruginosa* cells at an appropriate level in their environment. Moreover, bacterial cells is also able to change steady-state levels of 3O-C12-HSL to adapt to the changes in environmental condition.

In their previous publication, Rampioni et al (2007a) experimentally demonstrated that LasR and RsaL can bind to contiguous sites in the *rsaL-lasI* intergenic region. We can see in Fig. 5.7, how biochemical process of the *las* system reaches this stage.

In general, Rampioni et al (2007a) and Rampioni et al (2007b) has demonstrated the major function of RsaL in *P. aeruginosa*. They showed how *P. aeruginosa* cells govern the homeostasis of 3O-C12-HSL by controlling, in work out with LasR, the expression of both *lasI* and *rsaL* genes. They also successfully showed that RsaL is an integral part of the QS signalling network that regulates gene expression by non mutual mechanism, i.e. inhibition of 3O-C12-HSL signal molecule production.

However, there is insufficient biochemical evidence to determine whether the typical binding in the intergenic region is competitive, uncompetitive or non-competitive binding system. Furthermore, there is also no evidence whether the expression rates in each direction with all configurations of binding at the intergenic region displays symmetry or non-symmetry. Thus we try to investigate in more detail all of the possible binding types.

5.5.1   Possible types of binding inhibition in the *las* system

By definition, an enzyme inhibitor is a molecule that binds to an enzyme and decreases its activity (Cleland, 1963). They may broadly be classified as *reversible* and *irreversible* inhibitors. Irreversible inhibitors bind the target gene permanently. Irreversible inhibitors usually react and change the structure of the target gene chemically. Meanwhile, reversible inhibitors bind the target gene weakly. Reversible inhibitors only inhibit the activation of the enzyme and do not form any chemical bounds, is very rapid and can be easily removed (Rakesh, 2012).

RsaL is the key role of inhibition process in the *las* system. RsaL inhibits the activation of *lasI* gene and do not change the structure of *lasI* chemically. In addition, the time-scale of binding is very short compared to the functional lifetime of the enzyme itself. Thus RsaL can be categorized as reversible inhibitor. There are several types of reversible inhibitions. Here, we restrict attention to competitive, uncompetitive and non-competitive inhibition. As a competitive inhibitor, RsaL will block the activation of *lasI* genes by LasR/3O-C12-HSL complex (see Fig. 5.8a). Meanwhile, as an uncompetitive inhibitor, RsaL will bind to the *lasI* genes somewhere other than the binding site for LasR/3O-C12-HSL complex (see Fig. 5.8b). A combination of both competitive and uncompetitive inhibition, such that the RsaL inhibitor binds the *lasI* gene or the LasR/3O-C12-HSL+*lasI* gene with different affinities is called non-competitive inhibition (see Fig. 5.8c); mixed-competitive is the same as non-competitive inhibition if the genes are bound with equal affinity. Furthermore, we also examined the behaviour of the system when the expression rates for *lasI* and *rsaL* genes are symmetric or non-symmetric.

5.5.2 Competitive inhibition

Competitive binding occurs when both the LasR/3O-C12-HSL enzyme and RsaL inhibitor compete for binding to the active sites of the *lasI* gene (see Fig. 5.8). Thus the governing equations result from a blockade of either positive or negative *lasI* gene interaction by either LasR/3O-C12-HSL or RsaL, respectively. Furthermore, this competitive inhibition can be classified into non-symmetric and symmetric binding based on expression rates for LasR/3O-C12-HSL to *lasI* and *rsaL* genes.

Due to the overlapping of binding sites, *lasI* is completely inactive when the RsaL inhibitor binds *lasI* genes. For the non-symmetric case, the affinity constant between LasR/3O-C12-HSL and *rsaL* is relatively small. Meanwhile, in the symmetric case the affinity constant between LasR/3O-C12-HSL and *rsaL* gene is identical to the affinity constant between LasR/3O-C12-HSL and the *lasI* gene. Referring to theories of enzyme action by Chaplin and Bucke (1990), the equation of the non-symmetric and symmetric competitive inhibition can be written in Eq. 5.31-5.32 and Eq. 5.35-5.36, respectively.

Non-symmetric competitive inhibition.

Here, the governing equations are

$$\frac{d\hat{I}_L}{dt} = \beta_L \frac{R_{LH}^2}{K_L^2(1 + S_L/K_{SL})^2 + R_{LH}^2} - \gamma_{mL}\hat{I}_L + \beta_{L0}, \qquad (5.31)$$

$$\frac{d\hat{S}_L}{dt} = \beta_S \frac{R_{LH}}{K_S + R_{LH}} - \gamma_{mS}\hat{S}_L + \beta_{S0}. \qquad (5.32)$$

(a)

(b)

(c)
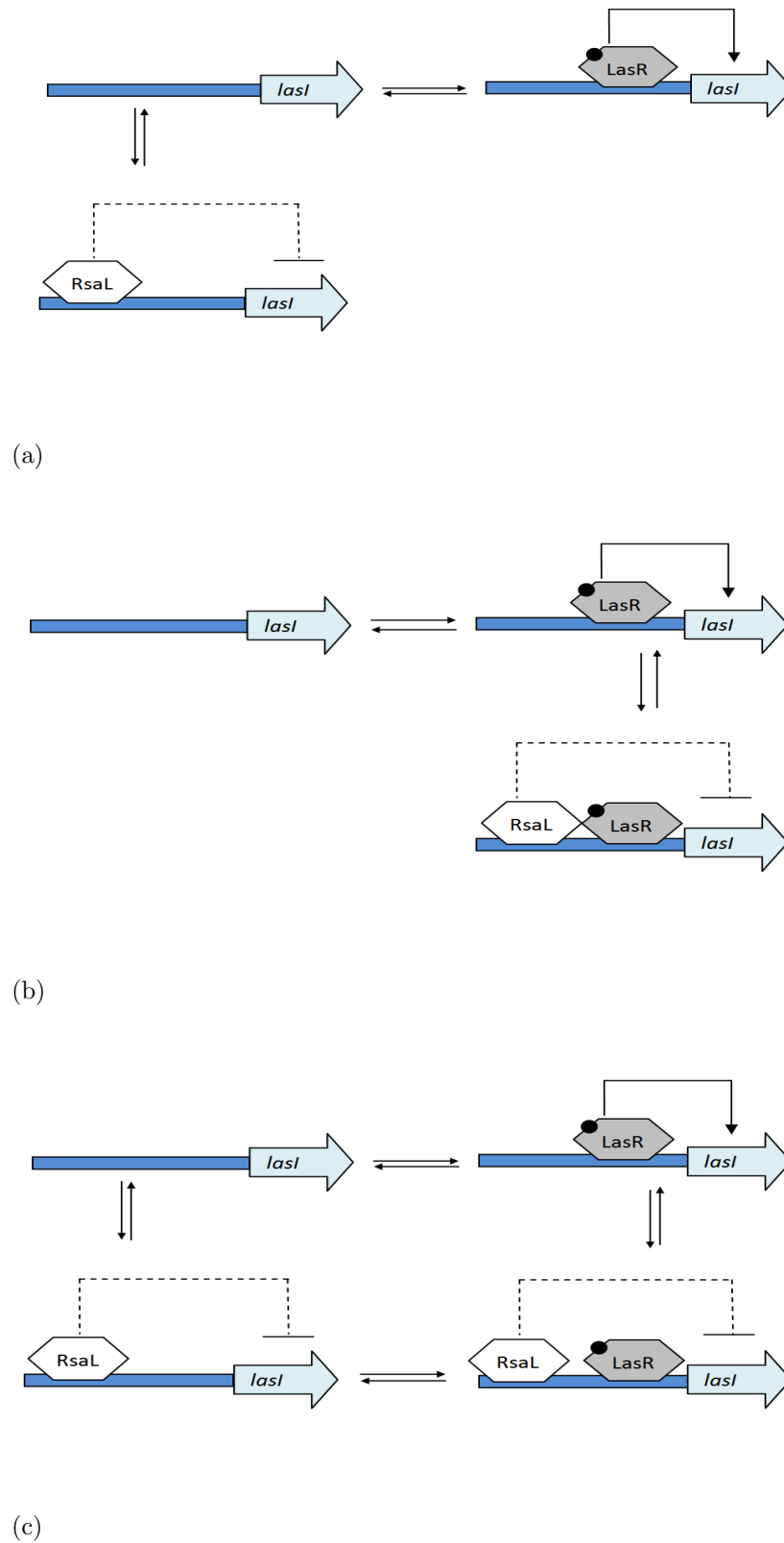
Figure 5.8: Binding types of inhibition: (a) competitive, (b) uncompetitive, and (c) non-competitive inhibition.
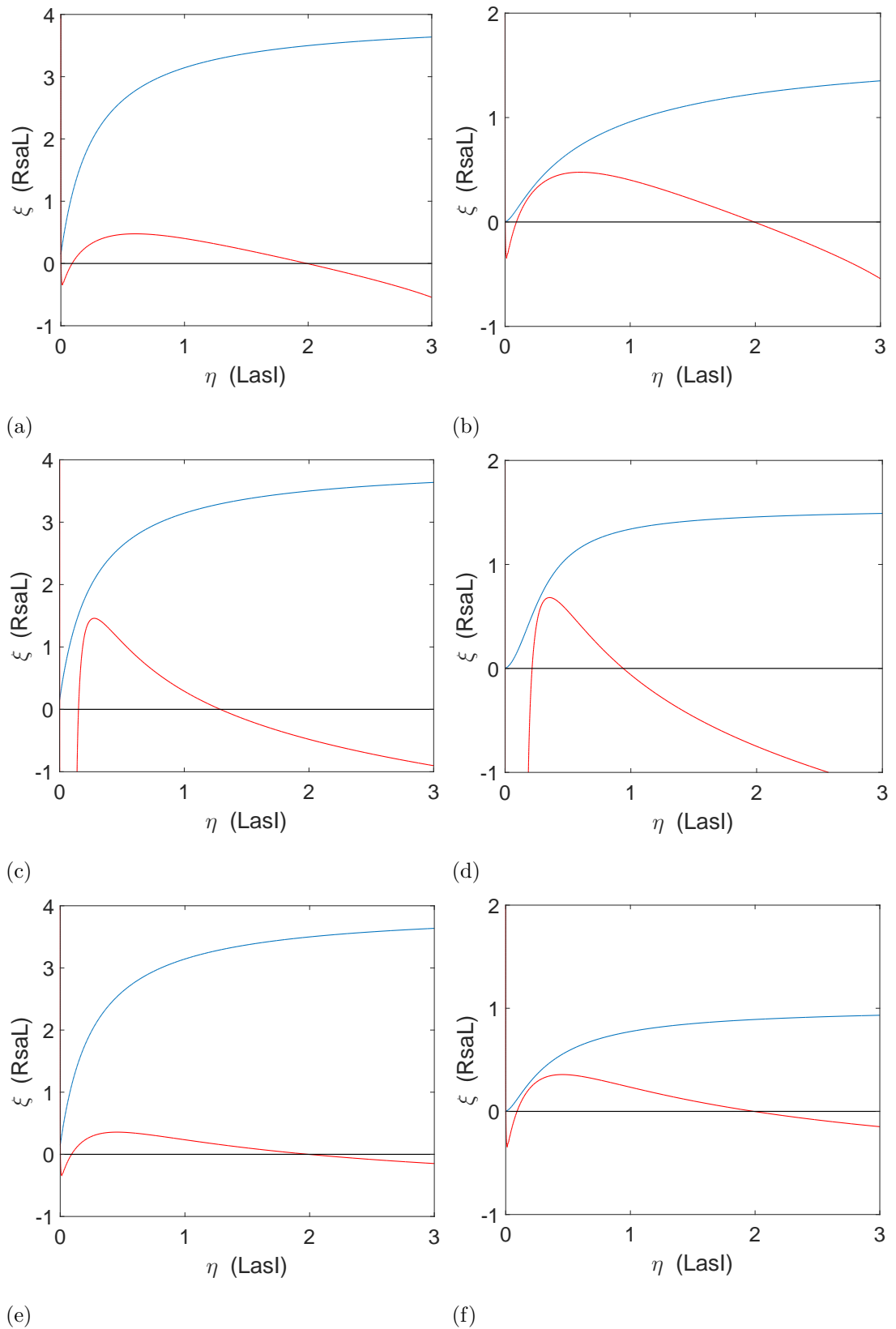
Figure 5.9: Intersection between LasI and RsaL concentration nullclines with different types of inhibition: (a) non-symmetric competitive, (b) symmetric competitive, (c) non-symmetric uncompetitive, (d) symmetric uncompetitive, (e) non-symmetric non-competitive, and (f) symmetric non-competitive.

Therefore, the non-dimensional model becomes

$$\frac{d\eta}{d\tau} = \frac{(\eta + a_1)^2}{a_2 (1 + \xi)^2 (\eta + a_1 + 1)^2 + (\eta + a_1)^2} - a_3\eta, \tag{5.33}$$

$$\frac{d\xi}{d\tau} = \frac{a_4 (\eta + a_1)}{a_6 (\eta + a_1 + 1) + (\eta + a_1)} - a_5\xi. \tag{5.34}$$

Symmetric competitive inhibition.

In this case, we find that

$$\frac{d\hat{I}_L}{dt} = \beta_L \frac{R_{LH}^2}{K_L^2(1 + S_L/K_{SL})^2 + R_{LH}^2} - \gamma_{mL}\hat{I}_L + \beta_{L0}, \tag{5.35}$$

$$\frac{d\hat{S}_L}{dt} = \beta_S \frac{R_{LH}^2}{K_L^2(1 + S_L/K_{SL})^2 + R_{LH}^2} - \gamma_{mS}\hat{S}_L + \beta_{S0}, \tag{5.36}$$

yielding the non-dimensional model

$$\frac{d\eta}{d\tau} = \frac{(\eta + a_1)^2}{a_2 (1 + \xi)^2 (\eta + a_1 + 1)^2 + (\eta + a_1)^2} - a_3\eta, \tag{5.37}$$

$$\frac{d\xi}{d\tau} = \frac{a_4 (\eta + a_1)^2}{a_2 (1 + \xi)^2 (\eta + a_1 + 1)^2 + (\eta + a_1)^2} - a_5\xi. \tag{5.38}$$

5.5.3   Uncompetitive inhibition

Uncompetitive binding occurs when the RsaL inhibitor binds to a site which only becomes available after the LasR/3O-C12-HSL enzyme has bound to the active site of the *lasI* gene. It can also be classified into non-symmetric and symmetric binding types. Referring to theories of enzyme action by Chaplin and Bucke (1990), the equation of the non-symmetric and symmetric uncompetitive inhibition can be written in Eq. 5.39-5.40 and Eq. 5.43-5.44, respectively.

Non-symmetric uncompetitive inhibition.

Here,

$$\frac{d\hat{I}_L}{dt} = \beta_L \frac{R_{LH}^2}{K_L^2 + R_{LH}^2(1 + S_L/K_{SL}')^2} - \gamma_{mL}\hat{I}_L + \beta_{L0}, \tag{5.39}$$

$$\frac{d\hat{S}_L}{dt} = \beta_S \frac{R_{LH}}{K_S + R_{LH}} - \gamma_{mS}\hat{S}_L + \beta_{S0}, \tag{5.40}$$

so that the non-dimensional model becomes

$$\frac{d\eta}{d\tau} = \frac{(\eta + a_1)^2}{a_2 (\eta + a_1 + 1)^2 + (\eta + a_1)^2 (1 + \xi')^2} - a_3\eta, \tag{5.41}$$

$$\frac{d\xi}{d\tau} = \frac{a_4 (\eta + a_1)}{a_6 (\eta + a_1 + 1) + (\eta + a_1)} - a_5\xi, \tag{5.42}$$

where ξ' is a rescaled ξ.

Symmetric uncompetitive inhibition.

For this case,

$$\frac{d\hat{I}_L}{dt} = \beta_L \frac{R_{LH}^2}{K_L^2 + R_{LH}^2(1 + S_L/K'_{SL})^2} - \gamma_{mL}\hat{I}_L + \beta_{L0}, \tag{5.43}$$

$$\frac{d\hat{S}_L}{dt} = \beta_S \frac{R_{LH}^2}{K_L^2 + R_{LH}(1 + S_L/K'_{SL})^2} - \gamma_{mS}\hat{S}_L + \beta_{S0}, \tag{5.44}$$

such that the non-dimensional model is

$$\frac{d\eta}{d\tau} = \frac{(\eta + a_1)^2}{a_2(\eta + a_1 + 1)^2 + (\eta + a_1)^2(1 + \xi')^2} - a_3\eta, \tag{5.45}$$

$$\frac{d\xi}{d\tau} = \frac{a_4(\eta + a_1)^2}{a_2(\eta + a_1 + 1)^2 + (\eta + a_1)^2(1 + \xi')^2} - a_5\xi. \tag{5.46}$$

Here, K'_{SL} represents the dissociation constant for the RsaL inhibition of binding of *lasI* genes to the LasR/3O-C12-HSL enzyme. It is different to K_{SL}, which represents the dissociation constant of inhibitor RsaL on *lasI* genes.

5.5.4 Non-competitive inhibition

Non-competitive inhibition occurs when the RsaL inhibitor can bind to the free *lasI* gene or the *lasI*-bound LasR/3O-C12-HSL enzyme. As explained above, the non-competitive inhibition form is a special case of mixed-competitive inhibition, where it binds to the target with two equal inhibition constants. Referring to theories of enzyme action by Chaplin and Bucke (1990), the equation of the non-symmetric and symmetric non-competitive inhibition can be written in Eq. 5.47-5.48 and Eq. 5.51-5.52, respectively.

Non-symmetric non-competitive inhibition.

Here,

$$\frac{d\hat{I}_L}{dt} = \beta_L \frac{R_{LH}^2}{K_L^2 + R_{LH}^2} \frac{1}{(1 + S_L/K_{SL})^2} - \gamma_{mL}\hat{I}_L + \beta_{L0}, \tag{5.47}$$

$$\frac{d\hat{S}_L}{dt} = \beta_S \frac{R_{LH}}{K_S + R_{LH}} - \gamma_{mS}\hat{S}_L + \beta_{S0}, \tag{5.48}$$

providing the non-dimensional model

$$\frac{d\eta}{d\tau} = \frac{(\eta + a_1)^2}{a_2(\eta + a_1 + 1)^2 + (\eta + a_1)^2} \frac{1}{(1 + \xi)^2} - a_3\eta, \tag{5.49}$$

$$\frac{d\xi}{d\tau} = \frac{a_4(\eta + a_1)}{a_6(\eta + a_1 + 1) + (\eta + a_1)} - a_5\xi. \tag{5.50}$$

Symmetric non-competitive inhibition.

Here, the governing equations are

$$\frac{d\hat{I}_L}{dt} = \beta_L \frac{R_{LH}}{K_L + R_{LH}} \frac{1}{(1 + S_L/K_{SL})} - \gamma_{mL}\hat{I}_L + \beta_{L0}, \tag{5.51}$$

$$\frac{d\hat{S}_L}{dt} = \beta_S \frac{R_{LH}}{K_L + R_{LH}} \frac{1}{(1 + S_L/K_{SL})} - \gamma_{mS}\hat{S}_L + \beta_{S0}, \tag{5.52}$$

and the non-dimensional model is

$$\frac{d\eta}{d\tau} = \frac{(\eta + a_1)^2}{a_2(\eta + a_1 + 1)^2 + (\eta + a_1)^2} \frac{1}{(1 + \xi)^2} - a_3\eta, \tag{5.53}$$

$$\frac{d\xi}{d\tau} = \frac{a_4(\eta + a_1)^2}{a_2(\eta + a_1 + 1)^2 + (\eta + a_1)^2} \frac{1}{(1 + \xi)^2} - a_5\xi. \tag{5.54}$$

Using the simplification steps highlighted in the main text, we determine appropriate nullclines for each binding type (see Fig. 5.9). The equations resulting from non-symmetric and symmetric competitive behaviour are presented in Fig. 5.9a and Fig. 5.9b, revealing the same qualitative behaviour as for the system in the main text. This suggests that competitive binding between RsaL and LasR/3O-C12-HSL with or without symmetry is sufficient for excitable behaviour. Therefore, although (Rampioni et al, 2007b) suggest there may be negative feedback from RsaL to its own production, this symmetrical binding is not required for excitable behaviour (c.f. general diagrams of the *las* system in Van Delden and Iglewski, 1998; De Kievit et al, 2002; Dockery and Keener, 2001; Fagerlind et al, 2005; Schaadt et al, 2013).

5.6 Downstream impact on *rhl* system

The *las* and *rhl* QS subsystems of *P. aeruginosa* do not act independently (Latifi et al, 1995; Pesci et al, 1997). Numerous research provides evidence that the regulation of Rhamnolipid production in *P.aeruginosa* is mediated by the *rhl* system involving the *las* system (Pearson et al, 1997).

Table 5.1: Description of dimensional variables of *rhl* system.

Variable	Description	Unit
H_L	3O-C12-HSL	nM
R_R	RhlR	nM
H_R	C4-HSL	nM
R_{RH}	RhlR/C4-HSL complex	nM
$\hat{R}_R$	rhlR mRNA	nM
I_R	RhlI	nM
$\hat{I}_R$	rhlI mRNA	nM

In *rhl* system, RhlR operates as a transcriptional activator in the presence of autoinducer C4-HSL. RhlR would bind C4-HSL, which leads to complex chemical form of RhlR/C4-HSL.
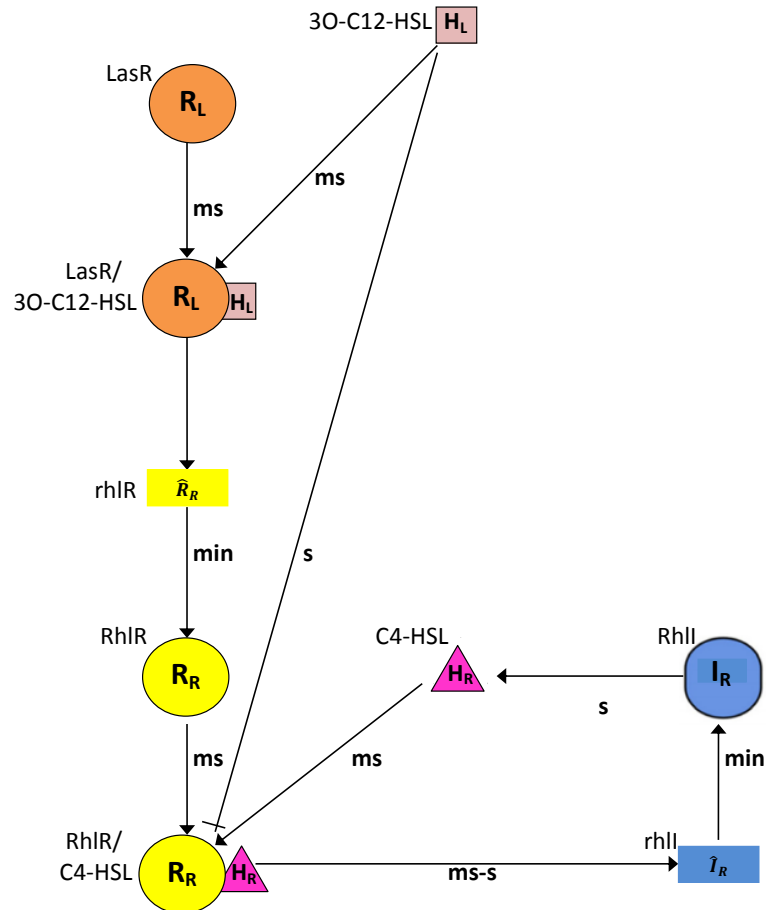
Figure 5.10: The signalling of *rhl* QS subsystem in *Pseudomonas aeruginosa*. Arrows and barred arrows indicate activating (positive) and inhibiting (negative) regulatory interactions, respectively. Shapes on the diagram depict autoregulation terminology. Letters associated with each arrow reflect the associated time scale (ms = millisecond, s = second, and min = minute). Symbols associated with each shape are detailed in Table 5.1

Following the process, complex chemical form of RhlR/C4-HSL would bind and activate the *rhlI* genes in which create a positive feedback on *rhl* system (Fagerlind et al, 2005). Transcription and translation process on *rhlI* genes induce the production of autoinducer synthase protein RhlI, which increases the amount of C4-HSL available to bind to RhlR.

As an individual system, dynamical behaviour of *rhl* system is similar to the positive feedback in the *las* system (Pesci et al, 1999). There will be a point of loop that is classic *S*-shape bifurcation diagram, which is one point of low stable steady state can leap to the highest steady state that represent the production of *RhlI* protein. However, as a hierarchy system, we try to link *las* system to this (*rhl)* system (see Fig. 5.10).

The *las* system presents positive and negative impacts on the *rhl* system. Once the concentration of autoinducer 3O-C12-HSL on the *las* system reach the quorum, LasR would bind 3O-C12-HSL, then form chemical complex of LasR/3O-C12-HSL. The LasR/3O-C12-HSL complex would not activate the *lasI* and *rsaL* genes on the *las* system only, but it also binds and activates *rhlR* genes on the *rhl* system in which induce the production of RhlR regulator (Pesci et al, 1997). On the other hand, QS signal molecule 3O-C12-HSL that is synthesized by LasI synthase in the *las* system would not bind LasR regulator only, but some of those signal molecules also bind RhlR as a regulator in the *rhl* system. Consequently, the signal molecule 3O-C12-HSL blocks the binding of C4-HSL to its regulator protein (RhlR) in which 3O-C12-HSL works as an inhibitor of the *rhl* system (Pesci et al, 1997).

In this section we are interested in the dynamics of the *rhl* system that is affected by the dynamics of the *las* system in *P. aeruginosa*. The expression of some genes, including *lasB*, *aprA*, and *rhlAB* genes are regulated by *rhl* system and are also under the control of the *las* system (Miller and Bassler, 2001). The *rhlAB* gene encodes rhamnosyltransferase and is involved in rhamnolipid production (Ochsner and Reiser, 1995) that affects bacterial spreading.

5.6.1   Model of *rhl* system

There are a considerable number of published model about modelling of *rhl* subsystem only (e.g., Chen et al, 2004) or both *las* and *rhl* subsystem (e.g., Fagerlind et al, 2003) for *P. aeruginosa*. However, to the best knowledge of the author, none of these studies connect the impact of the *las* to the *rhl* subsystem modelling, even though all of studies about QS in *P. aeruginosa* demonstrate that the placing of the *las* subsystem in a cell signalling hierarchy above the *rhl* subsystem. Thus we try to rebuild the existed *rhl* model by involving the role of the *las* system.

We construct the governing equations using mass action kinetics, guided by the literatures. First, consider the RhlR regulator (R_R), its binding activator, the autoinducer

C4-HSL (H_R) that compete with the binding of the autoinducer 3O-C12-HSL to its regulator, and the complex RhlR/C4-HSL (R_{RH}). In *rhl* system, we are interested in the downstream feedback of autoinducer 3O-C12-HSL. In this regard, we can assume the input of the RhlR/C4-HSL complex from the *las* system is constant, $R_R := R$ (constant). Basically, in the *las-rhl* systems of QS for *P. aeruginosa*, LasR (R_L) activates several genes' expressions including *Rhlr* gene that encodes RhlR (R_R) production. Here, we have assumed R_R to be constant in order to simplify the model equation and focus on the impact of the autoinducer 3O-C12-HSL on the *rhl* system without involving the whole *las* system. In the next chapter we will consider R_R to be affected by the *las* system rather than constant. By ignoring the *las* system, therefore, we consider H_L as a parameter in this model rather than a variable. We take an arbitrary value ($H_L = 50$ nM) for modelling purposes that generates high production of autoinducer 3O-C12-HSL.

In order to keep the number of equations low, we considered the *las* autoinducer signal inhibition of the complex RhlR/C4-HSL (R_{RH}) in manner akin to transcription inhibition rather than treating the *las* autoinducer signal as an antagonist that binds the complex RhlR/C4-HSL (R_{RH}). We represent this using mass action kinetics in similar manner to Fagerlind et al (2005). If the RhlR/C4-HSL complex is formed at α_{RH} through all of those processes and degrades at rate γ_{RR}, then we may write

$$\frac{dR_{RH}}{dt} = \alpha_{RH}\left(R - R_{RH}\right)\frac{H_R}{K_R\left(1 + \frac{H_L}{K_{HR}}\right) + H_R} - \gamma_{RR}R_{RH}. \tag{5.55}$$

where γ_{RR} is positive constant.

The autoinducer C4-HSL (H_R) is created in the system via the activity of the RhlI synthase (I_R), which we take to be at rate β_{HR}, and is naturally lost from the system at rate γ_{HR}. The most significant loss of the autoinducer from the cell is via diffusion through the cell membrane. Taking a simplified description of diffusion we can express the diffusive term as being proportional to the concentration difference across the membrane of H_R. Therefore, D_{HR} represents an additional loss rate, which is multiplied by the concentration H_R yielding

$$\frac{dH_R}{dt} = \beta_{HR}I_R - \gamma_{HR}H_R - D_{HR}H_R. \tag{5.56}$$

The enzyme RhlI (I_R) is produced by the *rhlI* gene through a transcription and translation process of *rhlI*-mRNA ($\hat{I}_R$) at rate α_I and degrades at rate γ_I, such that

$$\frac{dI_R}{dt} = \alpha_I\hat{I}_R - \gamma_I I_R. \tag{5.57}$$

Transcription at the *rhlI* promoter site ($\hat{I}_R$) is activated by the RhlR/C4-HSL complex (R_{RH}). The production process is assumed to follow a Hill form with a Hill number m. The *rhl* system has not been explored as massive as the *las* system. Many of researchers

Table 5.2: Parameters employed in the model of *rhl* system.

Par	Description	Standard value	Unit	Value/Range	Comments (Based on)/Ref
α_{RH}	rate at which RhlR/C4-HSL produced by RhlR, then inhibited by 3O-C12-HSL	0.5	min^{-1}	0.5 - 0.8	estimate
α_I	rate at which RhlI produced by rhlI mRNA	0.5	min^{-1}	0.5	2 min to translate protein, Alon (2006)
β_{HR}	rate at which C4-HSL produced by RhlI	8×10^2	min^{-1}	8×10^2	Raychaudhuri et al (2005)
β_I	max. production rate of RhlI at which rhlI mRNA is activated by RhlR/C4-HSL	1	nM min^{-1}	1	Estimate
β_{R0}	basal production rate of rhlR mRNA	0.1	nM min^{-1}	0.1	basal transcription rate of a protein, Alon (2006)
β_{I0}	basal production rate of rhlI mRNA	0.1	nM min^{-1}	0.1	basal transcription rate of a protein, Alon (2006)
K_R	affinity constant between *las* system and rhlR mRNA	250	nM	1-1000	Alon (2006)
K_I	affinity constant between RhlR/C4-HSL and rhlI mRNA	250	nM	1-1000	Alon (2006)

Table 5.2. continued

Par	Description	Standard value	Unit	Value/Range	Comments (Based on)/Ref
K_{HR}	dissociation constant of inhibitor 3O-C12-HSL to *rhl* system	250	nM	1-1000	Alon (2006)
γ_I	degradation rate of RhlI	0.01	$\min^{-1}$	0.01	Alon (2006)
γ_{HR}	degradation rate of C4-HSL	0.01	$\min^{-1}$	0.01	Alon (2006)
γ_{RR}	degradation rate of RhlR/C4-HSL	0.01	$\min^{-1}$	0.01 - 0.1	estimate
γ_{mI}	degradation rate of rhlI mRNA	0.14	$\min^{-1}$	0.2	2 min lifetime of RNA, Alon (2006)
D_{HR}	diffusion constant of C4-HSL	200	$\min^{-1}$	$0 - 10^4$	Pai and You (2009)

are interested to investigate rhamnolipid as a product of the *rhl* system, which is produced by *rhlAB* gene and activated by RhlR/C4-HSL complex rather than the system per se. Biochemically there is insufficient evidence to determine the value of the Hill number, m. For simplicity of the system, we adopt $m = 2$ as adopted from Alfiniyah et al (2017). With basal expression of β_{I0} and a loss rate of γ_{mI} this leads to the following expression for *rhlI*:

$$\frac{d\hat{I}_R}{dt} = \beta_I \frac{R_{RH}^2}{K_I^2 + R_{RH}^2} - \gamma_{mI}\hat{I}_R + \beta_{I0}. \tag{5.58}$$

In a similar way to the modelling of *las* system, we are able to make the same assumptions regarding the timescales to simplify the system. We assume that the dominant, slowest processes are protein production from mRNA via translation and folding. Therefore, other processes, namely the liganding of regulators, DNA binding, synthetase operation, and the transcription of DNA are much faster and we can assume that the differential equations for *rhlI* genes in the *rhl* system are at a quasi-steady state, such that

$$\hat{I}_R = \frac{\beta_I R_{RH}^2}{\gamma_{mI}\left(K_I^2 + R_{RH}^2\right)} + \frac{\beta_{I0}}{\gamma_{mI}}, \tag{5.59}$$

In addition, we make the simplifying assumption that HSL diffusion is rapid and $\gamma_{HR} \approx 0$, therefore, that the equation for C4-HSL, H_R can also be written in a quasi-steady state, providing

$$H_R = \frac{\beta_{HR}I_R}{D_{HR}}. \tag{5.60}$$

From system (see Fig. 5.10), we know that all processes involving binding activator C4-HSL, inhibitor 3O-C12-HSL, and transmission process from *las* to rhl system happen very fast. Thus we can assume that differential equation for the complex RhlR/C4-HSL (R_{RH}) in the *rhl* system is at a quasi-steady state, such that

$$\alpha_{RH}\left(R - R_{RH}\right)\frac{H_R}{K_R\left(1 + \frac{H_L}{K_{HR}}\right) + H_R} - \gamma_{RR}R_{RH} = 0. \tag{5.61}$$

Thus

$$R_{RH} = \frac{\alpha_{RH}R\frac{H_R}{K+H_R}}{\frac{\alpha_{RH}H_R}{K+H_R} + \gamma_{RR}}$$

$$= \frac{\alpha_{RH}\ R\ H_R}{H_R\left(\alpha_{RH} + \gamma_{RR}\right) + K\gamma_{RR}}, \tag{5.62}$$

where $K = K_R\left(1 + \frac{H_L}{K_{HR}}\right)$.

With the simplification above, the system of equations for the *rhl* system become just one differential equation. By assuming the basal production of *rhlI* genes is negligible ($\beta_{I0} = 0$), the governing equation becomes

$$\frac{dI_R}{dt} = \frac{\alpha_I\beta_I}{\gamma_{mI}}\frac{\alpha_{RH}^2\beta_{HR}^2R^2I_R^2}{K_I^2\left(\beta_{HR}I_R\left(\alpha_{RH} + \gamma_{RR}\right) + K\gamma_{RR}D_{HR}\right)^2 + \alpha_{RH}^2\beta_{HR}^2R^2I_R^2} - \gamma_I I_R. \tag{5.63}$$

We nondimensionalize this model by writing

$$I_R^* = \frac{I_R}{I_0}, \qquad \text{and} \qquad t^* = \frac{t}{t_0} \tag{5.64}$$

so the equation 5.63 becomes

$$\frac{dI_R^*}{dt^*} = \frac{b_1 I_R^{*2}}{b_2\left(I_R^* + b_3\right)^2 + I_R^{*2}} - b_4 I_R^*, \tag{5.65}$$

where

$$b_1 = \frac{\alpha_I\beta_I}{\gamma_{mI}}\frac{t_0}{I_0}, \qquad\qquad b_2 = \frac{K_I^2(\alpha_{RH}+\gamma_{RR})^2}{\alpha_{RH}^2R^2}, \tag{5.66}$$

$$b_3 = \frac{K}{I_0}\frac{\gamma_{RR}D_{HR}}{\beta_{HR}(\alpha_{RH}+\gamma_{RR})}, \qquad\qquad b_4 = \gamma_I t_0.$$

Here b_1, b_2, b_3 and b_4 are positive constants. The biological interpretation of this model is that 3O-C12-HSL inhibits the binding process of C4-HSL, which is represented by parameter $b_3 \propto K$(definition of Kcan be seen in Eqs. 5.62). The activation of *rhl* system that is affected by *las* system describes positive connection. This is reflected by parameter $b_2 \propto \frac{1}{R^2}$. In addition, I_R^* degrade exponentially.

Table 5.3: Non-dimensional Parameters involved in the model of *rhl* system.

Name	Description	Value
b_1	the production of signal molecules C4-HSL	3.51
b_2	The control of concentration of RhlR that is affected by the *las* system	1.69
b_3	The control binding of 3O-C12-HSL to RhlR/C4-HSL	1.47
b_4	The degradation of RhlI relative to the time	0.3

5.6.2   Dynamical system in *rhl* model

The non-dimensional differential Eq. 5.65 has been investigated analytically with the assistance of Maple (18; Maplesoft) and solved numerically using MATLAB (R2016a; MathWorks).

The nullclines for concentration RhlI is solution of $\frac{dI_R^*}{dt^*}$ equals zero. It can be seen clearly that Eq. 5.62 might have one, two or three fixed points. Those are $I_R^* = 0$ and two other fixed points that can be derived from equation below

$$(b_2 b_4 + b_4)\, I_R^{*2} + (2 b_2 b_3 b4 - b_1)\, I_R^* + b_2 b_3^2 b_4 = 0. \tag{5.67}$$

The stability of those three points can be seen in Fig. 5.11.
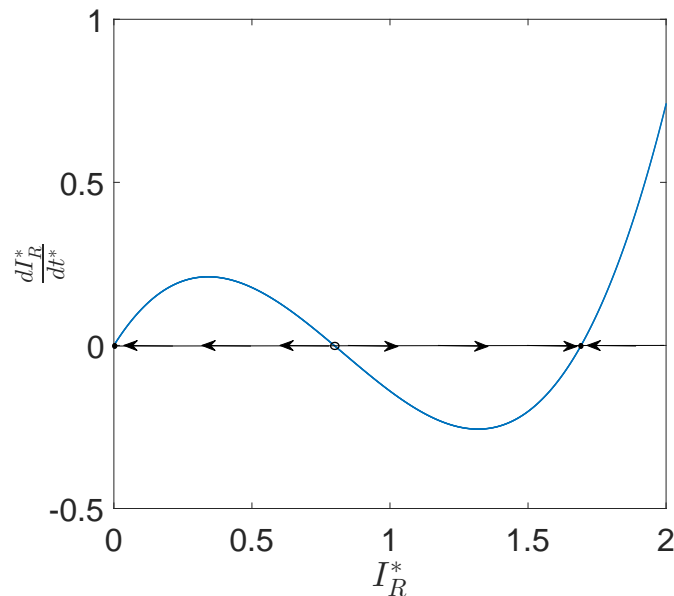
Figure 5.11: Three solutions are found at $\frac{dI_R^*}{dt^*}$ equals zero. Solid (open) circles denote stable (unstable) nodes. All parameters are in Table 5.3.

The *rhl* system that is represented by Eq. 5.65 yields fold bifurcation if the discriminant Eqs. 5.67 is greater than or equal to zero. At first the system has stable steady state and

nothing else, then there will be a point of loop that is classic S-shape bifurcation diagram. From that diagram, we can get the creation from low stable states that leap to the high stable state by passing the unstable state, or conversely.

Initially we investigated the dynamics of the rhl system with a one-parameter bifurcation, b_2. Non-dimensional parameter b_2 consist of R, which give information how the input from the las system affects the dynamical behaviour of the rhl system. We used continuation methods to track the evolution of solutions for I_R^* versus b_2.
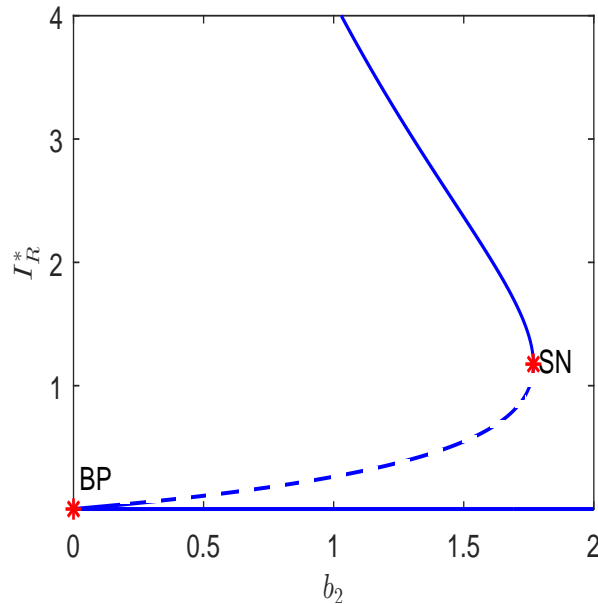
Figure 5.12: Bifurcation diagram for autoregulation of the rhl system with respect to b_2, which represents the concentration of activator as the outcome of the las system. Solid (dashed) lines depict stable (unstable) steady states. Co-dimension-1 singular points marked as BP (Branch point) as permanent solution, and SN indicate a saddle-node point. All parameters are in Table 5.3.

Figure 5.12 depicts a *reversible* bistability diagram and is also referred as *hysteresis*. The concentration of RhlI (I_R^*) is low until b_2 level exceeds the critical value, very small value that can be said it equals zero. This critical point is labelled BP (Branch Point), which is a permanent saddle-node. Any changes in parameter values of the model will not shift the position of BP point, at which point the concentration of RhlI increases abruptly to a high value. In a similar manner, starting with b_2 is very low, the concentration of RhlI does not drop significantly until b_2 reaches the high critical value, SN (see Fig. 5.12, $b_2 = 1.77$).

Furthermore, the non-dimensional parameter b_3 is also supposed to be essential parameter value in the rhl system. Once there is change in parameter value of b_3, the critical value (SN) in Fig. 5.12 moves to another value. Moreover, we can recognize that one of the constructor of b_3 is the K-parameter, which represents inhibition of 3O-C12-HSL to the

activator of C4-HSL. Thus b_2 and b_3 have different roles to determine the behaviour of the *rhl* system. Non-dimensional parameters b_2 and b_3 provide positive and negative affects, respectively, to the concentration of RhlI (Eqs. 5.65). In order to get clear understanding of the relation between b_2 and b_3, refer to Fig. 5.13.
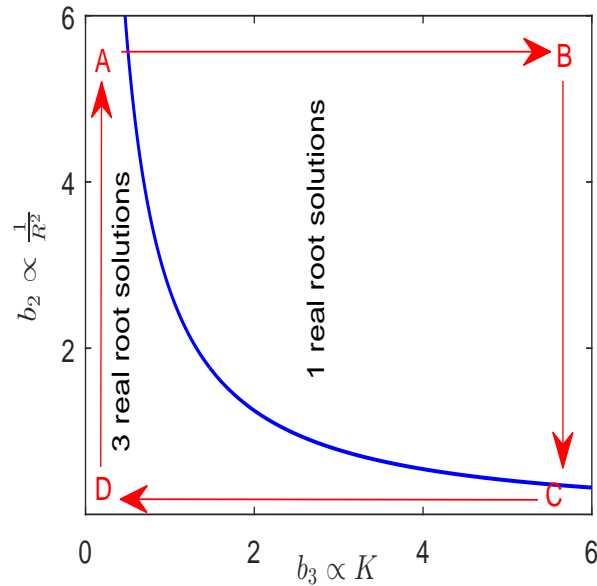
Figure 5.13: Two-dimensional bifurcation diagram for (b_3, b_2). The *bifurcation lines* divide the parameter regions. Two different regions that explain how binding inhibition 3O-C12-HSL to the C4-HS (K), affect the concentration of RhlR (R) that is affected by *las* system. All parameters are in Table 5.3.

Figure 5.13 demonstrates the downstream impact of *las* to *rhl* system. We start from region A $((K)$ and R are in the small value) which represents low level of both 3O-C12-HSL and RhlR. Then, there is pulse generation on the las system that generates pulse production of 3O-C12-HSL. In the region B, concentration of 3O-C12-HSL increased and reached the quorum level but the concentration of RhlR is still low. Once the quorum of 3O-C12-HSL is reached, then it increases the concentration of the LasR/3O-C12-HSL complex. This process triggers the transcription of some genes, including genes in the *las* system (*rsaL* gene, *lasI* gene) and in the *rhl* system (*rhlR* gene). In the case of *rhl* system, the transcription of *rhlR* gene increases the concentration of RhlR activator, R. Meanwhile, the consequent increase of 3O-C12-HSL levels also prevents the activation of RhlR by C4-HSL. However, the effect of pulses is still to increase the concentration of RhlR. This stage is referred to as 'handbraked acceleration', which represents the concentration of RhlR and 3O-C12-HSL in the high level (region C). Then, when the concentration of 3O-C12-HSL decreases as explained in Fig. 5.7, the handbrake of 3O-C12-HSL is removed and consequently increases the activation of *rhl* system. Thus in the region D, the concentration of 3O-C12-HSL is low, while RhlR is high

which leads to production of rhamnolipid. It is following that cells lose memory with no longer experience in the local environment with high concentration of 3O-C12-HSL. By a decrease in the level of 3O-C12-HSL concentration, in slow time it is followed by a decrease in the level of RhlR (return to the region A).

5.7 Discussion

By varying assumptions, the author investigated the behaviour of *las* system in more detail. The model showed that positive and negative feedback loops play an essential role in determining system dynamics. Numerical solution of the *las* system model without involving concentration of extracellular signal molecule, $H_{ex} = 0$, also reveals excitable pulse generation. Excitation occurs if there is large perturbation of 3O-C12-HSL, which induces pulse production of LasI. In the *las* system model with $H_{ex} \neq 0$ or as a constant, H_{ex} and $\frac{k_L^+}{k_L^-}$ (ratio between association and dissociation rate of LasR/3O-C12-HSL complex) compose a_1-non dimensional parameter. As $\frac{k_L^-}{k_L^+} \sim 1000 - 2000 nM$ (Welch et al, 2000), so the value of $a_1 = H_{ex} \frac{k_L^+}{k_L^-}$ is very small. This might be the reason why they present the same qualitative behaviour. In addition, we also explored numerical solution of the full system of seven differential equation. It provides very similar solution behaviour to the reduced system, including excitable pulse generation.

The dynamic complexity arises from interacting positive and negative feedback loops. We have demonstrated the dynamical system of *las* QS model, including its bifurcation analysis in the previous chapter. As a continuation of bifurcation analysis, we have investigated the phase diagrams of the dynamic solution behaviour for the *las* system that associate with two-dimensional bifurcation diagram. By investigating phase diagrams, we find three different solution behaviours, involving monostability, bistability or excitation, and oscillatory.

In addition, we have presented the possibilities of inhibition binding types in the *las* system, including competitive, uncompetitive and non-competitive inhibition. Moreover, we also explored symmetric and non-symmetric expression rate in each binding direction for all types of binding. By using similar steps in chapter 4, we derived forms of mathematical model to determine appropriate nullclines. The results of all binding types revealing the same qualitative behaviour as the system in chapter 4, which adopt a symmetric competitive binding form. This suggest that whatever the binding types between RsaL and LasR/3O-C12-HSL, even with symmetric or non-symmetric expression rate, the *las* system is sufficient for excitable behaviour. Therefore, basically negative feedback from RsaL to its own production with symmetrical binding as Rampioni et al (2007b) suggested is not required.

After investigating our *las* system model, we consider *las* system as black box controller that is involved in regulating the *rhl* system. Pesci et al (1997) demonstrated that the *rhl* system does not work independently, but that the *las* and *rhl* systems in *P. aeruginosa* have a hierarchical structure. We have shown how the *las* system affects the dynamical behaviour of the *rhl* system. This QS dynamical system, including *las* and *rhl* system, affects spreading of bacterial colony growth that we will discuss in the next chapter.

Chapter 6

The interaction of QS signalling and bacterial colony spreading

6.1 Introduction

Typically bacteria are found in communities and develop cooperative behaviour with capabilities of complex communication (Shapiro, 1988; Jacob and Cohen, 1998). Cooperative self-organization of bacterial colonies relies on the capability of cells to move in their environment and hence is recognized as an essential role in the expansion of colony (Shapiro, 1995; Giverso et al, 2015). In our case, we focus on cell signalling as quorum sensing and production of rhamnolipid "wetting agent" for the movement on the surface. We also consider nutrient together with the diffusion, as important factors that allow bacterial colonies to expand across the surface.

In this chapter, two different models are demonstrated, one simple and one complex to study bacterial spreading. We start by introducing a basic model that involves motile bacteria and nutrient concentration only. The ability of a bacterial species to manage quorum sensing signal molecules in colony growth is an index of its physiological state that has been discussed in the preliminary chapter (chapter 2). The physiological state of bacteria is controlled by biological factors such as bacterial growth, nutrient acquisition, and signal molecules production. We extend and modify the bacterial interaction model presented in chapter 2 to obtain a more comprehensive and realistic model by including motile behaviour. The main departure of our model from the basic model in chapter 2 is that non-motile bacteria are able to transform to become motile bacteria. Thus we include diffusion term in the model regarding the relationship between nutrient and spreading of colony growth.

We investigate the bifurcation phenomenon in that model by analysing the fixed points and also examine the existence of travelling waves. Following this, we expand the model

by including transition factor, i.e non-motile transform to motile bacteria and conversely. We approach these models analytically by employing similarity solutions, and numerically through travelling wave solutions. We present different types of bacterial growth on this model, and then we demonstrate the solutions for all those different types.

While the simple model helps to identify basic features of bacterial spreading, a more complex model is needed to discern the key roles of QS signalling in bacterial spreading. Therefore, in this chapter we also demonstrate the complex model of bacteria spreading by considering not only nutrient concentration, but also QS signal molecule production. In the QS signalling system of *P. aeruginosa*, the *las* and *rhl* systems regulate some gene expression including the *rhlAB* gene. This gene encodes rhamnosyltransferase that gives rise to the production of a biosurfactant identified as rhamnolipid. The biosurfactant allows expansion of the bacterial colony.

6.2 Motility transition

Bacteria employ several strategies to respond to changes in their environment. One of the popular strategies is employing flagella for motility to respond to changes in nutrient availability. Past research has studied the process of bacterial transition from motile to non-motile and vice versa extensively in *Escherichia coli* (Adler and Templeton, 1967; Sperandio et al, 2002; Douarche et al, 2009) and *Salmonella enterica* (Ohnishi et al, 1992; Iyoda et al, 2001; Wada et al, 2011a). It is suggested based on these studies that different species of organism present different responses to environment changes including changes in nutrient concentration. In *E. coli* for example, nutrient inhibit the expression of motile genes (Adler and Templeton, 1967) but in *S. enterica* nutrient enhance expression of motile genes (Wada et al, 2011a). Both of these bacteria therefore as described by (Wada et al, 2011b) have different schematic of flagellar gene network.

In another study, consistent with the previous findings by Saini et al (2010) and Wada et al (2011a), Koirala et al (2014) demonstrated that *S. enterica* population with inactive promoters existed at low concentration of nutrient, and became active cells at high concentration of nutrient. Koirala et al (2014) also investigated coexisting population of motile and non-motile in *S. enterica* cells and found that their distribution is determined by nutrient concentration in the growth culture.

Apart from the above different responses of various bacteria to the nutrient concentration, in this simple model of bacterial spreading we do not consider for specific species. We only explore the role of nutrient concentration in motile and non-motile bacterial interaction.

6.3   Simple model I : Motile bacteria and nutrient

Nutrient concentration supports the production of active cells. Active motility also requires a high level of particular nutrient that are used to synthesize and run flagellar apparatus. Thus we develop previous work by considering not only non-motile bacteria, but motile bacteria as well.

One of the important sources of collective motion on the cellular level is diffusion $(D_{\tilde{A}})$, which results from the random motion of individual cells. We assume that the bacteria grow under normal laboratory conditions and in the beginning the medium provides a convenient two-dimensional surface on which to grow. In two dimensions the diffusion equation is

$$\frac{\partial \tilde{A}}{\partial t} = \nabla \cdot \left(D_{\tilde{A}} \, \bigtriangledown \tilde{A} \right).$$

(6.1)

For our case, $D_{\tilde{A}}$ is constant, such that

$$\frac{\partial \tilde{A}}{\partial t} = D_{\tilde{A}} \Delta \tilde{A} = D_{\tilde{A}} \bigtriangledown^2 \tilde{A}.$$

(6.2)

The symbol Δ is the Laplacian; it stands for the combination $\nabla \cdot \nabla$ ("div dot grad"), also written ∇^2. For an axisymmetric solution in two-dimension in cylindrical coordinates, we have

$$\frac{\partial \tilde{A}}{\partial t} = D_{\tilde{A}} \left(\frac{\partial^2 \tilde{A}}{\partial r^2} + \frac{1}{r} \frac{\partial \tilde{A}}{\partial r} \right),$$

(6.3)

where r is the distances from the origin.
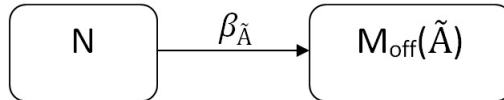
Figure 6.1: A simple diagram to describe the biological interaction between motile bacteria ($\tilde{A}$) and nutrient N that involve only growth process. $\beta_{\tilde{A}}$ is the growth rate of bacteria and is affected by nutrient concentration.

For the population of cells, it is appropriate to make a continuum assumption, that is, to depict discrete cells or organisms by continuous density distributions. This leads to partial differential equation models that are quite often analogous to classical models for cell diffusion. We begin with the base model that considers the nutrient concentration and the growth of the bacterial colony only (see Fig. 6.1).

Normally the experiment begins with a Petri dish containing a small volume of sterile nutrient-rich medium. The medium permits free diffusion of small molecules and provides a two-dimensional surface on which to grow microorganisms. A small number of cells are placed on the medium surface. By absorbing nutrient from below, they grow and multiply

to such an extent that the population gradually expands and spreads over the surface of substrate. Associated with Fig. 6.1, a simple set of equations to describe the interaction between motile bacteria $\tilde{A}$ and nutrient concentration N is constructed, such that

$$\frac{\partial \tilde{A}}{\partial t} = D_{\tilde{A}} \, \bigtriangledown^2 \tilde{A} + \beta_{\tilde{A}}(N)\tilde{A} - \mu \tilde{A}$$
$$= D_{\tilde{A}} \left(\frac{\partial^2 \tilde{A}}{\partial r^2} + \frac{1}{r}\frac{\partial \tilde{A}}{\partial r} \right) + \beta_{\tilde{A}}(N)\tilde{A} - \mu \tilde{A} \tag{6.4}$$

and

$$\frac{\partial N}{\partial t} = -\beta_{\tilde{A}}(N)\tilde{A}, \tag{6.5}$$

where the solution is assumed axisymmetric and

r	= radial distance from the centre of the dish,
$\tilde{A}(r,t)$	= the concentration $\tilde{A}$ at radial distance r and time t,
$D_{\tilde{A}}$	= diffusion coefficient of the bacteria $\tilde{A}$,
$\beta_{\tilde{A}}$	= growth rate of the bacteria $\tilde{A}$,
μ	= decay rate of bacterial concentration.

The pattern of bacterial colony *Erwinia carotovora* resembles a fried egg with a bumpy edge. Some part of the colony edge has light green fluorescent colour that expresses on-QS, and other part has dark colour that show there is no fluorescent (off-QS).

Consider here that the colony *E.carotovora* is axisymmetric. We solve the above equation using a similarity solution.

Applying the transformation $\tilde{A} = a(t)A$ to the equation (6.4), yields

$$\frac{\partial a}{\partial t}A + a\frac{\partial A}{\partial t} = aD_{\tilde{A}} \, \bigtriangledown^2 A + a\beta_{\tilde{A}}(N)A - \mu a A. \tag{6.6}$$

We choose a to satisfy

$$\frac{\partial a}{\partial t}A = a\beta_{\tilde{A}}(N)A - \mu a A, \tag{6.7}$$

such that

$$a = e^{\left(\beta_{\tilde{A}}(N)-\mu\right)t}. \tag{6.8}$$

Hence, substituting $a = e^{\left(\beta_{\tilde{A}}(N)-\mu\right)t}$ into equation (6.6), we obtain

$$\left(\beta_{\tilde{A}}(N) - \mu\right)A + \frac{\partial A}{\partial t} = D_{\tilde{A}}\left(\frac{\partial^2 A}{\partial r^2} + \frac{1}{r}\frac{\partial A}{\partial r}\right) + \left(\beta_{\tilde{A}}(N) - \mu\right)$$
$$\frac{\partial A}{\partial t} = D_{\tilde{A}}\left(\frac{\partial^2 A}{\partial r^2} + \frac{1}{r}\frac{\partial A}{\partial r}\right). \tag{6.9}$$

After that, let us now consider a possible similarity solution to equation (6.5 and 6.9), where

$$w(z) = A(r,t), \qquad n(z) = N(r,t), \qquad z = rt^{-1/2}. \tag{6.10}$$

Using equation (6.10) and the chain rule, we may conclude that

$$\frac{\partial A}{\partial t} = \frac{\partial w}{\partial z}\frac{\partial z}{\partial t} = -\frac{r}{2}t^{-\frac{3}{2}}\frac{\partial w}{\partial z}, \tag{6.11}$$

and

$$\frac{\partial A}{\partial r} = \frac{\partial w}{\partial z}\frac{\partial z}{\partial r} = t^{-\frac{1}{2}}\frac{\partial w}{\partial z}. \tag{6.12}$$

Thus equation (6.12) gives

$$
\begin{aligned}
\frac{\partial^2 A}{\partial r^2} &= \frac{\partial^2 A}{\partial z\,\partial r}\frac{\partial z}{\partial r} = \frac{\partial}{\partial z}\left(\frac{\partial A}{\partial r}\right)\frac{\partial z}{\partial r} \\
&= \frac{\partial}{\partial z}\left(t^{-\frac{1}{2}}\frac{\partial w}{\partial z}\right)t^{-\frac{1}{2}} \\
&= \frac{1}{t}\frac{\partial^2 w}{\partial z^2}.
\end{aligned}
\tag{6.13}
$$

Substitute (6.12) and (6.13) into equation (6.9), to give

$$
\begin{aligned}
0 &= -\frac{r}{2t\sqrt{t}}\frac{\partial w}{\partial z} - \frac{D_{\tilde{A}}}{t}\frac{\partial^2 w}{\partial z^2} + \frac{D_{\tilde{A}}}{r\sqrt{t}}\frac{\partial w}{\partial z} \\
&= \frac{1}{t}\left(-\frac{r}{2\sqrt{t}}\frac{\partial w}{\partial z} - D_{\tilde{A}}\frac{\partial^2 w}{\partial z^2} + \frac{\sqrt{t}D_{\tilde{A}}}{r}\frac{\partial w}{\partial z}\right) \\
&= -\frac{z}{2}\frac{\partial w}{\partial z} - D_{\tilde{A}}\frac{\partial^2 w}{\partial z^2} + \frac{D_{\tilde{A}}}{z}\frac{\partial w}{\partial z}.
\end{aligned}
\tag{6.14}
$$

Thus

$$\frac{\partial^2 w}{\partial z^2} + \left(\frac{z}{2D_{\tilde{A}}} - \frac{1}{z}\right)\frac{\partial w}{\partial z} = 0. \tag{6.15}$$

By using integrating factor,

$$I = e^{\int\left(\frac{z}{2D_{\tilde{A}}} - \frac{1}{z}\right)dz} = e^{\frac{z^2}{4D_{\tilde{A}}} - \ln z}, \tag{6.16}$$

we obtain

$$w'(z) = C_1 e^{\ln z - \frac{1}{4D_{\tilde{A}}}z^2}, \tag{6.17}$$

and get the analytic solution for concentration of bacteria $\tilde{A}$, such that

$$\tilde{A}(r,t) = K\, e^{\int \beta_{\tilde{A}}(N)dt}\, e^{-\frac{r^2}{4D_{\tilde{A}}t}}, \tag{6.18}$$

where K is a constant.

From the analytic solution, the equation (6.18) shows that the concentration of motile bacteria increases is proportional to the bacterial growth rate at any given time. When bacteria are placed in a medium that provides adequate nutrient that influence the growth rate, cell numbers will increase in logarithmic fashion and the radius of the colony become larger until nutrient is depleted, at which time the cell growth rate slows and some cells may begin die.

We have employed a similarity solutions to solve the equation above in which the boundary conditions are disregarded. Another type of solution is called travelling wave solutions, that is, solutions of the form $f(x - ct)$ with shape f and speed c.

In order to obtain travelling wave solution, we need initial and boundary conditions. The initial situation corresponds to a constant bacterial colony level within a disk of radius r_c. Thus at $t = 0$ the concentration of bacteria and nutrient can be described by the equation

$$\tilde{A}(r,0) = \begin{cases} a_0, & r < r_c \\ \\ 0, & r > r_c, \end{cases} \tag{6.19}$$

and

$$N(r,0) = N_0. \tag{6.20}$$

We expect that for long times the radius of the colony increases and N tends to zero in the centre, since nutrient has been consumed by bacteria. We also expect that bacteria $\tilde{A}$ will attain limiting concentration due to depletion of nutrient concentration. Furthermore, it is reasonable that

$$\frac{\partial N}{\partial r}(r,t) = 0 \quad \text{and} \quad \tilde{A}(r,t) \to 0 \quad \text{when } r \to \infty. \tag{6.21}$$

We shall investigate travelling wave solutions for different forms of $\beta_{\tilde{A}}(N)$. For case I, we start with exponential growth in which the growth such as

$$\beta_{\tilde{A}}(N)\tilde{A} := \beta_{\tilde{A}} N \tilde{A}. \tag{6.22}$$

Then for case II, we employ a power function in the growth form,

$$\beta_{\tilde{A}}(N)\tilde{A} := \beta_{\tilde{A}} N^n \tilde{A} = \beta_{\tilde{A}} N^2 \tilde{A}. \tag{6.23}$$

where n determines the shape and behaviour of the function. In this case, we take $n = 2$ for simplicity.

For case III we consider type III of Holling function, that is

$$\beta_{\tilde{A}}(N)\tilde{A} := \beta_{\tilde{A}} \frac{N^2}{k^2 + N^2} \tilde{A}, \tag{6.24}$$

where in this case $k = 0.5$ is arbitrary choice and not chosen for biological reasons.

The solutions of three different types of growth equation in the system can be seen in Fig. 6.2. Associated with these results, Fig. 6.2a, 6.2c, and 6.2e show that the colony density diminishes in response to the bacterial expansion and depletion of nutrient. At first, the bacterial concentration rapidly increases with certain radius, and begins to decrease after that point. The bacterial density decreases behind the travelling wave until it approaches zero density due to depletion of nutrient consumed by bacteria. The difference between those figures is the maximum increase of bacterial concentration that is affected by the dynamics of nutrient concentration due to different functions of bacterial growth.

Fig. 6.2b, 6.2d, and 6.2f show concentration of nutrient in the medium. They appear that the shapes of concentration profiles are virtually similar for all nutrient concentration.
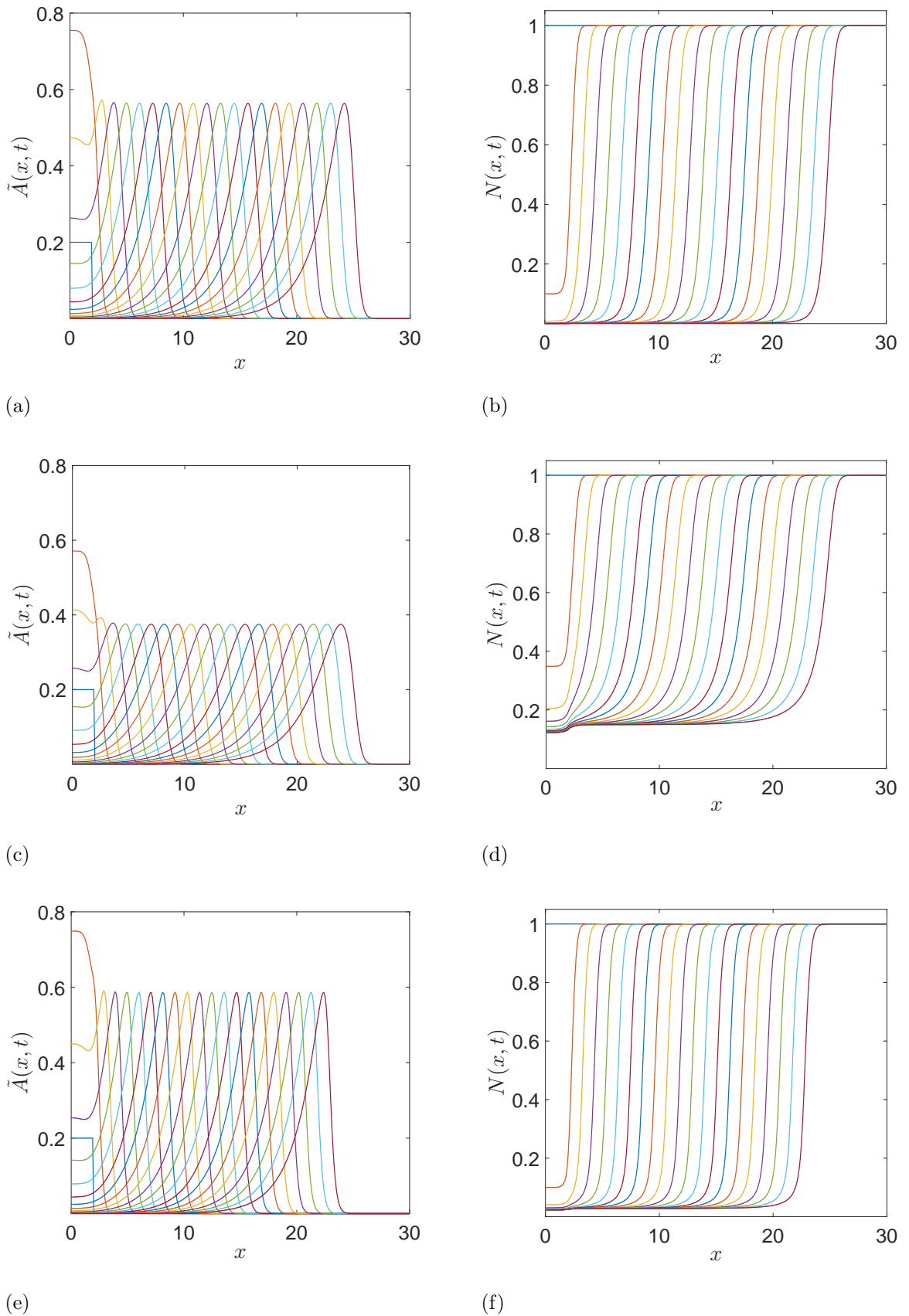
Figure 6.2: The concentration of motile bacteria and nutrient (a,b) type I, (c,d) type II and (e,f) type III. When the diffusion coefficient $D_{\tilde{A}}$ approaches 0, the colony does not spread much. Oppositely, for the larger value of $D_{\tilde{A}}$, the colony expands widely. Here $D_{\tilde{A}} = 0.05$, $\mu = 0.3$, initial value for nutrient concentration $= 1$ and for motile bacteria concentration $= 0.2$
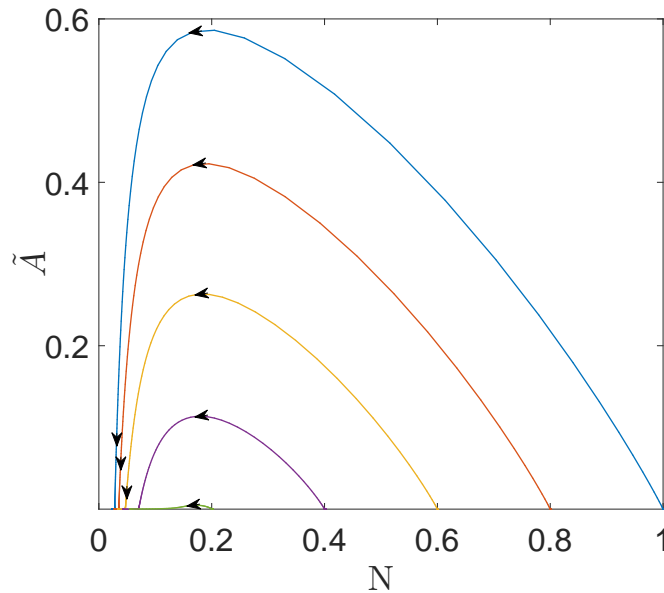
Figure 6.3: Phase portraits of the equations 6.4 and 6.5. Here $D_{\tilde{A}} = 0.05$, $\mu = 0.3$. Initial value for nutrient concentration $= 1, 0.8, 0.6, 0.4$, and 0.2 for blue, red, yellow, purple and green curve, respectively.

After some days of expansion, the nutrient concentration become exhausted, even if that medium initially contained a high concentration of nutrient. We can see the difference between those figures is in the tail. Figure 6.2b shows the solutions for rapidly decaying initial condition compare Fig.6.2d and Fig.6.2f. The nutrient concentration in Fig. 6.2b goes down to almost zero concentration, unlike Fig. 6.2d and Fig. 6.2f that end up with certain low level of nutrient concentration, $N(x, t) = 0.14$ and $N(x, t) = 0.03$, respectively.

In addition, phase plane Fig. 6.3 shows the qualitative behaviour of dynamical systems above become clearer. Here, we only plot the phase plane for type III. We can see from the Fig. 6.2 that the simple model with different forms of growth functions, $\beta_{\tilde{A}}(N)$, have the same behaviour, the simple models are only different in the value of stability points. Fig. 6.3 presents that all the trajectories will move in towards the equilibrium point as t increase, but it should be noted that in this case every trajectory has own equilibrium.

6.4 Bifurcation analysis of simple model I

In this section, we shall analyse the fixed points in the non-linear reaction-diffusion system and also the existence of travelling wave front solutions. Consider the equation for this

system,

$$\frac{\partial \tilde{A}}{\partial t} = D_{\tilde{A}} \nabla^2 \tilde{A} + \beta_{\tilde{A}}(N)\tilde{A} - \mu \tilde{A}$$
$$\frac{\partial N}{\partial t} = -\beta_{\tilde{A}}(N)\tilde{A}.$$
(6.25)

Typically we construct a solution of the system of equations 6.25 using ordinary differential equations. The solutions of 6.25 have the shape of a travelling wave as it propagates. Therefore we shall make the assumption that there exist some solutions with the following form

$$\tilde{A} = \tilde{A}(z) \qquad \text{and} \qquad N = N(z), \qquad z = x - ct \qquad \text{with} \qquad z \in \mathbb{R},$$
(6.26)

where c is the wave speed.

After applying the chain rule, the model becomes

$$-c\tilde{A}' = D_{\tilde{A}}\tilde{A}'' + \beta_{\tilde{A}}(N)\tilde{A} - \mu \tilde{A}$$
$$-cN' = -\beta_{\tilde{A}}(N)\tilde{A},$$
(6.27)

where the prime denotes differentiation with respect to z.

The next step is to get a system of first-order equations, such that

$$\tilde{A}' = B$$
$$B' = \frac{1}{D_{\tilde{A}}}\left(-cB - \beta_{\tilde{A}}(N)\tilde{A} + \mu \tilde{A}\right)$$
$$N' = \frac{\tilde{A}}{c}\beta_{\tilde{A}}(N).$$
(6.28)

Now there is a first-order system of equations that should satisfy the following boundary conditions:

$$\tilde{A}(\infty) = 0, \qquad \tilde{A}(-\infty) = 0,$$
$$B(\infty) = 0, \qquad B(-\infty) = 0,$$
$$N(\infty) = 1, \qquad N(-\infty) = N_*,$$
(6.29)

where $N_* \approx 0$ is a small value for the nutrient concentration.

As mentioned before, in this chapter we explore three different growth types of bacteria. For the **case I**, we have $\beta_{\tilde{A}}(N) := \beta_0 N$, then the original equations 6.28 may be rewritten as

$$\tilde{A}' = B$$
$$B' = \frac{1}{D_{\tilde{A}}}\left(-cB - \beta_0 N\tilde{A} + \mu \tilde{A}\right)$$
$$N' = \frac{\tilde{A}}{c}\beta_0 N.$$
(6.30)

where the prime denotes differentiation with respect to z.

From equations 6.30, we derive

$$B' = \frac{1}{D_{\tilde{A}}}\left(-c\tilde{A}' - cN' + \mu \frac{cN'}{\beta_0 N}\right).$$
(6.31)

From here, we can integrate to obtain

$$B = \frac{1}{D_{\tilde{A}}}\left(-c\tilde{A} - cN + \frac{\mu c}{\beta_0}lnN\right) + K \tag{6.32}$$

where K is a constant of integration.

We shall consider boundary conditions 6.29, $B(\infty) = 0$, such that

$$\text{BCs}\,(\infty): \qquad 0 = -\frac{c}{D_{\tilde{A}}} + K. \tag{6.33}$$

Thus we can obtain an explicit expression for the wave speed, after applying the boundary conditions 6.29, $B(-\infty) = 0$. This leads to

$$\text{BCs}\,(-\infty): \qquad N_* - 1 = \frac{\mu}{\beta_0}lnN_*. \tag{6.34}$$

We are interested in the value of $\frac{\mu}{\beta_0}$ such that the last equation has two roots for N_*. Thus we need to determine the value by plotting the equation 6.34 in Fig. 6.4. For a fixed c constant, we see how the solution N_* depend on $\frac{\mu}{\beta_0}$. This procedure is quite general for determining the solutions.

From Fig. 6.4, we can see if

1. $\frac{\mu}{\beta_0} > 1$, provides $N_* = 1$ or $N_* > 1$.

2. $\frac{\mu}{\beta_0} < 1$, provides $N_* = 1$ or $N_* < 1$.

Therefore $\frac{\mu}{\beta_0} < 1$ gives more realistic solution for the system 6.30. The N_* value should be less than or equal to the initial value of the nutrient concentration ($N = 1$).

In a similar manner, we can investigate other types of growth function by employing the same above steps. For the **case II**, we have $\beta_{\tilde{A}}(N) := \beta_0 N^2$, then the original equations 6.28 may be rewritten as

$$\tilde{A}' = B$$
$$B' = \frac{1}{D_{\tilde{A}}}\left(-cB - \beta_0 N^2\tilde{A} + \mu\tilde{A}\right) \tag{6.35}$$
$$N' = \frac{\tilde{A}}{c}\beta_0 N^2,$$

where the prime denotes differentiation with respect to z.

From equations 6.35, we derive

$$B' = \frac{1}{D_{\tilde{A}}}\left(-c\tilde{A}' - cN' + \frac{\mu cN'}{\beta_0 N^2}\right). \tag{6.36}$$

From here, we can integrate to obtain

$$B = \frac{1}{D_{\tilde{A}}}\left(-c\tilde{A} - cN + \frac{\mu c}{\beta_0 N}\right) + K \tag{6.37}$$
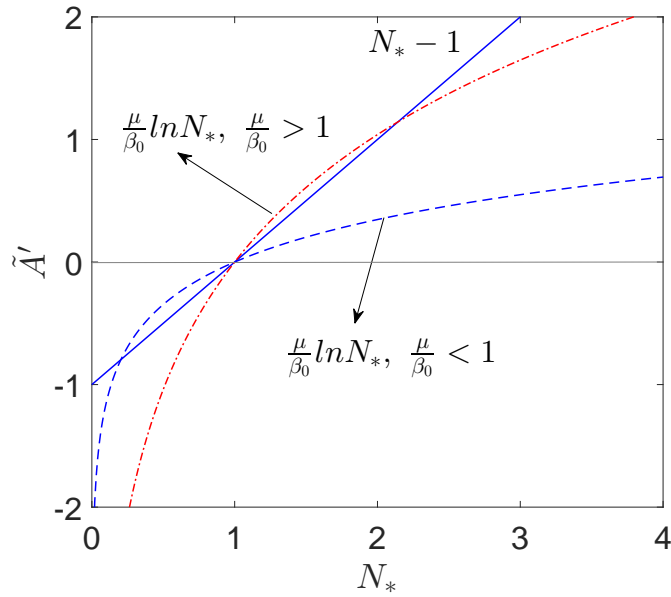
Figure 6.4: Approximate analytic procedure for determining the solution case I. Here $\mu = 0.3$, $\beta_0 = 0.5$ for case $\frac{\mu}{\beta_0} < 1$ (blue dashed-line) and $\beta_0 = 0.2$ for case $\frac{\mu}{\beta_0} > 1$ (red dashdotted-line).

where K is a constant of integration.

We shall consider boundary conditions 6.29, $B(\infty) = 0$, such that

$$\text{BCs}\,(\infty): \qquad 0 = \frac{1}{D_{\tilde{A}}}\left(-c + \frac{\mu c}{\beta_0}\right) + K. \tag{6.38}$$

Thus we can obtain an explicit expression for the wave speed c after applying the boundary conditions 6.29, $B(-\infty) = 0$. This lead to

$$\text{BCs}\,(-\infty): \qquad N_* - 1 = \frac{\mu}{\beta_0}\left(1 - \frac{1}{N_*}\right), \tag{6.39}$$

Fig. 6.5 represents equation 6.35. Then, we can see if

1. $\frac{\mu}{\beta_0} > 1$, provides $N_* = 1$ or $N_* > 1$.

2. $\frac{\mu}{\beta_0} < 1$, provides $N_* = 1$ or $N_* < 1$.

Therefore $\frac{\mu}{\beta_0} < 1$ gives more realistic solution for the system 6.35. Similar to the case I, the N_* value should be less than or equal to the initial value of the nutrient concentration $(N = 1)$.

For the **case III**, we have $\beta_{\tilde{A}}(N) := \frac{\beta_0 N^2}{k^2 + N^2}$, then the original equations 6.28 may be rewritten as

$$\tilde{A}' = B$$
$$B' = \frac{1}{D_{\tilde{A}}}\left(-cB - \beta_0\frac{N^2}{k^2 + N^2}\tilde{A} + \mu\tilde{A}\right) \tag{6.40}$$
$$N' = \frac{\beta_0}{c}\frac{N^2}{k^2 + N^2}\tilde{A},$$
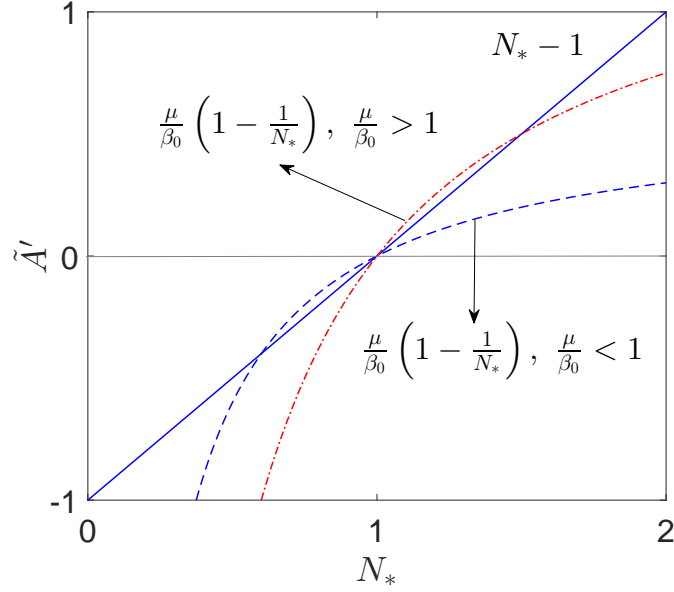
Figure 6.5: Approximate analytic procedure for determining the solution case I. Here $\mu = 0.3$, $\beta_0 = 0.5$ for case $\frac{\mu}{\beta_0} < 1$ (blue dashed-line) and $\beta_0 = 0.2$ for case $\frac{\mu}{\beta_0} > 1$ (red dashdotted-line).

where the prime denotes differentiation with respect to z.

From equations 6.40, we derive

$$B' = \frac{1}{D_{\tilde{A}}} \left(-c\tilde{A}' - cN' + \frac{\mu c}{\beta_0} N' + \frac{\mu c k^2 N'}{\beta_0 N^2} \right). \tag{6.41}$$

From here, we can integrate to obtain

$$B = \frac{1}{D_{\tilde{A}}} \left(-c\tilde{A} - cN + \frac{\mu c}{\beta_0} N - \frac{\mu c k^2}{\beta_0 N} \right) + K, \tag{6.42}$$

where K is a constant of integration.

We shall consider boundary conditions 6.29, $B(\infty) = 0$, such that

$$\text{BCs}\,(\infty): \qquad 0 = \frac{1}{D_{\tilde{A}}} \left(-c - \frac{\mu c}{\beta_0} - \frac{\mu c k^2}{\beta_0} \right) + K. \tag{6.43}$$

Then by substituting 6.43 and applying the boundary conditions 6.29, $B(-\infty) = 0$, we get

$$\text{BCs}\,(-\infty): \qquad N_* - 1 = \frac{\mu}{\beta_0} \left(N_* - \frac{k^2}{N_*} + k^2 - 1 \right). \tag{6.44}$$

Similar to the case I and II, we are interested in the value of $\frac{\mu}{\beta_0}$. The last equation has two roots for N_* with more possibilities compared to the previous cases. By plotting the equation 6.44 in Fig. 6.6, we see how the solution N_* depends on $\frac{\mu}{\beta_0}$ and k.

Rewriting equation 6.44 gives

$$aN^2 - (a + b) N + b = 0, \tag{6.45}$$

where equation 6.44 has two roots $N_* = 1$ or $N_* = \frac{b}{a}$ with

$$a := 1 - \frac{\mu}{\beta_0} \qquad \text{and} \qquad b := \frac{\mu k^2}{\beta_0}. \qquad (6.46)$$

From Fig. 6.6, we can see if

1. $\frac{\mu}{\beta_0} > 1$, provides $N_* = 1$ or N_* is negative for every k value.

2. $\frac{\mu}{\beta_0} < 1$ with $\frac{\mu}{\beta_0}\left(k^2 + 1\right) < 1$, provides $N_* = 1$ or $N_* < 1$.

3. $\frac{\mu}{\beta_0} < 1$ with $\frac{\mu}{\beta_0}\left(k^2 + 1\right) > 1$, provides $N_* = 1$ or $N_* > 1$.

Therefore $\frac{\mu}{\beta} < 1$ with $\frac{\mu}{\beta_0}\left(k^2 + 1\right) < 1$ gives more realistic solution for the system 6.40. Similar to the previous cases, the N_* value should be less than or equal to the initial value of the nutrient concentration $(N = 1)$.
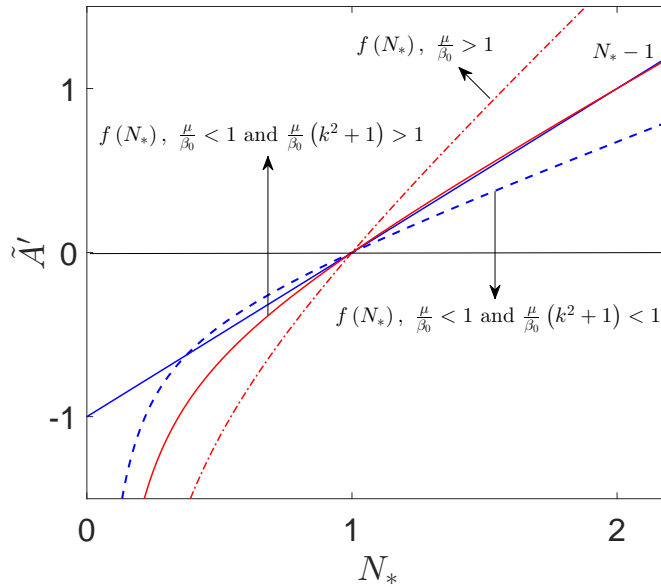
Figure 6.6: Approximate analytic procedure for determining the solution case I. Here $\mu = 0.3$, $\beta_0 = 0.5$ for case $\frac{\mu}{\beta_0}\left(k^2 + 1\right) < 1$ (blue dashed-line), $\beta_0 = 0.34$ for case $\frac{\mu}{\beta_0(k^2+1)} < 1$ (red solid-line) and $\beta_0 = 0.2$ for case $\frac{\mu}{\beta_0}\left(k^2 + 1\right) > 1$ (red dashdotted-line).

In addition, we shall provide phase plane analysis and explore travelling wave-front for equations 6.28. Phase plane analysis gives alternative meanings on the qualitative behaviour of the dynamical system. We can get information about stability of the system and the existence of the solutions related to the travelling wave. In this case, we consider only the case III that is more complex than case I and case II, which is expected to be able to cover case I and II.

The conditions in 6.29 can be expressed in a more compact form as

$$\lim_{z \to \infty} \left(\tilde{A}, B, N \right) = (0, 0, 1), \qquad \lim_{z \to -\infty} \left(\tilde{A}, B, N \right) = (0, 0, N_*) \tag{6.47}$$

The system 6.40 has critical points at $(0, 0, 1)$ and $(0, 0, N_*)$. In order to determine the stability of these points, it is required that we linearise the system present in 6.40. As such, the Jacobian matrix associated to the linearised system is expressed as,

$$J \left(\tilde{A}, B, N \right) = \begin{bmatrix} \frac{\partial}{\partial \tilde{A}} \tilde{A}' & \frac{\partial}{\partial B} \tilde{A}' & \frac{\partial}{\partial N} \tilde{A}' \\ \\ \frac{\partial}{\partial \tilde{A}} B' & \frac{\partial}{\partial B} B' & \frac{\partial}{\partial N} B' \\ \\ \frac{\partial}{\partial \tilde{A}} N' & \frac{\partial}{\partial B} N' & \frac{\partial}{\partial N} N' \end{bmatrix}$$

$$\tag{6.48}$$

$$= \begin{bmatrix} 0 & 1 & 0 \\ \\ -\frac{\beta_0}{D_{\tilde{A}}} \frac{N^2}{k^2 + N^2} + \frac{\mu}{D_{\tilde{A}}} & -\frac{c}{D_{\tilde{A}}} & -\frac{2\beta_0 k^2}{D_{\tilde{A}}} \frac{Nk^2}{(k^2 + N^2)^2} \tilde{A} \\ \\ \frac{\beta_0}{c} \frac{N^2}{k^2 + N^2} & 0 & \frac{2\beta_0 k^2}{c} \frac{Nk^2}{(k^2 + N^2)^2} \end{bmatrix}.$$

From here, we can obtain the characteristic equation defined as,

$$det \left(\lambda I - J \right) = \begin{vmatrix} \lambda & -1 & 0 \\ \\ \frac{\beta_0}{D_{\tilde{A}}} \frac{N^2}{k^2 + N^2} - \frac{\mu}{D_{\tilde{A}}} & \lambda + \frac{c}{D_{\tilde{A}}} & \frac{2\beta_0 k^2}{D_{\tilde{A}}} \frac{Nk^2}{(k^2 + N^2)^2} \tilde{A} \\ \\ -\frac{\beta_0}{c} \frac{N^2}{k^2 + N^2} & 0 & \lambda - \frac{2\beta_0 k^2}{c} \frac{Nk^2}{(k^2 + N^2)^2} \tilde{A} \end{vmatrix}, \tag{6.49}$$

where λ is an eigenvalue associated to the system 6.40 at a critical point. The characteristic equation is given by

$$\lambda \left(\lambda + \frac{c}{D_{\tilde{A}}} \right) \left(\lambda - \frac{2\beta_0 k^2}{c} \frac{Nk^2}{(k^2 + N^2)^2} \tilde{A} \right) + \left(\frac{2\beta_0 k^2}{D_{\tilde{A}}} \frac{Nk^2}{(k^2 + N^2)^2} \tilde{A} \right) \left(\frac{\beta_0}{c} \frac{N^2}{k^2 + N^2} \right)$$

$$\tag{6.50}$$

$$+ \left(\frac{\beta_0}{D_{\tilde{A}}} \frac{N^2}{k^2 + N^2} - \frac{\mu}{D_{\tilde{A}}} \right) \left(\lambda - \frac{2\beta_0 k^2}{c} \frac{Nk^2}{(k^2 + N^2)^2} \tilde{A} \right) = 0.$$

For the critical point $(0, 0, 1)$, equation 6.50 becomes,

$$\lambda^3 + \frac{c}{D_{\tilde{A}}} \lambda^2 + \left(\frac{\beta_0}{D_{\tilde{A}}} \frac{1}{k^2 + 1} - \frac{\mu}{D_{\tilde{A}}} \right) \lambda = 0. \tag{6.51}$$

Solving for eigenvalues $\lambda_{(0,0,1)}^{\pm}$ gives,

$$\lambda_{(0,0,1)}^{\pm} = \frac{-\frac{c}{D_{\tilde{A}}} \pm \sqrt{\frac{c^2}{D_{\tilde{A}}^2} - 4\left(\frac{\beta_0}{D_{\tilde{A}}}\frac{1}{k^2+1} - \frac{\mu}{D_{\tilde{A}}}\right)}}{2}. \tag{6.52}$$

We can obtain the eigenvectors associated with the eigenvalues by solving

$$(\lambda I - \tilde{J})\mathbf{v} = 0, \tag{6.53}$$

where $\tilde{J}$ is the coefficient matrix defined in 6.48, evaluated at the stationary point. Thus the equations corresponding to the eigenvectors associated to $\lambda_{(0,0,1)}^{\pm}$ are given by,

$$\tilde{A} = (\lambda I - \tilde{J})(N-1). \tag{6.54}$$

In a similar manner to analyse the critical point $(0,0,N_*)$, equation 6.50 becomes

$$\lambda^3 + \frac{c}{D_{\tilde{A}}}\lambda^2 + \left(\frac{\beta_0}{D_{\tilde{A}}}\frac{N_*}{k^2+N_*} - \frac{\mu}{D_{\tilde{A}}}\right)\lambda = 0. \tag{6.55}$$

Thus from equation 6.55, we can solve for the eigenvalues $\lambda_{(0,0,N_*)}^{\pm}$, providing

$$\lambda_{(0,0,N_*)}^{\pm} = \frac{-\frac{c}{D_{\tilde{A}}} \pm \sqrt{\frac{c^2}{D_{\tilde{A}}^2} - 4\left(\frac{\beta_0}{D_{\tilde{A}}}\frac{N_*}{k^2+N_*} - \frac{\mu}{D_{\tilde{A}}}\right)}}{2}. \tag{6.56}$$

By using 6.54, the equations representing the eigenvectors associated to $\lambda_{(0,0,N_*)}^{\pm}$ are

$$\tilde{A} = \lambda_{(0,0,N_*)}^{\pm}N \tag{6.57}$$
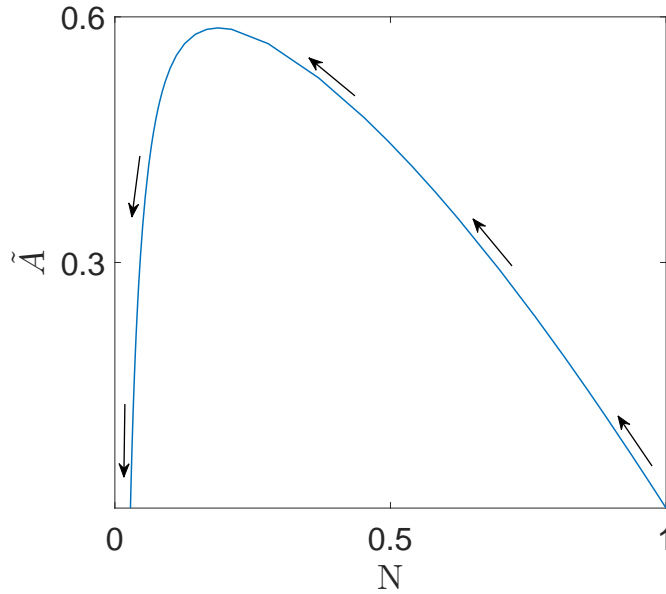
Figure 6.7: Phase portraits of the system 6.40. $\beta = 2$, $\mu = 0.3$, $k = 0.4$, and $D_{\tilde{A}} = 0.05$.

The phase portraits can be computed numerically by using MATLAB (see Fig. 6.7). In this figure, the motile-cells concentration, $\tilde{A}$, is plotted versus the nutrient concentration,

N. At first, nutrient concentration start from a sufficient level for colony growth and thus, motile-cells concentration increase. Then the nutrient concentration decreases (the point in the graph moves to the left) because it is consumed by bacteria, which is followed by a decrease of bacterial-cell concentration due to lack of nutrient. The arrows shows that the equilibrium $\left(\tilde{A}, N \right) = (0, N_0)$ is unstable (in this case $N_0 = 1$), whereas the equilibrium $\left(\tilde{A}, N \right) = (0, N_*)$ is stable with $N_* = \frac{\mu k^2}{\beta - \mu}$. Fig. 6.7 is exactly similar to the Fig. 6.3. This shows that linearisation of partial differential equation 6.4 and 6.5 become 6.28 does not change the behaviour of the travelling wave system.

In order for a travelling wave to exist, from the phase portraits depicted in Fig. 6.7, it is required that motile-cells concentration, $\tilde{A}$, must be positive. Therefore, the value of the *discriminant* in equation 6.52 and 6.56 should be greater than or equal to zero,

$$c^2 \geq 4D_{\tilde{A}} \left(\frac{\beta_0 N_*^2 - \mu \left(k^2 + N_*^2 \right)}{k^2 + N_*^2} \right). \tag{6.58}$$

Therefore, the minimum travelling wave speed is

$$c \geq \sqrt{4D_{\tilde{A}} \left(\frac{\beta_0 N_*^2 - \mu \left(k^2 + N_*^2 \right)}{k^2 + N_*^2} \right)}, \tag{6.59}$$

with some conditions that fulfil the solutions for equation system 6.40, i.e. $\frac{\mu}{\beta} < 1$ with $\frac{\mu}{\beta_0} \left(k^2 + 1 \right) < 1$, and $0 < N_* \leq 1$. This is illustrated in Figure 6.8,

(a)

(b)
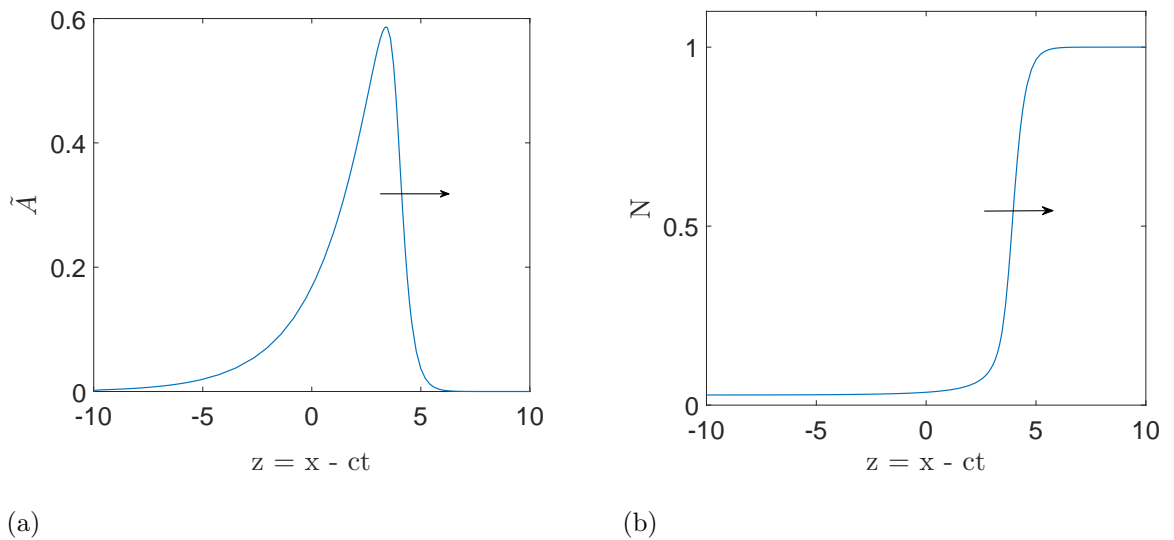
Figure 6.8: travelling wave front solution for (a) motile-cells concentration and (b) nutrient concentration with $c = 0.65$

6.5 Simple model II : Motile and non-motile bacteria

In this section, we give particular attention to non-motile and motile bacteria, which can be seen in Fig. 6.9. The underlying reason of this is that sufficient nutrient acquisition can

promote formation of the flagella that enables motile bacteria to actively expand the colony for more nutrient. Furthermore, the model is also extended from the model in chapter 2 through modifying the assumption of growth rate; bacteria have different growth rate because the required nutrient by non-motile and motile bacteria are not equal.
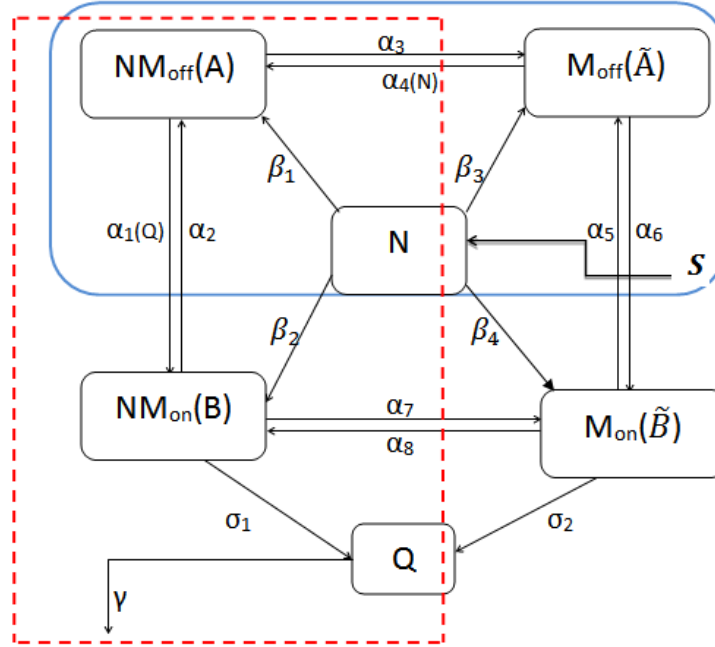
Figure 6.9: A flow diagram to describe the biological interactions between different types of bacteria (NM$_{\text{off}}$, NM$_{\text{on}}$, M$_{\text{off}}$, and M$_{\text{on}}$) that involve three processes: growth, transition, and signal molecule production. The diagram that is surrounded by red dashed-lines has been discussed in chapter 2. Now, we consider motile bacteria by looking at the diagram that is surrounded by blue solid-lines. The growth of bacteria is affected by nutrient concentration, N, which gets S as nutrient source. β_1 and β_3 associated with each *arrow* reflect the associated growth rate for bacteria A and $\tilde{A}$, respectively. NM = non-motile bacteria and M = motile bacteria, with "off" subscript representing down-regulated bacteria. α_3 and α_4 associated with each *arrow* reflect the associated transition rate between different types of bacteria, where α_4 is affected by nutrient concentration.

Associated with the model in Fig. 6.9, we assume bacteria $\tilde{A}$ diffuse but bacteria A do not. Furthermore, there are transition processes from bacteria A to $\tilde{A}$, and conversely.

A set of equations to describe the situation is as follows:

$$\frac{\partial A}{\partial t} = \beta_A(N)A + \alpha_4(N)\tilde{A} - \alpha_3 A, \tag{6.60}$$

and

$$\frac{\partial \tilde{A}}{\partial t} = D_{\tilde{A}} \, \nabla^2 \, \tilde{A} + \beta_{\tilde{A}}(N)\tilde{A} + \alpha_3 A - \alpha_4(N)\tilde{A}$$

$$= D_{\tilde{A}} \left(\frac{\partial^2 \tilde{A}}{\partial r^2} + \frac{1}{r}\frac{\partial \tilde{A}}{\partial r} \right) + \beta_{\tilde{A}}(N)A + \alpha_3 A - \alpha_4(N)\tilde{A} \qquad (6.61)$$

$$= \frac{D_{\tilde{A}}}{r}\frac{\partial}{\partial r}\left(r\frac{\partial \tilde{A}}{\partial r} \right) + \beta_{\tilde{A}}(N)\tilde{A} + \alpha_3 A - \alpha_4(N)\tilde{A},$$

where β_1 and β_3 represent the growth-rates of non-motile and motile bacteria, respectively. In addition, α_3 represents the transition rate from non-motile to motile bacteria. Conversely, α_4 represents the transition rate from motile to non-motile bacteria.

Referring to the earlier results, the level of nutrient in the medium is one of the important factors on the biological dynamics. It is clear that nutrient decreases as it is consumed by bacteria A and $\tilde{A}$. The rate-of-change of nutrient, N is given by

$$\frac{\partial N}{\partial t} = S - \beta_A(N)A - \beta_{\tilde{A}}(N)\tilde{A}. \qquad (6.62)$$

In order to proceed, we apply some assumptions for this system. We apply exponential growth rate on bacteria A and $\tilde{A}$. Moreover as we discussed in the beginning, transition between bacterial types from non-motile to motile cells or conversely is one bacterial behaviour to respond to nutrient availability in their environment, which has a different fashion for different species (see section 6.2). Here, we take one case by assuming that bacteria $\tilde{A}$ transform from motile to non-motile cells if the level of nutrient concentration is very low to save expensive energy. Thus α_4 is a function of nutrient concentration, $\alpha_4\,(N)$. Typically, the transition rate from motile to non-motile cells can be approximately modelled with a Hill function of the form $C_0 + (C_1 - C_0)\,\frac{N^p}{k^p + N^p}$. The three parameters of the Hill equation are C_0, C_1 and k, while p represents the Hill function coefficient that determines the shape of the transition rate function, which has value $p > 1$. Associated with the case that we have decided above, parameter values of C_0 and C_1 should fulfil $C_1 < C_0$. We can see the function of transition rate from motile to non-motile cells in Fig. 6.10. The transition rate from motile to non-motile is high when the concentration of nutrient is very low but, the transition rate decreases with increasing the nutrient level. There is always some transition from motile to non-motile bacteria even with a high level of nutrient. Bacteria does not necessarily only use nutrient for motility, but also for gene expression. Thus, some bacteria become non-motile even with high nutrient concentration. This is realistic and biologically relevant to the energy required for transcription and translation process in gene expression Ralston (2008b). Meanwhile, we take a constant value for the transition rate from non-motile to motile cells (α_3) to simplify the problem.

From the above system of partial differential equations, we imposed the following initial
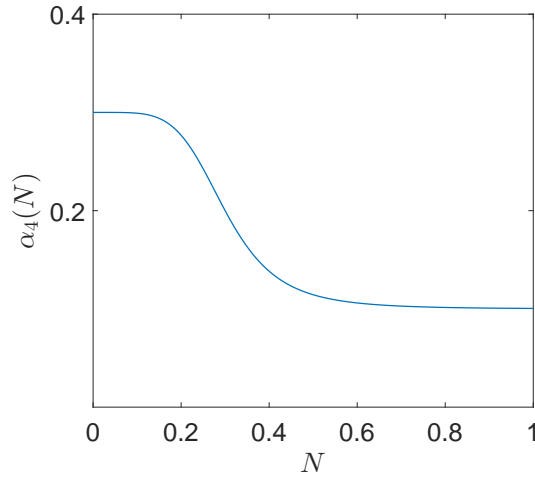
Figure 6.10: Transition process rate from motile to non-motile cells affected by the nutrient concentration. Here, $C_0 = 0.3$, $C_1 = 0.1$, $k = 0.3$ and coefficient Hill function $p = 5$.

conditions:

$$A = 0.05, \qquad \tilde{A} = 0.2 * (\text{radius of dish} < 0.5), \qquad N = 1, \tag{6.63}$$

and boundary conditions:

$$
\begin{aligned}
A(\infty) &= 0, & A(-\infty) &= 0, \\
\tilde{A}(\infty) &= 0, & \tilde{A}(-\infty) &= 0, \\
N(\infty) &= 1, & N(-\infty) &= N_*,
\end{aligned}
\tag{6.64}
$$

where $N_* \approx 0$ is a small value for the nutrient concentration.

We have obtained that the concentration of non-motile cells is roughly flat in the centre radius of the colony. From the simulation result, we can see that the concentration of non-motile cells increases with r a little before decreasing to zero (see Fig. 6.11a), which is affected by the transition process. The motile cells get converted into non-motile cells due to depletion of nutrient in any part of dish.

The concentration of motile bacteria increases due to diffusion into rich nutrient areas. The motile-cells diffuse and develop the bacterial colony size, spread to gain access to the nutrient availability and grow. We can see in Fig. 6.11b that the profile of motile-cells has a maximum level of concentration for a certain time near the centre of the colony. After going through that phase, the concentration of motile cells decreases to zero, similar to the non-motile cells. The dynamical behaviour of the total concentration between motile and non-motile cells can be seen in Fig. 6.11c.

At the same time, the concentration of nutrient is depleted due to consumption by non-motile and motile cells. The nutrient concentration become exhausted, even if that medium initially contained a high concentration of nutrient (see Fig. 6.11d).

(a)

(b)

(c)

(d)
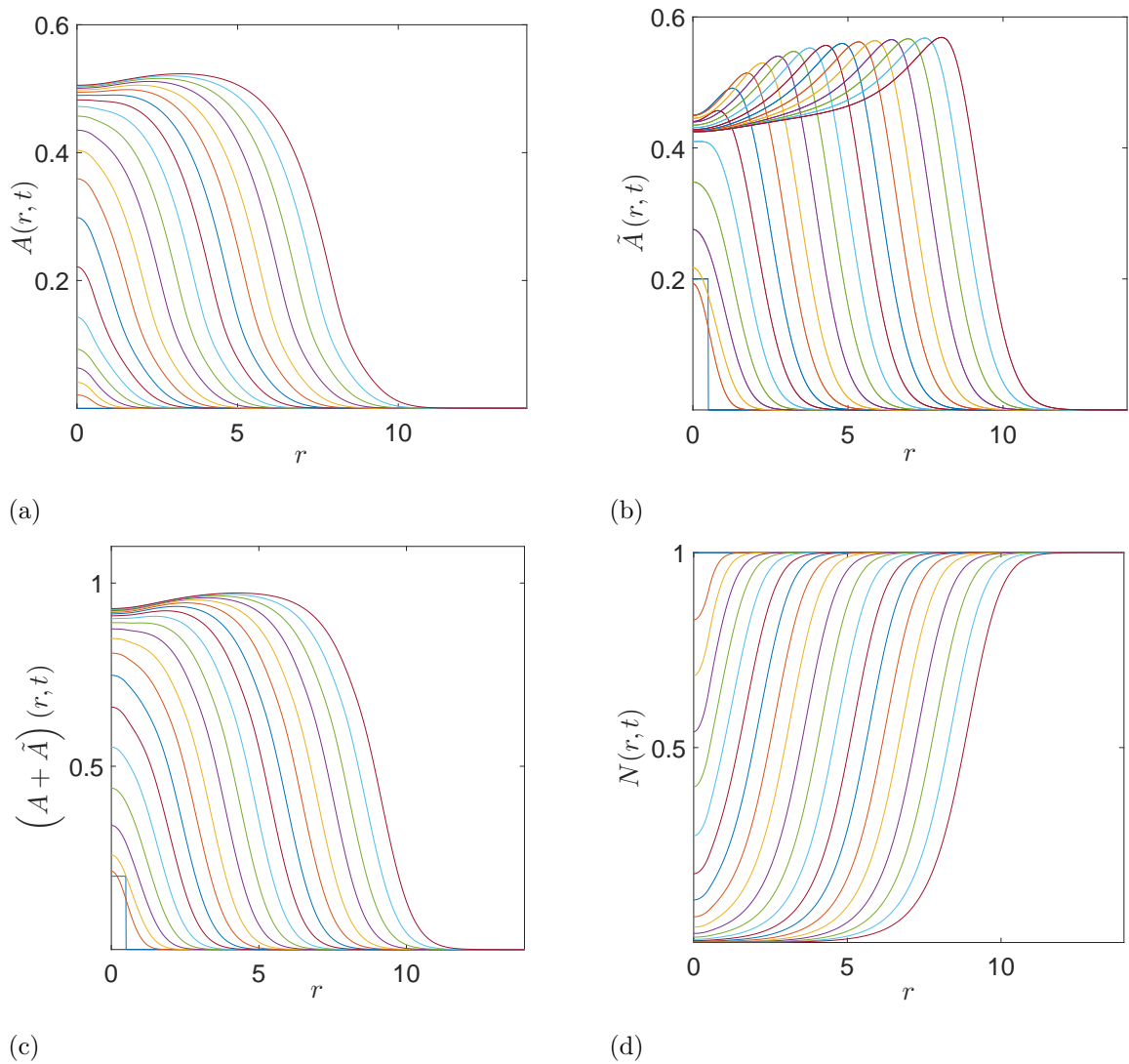
Figure 6.11: The concentration of (a) non-motile cells, (b) motile cells, (c) non-motile and motile cells and (d) nutrient. Here $\beta_1 = 0.3/\min$, $\beta_3 = 0.9/\min$, $D_{\tilde{A}} = 0.1 cm^2/\min$, $\alpha_3 = 0.25/\min$, and α_4 is Hill function in Fig. 6.10.

There are many mathematical models that have been published that discuss the factors that control the bacterial motility switch. Adler and Templeton (1967) examined the essential aspect of nutrient to stimulate the motility of *Escherichia coli* and also oxygen for particular conditions. Douarche et al (2009) showed that the motility transition of *E. coli* is correlated to oxygen concentration. They presented that oxygen penetrating into an anaerobic experiment induces the coexistence of two domains of non-motile and motile cells. Koirala et al (2014) investigated how nutrient affect motility in *Salmonella enterica* and observed coexisting populations of non-motile and motile cells, where the nutrient concentration in the growth medium determines the distribution of each population. Furthermore, it is not only nutrient and oxygen that affect regulation of motility behaviour, Tasaki et al (2017) demonstrated how environmental pH variations stimulate morphological change in *Bacillus subtilis* biofilms, which means indirectly they also affect bacterial motility.

While there are considerable number of studies about the transition of bacteria from non-motile to motile, none of these studies couple nutrient concentrations and QS signal molecule production to motility behaviour. Many papers have demonstrated the important role of QS signal molecule on bacterial motility. Daniels et al (2004) presented that bacteria produced signal molecules that regulate a flagella-driven movement in which bacteria can spread as a biofilm over a surface, then Daniels et al (2006) and Dixit et al (2017) showed that AHL molecule controls swarming behaviour of *Rhizobium etli*. Atkinson and Williams (2009) showed that autoregulated QS circuits of *Yersinia pseudotuberculosis* are able to produce up to eight different AHLs to control flagella-mediated motility by regulating the expression of the motility master regulator *flhDC*. Also Shrout et al (2011) demonstrated that some aspects of motility in *Pseudomonas aeruginosa* are influenced by QS signal molecule.

Therefore, as mentioned in the introduction, this basic model needs to be extended by considering regulation of QS signal molecules. Some bacteria produce surfactant as a wetting agent that is controlled by certain gene production, which is regulated by the QS signalling system. Biosurfactant play essential roles in bacterial cell motility, interaction and differentiation. Different types of bacteria produce different types of surfactant; for example rhamnolipids produced by *P. aeruginosa* (Jarvis and Johnson, 1949), serrawettins produced by *Serratia marcescens* (Matsuyama et al, 1989), Emulsan produced by *Acinetobacter calcoaceticus* (Shoham et al, 1983), Shoporolipids produced by *candida* and *Starmerella clade* (Kurtzman et al, 2010), syringafactin produced by *Pseudomonas syringae* (Burch et al, 2012), etc. Thus surfactant will be also considered in the model that we shall discuss in the next section.

Before we construct the complex model, we shall provide some biological background that has relevant information for the understanding and modelling of bacterial colony expansion. In particular, we present briefly information about rhamnolipid and its role in bacterial colony growth.

6.6   Background complex model : Further analysis of travelling wave on *las* system

In the previous chapter, we have demonstrated the pulse generator of the *las* system for single cells. We also illustrated how this potential pulse generator affects cell-cell communication within a colony in a linear chain of cells. In this section, we shall investigate travelling waves in response to a diffusing extracellular QS signal in spreading of bacterial colony.

Bacteria produce and release diffusible QS signal molecules. There have been extensive studies about the diffusing of QS signal molecules, but only a little research that focuses on

QS diffusion in spatially growing colonies. Ward et al (2003) introduced certain conditions for the existence of travelling waves in the model of a QS system by considering the diffusing of signal molecules. Dilanji et al (2012) demonstrated that diffusion of QS signal molecules generate spatial and temporal patterns that can synchronize gene expression. Based on Dilanji et al (2012)'s finding, Langebrake et al (2014) model a colony of the bacterium *Aliivibrio fischeri* and they found that LuxR-LuxI system can exhibit a travelling wave of QS activation in extended of colony. Most studies about spatially extended QS systems focus on biofilm development, for example (Dockery and Keener, 2001; Chopp et al, 2002; Anguige et al, 2006; Klapper and Dockery, 2010; Frederick et al, 2011).

At the first step, we focus on the *las* system only. In the previous chapter, Eqs. 4.15 and 4.16, we have two non-dimensional equations to describe the dynamic of the *las* QS system by considering extracellular 3O-C12-HSL as a constant, such that $\frac{d\eta}{d\tau}$ and $\frac{d\xi}{d\tau}$ with a_1 as a key non-dimensional parameter in the system that depends on the extracellular 3O-C12-HSL (H_{ex}), $a_1 = \frac{H_{ex}k_L^+}{k_L^-}$. Thus, once extracellular 3O-C12-HSL is considered as a variable on the *las* system, we define a_1 as a function of H_{ex} .

We also have introduced non-dimensional label for extracellular 3O-C12-HSL as ζ (see Eqs. 4.19). As extracellular 3O-C12-HSL is freely diffusible, we describe the spatial spread of H_{ex} (concentration $H_{ex}(x,t)$, nM) by the diffusion equation

$$\frac{\partial \zeta}{\partial \tau} = \frac{\partial^2 \zeta}{\partial \tilde{x}^2} \tag{6.65}$$

where $\zeta, \tilde{x}$ and τ are non-dimensional forms of H_{ex}, x and t.

Hence, we describe our complete non-dimensional model of the *las* system as

$$
\begin{aligned}
\frac{\partial \eta}{\partial \tau} &= \frac{(\eta + a_1(\zeta))^2}{a_2(1+\xi)^2(\eta + a_1(\zeta)+1)^2 + (\eta + a_1(\zeta))^2} - a_3\eta \\
\frac{\partial \xi}{\partial \tau} &= \frac{a_4(\eta + a_1(\zeta))^2}{a_2(1+\xi)^2(\eta + a_1(\zeta)+1)^2 + (\eta + a_1(\zeta))^2} - a_5\xi \\
\frac{\partial \zeta}{\partial \tau} &= \frac{\partial^2 \zeta}{\partial \tilde{x}^2} + \eta - a_6\zeta.
\end{aligned}
\tag{6.66}
$$

Using the non-dimensional parameter values listed in chapter 4, we solve the full model 6.66 numerically. To simplify the model of this phenomenon, we focus on a linear chain of cells in a colony. In this and later models, therefore, we are no longer working in polar coordinates. The model solutions exhibit propagation of pulses. Three types of figure are presented in Fig. 6.12 where each consist of two types of initial spike propagation. The left sides of figures (Fig. 6.12a, 6.12c, 6.12e) represent individual cells coupled together and impose left spike propagation in the initial condition of the system. Meanwhile, we impose centre spike initial condition of the system for the right figures (Fig. 6.12b, 6.12d, 6.12f).

These travelling pulses depend on the initial condition. Related to our finding in chapter 4, if there is large perturbation on 3O-C12-HSL production, then it results in a pulse

(a)

(b)

(c)

(d)

(e)

(f)
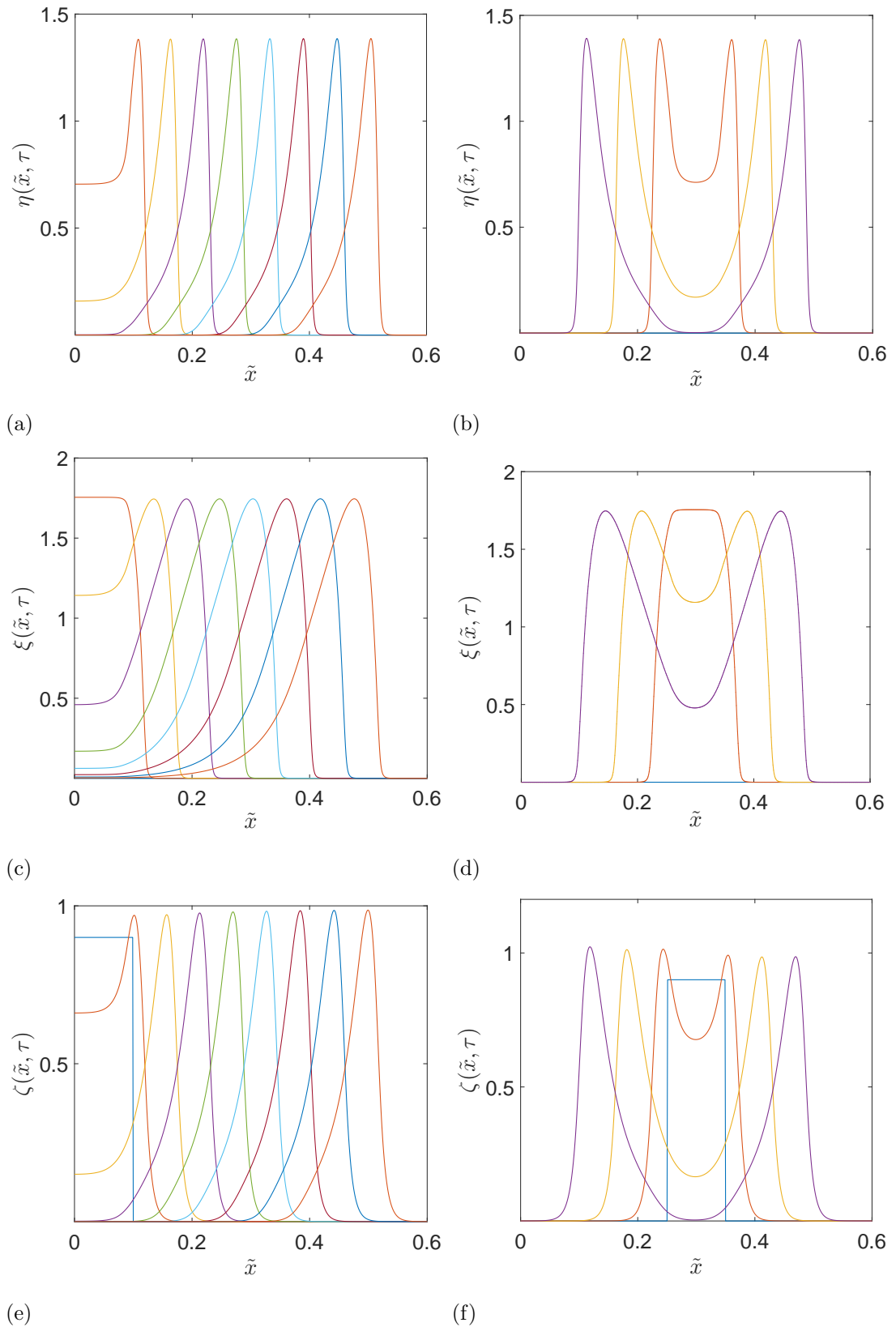
Figure 6.12: Travelling wave as simulations of system 6.66. Figures on the left (Fig. 6.12a, 6.12c, 6.12e) and right (Fig. 6.12b, 6.12d, 6.12f) sides are the simulation results when the individual cells are coupled together with left and centre spike propagation, respectively. x- and y- axes represent space variation of (a,b) LasI concentration η, (c,d) RsaL concentration ξ, (e,f) extracellular 3O-C12-HSL concentration ζ. All parameters value are in chapter 4.

generator on the *las* system, i.e. pulse production of LasI that is followed by RsaL. Thus in this model, we employ an initial condition that gives a pulse. At the same time, we impose the diffusion of extracellular 3O-C12-HSL to describe the spatial spread of signal molecules.

By considering the behaviour of a large perturbation in Fig. 4.2, Fig. 6.12a shows the concentration of LasI (η) increasing up to certain level and then decreasing to zero concentration. The variable ξ that represents concentration of RsaL will engage with the η increases and rapidly also deplete to a small steady value (see Fig. 6.12c). Consequently, there is also pulse generation on the concentration of extracellular 3O-C12-HSL due to the pulse generator in the *las* system (see Fig. 6.12e). In addition, Fig. 6.12b, 6.12d and 6.12f demonstrate clearly the spatial structure of the spreading colony, in which spike propagation is starting in the middle of the colony and creates symmetrical travelling pulses.

6.7 Model construction of interacting QS system and bacterial growth

Several well studied bacterial species are known to exhibit rapid spreading of colonies on surfaces due to production of extracellular signal molecules as a "wetting agent". Matsuyama et al (1989) demonstrated the effect of serrawettin W1 on spreading growth of *S. marcescens*. Burch et al (2012) also presented that syrigafactin as biosurfactant of *P. syringae* plays an important role in allowing the bacteria to colonize and move on surfaces. Furthermore, Caiazza et al (2005) showed through experimental work that rhamnolipids modulate complex motility in *P. aeruginosa*. They also discussed the ability of *P. aeruginosa* in the context of colony behaviour including bacterial colony movement by producing and responding to rhamnolipids.
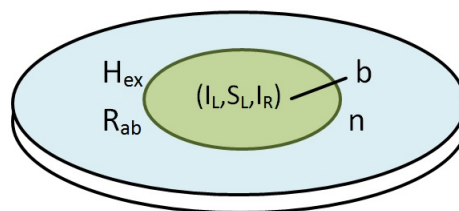
Figure 6.13: Illustration for bacterial colony of *P. aeruginosa* in the surface of nutrient. Every single cells has a QS signalling system that consists of two main QS sub-system, the *las* and *rhl* systems. *P. aeruginosa* produce rhamnolipids as a biosurfactant product that is regulated by the *rhl* system and controlled by the *las* system. Rhamnolipid functions as a wetting-agent to facilitate colony spreading. *Descriptions* associated with each *symbol* are detailed in table 6.1

Table 6.1: Description of variables in the model of bacterial spreading.

Variable	Description	Non-dimensional variable
b	bacteria concentration	B
n	nutrient concentration	N
I_L	LasI concentration	η
S_L	RsaL concentration	ξ
H_{ex}	extracellular 3O-C12-HSL concentration	H
I_R	RhlI concentration	ϕ
R_{ab}	rhamnolipids concentration	R_{AB}
R_R	total RhlR concentration that is affected by *las* system	ϱ

In this section, we shall construct a model to describe the spreading of a bacterial colony in the surface of nutrient by involving our findings from the previous chapters. In this case, we do not consider varying hardness of surface. For simplicity, we assume there is no fluid in the bacterial culture (see Fig. 6.13)

We deal with a continuous model of bacterial growth with reaction-diffusion equations. The model is in the two-dimensional (2D), with $b(\mathbf{x}, t)$ presenting the concentration of bacteria on a 2D plane and $n(\mathbf{x}, t)$ for the 2D nutrient concentration.

We have demonstrated in previous chapters how QS signal molecule of *P. aeruginosa* affects the production of rhamnolipid as a bio-surfactant product, $R_{ab}(\mathbf{x}, t)$ presenting the concentration of rhamnolipid on a 2D plane. Rhamnolipid-biosurfactant is able to break down the barriers that prevent liquid spreading. The diffusion rate is low when the concentration of rhamnolipids is very low and increases with increasing rhamnolipid concentration. The use of a diffusion term allows us to model this behaviour. Thus the movement of bacteria can be written as diffusion equation of bacteria that depends on the rhamnolipid, $\frac{\partial}{\partial x}\left(D_b(R_{ab})\frac{\partial b}{\partial x}\right)$, where $D_b(R_{ab})$ can be presented as a function of R_{ab} such that

$$D_b(R_{ab}) = C_0 + C_1 \frac{R_{ab}^2}{K_{Rab}^2 + R_{ab}^2}, \tag{6.67}$$

where C_0, C_1 are positive constants and K_{Rab} is maximum production capacity of rhamnolipids. The Hill coefficient of 2 is an arbitrary value, chosen to describe diffusion rate profile in this model.

Thus the rate of change of the bacterial concentration, with growth rate β_b and death

rate γ_b can be described by

$$\frac{\partial b}{\partial t} = \frac{\partial}{\partial x}\left(D_b(R_{ab})\frac{\partial b}{\partial x}\right) + \beta_b\left(1 - \frac{b}{K}\right)bn - \gamma_b b, \tag{6.68}$$

where we impose a model of logistic growth instead of exponential growth on the bacterial cells. A logistic growth model is able to represent the dynamics of bacterial spreading in a colony, while an exponential growth model only shows that bacterial concentration continues to increase with time. Thus exponential growth no longer works for this model.

Nutrients are one of the important factors in bacterial life. Nutrient diffuse in the local environment and deplete due to consumption by bacteria, providing

$$\frac{\partial n}{\partial t} = \frac{\partial}{\partial x}\left(D_n\frac{\partial n}{\partial x}\right) - \beta_b\left(1 - \frac{b}{K}\right)bn, \tag{6.69}$$

where D_n is coefficient of diffusion of nutrient.

In this model (Fig. 6.13), we consider rhamnolipid as the main factor allowing expansion of the bacterial colony. Moreover, nutrient are also important for growth and thus colony expansion.

The first stage of colony spreading is composed of dispersed single cells (Jacobson and Dove, 1975). Bacteria have QS systems that regulate the activation of some genes, including rhamnolipids production as surfactant in spreading colony of *P. aeruginosa* (Jarvis and Johnson, 1949). Starting from single cell, we have investigated the behaviour of QS signalling system of *P. aeruginosa*. In chapter 4, we have the non-dimensional equations for η and ξ that demonstrate the dynamical system of LasI and RsaL in the *las* system of *P. aeruginosa*. Following the dynamical system of LasI and RsaL, we also get the dynamical system of extracellular 3O-C12-HSL. We can see the dynamical system for extracellular 3O-C12-HSL, ζ, for single cell in Eqs. 4.19 chapter 4, it is generated by η and decreases linearly with the concentration of ζ.

For convenience, we try to differentiate the variable symbols. We use *Greek letters* and *Roman letters* for internal and external variables, respectively. Thus in this system, we define

$$\zeta \equiv H, \tag{6.70}$$

as a symbol for non-dimensional extracellular 3O-C12-HSL concentration.

By assuming the LasI and RsaL concentration in every single cells diffuse as the diffusion process on bacterial cells, both non-dimensional equations become

$$\begin{aligned}
\frac{\partial \eta}{\partial \tau} &= \frac{\partial}{\partial \tilde{x}}\left(\tilde{D}_B(R_{AB})\frac{\partial \eta}{\partial \tilde{x}}\right) + \frac{(\eta + a_1\,(H))^2}{a_2\,(1 + \xi)^2\,(\eta + a_1\,(H) + 1)^2 + (\eta + a_1\,(H))^2} - a_3\eta \\
\frac{\partial \xi}{\partial \tau} &= \frac{\partial}{\partial \tilde{x}}\left(\tilde{D}_B(R_{AB})\frac{\partial \xi}{\partial \tilde{x}}\right) + \frac{a_4\,(\eta + a_1\,(H))^2}{a_2\,(1 + \xi)^2\,(\eta + a_1\,(H) + 1)^2 + (\eta + a_1\,(H))^2} - a_5\xi,
\end{aligned} \tag{6.71}$$

where $\tilde{x}, B, R_{AB}$ are non-dimensional form of x, b, R_{ab}, which represent length, bacteria and rhamnolipid concentration, respectively. Then $\tilde{D}_B(R_{AB})$ is the non-dimensional form of diffusion constant equal to $\frac{D_b(R_{ab})}{D_{Hex}}$.

In this system, we consider bacteria as a colony so the concentration of extracellular 3O-C12-HSL in the colony of cells should be proportional to the total concentration of bacteria, such that the dynamical system for H in Eqs. 4.19 becomes

$$\frac{\partial H}{\partial \tau} = \frac{\partial}{\partial \tilde{x}} \frac{\partial H}{\partial \tilde{x}} + \eta B - a_6 H, . \tag{6.72}$$

It has been discussed that the expression of $rhlR$ is induced by LasR/3O-C12-HSL complex placing the rhl-system in cell-signalling hierarchy below the las-system of $P. aeruginosa$. Therefore, the dynamical system of the las system affects the dynamical system of the rhl system that we have presented in chapter 4 and 5. We have the governing equation of rhl system (Eqs. 5.63),

$$\frac{dI_R}{dt} = \frac{\alpha_I \beta_I}{\gamma_{mI}} \frac{\alpha_{RH}^2 \beta_{HR}^2 R^2 I_R^2}{K_I^2 \left(\beta_{HR} I_R \left(\alpha_{RH} + \gamma_{RR}\right) + K \gamma_{RR} D_{HR}\right)^2 + \alpha_{RH}^2 \beta_{HR}^2 R^2 I_R^2} - \gamma_I I_R.$$

By adjusting the form of non-dimensional term in the las system that defined $\tau = \frac{\alpha_L \beta_L \beta_{HL} k_L^+}{\gamma_{mL} D_{HL} k_L^-} t$, we can non-dimensionalize the model of rhl system by writing

$$\phi = \frac{\gamma_{mI}}{\beta_I} I_R. \tag{6.73}$$

In a similar manner, it diffuses as the diffusion process on bacterial cells. Thus the equation for RhlI becomes

$$\frac{d\phi}{d\tau} = \frac{\partial}{\partial \tilde{x}} \left(\tilde{D}_B(R_{AB}) \frac{\partial \phi}{\partial \tilde{x}} \right) + \frac{a_7 \left(R\right) \phi^2}{\left(\phi + a_8 \left(\eta, H\right)\right)^2 + a9 \left(R\right) \phi^2} - a_{10} \phi, \tag{6.74}$$

where

$$a_7 = \frac{\gamma_{mL} D_{HL} k_L^- \alpha_I}{\alpha_L \beta_L \beta_{HL} k_L^+} \frac{\alpha_{RH}^2 R^2}{K_I^2 \left(\alpha_{RH} + \gamma_{RR}\right)^2} = a_3 \frac{\alpha_I \alpha_{RH}^2}{\gamma_{IL} K_I^2 \left(\alpha_{RH} + \gamma_{RR}\right)^2} R^2,$$

$$a_8 = \frac{\gamma_{mI} \gamma_{RR} D_{HR}}{\beta_I \beta_{HR} \left(\alpha_{RH} + \gamma_{RR}\right)} K, \qquad \text{and} \qquad K = f(\eta, H)$$

$$\tag{6.75}$$

$$a_9 = \frac{\alpha_{RH}^2}{K_I^2 \left(\alpha_{RH} + \gamma_{RR}\right)^2} R^2,$$

$$a_{10} = \frac{\gamma_{mL} D_{HL} k_L^- \gamma_I}{\alpha_L \beta_L \beta_{HL} k_L^+} = a_3 \frac{\gamma_I}{\gamma_{IL}}.$$

Unlike the previous chapter that considered $R_R = R$ is a constant, in this system R_R represents the total concentration of RhlR that is affected by the *las* system. LasI synthase positively affects the concentration of LasR/3O-C12-HSL complex. Once the concentration of 3O-C12-HSL signal molecule reaches quorum level, they bind LasR to form LasR/3O-C12-HSL complex, which activates some genes' expression including *rhlR* genes that induce the production of RhlR enzyme (R_R). Thus we can construct a differential equation for R as a function of LasI, and define $R \equiv \varrho$ as an internal variable in the system. To the best of our knowledge, the connection form between the *las* and *rhl* systems remains unclear. In this case, we chose a simple form by defining

$$\frac{d\varrho}{d\tau} = a_{11}\eta^2 - a_{12}\varrho,$$

(6.76)

where a_{11}, a_{12} are the non-dimensional form of production and loss rate of RhlR.

As we discussed in the beginning of this chapter, rhamnolipids are a surfactant product of *P. aeruginosa* that has a function as a "wetting agent". Rhamnolipid plays a major role in bacterial spreading and it is regulated by the *rhl* system. Once C4-HSL binds RhlR, the complex RhlR/C4-HSL activates *rhlI* and *rhlAB* that encodes the production of RhlI synthase and rhamnosylntransfese, respectively. The real stage of rhamnolipid production is very complex. In order to simplify the system, we consider rhamnosylntransfese as a rhamnolipid (see Fig. 1.8). The rhamnolipid (R_{ab}) is produced by the *rhlAB* gene through transcription and translation process of *rhlAB*-mRNA $\left(\hat{R}_{ab}\right)$ at rate α_{ab} and degrades at rate γ_{Rab}, such that

$$\frac{dR_{ab}}{dt} = \alpha_{ab}\hat{R}_{ab} - \gamma_{Rab}R_{ab}.$$

(6.77)

Transcription at the *rhlAB* promoter site ($\hat{R}_{ab}$) is activated by the RhlR/C4-HSL complex (R_{RH}). We can construct a differential equation for *rhlAB* gene $\hat{R}_{ab}$ with basal expression β_{ab0} and a loss rate of γ_{ab}, such that

$$\frac{d\hat{R}_{ab}}{dt} = \beta_{ab}\frac{R_{RH}^2}{K_{ab}^2 + R_{RH}^2} - \gamma_{ab}\hat{R}_{ab} + \beta_{ab0}.$$

(6.78)

In similar way to the previous assumptions regarding the rate of change of gene transcription, we can assume that the differential equations for *rhlAB* genes in the *rhl* system are at a quasi-steady state, such that

$$\hat{R}_{ab} = \frac{\beta_{ab}R_{RH}^2}{\gamma_{ab}\left(K_{ab}^2 + R_{RH}^2\right)} + \frac{\beta_{ab0}}{\gamma_{ab}}.$$

(6.79)

By assuming the basal transcription of *rhlAB* genes is negligible ($\beta_{AB0} = 0$), the governing equation for rhamnolipid (R_{AB}) becomes

$$\frac{dR_{ab}}{dt} = \frac{\alpha_{ab}\beta_{ab}}{\gamma_{ab}}\frac{\alpha_{RH}^2\beta_{HR}^2R^2I_R^2}{K_{ab}^2\left(\beta_{HR}I_R\left(\alpha_{RH} + \gamma_{RR}\right) + K\gamma_{RR}D_{HR}\right)^2 + \alpha_{RH}^2\beta_{HR}^2R^2I_R^2} - \gamma_{Rab}R_{ab}.$$

(6.80)

Similar to the equation of synthase RhlI, we can write the non-dimensional form for rhamnolipids equation by writing

$$R_{AB} = \frac{\gamma_{ab}}{\beta_{ab}} R_{ab} \tag{6.81}$$

so the equation for rhamnolipids concentration become

$$\frac{\partial R_{AB}}{\partial \tau} = \frac{\partial}{\partial \tilde{x}} \left(\tilde{D}_{R_{AB}} \frac{\partial R_{AB}}{\partial \tilde{x}} \right) + \frac{a_{13}(R)\phi^2}{(\phi + a_{14}(\eta, H))^2 + a_{15}(R)\phi^2} - a_{16} R_{AB}, \tag{6.82}$$

where

$$a_{13} = \frac{\gamma_{mL} D_{HL} k_L^- \alpha_{ab}}{\alpha_L \beta_L \beta_{HL} k_L^+} \frac{\alpha_{RH}^2 R^2}{K_{ab}^2 (\alpha_{RH} + \gamma_{RR})^2} = a_3 \frac{\alpha_{ab} \alpha_{RH}^2}{\gamma_{IL} K_{ab}^2 (\alpha_{RH} + \gamma_{RR})^2} R^2,$$

$$a_{14} = \frac{\gamma_{ab} \gamma_{RR} D_{HR}}{\beta_{ab} \beta_{HR} (\alpha_{RH} + \gamma_{RR})} K, \qquad \text{and} \qquad K = f(\eta, H)$$

$$\tag{6.83}$$

$$a_{15} = \frac{\alpha_{RH}^2}{K_{ab}^2 (\alpha_{RH} + \gamma_{RR})^2} R^2,$$

$$a_{16} = \frac{\gamma_{mL} D_{HL} k_L^- \gamma_{Rab}}{\alpha_L \beta_L \beta_{HL} k_L^+} = a_3 \frac{\gamma_{Rab}}{\gamma_{IL}}.$$

Here, $\tilde{D}_{R_{AB}}$ is the non-dimensional form of diffusion coefficient of rhamnolipid that is equal to $\frac{D_{Rab}}{D_{Hex}}$.

By using a similar argument regarding the timescale, the activation process of *rhlR* by LasR/3O-C12-HSL is very fast and we can assume that the differential equation for ϱ (see Eqs. 6.76) is at steady state, such that

$$\varrho = \frac{a_{11}}{a_{12}} \eta. \tag{6.84}$$

Therefore the complete model represented by Fig. 6.13 is composed of four external variables (bacteria, nutrient, extracellular 3O-C12-HSL, rhamnolipids), and three internal variables (LasI, RsaL, and RhlI concentration). The non-dimensional processes of LasI, RsaL, extracellular concentration 3O-C12-HSL, RhlI ,RhlR, RhlAB $(\eta, \xi, H, \phi, R_{AB})$ have been presented. Meanwhile, we can get non-dimensional form for variables B and N by simply writing

$$B = \frac{b}{b_0}, \qquad N = \frac{n}{n_0}, \tag{6.85}$$

with the definition of non-dimensional parameter β and γ, such that

$$\beta = a_3 \frac{\beta_b n_0}{\gamma_{IL}}, \qquad \gamma = a_3 \frac{\gamma_b}{\gamma_{IL}}. \tag{6.86}$$

Therefore the complete equations for the model of bacterial spreading by involving the dynamical behaviour of QS signalling system of *P. aeruginosa* (Eqs. 6.68 to Eqs. 6.82) can be written in dimensionless units as

$$\frac{\partial B}{\partial \tau} = \frac{\partial}{\partial \tilde{x}} \left(\tilde{D}_B(R_{AB}) \frac{\partial B}{\partial \tilde{x}} \right) + \beta \left(1 - \frac{B}{K} \right) BN - \gamma B$$

$$\frac{\partial N}{\partial \tau} = \frac{\partial}{\partial \tilde{x}} \left(\tilde{D}_N \frac{\partial N}{\partial \tilde{x}} \right) - \beta \left(1 - \frac{B}{K} \right) BN$$

$$\frac{\partial \eta}{\partial \tau} = \frac{\partial}{\partial \tilde{x}} \left(\tilde{D}_B(R_{AB}) \frac{\partial \eta}{\partial \tilde{x}} \right) + \frac{\left(\eta + a_1 \left(H \right) \right)^2}{a_2 \left(1 + \xi \right)^2 \left(\eta + a_1 \left(H \right) + 1 \right)^2 + \left(\eta + a_1 \left(H \right) \right)^2} - a_3 \eta$$

$$\frac{\partial \xi}{\partial \tau} = \frac{\partial}{\partial \tilde{x}} \left(\tilde{D}_B(R_{AB}) \frac{\partial \xi}{\partial \tilde{x}} \right) + \frac{a_4 \left(\eta + a_1 \left(H \right) \right)^2}{a_2 \left(1 + \xi \right)^2 \left(\eta + a_1 \left(H \right) + 1 \right)^2 + \left(\eta + a_1 \left(H \right) \right)^2} - a_5 \xi$$

$$\frac{\partial H}{\partial \tau} = \frac{\partial}{\partial \tilde{x}} \frac{\partial H}{\partial \tilde{x}} + \eta B - a_6 H$$

$$\frac{d\phi}{d\tau} = \frac{\partial}{\partial \tilde{x}} \left(\tilde{D}_B(R_{AB}) \frac{\partial \phi}{\partial \tilde{x}} \right) + \frac{a_7 \frac{a_{11}}{a_{12}} \left(\eta \right)^2 \phi^2}{\left(\phi + a_8 \left(\eta, H \right) \right)^2 + a9 \frac{a_{11}}{a_{12}} \left(\eta \right)^2 \phi^2} - a_{10} \phi$$

$$\frac{\partial R_{AB}}{\partial \tau} = \frac{\partial}{\partial \tilde{x}} \left(\tilde{D}_R \frac{\partial R_{AB}}{\partial \tilde{x}} \right) + B \left(\frac{a_{13} \frac{a_{11}}{a_{12}} \left(\eta \right)^2 \phi^2}{\left(\phi + a_{14} \left(\eta, H \right) \right)^2 + a_{15} \frac{a_{11}}{a_{12}} \left(\eta \right)^2 \phi^2} \right) - a_{16} R_{AB}.$$

(6.87)

Here a_1 to a_{16} are positive constants. The biological interpretation of this model consists of dynamical processes inside and outside of the cell (see Fig. 6.14) : η positively affects the production of η, ξ, H, ϕ and R_{AB}. The expression of the *lasI* gene induces the production of LasI synthase (η) that leads to increased 3O-C12-HSL concentration or, implicitly, it also increases the secretion level of 3O-C12-HSL concentration to the outside of cell body, extracellular 3O-C12-HSL (H). The consequent increase of 3O-C12-HSL concentration and thus activated LasR generates a positive feedback loop and is responsible for the activation of *lasI* and *rsaL* gene expression, which induces the production of LasI (η) and RsaL (ξ). In addition, the LasR/3O-C12-HSL complex is also responsible for the activation of *rhlR* gene expression that leads to the production of RhlR regulator. This process explains the initial stage of how η as a main component in the *las* system regulates the *rhl* signalling system. Meanwhile, another main component in the *las* system, ξ, inhibits the expression of η, which describes negative feedback from competitive inhibition by RsaL to the expression of the *lasI* gene.
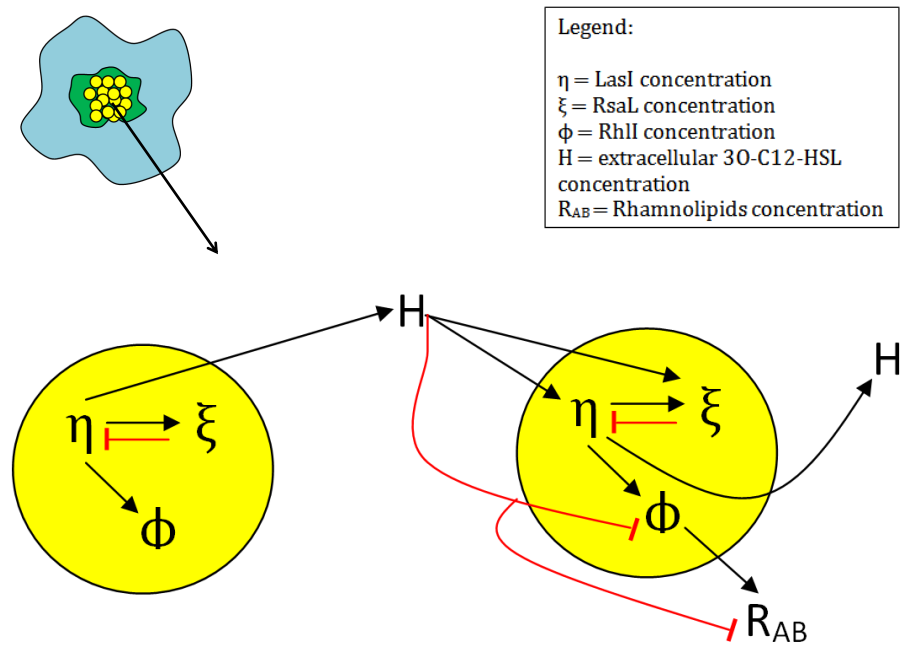
Figure 6.14: Illustration of the cell communication mechanism by secreting a signal molecule (ligand) that reversibly binds from one cell to another cell. Black and red arrows represent positive and negative effect, respectively.

Still inside of the cell, the consequent increase of RhlR concentration is followed by RhlR/C4-HSL forming. This leads to the activation of some gene expression, especially *rhlI*, *rhlA* and *rhlB*. The *rhlI* gene encodes the production of RhlI enzyme (ϕ). Meanwhile *rhlA* and *rhlB* genes encode the production of rhamnosyltransferase that leads to rhamnolipid production (R_{AB}).

Outside of the cell body, extracellular signal molecules play a key role in the communication mechanism between bacterial cells. H carries information from one cell to another cell. H binds intracellular receptors on the *las* system (LasR), then activates gene expression that leads to increased enzyme production, such as η, ξ and ϕ. On the other hand, H also binds intracellular receptor on the *rhl* system (RhlR) and thereby blocks the binding of C4-HSL to its transcriptional activator. This inhibits the activation of *rhlA* and *rhlB* genes expression and negatively affects rhamnolipid production (R_{AB}).

Chrzanowski et al (2012) demonstrated why *P. aeruginosa* produce rhamnolipid and confirmed that rhamnolipid plays a role in surface associated bacterial motility. Thus it is reasonable that the diffusion coefficient of bacteria does not only depend on the nutrient, but also rhamnolipid concentration. For our system, we assume that the diffusion coefficient of nutrient is very small compared to rhamnolipids.

The non-dimensional set of differential Eqs. 6.87 has been solved numerically using MAT-

LAB (R2016a; MathWorks). Some parameters of the model have been employed in the previous chapters. We add description of other parameter values in the table and provide numerical results in Fig. 6.15 and 6.16.

Table 6.2 lists parameters that have either been adopted from the literature based on experimental evidence or estimated, as stated. The basal production rate of $rhlAB$ gene-mRNA can be considered as similar to the basal production of protein. This is because the RhlR/C4-HSL complex activates $rhlAB$ gene-mRNA in a very fast process before encoding rhamnosiltransferase that leads to the rhamnolipids production. As described before, we simplify the governing equations by assuming quasi-steady states for the fast reactions. This complex model results in 16 non-dimensional parameters and 4 non-dimensional diffusion coefficients (see table 6.3). In order to investigate the dynamical behaviour of bacterial spreading in a colony, we vary the non-dimensional parameter values. If we only used the parameter values $a_1 - a_5$ of chapter 4, it would be difficult to find other parameter values $a_6 - a_{16}$ that give interesting results. For modelling purpose, therefore, we set non-dimensional parameter values $a_1 - a_5$ different to that of chapter 4 but they are still in the range of values in table 4.2.

In a previous chapter, we have demonstrated the potential for the las system to act as a pulse generator and illustrated how this effect translates into cell-cell communication in a simple linear chain of cells. By putting this phenomenon as a starting point of the dynamical system in bacterial colony expansion (see Fig. 6.15a and 6.15b), we get dynamical behaviour of the rhl system (see Fig. 6.15c). As an illustration of travelling wave of a pulse in a linear chain of cells, we assume that diffusion of 3O-C12-HSL and C4-HSL across each cell membrane are such that the intracellular autoinducers of las and rhl system are at a kinetic equilibrium (i.e $\frac{dH_L}{dt} = 0$ and $\frac{dH_R}{dt} = 0$, as stated in chapter 4 and 5, respectively). The difference between this model and the previous model in section 4.4 is in how diffusion is modelled. Therefore, we can see in Fig. 6.15a, 6.15b and 6.15c, all of the genes products including LasI synthase (η), RsaL inhibitor (ξ), and RhlI synthase (ϕ) diffuse as bacteria diffuse due to the impact of rhamnolipid.

Moreover, we assume that extracellular signal molecules are the main actors in the neighbourhood surrounding each cell. We have explained how LasI synthesizes 3O-C12-HSL signal molecule and increases the level of extracellular 3O-C12-HSL that is freely diffusible. Thus the dynamical system of extracellular 3O-C12-HSL in Fig. 6.16c diffuses with its own coefficient of diffusion and is affected by the behaviour of Fig. 6.15a. The coefficient of diffusion of extracellular 3O-C12-HSL is bigger than others. Fig. 6.16c also illustrates how signal molecules spread in the local environment of the colony and affect rhamnolipid production.

Table 6.2: Parameters employed in the complex system, some other parameter values have been stated in table 4.2 and table 5.2.

Par	Description	Standard value	Unit	Value/ Range	Comments (Based on)/Ref
α_{ab}	rate at which rhamnolipids produced by rhlAB mRNA	0.5	$\min^{-1}$	0.5	2 min to translate protein, Alon (2006)
β_{ab}	max. production rate of rhamnolipids at which rhlAB mRNA is activated by RhlR/C4-HSL	1	$nM\ \min^{-1}$	1	Estimate
β_{ab0}	basal production rate of rhlAB mRNA	0.1	$nM\ \min^{-1}$	0.1	basal transcription rate of a protein, Alon (2006)
K_{ab}	affinity constant between RhlR/C4-HSL and rhlAB mRNA	230	nM	1-1000	Alon (2006)
γ_{Rab}	degradation rate of rhamnolipids	0.01	$\min^{-1}$	0.01 - 0.02	estimate
γ_{ab}	degradation rate of rhlAB mRNA	0.2	$\min^{-1}$	0.2	2 min lifetime of RNA, Alon (2006)
D_n	Diffusion constant of nutrient	10^{-7}	$cm^2 \min^{-1}$	6×10^{-5}	Bees et al (2000)
D_b	Diffusion constant of bacterial cells	$10^{-5} - 10^{-3}$	$cm^2 \min^{-1}$	6×10^{-5}	Bees et al (2000)
D_{Hex}	Diffusion constant of extracellular	10^{-1}	$cm^2 \min^{-1}$		estimate
D_{Rab}	Diffusion constant of rhamnolipids	10^{-4}	$\min^{-1}$		estimate

Table 6.3: Non-dimensional Parameters involved in the complex system.

Name	Description	Value
β	the growth rate of bacterial concentrations	0.5
γ	the degradation of bacterial concentrations	0.02
a_1	the effect of extracellular signal molecules	0.2
a_2	a squared ratio of concentration of Las components	0.3
a_3	the degradation of LasI relative to signal molecule production	0.15
a_4	the control of binding of RsaL to LasI	0.4
a_5	the degradation of RsaL relative to signal molecule production	0.02
a_6	the degradation of extracellular 3O-C12-HSL	1.1
a_7	The control of activation of rhl system by las system through RhlR that involves the production of LasI and affinity binding RhlR/C4-HSL to $rhlI$ mRNA	0.33
a_8	The control inhibition of extracellular 3O-C12-HSL to the transcriptional regulator in the rhl system, RhlR	0.15
a_9	The control of activation of rhl system by las system through RhlR that involves affinity binding RhlR/C4-HSL to $rhlI$ mRNA	0.2
a_{10}	The degradation of RhlI relative to the C4-HSL production	0.15
a_{11}	The production of RhlR relative to the las system	0.3
a_{12}	The degradation of RhlR	0.1
a_{13}	The control of activation of rhl system by las system through RhlR that involves the production of LasI and affinity binding RhlR/C4-HSL to $rhlI$ mRNA	0.3

(a)

(b)

(c)
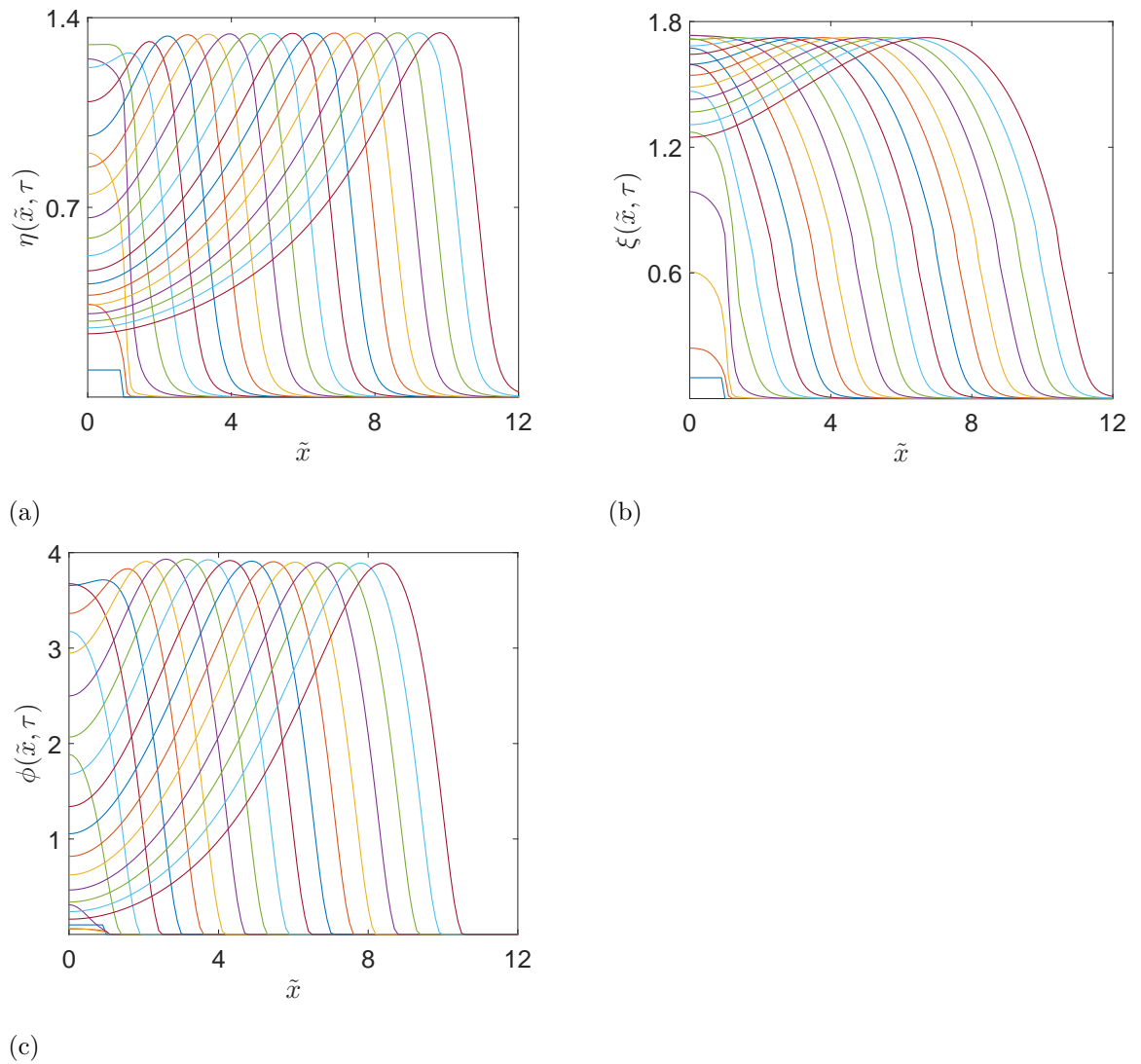
Figure 6.15: Propagation of pulse waves inside of the cell. Pulse generation of LasI (η) triggers pulse generation of RsaL (ξ) by increasing 3O-C12-HSL concentration. This also leads to pulse production of RhlI (ϕ), a downstream impact of *las* to *rhl* system. All parameter values are in table 6.3
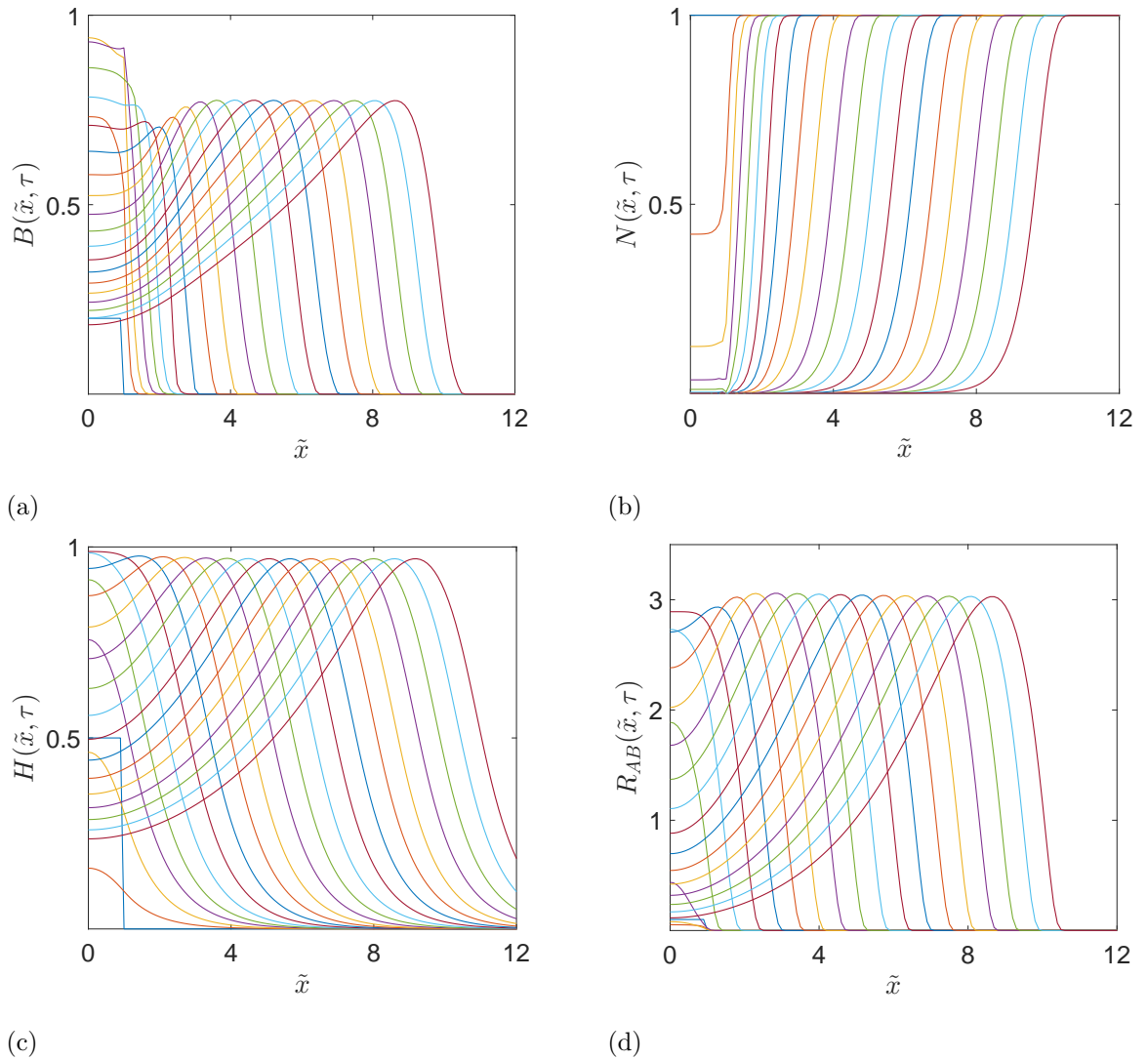
Figure 6.16: (a) Bacteria adapt as the environmental conditions change. The bacterial colony expands in relation to the decrease of nutrient concentration in the middle of the colony and dispersion of rhamnolipid. (b) After a certain time of colony expansion, the nutrient concentration becomes exhausted in the colony centre. (c) Travelling pulses of extracellular 3O-C12-HSL are a consequence of the dynamical system in the inside of the cell and diffusion. (d) Dispersion of rhamnolipid assist the expansion of the colony. See text for detailed explanation. All parameter values are in table 6.3

Table 6.3. continued

Name	Description	Value
a_{14}	The control inhibition of extracellular 3O-C12-HSL to the transcriptional regulator in the *rhl* system,RhlR	0.1
a_{15}	The control of activation of *rhl* system by *las* system through RhlR that involves affinity binding RhlR/C4-HSL to *rhlI* mRNA	0.2
a_{16}	The degradation of RhlI relative to the C4-HSL production	0.2
$\tilde{D}_B\,(R_{AB})$	The diffusion constant of bacteria that depends on rhamnolipids concentration	$10^{-4} - 10^{-2}$
$\tilde{D}_N$	The diffusion constant of nutrient	10^{-6}
$\tilde{D}_{R_{AB}}$	The diffusion constant of rhamnolipids	10^{-3}
$\tilde{D}_H$	The diffusion constant of extracellular 3O-C12-HSL	1

We have demonstrated how LasI and RhlI are involved in rhamnolipid production with an inhibition due to 3O-C12-HSL. As a consequence, the dynamical behaviour of rhamnolipids (see Fig. 6.16d) is affected by the behaviour of η, ϕ, and H (Fig. 6.15a, 6.15c, and 6.16c). In addition, Fig. 6.16d also illustrates dispersion of rhamnolipid that assists the expansion of the bacterial colony. In the absence of rhamnolipid, the relative low coefficient of diffusivity of bacterial cells does not lead to expansion of the colony (see Fig. 6.16a). Associated with Fig. 6.16a that bacterial density diminishes in response to the bacterial expansion and depletion of nutrient in the centre of the colony, Fig. 6.16b; after a certain time the nutrient concentration becomes exhausted.

In order to get a better understanding of the downstream impact of the *las* system on the *rhl* system, Fig. 6.17 illustrates how the extracellular 3O-C12-HSL modulates rhamnolipid production. If the degradation of extracellular 3O-C12-HSL is high, the potential of the *las* system to act as a pulse generator affects the pulse activation of *rhl* system and is followed by sufficient rhamnolipid production to assist the expansion of the colony. Meanwhile, if the degradation of extracellular 3O-C12-HSL is very small, the extracellular 3O-C12-HSL diffuses freely and effectively prevents the activation of RhlR by C4-HSL. Consequently, it inhibits the activation of the *rhlAB* gene by RhlR/C4-HSL complex and leads to the low production of rhamnolipid and low colony expansion. In this complex model, we were
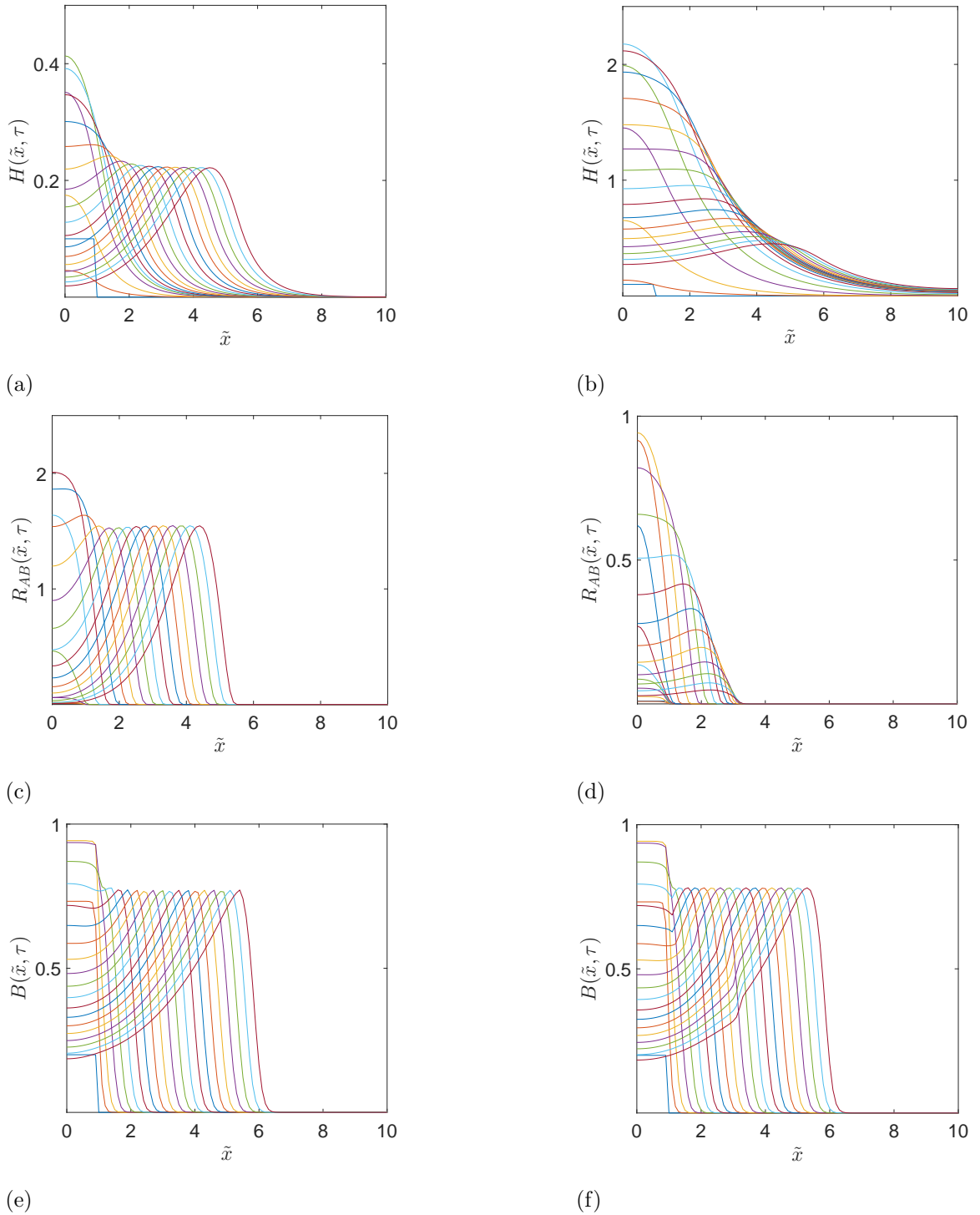
Figure 6.17: Extracellular signal molecules 3O-C12-HSL modulate the rhamnolipid production. Left figures (a, c, e) The *las* system has high degradation of extracellular 3O-C12-HSL ($a_6 = 2$), so the effect of pulse generation on the *las* system remains stable on the activation of the *rhl* system and directs the rhamnolipid production. Right figures (b, d, f) The *las* system has small degradation of extracellular 3O-C12-HSL ($a_6 = 0.3$), so the extracellular 3O-C12-HSL effectively inhibits the activation of RhlR by C4-HSL and results in small production of rhamnolipids. Other parameters values are in table 6.3

only concerned with colony spreading. The current model does not show the dynamical behaviour of colony spreading at the edge of the colony (Fig. 6.17e and Fig. 6.17f). Future work should consider the rate of change of $B\eta$, $B\xi$, and $B\phi$ to provide a more accurate model of the dynamical system of colony expansion, which includes behaviour at the center and edge of the colony in a similar manner to Bees et al (2000).

6.8   Discussion

This chapter presented two different models, one simple and one complex to study bacterial spreading. In the simple model, we have improved an introductory model of bacterial interaction that has been discussed in chapter 2 by considering motile-cells in the model. We give particular attention to nutrient acquisition and how it affects the transition process from non-motile to motile cells and conversely. We use a system of partial differential equations to describe a diffusion process in motile bacteria. Then, we linearised the system to become ordinary differential equations for assessing the stability of an equilibrium point of the system. In the first part, we analysed the model that consists of nutrient and motile-cell concentration. After that, we extended the system by involving concentration of non-motile cells.

In the simulations of the simple model, the parameter values are not based on experiments. We take arbitrary values and have surveyed parameter space to get results that agree with biological expectations. In addition, we have discussed three different types of bacterial growth function: a linear function (exponential growth), a power function, and a type III Holling function. From the simulations, we show how nutrient concentration plays a role in the bacterial motility. The difference in simulation results between those functions is in the speed of decaying nutrient concentration in the tail of the travelling wave of nutrient concentration. With a similar technique to the previous chapters, we explore the dynamical behaviour of the system through bifurcation analysis. In order to explore the dynamical behaviour of the model for motile-cells, we analysed the fixed points that is followed by phase plane analysis to get information about stability of the system, where the existence of the solutions corresponds to travelling waves.

We have extended the simple model of bacterial spreading by considering QS signal molecules and imposing a QS dynamical system that has been discussed in chapters 3 to 5. In addition, rhamnolipid, a surfactant product that is regulated by the QS signalling system is also considered. We employed parameters that have been adopted from the literature based on experimental evidence and estimates. We are confident that our dimensionless parameters are located in a biologically reasonable region of parameter space. Thus the parameters are able to capture the processes of the communication mechanism between

bacterial cells, even though we acknowledge that the model is sensitive to the value of these parameters.

From the numerical results, we have demonstrated that the pulse generation of the LasI synthase in the *las* system generates pulse production of RhlI synthase in the *rhl* system. At the same time it also increases the extracellular 3O-C12-HSL level preventing the activation of the transcriptional activator RhlR by C4-HSL and results in a decrease of RhlI synthase production. However, we have showed that the effect of the pulses on *las* system are able to increase the concentration of RhlR and this is revealed by the existence of RhlI pulses. The comprehensive numerical results suggest that pulse generation in the *las* system of *P. aeruginosa* presents downstream impact on the *rhl* system and creates a 'handbraked acceleration' due to significant amount of extracellular 3O-C12-HSL. This leads to the dynamical behaviour of rhamnolipids production as a *rhl* system product that is controlled by the *las* system. Finally, we have demonstrated the dynamical behaviour of bacterial spreading in which rhamnolipids assist the expansion of the colony.

Chapter 7

General discussion

7.1 Summary of thesis aims

The overall aim of this thesis was to establish a description that can be used to explain the essential role of QS signalling system related to gene expression in bacterial colony behaviour. It was also to explain how biological and physical interaction has effects on the spatial structure of bacterial spreading. To address these aims, firstly, the role of QS signal molecules was explored in a simple bacterial interaction that consists of nutrients, motile and non-motile cells. Secondly, the dynamic QS signalling system was investigated and the reason to use the QS signalling system of *P. aeruginosa* as the research object of this thesis was explained in the main chapters. Thirdly, the dynamic system of QS was investigated to understand how QS plays a role in bacterial spreading.

7.2 Role of the QS signalling system in the behaviour of bacterial colony

Bacteria produce and release QS signal molecules as a communication mechanism that allows bacterial cells to control many of the gene expressions related to activities including population density, cell motility, bio-surfactant production, etc. It is therefore necessary to investigate the role of QS in bacterial activities and modelling at every scale of activation and inhibition regulatory interactions within the signalling process in order fully to understand the system.

In this thesis we have shown how the QS signalling system plays a role in bacterial interaction. We have also demonstrated the dynamic nature of the QS regulatory network that is followed by its impacts on bacterial spreading. In this case, we employ the QS signalling system of *P. aeruginosa* as a research object. Then, in order to get excellent results that can describe the real process of QS signalling, we have studied the system

through previously published theoretical and experimental work on the QS system before we constructed our model. We also compared parameter values in existing mathematical biology manuscripts with biological estimates to get rational parameter values for our model. This highlights the strength of this work.

In chapter 2, simple bacterial interactions involving bacterial growth, transition of bacterial types and signal molecule production were demonstrated. As a preliminary to the research, the first model focusses attention on the diffusion effect of QS signal molecules on the population density or colony growth, which does not consider the motile behaviour of the bacteria. We constructed the model by describing that there is transition process from up-regulated to down-regulated bacteria or conversely, where the rate of signal molecule production from up-regulated bacteria is much larger than from down-regulated bacteria. In addition, both kinds of bacterial growth depend on the nutrient concentration. The results showed that an effective rate of diffusion of QS signal molecules decreases on a slow time scale as the colony grows, which also explained the existence of bistability of colony growth by considering the slope of the transition rate from off-QS to on-QS bacteria (κ) and effective loss rate of signal molecule (γ) as bifurcation parameters.

We then sought to extend the simple model of bacterial interaction in chapter 2, by also considering the dynamic system of QS signal molecules in the inside of individual cells, which is known to affect bacterial behaviour or interactions. This became the main research in this thesis. We started to explore the QS signalling itself by investigating the dynamic behaviour of the system, preceded by a literature review of QS mathematical models in chapter 3. There are four findings in chapter 3: firstly, the Hill form for the rates of change in gene production that strongly suggests that the number of the Hill coefficient has to be greater than one. Secondly, the functional form for the transcription of both *lasI* and *rsaL* genes is identical, which suggest that we should add a repressor-line from RsaL transcriptional repressor to *rsal* gene in the QS signalling diagram of *P. aeruginosa*. Thirdly, there is insufficient evidence to determine the binding types in the intergenic region, and also there is no information about expression rates in each direction for all configurations of binding types. Fourthly, the parameter values that are used in some literature on QS modelling are significantly different to the biological estimates.

Based on the findings in chapter 3, in chapter 4 we constructed a QS model of *P. aeruginosa*. We started by describing the biological system of QS signalling in *P. aeruginosa* in greater detail, as well as the mathematical approach. Then, we conducted a numerical investigation of the model by highlighting the key parameters to determine system equilibria and to explore the dynamical behaviour. The results demonstrated the potential for the *las* system to act as a pulse generator. We also demonstrated that this can lead to the

generation of a pulse train when the individual cells are coupled in a linear chain through diffusion of the HSL signal molecule. The *las* system is coupled to the *rhl* system by the LasR transcription factor and 3O-C12-HSL signal molecules. The LasR transcription factor promotes the transcription of *rhlR* gene that induces the production of RhlR in the *rhl* system. On the other hand, 3O-C12-HSL inhibits the activation of RhlR by C4-HSL. This creates an interesting effect in the combined system that we might call a 'handbraked acceleration'. The hierarchy of the QS system in *P. aeruginosa* places the *las* system above the *rhl* system. Thus, by assuming that the *rhl* system follows the same dynamics as the *las* system, the *las* system, through the complex LasR/3O-C12-HSL, increases the production of RhlR even though it is also handbraked by the presence of a significant concentration of 3O-C12-HSL, inhibiting the activation of the *rhlR* gene and the downstream consequences.

In chapter 5 we provide further analysis and demonstrate the downstream impact of the *las* system. We explored the behaviour of the *las* system by applying varying assumptions. We presented that the *las* system model with a zero concentration of extracellular signal molecules also reveals excitable pulse generation behaviour. The dynamic complexity arises from the interaction between the LasI loop and the RsaL loop as positive and negative feedback loops, respectively. Then, we conducted bifurcation analysis and investigated the equilibria of the system that associates with the bifurcation diagram. In addition, this chapter also presents a further investigation of the phase plane in relation to the possibilities of inhibition types in the *las* system. We explored binding inhibition types including competitive, non-competitive and competitive inhibition with symmetric and non-symmetric expression rates in each binding type for all types of binding. The results of all binding types presented the same qualitative behaviour. This suggests that whatever the binding types between RsaL and LasR/3O-C12-HSL, with symmetric or non-symmetric expression rate, the *las* system is sufficient for excitable behaviour. This finding, therefore, also indicates that the symmetrical binding negative feedback from RsaL to its own production is not required for excitable behaviour as in the general diagrams of the QS signalling system that have been published (c.f. general diagrams of the *las* system in Van Delden and Iglewski, 1998; De Kievit et al, 2002; Dockery and Keener, 2001; Fagerlind et al, 2005; Schaadt et al, 2013). In this chapter, we also constructed a mathematical model for the *rhl* system in order to understand its dynamic behaviour and the downstream impact of the *las* system to the *rhl* system. This demonstrated the competition between production of the two signal molecules, 3O-C12-HSL and C4-HSL, which are produced by the *las* and *rhl* systems, respectively, in terms of generating quorum memory in the *rhl* system. This may enable cells to trigger rhamnolipid production (as a surfactant product of the *rhl* system) only when they are at the edge of colony.

Finally, in chapter 6 we constructed a simultaneous model of bacterial spreading. Started with a simple model, we extended the preliminary model by including motile-cells in the system in order to get a more realistic model. The bacterial cells are able to transform from non-motile to motile cells, or conversely. By involving motile cells in the system, we include a diffusion term in the model to take account of the dynamic system of motile cells. The results presented the centrality of nutrient concentration in the bacterial motility. In this model, we explored three different types of bacterial growth. Nutrients are consumed by bacteria and we can see that, for every type, the difference in the simulation results is dependent on the the speed of the decay in the nutrients concentration. We also analysed the stability of the system through fixed points and phase plane to investigate the existence of the travelling wave solution. Lastly, we reconcile of all the findings in the previous chapters to construct a model involving seven variables (four external and three internal variables). The external variables consist of bacteria, nutrients, extracellular signal molecules and rhamnolipid concentration. Meanwhile, the internal variable consists of the key components in the QS signalling system of *P. aeruginosa*, which are LasI, RsaL and RhlI concentration. In this model, we impose a reaction-diffusion model. The spread of a bacterial colony on a surface is through a process of diffusion that is affected by rhamnolipid concentration. Thus the constant diffusion of bacteria can be expressed as a function of rhamnolipids. As a consequence, the constant diffusion all of the main components inside the cells (LasI, RsaL and RhlI) is similar to the constant diffusion of bacteria because they diffuse as the bacteria diffuse. Meanwhile, external factors such as nutrients, extracellular and rhamnolipid concentration have their own constant diffusion. This model suggests that the potential for the *las* system to act as a pulse generator, also induces pulse production in the *rhl* system, which leads to rhamnolipid production at the edge of colony, rapid expansion and access to more nutrients.

The autoinducer based QS system is a form of cell-cell communication, which is common among Gram-negative bacteria. Although QS of *P. aeruginosa* has been intensively studied, it is still unclear how the QS system acts as a global regulator of genes expression in the cell. In order to get a better understanding of the QS system and its dynamics, we developed the QS system of *P. aeruginosa*. Mathematical modelling has gained attention as a research tool to identify the process and key parameters for the system being studied. The models developed here are based on those of Dockery and Keener (2001) and Fagerlind et al (2005). Our three different QS models exhibit expected QS dynamics, i.e. the QS activator works by switching between two stable steady states that represent low and high concentrations of the QS signal molecule. In contrast to the model by Dockery and Keener (2001), the expression of RsaL is included as an inhibitor of QS signal molecule production in the QS model

system developed here. In addition, unlike Fagerlind et al (2005), we have used parameter values that correspond to biological estimates. This allowed the dynamical behaviour of the QS system to be investigated, thereby improving understanding of how the QS system is regulated. To the best my knowledge, this was the first QS model that demonstrate the potential for the *las* system to act as a pulse production of 3O-C12-HSL. By investigating pulse generation in the QS system of *P. aeruginosa*, we have shown that this can lead to the generation of a pulse train when the individual cell coupled is by diffusion to a QS signal molecule. This also enables cells to trigger rhamnolipid production that supports colony spreading.

7.3 Recommendations for future research

This thesis has contributed to current understanding about the role of QS signalling systems in bacterial colony dynamics. Prior to this work, the pulse generation in the quorum machinery of *P. aeruginosa* had been unexplored. By understanding the potential of the *las* system to act as a pulse generator and also its affect on the dynamic behaviour of the *rhl* system, we get a clear description of how rhamnolipids play a role in bacterial spreading. Although this work has revealed significant findings in understanding the dynamic behaviour of QS systems for *P. aeruginosa*, and has contributed to the mathematical model of QS bacteria, there is a need to investigate several areas further, as detailed below.

In the preliminary studies, chapter 2, we have introduced a simple mathematical model of bacteria, describing the relationship between the effective loss rate of signal molecule concentration and bacterial population growth. The model only focuses on a simple QS signal molecules, however, and just two bacterial states. This preliminary model simplifies the more complicated biological reality. For example, there are numerous types of QS signal molecule in local environments inhabited by a variety of species, thus it involves complex communication mechanisms between species. The simple model in chapter 2 is intended as a first study on the mathematical modelling of bacterial behaviours, which can be extended in any direction of the research. In this case, we can move one step ahead for this model by investigating the effect of the production of QS signal molecules on a bacterial population when a QS switch is imposed. In addition, this model can be conducted using experimental work in a similar manner to Ward et al (2001).

In chapter 3, we review the existing theoretical and experimental work on QS, especially the QS model of Dockery and Keener (2001), revealing how the theoretical and experimental understanding of bacterial communication has made significant progress. We conclude the review in chapter 3 by discussing the future potential of modelling in QS and employed this knowledge in chapter 4 to construct the QS model of *P. aeruginosa*. In addition, biochemical

theories of QS signalling system have been extensively developed in the last decades. It is inevitable, therefore, that by updating and exploring the development of QS studies we can expand this review.

We construct a QS model of *P. aeruginosa* in chapter 4 with further analysis in chapter 5. Although this chapter has been published, we have highlighted the weakness of this work. Specifically, although most of the parameter values were acquired from the published data, not all have been verified experimentally. Further studies should therefore be conducted using experimental work. In addition, the quantitative properties of the pulse in terms of its duration and amplitude is a very important issue in biology. For example the excitable neuronal behaviour (spikes) are very regular in amplitude and duration while excitable behaviour in *Bacillus Subtilis* competence can be very variable in duration. Thus further analysis of spatial description on the existence of pulse behaviour would be more interesting. It also would be exciting if this signalling role were connected to biofilm formation. Numerous research by theoretical or experimental studies has discussed the role played by biofilms in human life.

At the end of this thesis, we constructed a mathematical model for bacterial spreading by involving the factors that were discussed in the previous chapters. In this case, we construct a simple model of a spreading colony on a surface of nutrients where there is no fluid between the colony and the surface of nutrients. In future work, therefore, we can extend this model by considering more complicated cases in terms of how the physical mechanisms of rhamnolipid dispersal interact with the biological mechanisms of bacterial transition (up-regulated to down-regulated, or conversely) and cell-to-cell signalling. In terms of the medium within which the bacterial spread occurs, we can also consider bacterial colony spread in hard, soft, very soft or mixed media, which incorporates aspects of thin film flow with wetting due to rhamnolipid production.

Bibliography

Abadal S, Akyildiz IF (2011) Automata modeling of quorum sensing for nanocommunication networks. Nano Communication Networks 2(1):74–83

Abadal S, Llatser I, Alarcn E, Cabellos-Aparicio A (2014) Cooperative signal amplification for molecular communication in nanonetworks. Wireless Networks 20(6):1611–1626

Adler J, Templeton B (1967) The effect of environmental conditions on the motility of *Escherichia coli*. Journal of General Microbiology 46(2):175–184

Agrawal V, Kang SS, Sinha S (2014) Realization of morphing logic gates in a repressilator with quorum sensing feedback. Physics Letters, Section A: General, Atomic and Solid State Physics 378(16-17):1099–1103

Alberghini S, Polone E, Corich V, Carlot M, Seno F, Trovato A, Squartini A (2009) Consequences of relative cellular positioning on quorum sensing and bacterial cell-to-cell communication. FEMS Microbiology Letters 292(2):149–161

Alfiniyah C, Bees MA, Wood AJ (2017) Pulse generation in the quorum machinery of *Pseudomonas aeruginosa*. Bulletin of Mathematical Biology 79(6):1360–1389

Alon U (2006) An Introduction to System Biology: Design Principles of Biological Circuits. Chapman and Hall or CRC Press, Boca Raton, FL

Alves F, Dilo R (2005) A simple framework to describe the regulation of gene expression in prokaryotes. Comptes Rendus - Biologies 328(5):429–444

Anand SK, Griffiths MW (2003) Quorum sensing and expression of virulence in *Escherichia coli* o157:h7. International Journal of Food Microbiology 85(1-2):1–9

Angeli D, Ferrell Jr JE, Sontag ED (2004) Detection of multistability, bifurcations, and hysteresis in a large class of biological positive-feedback systems. Proceedings of the National Academy of Sciences of the United States of America 101(7):1822–1827

Anguige K, King JR, Ward JP, Williams P (2004) Mathematical modelling of therapies targeted at bacterial quorum sensing. Mathematical Biosciences 192(1):39–83

Anguige K, King JR, Ward JP (2005) Modelling antibiotic- and anti-quorum sensing treatment of a spatially-structured *Pseudomonas aeruginosa* population. Journal of Mathematical Biology 51(5):557–594

Anguige K, King JR, Ward JP (2006) A multi-phase mathematical model of quorum sensing in a maturing *Pseudomonas aeruginosa* biofilm. Mathematical Biosciences 203(2):240–276

Atkinson S, Williams P (2009) Quorum sensing and social networking in the microbial world. Journal of the Royal Society Interface 6(40):959–978

Balco VM, Barreira SVP, Nunes TM, Chaud MV, Tubino M, Vila MMDC (2014) Carbohydrate hydrogels with stabilized phage particles for bacterial biosensing: Bacterium diffusion studies. Applied Biochemistry and Biotechnology 172(3):1194–1214

Barbarossa MV, Kuttler C (2016) Mathematical modeling of bacteria communication in continuous cultures. Applied Sciences (Switzerland) 6(5):149

Barbarossa MV, Kuttler C, Fekete A, Rothballer M (2010) A delay model for quorum sensing of *Pseudomonas putida*. BioSystems 102(2-3):148–156

Barbuti R, Maggiolo-Schettini A, Milazzo P, Pardini G (2009) Spatial calculus of looping sequences. Electronic Notes in Theoretical Computer Science 229(1):21–39

Barbuti R, Maggiolo-Schettini A, Milazzo P, Tiberi P, Troina A (2009b) Stochastic calculus of looping sequences for the modelling and simulation of cellular pathways. In: Lecture Notes in Computer Science (including subseries Lecture Notes in Artificial Intelligence and Lecture Notes in Bioinformatics), vol 5121, Springer, pp 86–113

Barbuti R, Maggiolo-Schettini A, Milazzo P, Pardini G (2011) Spatial calculus of looping sequences. Theoretical Computer Science 412(43):5976–6001

Bassler BL (2002) Small talk: Cell-to-cell communication in bacteria. Cell 109(4):421–424

Beckmann BE, Knoester DB, Connelly BD, Waters CM, McKinley PK (2012) Evolution of resistance to quorum quenching in digital organisms. Artificial Life 18(3):291–310

Bees MA, Andresen P, Mosekilde E, Givskov M (2000) The interaction of thin-film flow, bacterial swarming and cell differentiation in colonies of *Serratia liquefaciens*. Journal of Theoretical Biology 40:27–63

Bees MA, Andresen P, Mosekilde E, Givskov M (2002) Quantitative effects of medium hardness and nutrient availability on the swarming motility of *Serratia liquefaciens*. Bulletin of Mathematical Biology 64(3):565–587

Ben-Jacob E, Schochet O, Tenenbaum A, Cohen I, Czirk A, Vicsek T (1994) Generic modelling of cooperative growth patterns in bacterial colonies. Nature 368(6466):46–49

Berg JM, Tymoczko JL, Stryer L (2002) Prokaryotic DNA-binding proteins bind specifically to regulatory sites in operons. In Biochemistry (5th ed., section 31.1), New York

Bianco L, Pescini D, Siepmann P, Krasnogor N, Romero-Campero FJ, Gheorghe M (2006) Towards a p systems *Pseudomonas* quorum sensing model. In: 7th International Workshop on Membrane Computing, WMC 2006, vol 4361, Lecture Notes in Computer Science, Springer, pp 197–214

Bowden GH, Li YH (1997) Nutritional influences on biofilm development. Advances in dental research 11(1):81–99

Bressloff PC (2016) Ultrasensitivity and noise amplification in a model of *Vibrio harveyi* quorum sensing. Physical Review E - Statistical, Nonlinear, and Soft Matter Physics 93(6):062,418

Bressloff PC (2017) Stochastic switching in biology: From genotype to phenotype. Journal of Physics A: Mathematical and Theoretical 50(13):133,001

Brown D (2010) A mathematical model of the *Gac/Rsm* quorum sensing network in *Pseudomonas* fluorescens. BioSystems 101(3):200–212

Brown D (2013) Linking molecular and population processes in mathematical models of quorum sensing. Bulletin of Mathematical Biology 75(10):1813–1839

Brown JR, Doolittle WF (1997) Archaea and the prokaryote-to-eukaryote transition. Microbiology and Molecular Biology Reviews 61(4):456–502

Burch AY, Shimada BK, Mullin SWA, Dunlap CA, Bowman MJ, Lindow SE (2012) *Pseudomonas syringae* coordinates production of a motility-enabling surfactant with flagellar assembly. Journal of Bacteriology 194(6):1287–1298

Byers JT, Lucas C, Salmond GPC, Welch M (2002) Nonenzymatic turnover of an *Erwinia carotovora* quorum-sensing signaling molecule. Journal of Bacteriology 184(4):1163–1171

Caiazza NC, Shanks RMQ, O'Toole GA (2005) Rhamnolipids modulate swarming motility patterns of *Pseudomonas aeruginosa*. Journal of Bacteriology 187(21):7351–7361

Carstea AS, Grecu AT, Grecu D (2010) Proteomic signals in modular transcriptional cascades: A discrete time and cellular automaton approach. Physica D: Nonlinear Phenomena 239(12):967–971

Castillo-Juarez I, Maeda T, Mandujano-Tinoco EA, Perez-Eretza B, Garcia-Contreras J, Wood TK, Garcia-Contreras R (2015) Role of quorum sensing in bacterial infections. World Journal of Clinical Cases: WJCC 3(7):575–598

Chaplin M, Bucke C (1990) Enzyme Technology. Cambridge University Press, URL `https://books.google.co.uk/books`

Chaves GS, Lepine F, Deziel E (2005) Production of rhamnolipids by *Pseudomonas aeruginosa*. Applied Microbiology Biotechnology 68(6):718–725

Chen F, Chen CC, Riadi L, Ju LK (2004) Modeling *rhl* quorum-sensing regulation on rhamnolipid production by *Pseudomonas aeruginosa*. Biotechnology Progress 20(5):1325–1331

Chen L, Wang R, Zhou T, Aihara K (2005) Noise-induced cooperative behavior in a multicell system. Bioinformatics 21(11):2722–2729

Chopp DL, Kirisits MJ, Moran B, Parsek MR (2002) A mathematical model of quorum sensing in a growing bacterial biofilm. Journal of Industrial Microbiology and Biotechnology 29(6):339–346

Chopp DL, Kirisits MJ, Moran B, Parsek MR (2003) The dependence of quorum sensing on the depth of a growing biofilm. Bulletin of Mathematical Biology 65(6):1053–1079

Chrzanowski L, Lawniczak L, Czaczyk K (2012) Why do microorganisms produce rhamnolipids? World Journal of Microbiology and Biotechnology 28(2):401–419

Cleland WW (1963) The kinetics of enzyme-catalyzed reactions with two or more substrates or products. II. Inhibition: nomenclature and theory. Biochimica et Biophyica Acta

Cogan NG (2013) Concepts in disinfection of bacterial populations. Mathematical Biosciences 245(2):111–125

Cogan NG, Chellam S (2009) Incorporating pore blocking, cake filtration, and eps production in a model for constant pressure bacterial fouling during dead-end microfiltration. Journal of Membrane Science 345(1-2):81–89

Cogan NG, Gunn JS, Wozniak DJ (2011) Biofilms and infectious diseases: Biology to mathematics and back again. FEMS Microbiology Letters 322(1):1–7

Contois DE (1959) Kinetics of bacterial growth: relationship between population density and specific growth rate of continuous cultures. Journal of General Microbiology 21(1):40–50

Costa SGVAO, De Souza SR, Nitschke M, Franchetti SMM, Jafelicci Jr M, Lovaglio RB, Contiero J (2009) Wettability of aqueous rhamnolipids solutions produced by *Pseudomonas aeruginosa* lbi. Journal of Surfactants and Detergents 12(2):125–130

Daniels R, Vanderleyden J, Michiels J (2004) Quorum sensing and swarming migration in bacteria. FEMS Microbiol Review 28(3):261–289

Daniels R, Reynaert S, Hoekstra H, Verreth C, Janssens J, Braeken K, Fauvart M, Beullens S, Heusdens C, Lambrichts I, De Vos DE, Vanderleyden J, Vermant J, Michiels J (2006) Quorum signal molecules as biosurfactants affecting swarming in *Rhizobium etli*. Proceedings of the National Academy of Sciences of the United States of America 103(40):14,965–14,970

Davies DG, Parsek MR, Pearson JP, Iglewski BH, Costerton JW, Greenberg EP (1998) The involvement of cell-to-cell signals in the development of a bacterial biofilm. Science 280(5361):295–298

De Kievit T, Seed PC, Nezezon J, Passador L, Iglewski BH (1999) Rsal, a novel repressor of virulence gene expression in *Pseudomonas aeruginosa*. Journal of Bacteriology 181(7):2175–2184

De Kievit TR, Iglewski BH (2000) Bacterial quorum sensing in pathogenic relationships. Infection and Immunity 68(9):4839–4849

De Kievit TR, Kakai Y, Register JK, Pesci EC, Iglewski BH (2002) Role of the *Pseudomonas aeruginosa las* and *rhl* quorum-sensing systems in *rhlI* regulation. FEMS Microbiology Letters 212(1):101–106

Denyer SP, Maillard JY (2002) Cellular impermeability and uptake of biocides and antibiotics in gram-negative bacteria. Journal Applied Microbiology 92:35S–45S

Diggle SP, West SA, Gardner A, Griffin AS (2008) Communication in bacteria, in Sociobiology of Communication: An Interdisciplinary Perspective, P. d'Ettorre and D. P. Hughes, Eds. Oxford University Press, United Kingdom

Dilanji GE, Langebrake JB, De Leenheer P, Hagen SJ (2012) Quorum activation at a distance: Spatiotemporal patterns of gene regulation from diffusion of an autoinducer signal. Journal of the American Chemical Society 134(12):5618–5626

Dixit S, Dubey RC, Maheshwari DK, Seth PK, Bajpai VK (2017) Roles of quorum sensing molecules from *Rhizobium etli* rt1 in bacterial motility and biofilm formation. Brazilian Journal of Microbiology DOI http://dx.doi.org/10.1016/j.bjm.2016.08.005

Dockery JD, Keener JP (2001) A mathematical model for quorum sensing in *Pseudomonas aeruginosa*. Bulletin of Mathematical Biology 63(1):95–116

Douarche C, Buguin A, Salman H, Libchaber A (2009) *Eschericia coli* and oxygen: A motility transition. Physical Review Letters 102(19):198,101

Du H, Xu Z, Shrout JD, Alber M (2011) Multiscale modeling of *Pseudomonas aeruginosa* swarming. Mathematical Models and Methods in Applied Sciences 21(1):939–954

Du H, Xu Z, Anyan M, Kim O, Leevy WM, Shrout JD, Alber M (2012) High density waves of the bacterium *Pseudomonas aeruginosa* in propagating swarms result in efficient colonization of surfaces. Biophysical Journal 103(3):601–609

Dubern JF, Diggle SP (2008) Quorum sensing by 2-alkyl-4-quinolones in *Pseudomonas aeruginosa* and other bacterial species. Molecular Biosystems 4(9):882–888

Duddu R, Bordas S, Chopp D, Moran B (2008) A combined extended finite element and level set method for biofilm growth. International Journal for Numerical Methods in Engineering 74(5):848–870

Duddu R, Chopp DL, Moran B (2009) A two-dimensional continuum model of biofilm growth incorporating fluid flow and shear stress based detachment. Biotechnology and Bioengineering 103(1):92–104

Eberhard A (1972) Inhibition and activation of bacterial *Luciferase* synthesis. Journal of Bacteriology 109(3):1101–1105

Eberhard A, Burlingame AL, Eberhard C, Kenyon GL, Nealson KH, Oppenheimer NJ (1981) Structural identification of autoinducer of photobacterium *Fischeri luciferase*. Biochemistry 20(9):2444–2449

Edelstein L (2005) Mathematical models in Biology. SIAM-Classics in Applied Mathematics, New York

Emerenini BO, Hense BA, Kuttler C, Eberl HJ (2015) A mathematical model of quorum sensing induced biofilm detachment. PLoS ONE 10(7):e0132,385

Fagerlind MG (2008) Mathematical modelling of bacterial quorum sensing and bioflm formation. Doctoral thesis, University of New South Wales, Sydney, Australia

Fagerlind MG, Rice SA, Nilsson P, Harlen M, James S, Charlton T, Kjelleberg S (2003) The role of regulators in the expression of quorum-sensing signals in *Pseudomonas aeruginosa*. Journal of Molecular Microbiology and Biotechnology 6(2):88–100

Fagerlind MG, Nilsson P, Harln M, Karlsson S, Rice SA, Kjelleberg S (2005) Modeling the effect of acylated homoserine lactone antagonists in *Pseudomonas aeruginosa*. BioSystems 80(2):201–213

Fekete A, Kuttler C, Rothballer M, Hense BA, Fischer D, Buddrus-Schiemann K, Lucio M, Mller J, Schmitt-Kopplin P, Hartmann A (2010) Dynamic regulation of n-acyl-homoserine lactone production and degradation in *Pseudomonas putida* isof. FEMS Microbiology Ecology 72(1):22–34

Frank SA (2013) Input-output relations in biological systems: measurement, information and hill equation. URL `http://www.biology-direct.com/content/8/1/31`

Frederick MR, Kuttler C, Hense BA, Eberl HJ (2011) A mathematical model of quorum sensing regulated eps production in biofilm communities. Theoretical Biology and Medical Modelling 8:8

Frieden BR, Gatenby RA (2007) Exploratory data analysis using fisher information. Exploratory Data Analysis Using Fisher Information, Springer London

Fujikawa H, Matsushita M (1988) Fractal growth of *Bacillus subtilis* on agar plates. journal of the physical society of japan 58(11):3875–3878

Fujimoto K, Sawai S (2013) A design principle of group-level decision making in cell populations. PLoS Computational Biology 9(6):e1003,110

Fuqua C, Parsek MR, Greenberg EP (2001) Regulation of gene expression by cell-to-cell communication: acyl-homoserine lactone quorum sensing. Annual Review of Genetics 35(1):439–468

Gallegos A, Mazzag B, Mogilner A (2006) Two continuum models for the spreading of myxobacteria swarms. Bulletin of Mathematical Biology 68(4):837–861

Galloway DR (1991) *Pseudomonas aeruginosa* elastase and elastolysis revisited: recent developments. Molecular Microbiology 5(10):2315–2321

Garca-Contreras R, Maeda T, Wood TK (2013) Resistance to quorum-quenching compounds. Applied and Environmental Microbiology 79(22):6840–6846

Garcia-Ojalvo J, Elowitz MB, Strogatz SH (2004) Modeling a synthetic multicellular clock: Repressilators coupled by quorum sensing. Proceedings of the National Academy of Sciences of the United States of America 101(30):10,955–10,960

Gatenby RA, Frieden BR (2007) Information theory in living systems, methods, applications, and challenges. Bulletin of Mathematical Biology 69(2):635–657

Gheorghe M (2006) P systems - a new computational approach in systems biology. In: 1st International Conference on Bio-Inspired Computing - Theory and Applications, BIC-TA 2006, pp 7–14

Giverso C, Verani M, Ciarletta P (2015) Branching instability in expanding bacterial colonies. Journal of the Royal Society Interface 12(104):20141,290

Glessner A, Smith RS, Iglewski BH, Robinson JB (1999) Roles of *Pseudomonas aeruginosa las* and *rhl* quorum-sensing systems in control of twitching motility. Journal of Bacteriology 181(5):1623–1629

Glick D, Barth S, Macleod KF (2010) Autophagy: Cellular and molecular mechanisms. Journal of Pathology 221(1):3–12

Gloag ES, Turnbull L, Whitchurch CB (2015) Bacterial stigmergy: an organising principle of multicellular collective behaviours of bacteria. Scientifica 2015(2015):387,352

Golding I, Kozlovsky Y, Cohen I, Ben-Jacob E (1998) Studies of bacterial branching growth using reaction-diffusion models for colonial development. Physica A: Statistical Mechanics and its Applications 260(3-4):510–554

Goryachev AB (2009) Design principles of the bacterial quorum sensing gene networks. Wiley Interdisciplinary Reviews: Systems Biology and Medicine 1(1):45–60

Goryachev AB (2011) Understanding bacterial cell-cell communication with computational modeling. Chemical Reviews 111(1):238–250

Goryachev AB, Toh DJ, Wee KB, Lee T, Zhang HB, Zhang LH (2005) Transition to quorum sensing in an *Agrobacterium* population: A stochastic model. PLoS Computational Biology 1(4):e37

Goryachev AB, Toh DJ, Lee T (2006) Systems analysis of a quorum sensing network: design constraints imposed by the functional requirements, network topology and kinetic constants. Biosystems 83(2-3):178–187

Gram HC (1884) Uber die isolierte farbung der schizomyceten in schnitt- und trockenpraparaten. Fortschritte der Medizin (in German) 2:185–189, english translation in : Brock, T.D. "Pioneers in Medical Laboratory Science: Christian Gram 1884". Hoslink. Retrieved 2017-07-04.

Grover JP (1997) Resource competition, population and community biology series 19. Chapman and Hall, New York

Gunther Iv NW, Nuez A, Fett W, Solaiman DKY (2005) Production of rhamnolipids by *Pseudomonas chlororaphis*, a nonpathogenic bacterium. Applied and Environmental Microbiology 71(5):2288–2293

Gustafsson E, Nilsson P, Karlsson S, Arvidson S (2005) Characterizing the dynamics of the quorum-sensing system in *Staphylococcus aureus*. Journal of Molecular Microbiology and Biotechnology 8(4):232–242

Haseltine EL, Arnold FH (2008) Implications of rewiring bacterial quorum sensing. Applied and Environmental Microbiology 74(2):437–445

Hat B, Kochaczyk M, Bogda MN, Lipniacki T (2016) Feedbacks, bifurcations, and cell fate decision-making in the p53 system. PLoS Computational Biology 12(2):e1004,787

Hense BA, Mller J, Kuttler C, Hartmann A (2012) Spatial heterogeneity of autoinducer regulation systems. Sensors 12(4):4156–4171

Horn H, Lackner S (2014) Modeling of biofilm systems: A review. In: Advances in Biochemical Engineering/Biotechnology, vol 146, Springer Science and Business Media Deutschland GmbH, pp 53–76

Hunter GAM, Keener JP (2014) Mechanisms underlying the additive and redundant qrr phenotypes in *Vibrio harveyi* and *Vibrio cholerae*. Journal of Theoretical Biology 340:38–49

Hunter GAM, Vasquez FG, Keener JP (2013) A mathematical model and quantitative comparison of the small rna circuit in the *Vibrio harveyi* and *Vibrio cholerae* quorum sensing systems. Physical Biology 10(4):046,007

Hussler S, Nimtz M, Domke T, Wray V, Steinmetz I (1998) Purification and characterization of a cytotoxic exolipid of *Burkholderia pseudomallei*. Infection and Immunity 66(4):1588–1593

Ingraham JL, Maaloe O, Neidhardt FC (1983) Growth of the bacterial cell. Sinaur Associates Inc, Massachusetts

Ishihama A, Kori A, Koshio E, Yamada K, Maeda H, Shimada T, Makinoshima H, Iwata A, Fujitac N (2014) Intracellular concentrations of 65 species of transcription factors with known regulatory functions in *Escherichia coli*. Journal of Bacteriology 196(15):2718–2727

Iyoda S, Kamidoi T, Hirose K, Kutsukake K, Watanabe H (2001) A flagellar gene fliz regulates the expression of invasion genes and virulence phenotype in *Salmonella enterica serovar Typhimurium*. Microbial Pathogenesis 30(2):81–90

Jabbari S, King JR, Koerber AJ, Williams P (2010) Mathematical modelling of the *agr* operon in *Staphylococcus aureus*. Journal of Mathematical Biology 61(1):17–54

Jacob EB (2008) Social behavior of bacteria: from physics to complex organization. The European Physical Journal B 65(3):315–322

Jacob EB, Cohen HL (1998) Cooperative self-organization of microorganisms. Scientific American in press, New York

Jacobson DN, Dove WF (1975) The amoebal cell of *Physarum polycephalum*: Colony formation and growth. Developmental Biology 47(1):97–105

Jalihal A, Praveen Krishna V, Adline Princy S (2014) A neoteric approach: Designing the virulence regulation model for *Staphylococcus aureus* by contemplating boolean network. BioTechnology: An Indian Journal 9(6):242–247

James S, Nilsson P, James G, Kjelleberg S, Fagerstrom T (2000) Luminescence control in the marine bacterium *Vibrio fischeri*: An analysis of the dynamics of *lux* regulation. Journal of Molecular Biology 296:1127–1137

Janakiraman V, Englert D, Jayaraman A, Baskaran H (2009) Modeling growth and quorum sensing in biofilms grown in microfluidic chambers. Annals of Biomedical Engineering 37(6):1206–1216

Jarrett AM, Cogan NG, Hussaini MY (2015) Mathematical model for mrsa nasal carriage. Bulletin of Mathematical Biology 77(9):1787–1812

Jarvis FG, Johnson MJ (1949) A glycolipide produced by *Pseudomonas aeruginosa*. Jounal of American Chemical Society 71(12):4124–4126

Karlsson D, Karlsson S, Gustafsson E, Normark BH, Nilsson P (2007) Modeling the regulation of the competence-evoking quorum sensing network in *Streptococcus pneumoniae*. BioSystems 90(1):211–223

Keener JP (2006) How *Salmonella typhimurium* measures the length of flagellar filaments. Bulletin of Mathematical Biology 68(7):1761–1778

Kepseu WD, Woafo P, Sepulchre JA (2010) Dynamics of the transition to pathogenicity in *Erwinia chrysanthemi*. Journal of Biological Systems 18(1):173–203

Kepseu WD, Van Gijsegem F, Sepulchre JA (2012) Modelling the onset of virulence in pathogenic bacteria. Methods in Molecular Biology 804:501–517

Khan HA, Gbosi A, Britton LN, Bryant SL (2008) Mechanistic models of microbe growth in heterogeneous porous media. In: 16th SPE/DOE Improved Oil Recovery Symposium 2008 - "IOR: Now More Than Ever.", vol 2, pp 886–894

Khanacademy (2017) Overview: Gene regulation in bacteria. URL `https://www.khanacademy.org`, retrieved 20-04-17

Kim M, Lee S, Park HD, Choi SI, Hong S (2012) Biofouling control by quorum sensing inhibition and its dependence on membrane surface. Water Science and Technology 66(7):1424–1430

King JR, Koerber AJ, Croft JM, Ward JP, Williams P, Sockett RE (2003) Modelling host tissue degradation by extracellular bacterial pathogens. Mathematical Medicine and Biology 20(3):227–260

Klapper I, Dockery J (2010) Mathematical description of microbial biofilms. SIAM Review 52(2):221–265

Koch AL, Robinson JA, Milliken GA (1998) Mathematical modelling in microbial ecology. Chapman and Hall, New York

Koerber AJ, King JR, Ward JP, Williams P, Croft JM, Sockett RE (2002) A mathematical model of partial-thickness burn-wound infection by *Pseudomonas aeruginosa*: Quorum sensing and the build-up to invasion. Bulletin of Mathematical Biology 64(2):239–259

Koerber AJ, King JR, Williams P (2005) Deterministic and stochastic modelling of endosome escape by *Staphylococcus aureus*: "quorum" sensing by a single bacterium. Journal of Mathematical Biology 50(4):440–488

Kohler T, Curty LK, Barja F, Van Delden C, Pechere JC (2000) Swarming of *Pseudomonas aeruginosa* is dependent on cell-to-cell signaling and requires flagella and pili. Journal of Bacteriology 182(21):5990–5996

Koirala S, Mears P, Sim M, Golding I, Chemla YR, Aldridge PD, Rao CV (2014) A nutrient-tunable bistable switch controls motility in *Salmonella enterica serovar typhimurium*. mBio 5(5):e01,611–e01,614

Kokare C, Chakraborty S, Khopade A, Mahadik K (2009) Biofilm: Importance and application. Indian Journal of Biotechnology 8:159–168

Kong KF, Vuong C, Otto M (2006) *Staphylococcus* quorum sensing in biofilm formation and infection. International Journal of Medical Microbiology 296(2-3):133–139

Kong W, Liang H, Shen L, Duan K (2009) Regulation of type iii secretion system by rhl and pqs quorum sensing systems in *Pseudomonas aeruginosa*. Wei sheng wu xue bao = Acta microbiologica Sinica 49(9):1158–1164

Kurtzman CP, Price NPJ, Ray KJ, Kuo TM (2010) Production of sophorolipid biosurfactants by multiple species of the *Starmerella (Candida) bombicola yeast clade*. FEMS Microbiology Letters 311(2):140–146

Langebrake JB, Dilanji GE, Hagen SJ, De Leenheer P (2014) Traveling waves in response to a diffusing quorum sensing signal in spatially-extended bacterial colonies. Journal of Theoretical Biology 363:53–61

Latifi A, Winson MK, Foglino M, Bycroft BW, Stewart GS, Lazdunski A, Williams P (1995) Multiple homologues of luxr and luxi control expression of virulence determinants and secondary metabolites through quorum sensing in *Pseudomonas aeruginosa* pao1. Molecular Microbiology 17(2):333–343

Latifi A, Foglino M, Tanaka K, Williams P, Lazdunski A (1996) A hierarchical quorum-sensing cascade in *Pseudomonas aeruginosa* links the transcriptional activators lasr and rhir (vsmr) to expression of the stationary-phase sigma factor rpos. Molecular Microbiology 21(6):1137–1146

Lewenza S, Conway B, Greenberg EP, Sokol PA (1999) Quorum sensing in *Burkholderia cepacia*: Identification of the luxri homologs cepri. Journal of Bacteriology 181(3):748–756

Li F, Lin L, Ma S (2015) Research of diffusion-based molecular oscillation and synchronization in nanonetworks. Xitong Fangzhen Xuebao / Journal of System Simulation 27(9):1960–1966

Li YH, Tian X (2012) Quorum sensing and bacterial social interactions in biofilms. Sensors 12(3):2519–2538

Liu K, Zeng X, Qiao L, Li X, Yang Y, Dai C, Hou A, Xu D (2014) The sensitivity and significance analysis of parameters in the model of ph regulation on lactic acid production by *Lactobacillus bulgaricus*. BMC Bioinformatics 15(13):S5

Liu YQ, Liu Y, Tay JH (2004) The effects of extracellular polymeric substances on the formation and stability of biogranules. Applied Microbiology and Biotechnology 65(2):143–148

Lo C, Wei G, Marculescu R (2015) Towards autonomous control of molecular communication in populations of bacteria. In: 2nd ACM International Conference on Nanoscale Comput-

ing and Communication, ACM NANOCOM 2015, Association for Computing Machinery, Inc

Long T, Tu KC, Wang Y, Mehta P, Ong NP, Bassler BL, Wingreen NS (2009) Quantifying the integration of quorum-sensing signals with single-cell resolution. PLoS Biology 7(3):e68

Lowy F (2009) Bacterial classification, structure and function. URL `http://www.columbia.edu/itc/hs/medical/pathophys/id/2009/`, retrieved 2015-04-27

Ma XY, Wang XC, Ngo HH, Guo W, Wu MN, Wang N (2014) Bioassay based luminescent bacteria: Interferences, improvements, and applications. Science of the Total Environment 468-469:1–11

Maier RM, Soberon-Chavez G (2000) *Pseudomonas aeruginosa* rhamnolipids: Biosynthesis and potential applications. Applied Microbiology and Biotechnology 54(5):625–633

Malthus T (1798) An essay on the principle of population. Oxford World's Classics reprint (Chapter VII, p.61)

Marenda M, Zanardo M, Trovato A, Seno F, Squartini A (2016) Modeling quorum sensing trade-offs between bacterial cell density and system extension from open boundaries. Scientific Reports 6:39,142

Mata L, Gaspar H, Santos R (2012) Carbon/nutrient balance in relation to biomass production and halogenated compound content in the red alga *Asparagopsis taxiformis (bonnemaisoniaceae)*. Journal of Phycology 48(1):248–253

Matsushita M, Fujikawa H (1990) Diffusion-limited growth in bacterial colony formation. Physica A: Statistical Mechanics and its Applications 168(1):498–506

Matsuyama T, Sogawa M, Nakagawa Y (1989) Fractal spreading growth of *Serratia marcescens* which produces surface active exolipids. FEMS Microbiology Letters 61(3):243–246

McGary K, Nudler E (2014) Rna polymerase and the ribosome: the close relationship. Current Opinion in Microbiology 16(2):112–117

McMillen D, Kopell N, Hasty J, Collins JJ (2002) Synchronizing genetic relaxation oscillators by intercell signaling. Proceedings of the National Academy of Sciences of the United States of America 99(2):679–684

Medina G, Jurez K, Valderrama B, Soberon-Chavez G (2003) Mechanism of *Pseudomonas aeruginosa* rhlr transcriptional regulation of the *rhlAB* promoter. Journal of Bacteriology 185(20):5976–5983

Medved M (1992) Fundamentals of dynamical systems and bifurcation theory. IOP publishing Ltd, England

Melke P, Sahlin P, Levchenko A, Jnsson H (2010) A cell-based model for quorum sensing in heterogeneous bacterial colonies. PLoS Computational Biology 6(6):1–13

Miller MB, Bassler BL (2001) Quorum sensing in bacteria. Annual Review Microbiology 55:165–199

Mimura M, Sakaguchi H, Matsushita M (2000) Reaction-diffusion modelling of bacterial colony. Physica A 282(1-2):283–303

Mok KC, Wingreen NS, Bassler BL (2003) *Vibrio harveyi* quorum sensing: A coincidence detector for two autoinducers controls gene expression. EMBO Journal 22(4):870–881

Monod J (1947) The phenomenon of enzymatic adaptation. Growth 11:223–289

Muller J, Uecker H (2013) Approximating the dynamics of communicating cells in a diffusive medium by odes-homogenization with localization. Journal of Mathematical Biology 67(5):1023–1065

Muller J, Kuttler C, Hense BA, Rothballer M, Hartmann A (2006) Cell-cell communication by quorum sensing and dimension-reduction. Journal of Mathematical Biology 53(4):672–702

Muller MM, Hrmann B, Syldatk C, Hausmann R (2010) *Pseudomonas aeruginosa* pao1 as a model for rhamnolipid production in bioreactor systems. Applied Microbiology and Biotechnology 87(1):167–174

Mund A, Kuttler C, Prez-Velzquez J, Hense BA (2016) An age-dependent model to analyse the evolutionary stability of bacterial quorum sensing. Journal of Theoretical Biology 405:104–115

Murray JD (1989) Mathematical Biology:I.An Introduction. Springer-Verlag, USA

Murray JD (1993) Mathematical Biology, 2nd ed. Springer-Verlag, New York

Musselman SW, Chander S (2002) Wetting and adsorption of acetylenic diol based non-ionic surfactants on heterogeneous surfaces. Colloids and Surfaces A: Physicochemical and Engineering Aspects 206(1-3):497–513

Navid A, Ghim CM, Fenley AT, Yoon S, Lee S, Almaas E (2009) Systems biology of microbial communities. Methods in Molecular Biology 500:469–494

Nealson KH, Hastings JW (1979) Bacterial bioluminescence: Its control and ecological significance. Microbiological Reviews 43(4):496–518

Nealson KH, Platt T, Hastings JW (1970) Cellular control of the synthesis and activity of the bacterial luminescent system. Journal of Bacteriology 104(1):313–322

Nelson LK, D'Amours GH, Sproule-Willoughby KM, Morck DW, Ceri H (2009) *Pseudomonas aeruginosa las* and *rhl* quorum-sensing systems are important for infection and inflammation in a rat prostatitis model. Microbiology 155(8):2612–2619

Nikolaev EV, Sontag ED (2016) Quorum-sensing synchronization of synthetic toggle switches: A design based on monotone dynamical systems theory. PLoS Computational Biology 12(4):e1004,881

Nilsson P, Olofsson A, Fagerlind M, Fagerstrm T, Rice S, Kjelleberg S, Steinberg P (2001) Kinetics of the ahl regulatory system in a model biofilm system: How many bacteria constitute a "quorum"? Journal of Molecular Biology 309(3):631–640

Nouwens AS, Beatson SA, Whitchurch CB, Walsh BJ, Schweizer HP, Mattick JS, Cordwell SJ (2003) Proteome analysis of extracellular proteins regulated by the *las* and *rhl* quorum sensing systems in *Pseudomonas aeruginosa* pao1. Microbiology 149(5):1311–1322

Ochsner UA, Reiser J (1995) Autoinducer-mediated regulation of rhamnolipid biosurfactant synthesis in *Pseudomonas aeruginosa*. Proceedings of the National Academy of Sciences of the United States of America 92(14):6424–6428

Ohnishi K, Kutsukake K, Suzuki H, Lino T (1992) A novel transcriptional regulation mechanism in the flagellar regulon of *Salmonella typhimurium*: an antisigma factor inhibits the activity of the flagellumspecific sigma factor, f. Molecular Microbiology 6(21):3149–3157

O'Loughlin CT, Miller LC, Siryaporn A, Drescher K, Semmelhack MF, Bassler BL (2013) A quorum-sensing inhibitor blocks *Pseudomonas aeruginosa* virulence and biofilm formation. Proceedings of the National Academy of Sciences of the United States of America 110(44):17,981–17,986

Pai A, You L (2009) Optimal tuning of bacterial sensing potential. Molecular Systems Biology 5(1):286

Panikov NS (1995) Microbial growth kinetics. Chapman and Hall, London

Paton KM, Anderson L, Flottat P, Cytrynbaum EN (2015) A model of chloroplast growth regulation in mesophyll cells. Bulletin of Mathematical Biology 77(9):1653–1667

Pearson JP, Passador L, Iglewski BH, Greenberg EP (1995) A second n-acylhomoserine lactone signal produced by *Pseudomonas aeruginosa*. Proceedings of the National Academy of Sciences of the United States of America 92(5):1490–1494

Pearson JP, Pesci EC, Iglewski BH (1997) Roles of *Pseudomonas aeruginosa las* and *rhl* quorum-sensing systems in control of elastase and rhamnolipid biosynthesis genes. Journal of Bacteriology 179(18):5756–5767

Perez-Velazquez J, Quinones B, Hense BA, Kuttler C (2015) A mathematical model to investigate quorum sensing regulation and its heterogeneity in *Pseudomonas syringae* on leaves. Ecological Complexity 21:128–141

Perez-Velazquez J, Golgeli M, Garcia-Contreras R (2016) Mathematical modelling of bacterial quorum sensing: A review. Bulletin of Mathematical Biology 78(8):1585–1639

Pesci EC, Pearson JP, Seed PC, Iglewski BH (1997) Regulation of *las* and *rhl* quorum sensing in *Pseudomonas aeruginosa*. Journal of Bacteriology 179(10):3127–3132

Pesci EC, Milbank JBJ, Pearson JP, McKnight S, Kende AS, Greenberg EP, Iglewski BH (1999) Quinolone signaling in the cell-to-cell communication system of *Pseudomonas aeruginosa*. Proceedings of the National Academy of Sciences of the United States of America 96(20):11,229–11,234

Pfeuty B, Kaneko K (2009) The combination of positive and negative feedback loops confers exquisite flexibility to biochemical switches. Physical Biology 6(4):046,013

Poignard C (2014) Inducing chaos in a gene regulatory network by coupling an oscillating dynamics with a hysteresis-type one. Journal of Mathematical Biology 69(2):335–368

Potapov I, Zhurov B, Volkov E (2012) "quorum sensing" generated multistability and chaos in a synthetic genetic oscillator. Chaos 22(2):023,117

Pratt LA, Kolter R (1998) Genetic analysis of *Escherichia coli* biofilm formation: Roles of flagella, motility, chemotaxis and type i pili. Molecular Microbiology 30(2):285–293

Quan DN, Tsao CY, Wu HC, Bentley WE (2016) Quorum sensing desynchronization leads to bimodality and patterned behaviors. PLoS Computational Biology 12(4):e1004,781

Rahim R, Ochsner UA, Olvera C, Graninger M, Messner P, Lam JS, Soberon-Chavez G (2001) Cloning and functional characterization of the *Pseudomonas aeruginosa rhlC* gene

that encodes rhamnosyltransferase 2, an enzyme responsible for di-rhamnolipid biosynthesis. Molecular Microbiology 40(3):708–718

Rahman KSM, Rahman TJ, McClean S, Marchant R, Banat IM (2002) Rhamnolipid biosurfactant production by strains of pseudomonas aeruginosa using low-cost raw materials. Biotechnology Progress 18(6):1277–1281

Rakesh S (2012) Enzyme Inhibition: Mechanisms and Scope, Enzyme Inhibition and Bioapplications. In Tech, Rijeka

Ralston A (2008a) Operons and prokaryotic gene regulation. Nature Education 1(1):216

Ralston A (2008b) Simultaneous gene transcription and translation in bacteria. Nature Education 1(1):4

Ramesh Kumar VVS, Kumar P (2017) Biofilm: Importance and applications in bio-medical sciences. URL `http://www.medindia.net/health-press-release/Biofilm-Importance-and-Applications-in-Bio-Medical-Sciences-176653-1.htm`, retrieved 2017-07-06

Rampioni G, Policelli F, Bertani I, Righetti K, Venturi V, Zennaro E, Leoni L (2007a) The *Pseudomonas* quorum-sensing regulator rsal belongs to the tetrahelical superclass of h-t-h proteins. Journal of Bacteriology 189(5):1922–1930

Rampioni G, Schuster M, Greenberg EP, Bertani I, Grasso M, Venturi V, Zennaro E, Leoni L (2007b) Rsal provides quorum sensing homeostasis and functions as a global regulator of gene expression in *Pseudomonas aeruginosa*. Molecular Microbiology 66(6):1557–1565

Raychaudhuri A, Jerga A, Tipton PA (2005) Chemical mechanism and substrate specificity of rhli, an acylhomoserine lactone synthase from *Pseudomonas aeruginosa*. Biochemistry 44(8):2974–2981

Redfield RJ (2002) Is quorum sensing a side effect of diffusion sensing? Trends in Microbiology 10(8):365–370

Renfro TD (2013) Rhamnolipids biosurfactant transport in agricultural soils. Doctoral thesis, Florida State University, USA

Russo G, Slotine JJE (2010) Global convergence of quorum-sensing networks. Physical Review E - Statistical, Nonlinear, and Soft Matter Physics 82(4):041,919

Saini S, Koirala S, Floess E, Mears PJ, Chemla YR, Golding I, Aldridge C, Aldridge PD, Rao CV (2010) Fliz induces a kinetic switch in flagellar gene expression. Journal of Bacteriology 192(24):6477–6481

Schaadt NS, Steinbach A, Hartmann RW, Helms V (2013) Rule-based regulatory and metabolic model for quorum sensing in *Pseudomonas aeruginosa*. BMC Systems Biology 7:81

Schachter B (2003) Slimy business the biotechnology of biofilms. Nature Biotechnology 21(4):361–365

Schuster M, Greenberg EP (2006) A network of networks: Quorum-sensing gene regulation in *Pseudomonas aeruginosa*. International Journal of Medical Microbiology 296(2-3):73–81

Scutera S, Zucca M, Savoia D (2014) Novel approaches for the design and discovery of quorum-sensing inhibitors. Expert Opinion on Drug Discovery 9(4):353–366

Seed PC, Passador L, Iglewski BH (1995) Activation of the *Pseudomonas aeruginosa lasI* gene by lasr and the *Pseudomonas* autoinducer pai: An autoinduction regulatory hierarchy. Journal of Bacteriology 177(3):654–659

Shadel BS, Baldwin TO (1991) The *Vibrio fischeri* luxr protein is capable of bidirectional stimulation of transcription and both positive and negative regulation of the *luxR* gene. Journal of Bacteriology 173(2):568–574

Shankaran H, Steven HS, Resat H (2007) Receptor downregulation and desensitization enhance the information processing ability of signalling receptors. BMC Systems Biology 1:48

Shapiro JA (1988) Bacteria as multicellular organisms. Scientific American, New York

Shapiro JA (1995) The significances of bacterial colony patterns. BioEssays 17(7):597–607

Shih PC, Huang CT (2002) Effects of quorum-sensing deficiency on *Pseudomonas aeruginosa* biofilm formation and antibiotic resistance. Journal of Antimicrobial Chemotherapy 49(2):309–314

Shoham Y, Rosenberg M, Rosenberg E (1983) Bacterial degradation of emulsan. Applied and Environmental Microbiology 46(3):573–579

Shrout JD, Chopp DL, Just CL, Hentzer M, Givskov M, Parsek MR (2006) The impact of quorum sensing and swarming motility on *Pseudomonas aeruginosa* biofilm formation is nutritionally conditional. Molecular Microbiology 62(5):1264–1277

Shrout JD, Tolker-Nielsen T, Givskov M, Parsek MR (2011) The contribution of cell-cell signaling and motility to bacterial biofilm formation. MRS Bulletin 36(5):367–373

Singh D, Manjunatha BS, Meena RP, Taria S (2015) Bacterial biofilm and quorum sensing. Annals of Biology 31(1):13–17

Sitnikov DM, Schineller JB, Baldwin TO (1995) Transcriptional regulation of bioluminesence genes from *Vibrio fischeri*. Molecular Microbiology 17(5):801–812

Skindersoe ME, Alhede M, Phipps R, Yang L, Jensen PO, Rasmussen TB, Bjarnsholt T, Tolker-Nielsen T, Hoiby N, Givskov M (2008) Effects of antibiotics on quorum sensing in *Pseudomonas aeruginosa*. Antimicrobial Agents and Chemotherapy 52(10):3648–3663

Smith HL, Waltman P (1995) The theory of the chemostat. Cambridge University Press, Cambridge, UK

Song H, Smolen P, Av-Ron E, Baxter DA, Byrne JH (2007) Dynamics of a minimal model of interlocked positive and negative feedback loops of transcriptional regulation by camp-response element binding proteins. Biophysical Journal 92(10):3407–3424

Sotirova A, Spasova D, Vasileva-Tonkova E, Galabova D (2009) Effects of rhamnolipid-biosurfactant on cell surface of *Pseudomonas aeruginosa*. Microbiological Research 164(3):297–303

Sperandio V, Torres AG, Kaper JB (2002) Quorum sensing *Escherichia coli* regulators b and c (qsebc): A novel two-component regulatory system involved in the regulation of flagella and motility by quorum sensing in *Eschericia coli*. Molecular Microbiology 43(3):809–821

Stanghellini ME, Miller RM (1997) Their identity and potential efficacy in the biological control of zoosporic plant pathogens. Plant Disease 81(1):4–12

Stewart PS (2003) Diffusion in biofilms. Journal of Bacteriology 185(5):1485–1491

Stipcevic T, Piljac A, Piljac G (2006) Enhanced healing of full-thickness burn wounds using di-rhamnolipid. Burns 32(1):24–34

Strogatz HS (2000) Nonlinear and dynamics chaos (with applications to physics, biology, chemistry, and engineering). Westview Press, USA

Su Y, Mennerich A, Urban B (2012) Comparison of nutrient removal capacity and biomass settleability of four high-potential microalgal species. Bioresource Technology 124:157–162

Swift S, Karlyshev AV, Fish L, Durant EL, Winson MK, Chhabra SR, Williams P, Macintyre S, Stewart GSAB (1997) Quorum sensing in *Aeromonas hydrophila* and *Aeromonas salmonicida*: Identification of the luxri homologs ahyri and asari and their cognate n-acylhomoserine lactone signal molecules. Journal of Bacteriology 179(17):5271–5281

Syldatk C, Lang S, Matulovic U, Wagner F (1985) Production of four interfacial active rhamnolipids from -alkanes or glycerol by resting cells of *Pseudomonas* species dsm 2874. Zeitschrift fur Naturforschung - Section C Journal of Biosciences 40(1-2):61–67

Szabo E (2015) Oregonator generalization as a minimal model of quorum sensing in belousov-zhabotinsky reaction with catalyst confinement in large populations of particles. RSC Advances 5(120):99,547–99,554

Tasaki S, Nakayama M, Shoji W (2017) Self-organization of bacterial communities against environmental ph variation: Controlled chemotactic motility arranges cell population structures in biofilms. PLoS ONE 12(3):e0173,195

Terrazas G, Krasnogor N, Gheorghe M, Bernardini F, Diggle S, Cmara M (2005) An environment aware p-system model of quorum sensing. In: Cooper SB, Lowe B, Torenvliet L (eds) First Conference on Computability in Europe, CiE 2005: New Computational Paradigms, vol 3526, pp 479–485

Tilman D (1982) Resource competition and community structure. Priceton University Press, Priceton

Tinsley MR, Taylor AF, Huang Z, Showalter K (2009) Emergence of collective behavior in groups of excitable catalyst-loaded particles: Spatiotemporal dynamical quorum sensing. Physical Review Letters 102(15):158,301

Tinsley MR, Taylor AF, Huang Z, Wang F, Showalter K (2010) Dynamical quorum sensing and synchronization in collections of excitable and oscillatory catalytic particles. Physica D: Nonlinear Phenomena 239(11):785–790

Todar K (2015) The growth of bacterial population. URL `http://textbookofbacteriology.net/growth_3.html`, retrieved 2015-03-16

Trovato A, Seno F, Zanardo M, Alberghini S, Tondello A, Squartini A (2014) Quorum vs. diffusion sensing: A quantitative analysis of the relevance of absorbing or reflecting boundaries. FEMS Microbiology Letters 352(2):198–203

Tuleva BK, Ivanov GR, Christova NE (2002) Biosurfactant production by a new *Pseudomonas putida* strain. Zeitschrift fur Naturforschung - Section C Journal of Biosciences 57(3-4):356–360

Uecke H, Mller J, Hense BA (2014) Individual-based model for quorum sensing with background flow. Bulletin of Mathematical Biology 76(7):1727–1746

Van Delden C, Iglewski BH (1998) Cell-to-cell signaling and *Pseudomonas aeruginosa* infections. Emerging Infectious Diseases 4(4):551–560

Van Der Tol MWM, Scholten H (1997) A model analysis on the effect of decreasing nutrient loads on the biomass of benthic suspension feeders in the oosterschelde ecosystem (sw netherlands). Aquatic Ecology 31(4):395–408

Verhulst PF (1838) Notice sur la loi que la population suit dans son accroissement. Correspondence Mathematique et Physique Publiee par a *Quetelet* 10:113–121

Viretta AU, Fussenegger M (2004) Modeling the quorum sensing regulatory network of human-pathogenic *Pseudomonas aeruginosa*. Biotechnology Progress 20(3):670–678

Von Bodman SB, Farrand SK (1995) Capsular polysaccharide biosynthesis and pathogenicity in *Erwinia stewartii* require induction by an n-acylhomoserine lactone autoinducer. Journal of Bacteriology 177(17):5000–5008

Wada T, Morizane T, Abo T, Tominaga A, Inoue-Tanaka K, Kutsukake K (2011a) Eal domain protein ydiv acts as an anti-flhd4c2 factor responsible for nutritional control of the flagellar regulon in *Salmonella enterica serovar typhimurium*. Journal of Bacteriology 193(7):1600–1611

Wada T, Tanabe Y, Kutsukake K (2011b) Fliz acts as a repressor of the *ydiV* gene, which encodes an anti-flhd 4c 2 factor of the flagellar regulon in *Salmonella enterica serovar typhimurium*. Journal of Bacteriology 193(19):5191–5198

Wang R, Chen L (2005) Synchronizing genetic oscillators by signaling molecules. Journal of Biological Rhythms 20(3):257–269

Ward JP, King JR (2012) Thin-film modelling of biofilm growth and quorum sensing. Journal of Engineering Mathematics 73(1):71–92

Ward JP, King JR, Koerber AJ, Williams P, Croft JM, Sockett RE (2001) Mathematical modelling of quorum sensing in bacteria. Ima Journal of Mathematics Applied in Medicine and Biology 18(3):263–292

Ward JP, King JR, Koerber AJ, Croft JM, Sockett RE, Williams P (2003) Early development and quorum sensing in bacterial biofilms. Journal of Mathematical Biology 47(1):23–55

Webber MA, Piddock LJV (2003) The importance of efflux pumps in bacterial antibiotic resistance. Journal of Antimicrobial Chemotherapy 51(1):9–11

Weber M, Buceta J (2013) Dynamics of the quorum sensing switch: stochastic and nonstationary effects. BMC Systems Biology 7:6

Wei G, Walsh C, Cazan I, Marculescu R (2015) Molecular tweeting: Unveiling the social network behind heterogeneous bacteria populations. In: 6th ACM Conference on Bioinformatics, Computational Biology, and Health Informatics, BCB 2015, Association for Computing Machinery, Inc, pp 366–375

Wei G, Lo C, Walsh C, Hiller NL, Marculescu R (2016) In silico evaluation of the impacts of quorum sensing inhibition (qsi) on strain competition and development of qsi resistance. Scientific Reports 6:35,136

Welch M, Todd DE, Whitehead NA, McGowan SJ, Bycroft BW, Salmond GPC (2000) N-acyl homoserine lactone binding to the carr receptor determines quorum-sensing specificity in *Erwinia*. EMBO Journal 19(4):631–641

Wilder CN, Diggle SP, Schuster M (2011) Cooperation and cheating in *Pseudomonas aeruginosa*: The roles of the *las*, *rhl* and *pqs* quorum-sensing systems. ISME Journal 5(8):1332–1343

Winson MK, Camara M, Latifi A, Foglino M, Chhabra SR, Daykin M, Bally M, Chapon V, Salmond GPC, Bycroft BW, Lazdunski A, Stewart GSAB, Williams P (1995) Multiple n-acyl-l-homoserine lactone signal molecules regulate production of virulence determinants and secondary metabolites in *Pseudomonas aeruginosa*. Proceedings of the National Academy of Sciences of the United States of America 92(20):9427–9431

Wolf DM, Arkin AP (2003) Motifs, modules and games in bacteria. Current Opinion in Microbiology 6(2):125–134

Xie XS, Choi PJ, Li GW, Nam KL, Lia G (2008) Single-molecule approach to molecular biology in living bacterial cells. Annual Review of Biophysics 37:417–444

Zhang L, Murphy PJ, Kerr A, Tate ME (1993) Agrobacterium conjugation and gene regulation by n-acyl-l-homoserine lactones. Nature 362(6419):446–448

Zhang T, Pabst B, Klapper I, Stewart PS (2013) General theory for integrated analysis of growth, gene, and protein expression in biofilms. PLoS ONE 8(12):e83,626

Zhang Z, Peng J, Zhang J (2008) Analysis of a bacteria-immunity model with delay quorum sensing. Journal of Mathematical Analysis and Applications 340(1):102–115

Zhang Z, Suo Y, Zhang J (2015) Stability and sensitive analysis of a model with delay quorum sensing. Abstract and Applied Analysis 2015:1–11

Zhang ZH, Suo YH (2009) Analysis of an epidemic model with quorum sensing mechanism. Fangzhi Gaoxiao Jichukexue Xuebao 22(3):303–307

Zhao J, Shen Y, Haapasalo M, Wang Z, Wang Q (2016) A 3D numerical study of antimicrobial persistence in heterogeneous multi-species biofilms. Journal of Theoretical Biology 392:83–98

Zhao L, Montville TJ, Schaffner DW (2002) Time-to-detection, percent-growth-positive and maximum growth rate models for *Clostridium botulinum* 56a at multiple temperatures. International Journal of Food Microbiology 77(3):187–197

Zhao L, Montville TJ, Schaffner DW (2006) Evidence for quorum sensing in *Clostridium botulinum* 56a. Letters in Applied Microbiology 42(1):54–58

Zhonghua Z, Yaohong S, Juan Z, Xinyu S (2015) Stability and bifurcations in a model of bacteria immunity with quorum sensing. Mathematical Population Studies 22(4):209–233